



University
of Glasgow

Smith, Richard (1998) *Investigations of low levels of stellar polarimetric variability*. PhD thesis.

<http://theses.gla.ac.uk/2804/>

Copyright and moral rights for this thesis are retained by the author

A copy can be downloaded for personal non-commercial research or study, without prior permission or charge

This thesis cannot be reproduced or quoted extensively from without first obtaining permission in writing from the Author

The content must not be changed in any way or sold commercially in any format or medium without the formal permission of the Author

When referring to this work, full bibliographic details including the author, title, awarding institution and date of the thesis must be given

Investigations of Low Levels of Stellar Polarimetric Variability.

by

Richard Smith B.Sc.

Thesis

submitted to the

University of Glasgow

for the degree of

Ph.D.

Astronomy and Astrophysics Group
Department of Physics and Astronomy,
University of Glasgow,
Glasgow G12 8QQ

November 1998

© Richard Smith 1999

Acknowledgements

My sincere thanks go out to a number of people who have made my life at Glasgow, whilst completing this work, both enjoyable, and at times endurable ! First and foremost, I would like to acknowledge Dr. David Clarke, to whom I am deeply emdebted for his help and expertise. I have lost count of the number of times I have knocked on his door for those crucial supervisory chats which have steered me in the right direction. Thank you Dave for your help, friendship, and most of all, for your patience !

I also extend my warm thanks to those other characters who have helped to brighten up my life at the observatory, and provide me with a good few tails to remember. These include of course, my good friends Jaber and Victor, who have aided me considerably with the various Starlink packages I have used, and provided me with more laughs than I can remember. A great thanks to Colin Hunter, the technician for assembling the various instruments I have used, and for tolerating my antics over the years. Thanks also, to the janitor David, for participating in the general level of comaradirie, and for being so cheerful all the time. How do you do it ?

Whilst I have studied here, a great portion of my life has been spent with the boys from the RMR, who have knocked me down when I was feeling blue, and laughed at me when things were going wrong ! A great thanks go out to them all, for reminding me of the funny side of life, no matter how bad things were going, especially Dickie, Stewart, Chris, Brooksie, Boycie, and not forgetting good friends lost - John, Jaz and Tony.

A big thanks and love to my parents for being the best parents I could have hoped for over those most trying of times, and for being so supportive and understanding. Love also for my girlfriend, Hilary for putting up with me over these last two years and for bringing so much happiness into my life.

Summary

The aim of this thesis is the investigation of stars which show very low levels of polarimetric variability. A sample of such stars has been observed and assessed statistically to determine small differences, and temporal changes in polarisation. A statistical test has been improved upon, and used in a more rigorous, but more conservative fashion, emphasising the need for great care and thorough statistical assessment of such sources, to detect *true* temporal change. A new idea for an astronomical polarimeter has been introduced and discussed. The device, incorporating liquid crystals as phase modulators, has been theoretically modeled, designed and developed. Finally the instrument has been tested to ascertain its sensitivity and to investigate the repeatability of any results accrued from its use.

Chapter 1 is a basic introduction to the concepts employed within the thesis. Initially, basic polarimetric definitions are introduced, with the mathematical technique of using Mueller matrices (Mueller (1948)) as a means of examining the effect on a polarised light beam as it passes through a series of retarders. This will be of great importance in considering the design of the new polarimeter. The chapter also briefly introduces some of the basic mechanisms which are responsible for producing polarisation, either in or around a star, or in the interstellar space between an observed star and the observer. Such processes include electron scattering and atomic scattering. A discussion of solar type stars will then follow, as a preview to the observations of a sample of such stars observed and analysed later in the thesis. Finally, this chapter discusses some of the present instruments used for polarimetry, and their draw backs. It will be suggested that there is a need for a new breed of polarimeters which may be used to assess completely, the polarisation state of stellar light, without the need for any mechanically moving parts within the instrument itself. The employment of two liquid crystal variable retarders

aligned in succession to each other is suggested as a method for investigation.

Chapter 2 is concerned with measurements taken over seven nights in May 1996 on the 0.75m telescope at Sutherland, South Africa, using the Cape Town Polarimeter. The program was chosen to observe solar type stars, and the stars were selected by having a spectral classification around G5V. Whilst it is known that the optical radiation of about 85 % of young stars at both ends of the spectral classification sequence, exhibit intrinsic linear polarisation, there is little information on the polarimetric properties for intermediate spectral types. These types range between F and early G8, and they represent about 15% of the total objects, and most have not been studied polarimetrically. Recently it has been suggested that the polarimetric properties of such stars might be considered from the point of view of their circumstellar evolution (Tamura and Sato (1989) and Yudin (1994)). Such ideas are discussed in Chapter 2 and the results of the observing campaign are analysed for temporal variability, using known statistical tests, with the aim of detecting any change in polarisation.

The concern of Chapter 3 is to investigate the use of the Kolmogorov statistical technique (Conover (1980)) as a means of detecting low levels of polarimetric variability. Traditionally used to assess the similarity between two distributions, it is particularly useful as a means of obtaining a reasonable hypothesised distribution, as an approximation to a real distribution. The aim of this chapter will be to use the technique to compare the data from a set of polarised stars, with their calculated theoretical normal distributions. A significant deviation points to the presence of some underlying variability. Consideration is given to the standard error on the mean of the distribution, leading to a more conservative test than previously appreciated. This becomes increasingly important when investigating very low levels of temporal variability.

The development of a *Twin Liquid Crystal Polarimeter* is the theme of Chapter 4. The need for a polarimeter with no mechanically moving components is explained, and to this end, the possible use of liquid crystals is discussed. Initially a device incorporating just one liquid crystal is described, but inevitably this system still requires some mechanical rotation. The subsequent theory behind developing a system with two liquid crystals, to eliminate the need for any rotation, is then developed. It is made apparent that for successful operation of such a device, the cells need be aligned very precisely to each other. Procedures for doing this are considered and assessed. The final optical arrangement

is then calibrated with the aid of the Sénarmont Compensator, used to determine the retardation of any phase plate. The final polarimeter is tested to determine the effective modulation of the system, by passing light beams of known wavelength and polarisation, through it. Such real values of polarisation, and direction of vibration, are compared with those values calculated from the output of the polarimeter. The possible errors present in the system are then discussed, and some detailed theoretical modeling is provided, assessing the effect on the output values, when these errors are applied.

Finally, the thesis is concluded in Chapter 5 with a brief overview of the results and conclusions made. The results from each individual chapter are summarised neatly in an easily digestible form. Suggestions for further avenues of research are made, with the aim of improving knowledge in the fields discussed.

Contents

Acknowledgements	ii
Summary	iii
1 Introduction	1
1.1 Polarimetric Definitions	2
1.2 Mueller Matrices	5
1.3 Astrophysical Mechanisms That Produce Polarisation	7
1.3.1 Electron and Thomson Scattering	7
1.3.2 Atomic and Molecular Scattering	8
1.3.3 Scattering by Dust Particles	8
1.3.4 Magnetic fields	9
1.4 Polarisation of Solar and Late Type Stars	9
1.4.1 Activity in F to M Type Stars	11
1.5 General Polarimetric Modulators	13
2 UCT Polarimeter Observations	17
2.1 Introduction	17
2.2 The Measurements	19
2.3 Statistical analyses	21
2.3.1 Testing for Temporal Variability of Polarisation Using the Welch Test	22
2.3.2 Unpolarised Standard Stars	23
2.3.3 Polarised Standard Stars	29
2.4 The program stars	33
2.4.1 Observations of Tu Pyx - SAO 154972	35

2.4.2	Observations of SAO 251015	38
2.4.3	Observations of 59 VIR : HD115383	38
2.4.4	Observations of HD128400	40
2.4.5	Observations of HD 155555	40
2.4.6	Observations of HD 1835	42
2.5	Conclusion of G-Type Discussion	44
2.6	Observations of HD 139614	45
2.6.1	Observations	45
2.6.2	Discussion	46
2.6.3	Future Work	48
2.7	Observations of HD 100546	48
2.7.1	Measurements	49
2.7.2	Discussion and Conclusion of Results for HD 100546	53
3	Kolmogorov Testing for Temporal Variability	54
3.1	Kolmogorov-Smirnoff Technique	55
3.2	Kolmogorov Technique Analysis to Detect Real Temporal Variability by Consideration of Errors	59
3.2.1	Analysis ϕ Cas	60
3.2.2	Analysis ξ Per	63
3.2.3	Analysis λ Cep	69
3.2.4	Analysis of Alternative Data on λ Cep	72
3.3	Kolmogorov Technique for Analysis of the Polarisation Angle	75
3.3.1	Analysis ϕ Cas	77
3.3.2	Analysis ξ Per	80
3.3.3	Analysis λ Cep	80
3.4	Conclusion	83
3.4.1	ϕ Cas	84
3.4.2	ξ Per	85
3.4.3	λ Cep	85
3.4.4	Summary	86

4	A Liquid Crystal Polarimeter	88
4.1	The Meadowlark Liquid Crystal Variable Retarder	89
4.1.1	D1040 Liquid Crystal Digital Interface	96
4.2	Selection of Liquid Crystal Configuration	97
4.2.1	The Single Liquid Crystal Polarimeter	97
4.2.2	The Twin Liquid Crystal Polarimeter	100
4.3	Alignment Of Optical Components For Calibration	105
4.4	Sénarmont Compensator	109
4.5	Experimental Testing of the Polarimeter	112
4.6	Theoretical Analysis of Errors and the Effect on Determined Polarisation and Polarisation Angle	114
4.6.1	The Individual Effect of the Three Important Errors	116
4.6.2	The Combined Effect of the Three Important Errors	125
4.6.3	Effects of the Passband	129
4.7	Summary	131
5	Conclusion	134
A	UCT Data Prior To Reduction	141
	Bibliography	155

List of Figures

2.1	The Stokes parameter plot (q, u in %) displays the four B band polarisation measurements of HD 202940 made on the nights of JD 0225, 0226, 0229, 0230. Each point is the weighted mean of all measurements taken on those nights. The star is an unpolarised standard, but the data clearly reveal an instrumental polarisation of $\sim 0.3\%$	24
2.2	The Stokes parameter plot (q, u in %) displays the four V band polarisation measurements of HD 202940 made on the nights of JD 0225, 0226, 0229, 0230. Each point is the weighted mean of all measurements taken on those nights.	25
2.3	The Stokes parameter plot (q, u in %) displays the two R band polarisation measurements of HD 202940 made on the nights of JD 0225, 0230. Each point is the weighted mean of all measurements taken on those nights. . . .	25
2.4	The Stokes parameter plot (q, u in %) displays the four V band (\bullet) polarisation measurements of HD 100623 made on the night of JD 0229; 25 May 1996. Comparison is made with the higher quality data for HD 202940 (\oplus)	26
2.5	The Stokes parameter plot displays the four R band polarisation measurements (\bullet) of HD 100623 made on the night of JD 0229;25 May 1996. Also plotted are the individual observations for HD 202940 (\square)	27
2.6	The Stokes parameter plot (q, u in %) for HD 147084 showing the weighted mean data points for the U,B,V,R,I bands, in percentage polarisation. . . .	30
2.7	The Stokes parameter plot (q, u in %) for HD 160529 showing the weighted mean data points for bands U,B,V,R,I in percentage polarisation.	30

2.8	The Stokes parameter plot (q, u in %) displays the 5 data points, for TU Pyx, representing the average point for the nights of JD 0226, 0227, 0229, 0230 and 0231 respectively. The measurements indicate an intrinsic polarisation of about 0.5% which suddenly increased to $\sim 2\%$ on the night of JD 0231.	36
2.9	The Stokes parameter plot (q, u in %) displays the average data points, in the R band, for the nights of JD 0227, 0229 and 0230 respectively, indicating that the data sets for the unpolarised standard HD 202940 (\bullet) and TU Pyx (\circ), can not be considered as being generated from the same parent distribution.	36
2.10	The Stokes parameter (q, u in %) plot displays the six V band polarisation measurements of TU Pyx made on the night of JD 0231. The time sequence covering about 20 minutes shows that the first three are bunched close to the origin while the final three display $p \sim 2\%$	37
2.11	The Stokes parameter plot for 59 Vir in the B band on the night JD 0230, showing a possible fluctuation.	39
2.12	The Stokes parameter plot (q, u in %) of the B (\bullet) and V (\circ) band measurements made of 59 Vir on four different nights indicate polarimetric changes that may be related to its associated photometric period. The numbers 2, 3, 5, 6 refer respectively to the nights of JD 0226, 0227, 0229 and 0230. . .	40
2.13	The Stokes parameter plot (q, u in %) displays the B band measurements for HD 128400 on the nights of JD0229 (\bullet) and JD 0230 (\circ). Welch tests indicate that the two distributions cannot be considered as belonging to the same parent distribution in q	41
2.14	The Stokes parameter plot displays the V band measurements for HD 128400 on the nights of JD0229 (\circ) and JD 0230 (\bullet). Welch tests indicate that the two distributions cannot be considered as belonging to the same parent distribution in u	41

2.15	The Stokes parameter plot (q, u in %) depicts the V band polarimetric values for HD 155555 for each period, on the four nights of observation; \bullet = JD 0225, \triangle = JD 0227, \circ = JD 0229 and \times = JD 0230. It may be noted that for JD 0229, all the data lie in the fourth quadrant and Welch tests indicate variations in the parent distributions from which night-to-night data have been sampled, suggesting a low level of polarimetric variability.	43
2.16	The Stokes parameter plot (q, u in %), for HD 1835, in the B band. There is a marginal suggestion that the star may exhibit a polarisation $\sim 0.07\%$. .	43
2.17	V band polarisation measurements of HD 139614 plotted in the q, u -plane. .	47
2.18	The Stokes parameter plot (q, u in %) depicts the mean polarimetric values for HD 100546 for each of the three nights of observation, for the B and V bands.	51
2.19	The Stokes parameter plot depicts the individual V-band polarimetric records for HD 100546 for the night of JD 245 0229.	52
3.1	The hypothesized distribution function $F^*(x)$, the empirical distribution function (EDF), $S(x)$, and the Kolmogorov Statistic, T	57
3.2	58
3.3	Flow chart showing the analysis process for the program stars. The data for the normalised Stokes parameter in question, may be considered as showing some temporal variability, if H_0 is rejected at the level α	61
3.4	ϕ Cas. Plots of the empirical distribution function $S(q)$, and the hypothesised distribution functions $F^*(q)$, $F^*(q+se)$ and $F^*(q-se)$, where se is the standard error of the observed mean. The four plots (a), (b), (c) and (d), correspond to the four nights of observation 16 th , 17 th , 19 th and 20 th October 1989. The Julian dates given are for the first data point of that night. Kolmogorov tests for the 19 th reveal temporal variability on this night at the 95% confidence level.	64

- 3.5 ϕ Cas. Plots of the empirical distribution function $S(u)$, and the hypothesised distribution functions $F^*(u)$, $F^*(u+se)$ and $F^*(u-se)$, where se is the standard error of the observed mean. The four plots (a), (b), (c) and (d), correspond to the four nights of observation 16th, 17th, 19th and 20th October 1989. The Julian dates given are for the first data point of that night. Kolmogorov tests for the 19th reveal temporal variability on this night at the 90% confidence level. 65
- 3.6 ξ Per. Plots of the empirical distribution function $S(q)$, and the hypothesised distribution functions $F^*(q)$, $F^*(q+se)$ and $F^*(q-se)$, where se is the standard error of the observed mean. The four plots (a), (b), (c) and (d), correspond to the four nights of observation 16th, 17th, 19th and 20th October 1989. The Julian dates given are for the first data point of that night. Kolmogorov tests for the 19th reveal temporal variability on this night at the 95% confidence level. 67
- 3.7 ξ Per. Plots of the empirical distribution function $S(u)$, and the hypothesised distribution functions $F^*(u)$, $F^*(u+se)$ and $F^*(u-se)$, where se is the standard error of the observed mean. The four plots (a), (b), (c) and (d), correspond to the four nights of observation 16th, 17th, 19th and 20th October 1989. The Julian dates given are for the first data point of that night. Kolmogorov tests for the 19th reveal temporal variability on this night at the 95% confidence level. 68
- 3.8 λ Cep. Plots of the empirical distribution function $S(q)$, and the hypothesised distribution functions $F^*(q)$, $F^*(q+se)$ and $F^*(q-se)$, where se is the standard error of the observed mean. The four plots (a), (b), (c) and (d), correspond to the four nights of observation 16th, 17th, 19th and 20th October 1989. The Julian dates given are for the first data point of that night. Kolmogorov tests detect no temporal variability of q during any of the observed nights. 70

3.9	<p>λ Cep. Plots of the empirical distribution function $S(u)$, and the hypothesised distribution functions $F^*(u)$, $F^*(u+se)$ and $F^*(u-se)$, where se is the standard error of the observed mean. The four plots (a), (b), (c) and (d), correspond to the four nights of observation 16th, 17th, 19th and 20th October 1989. The Julian dates given are for the first data point of that night.</p>	71
3.10	<p>λ Cep. Plots of the empirical distribution function $S(q)$, $S(u)$ and the respective hypothesised distribution functions, where se is the standard error of the observed mean. Each plot represents the cumulative data over the four nights of observation.</p>	72
3.11	<p>λ Cep. Daniel Hayes data (Hayes, 1977). (a) and (b) show plots of the empirical distribution function $S(x)$, and the hypothesised distribution functions $F^*(x)$, $F^*(x+se)$ and $F^*(x-se)$, where for (a) $x=q$, and for (b) $x=u$. se is the standard error of the observed mean. (c) and (d) show the individual normalised Stokes parameters binned to produce histograms as an approximation of the real distribution, plotted with the normal distribution generated from the observed mean and standard deviation. The data is from the Harriman Observatory of Columbia, and spans 32 months. In all, 74 observations were made on 31 nights.</p>	74
3.12	<p>The CDF for θ for an unpolarised source, or a polarised standard viewed in the centre of gravity coordinate system.</p>	76
3.13	<p>Plot in q,u space with the centre of gravity, q_0, u_0 as the origin. Due to the standard error on the observed mean, there is an error on the determination of the centre of gravity position. It is possible that it may be anywhere within the 1σ circle. The EDF plots in the Kolmogorov plots for the polarisation angle, θ, will show three sample EDF's calculated with origins at (q_0, u_0), $(q_0+s.e, u_0)$ and $(q_0, u_0+s.e.)$, where $s.e.$ is the standard error of the observed mean.</p>	76

3.14	ϕ Cas. Plots of the empirical distribution functions $S(\theta_0)$, $S(\theta_{q_0+se, u_0})$ and $S(\theta_{q_0, u_0+se})$ where se is the standard error of the observed mean, and the hypothesised distribution function $F(\theta)$ for a normally distributed set of θ . The four plots (a), (b), (c) and (d), correspond to the four nights of observation 16 th , 17 th , 19 th and 20 th October 1989. The Julian dates given are for the first data point of that night.	78
3.15	ϕ Cas. The four CDF plots for ϕ Cas on the night of 19 th October 1989 showing the effect upon the empirical distribution functions of the real data, calculated from different centre of gravity positions, where u_0 and q_0 are varied by different factors of the s.e., up to -1.0 s.e. A better fit to $S(\theta_0)$ is obtained with $S(\theta_{q_0-se, u_0})$	79
3.16	ξ Per. Plots of the empirical distribution functions $S(\theta_0)$, $S(\theta_{q_0+se, u_0})$ and $S(\theta_{q_0, u_0+se})$ where se is the standard error of the observed mean, and the hypothesised distribution function $F(\theta)$ for a normally distributed set of θ . The four plots (a), (b), (c) and (d), correspond to the four nights of observation 16 th , 17 th , 19 th and 20 th October 1989. The Julian dates given are for the first data point of that night.	81
3.17	λ Cep. Plots of the empirical distribution functions $S(\theta_0)$, $S(\theta_{q_0+se, u_0})$ and $S(\theta_{q_0, u_0+se})$ where se is the standard error of the observed mean, and the hypothesised distribution function $F(\theta)$ for a normally distributed set of θ . The four plots (a), (b), (c) and (d), correspond to the four nights of observation 16 th , 17 th , 19 th and 20 th October 1989. The Julian dates given are for the first data point of that night.	82
3.18	CDF plots for the total data of the four nights of observation of λ Cep. It is interesting to note the wave-like nature of the curve. The curve expected elliptical distribution in q, u space, would be expected to cross the straight line $F(\theta)$ only twice.	83
4.1	Cross-sections of the liquid crystal variable retarder cell. Dimensions are shown in inches and fast, f , and slow, s , axes are indicated. D is 1.99 inches, the Clear Aperture, C.A., is 0.80 inches, and the thickness, t , is 0.79 inches. The SMB connector is attached to the power supply.	90

4.2	The output polarisation forms for the different retardance values, when the liquid crystal is positioned with fast axis at 45° to the horizontally polarised input.	90
4.3	The construction of the liquid crystal variable retarder, showing molecular alignment with no voltage applied, and at high voltage.	91
4.4	Performance curve for the retarder at 632.8nm, and 21°C	92
4.5	Performance curve for the retarder at 632.8nm, and 21°C , with a compensator attached, such that axes are aligned, (Meadowlark 1992).	92
4.6	Plot demonstrating how the birefringence of the liquid crystal variable retarder decreases at longer wavelengths.	93
4.7	Plot demonstrating the temperature sensitivity of the liquid crystal variable retarder.	94
4.8	Normalised transmittance of a liquid crystal variable retarder between crossed polaroids, at a single wavelength, (Meadowlark 1992).	95
4.9	The transmittance as a function of wavelength for a liquid crystal variable retarder between crossed polaroids, optimised at 550nm.	95
4.10	Typical contrast ratio of a liquid crystal variable retarder between crossed polaroids, optimised at 550nm.	95
4.11	Typical response time for a liquid crystal variable retarder. The upper diagram shows normal response, whereas the lower diagram shows the more rapid response employing the Transient Nematic Effect (see Meadowlark 1992).	96
4.12	The Meadowlark liquid crystal digital interface, used to allow precision control of the liquid crystal by PC.	97
4.13	The output linear polarisation forms needed for the determination of the Stokes parameters, Q and U.	98
4.14	Instrumental setup, for the Single Liquid Crystal Polarimeter. The Stokes parameter Q, is determined with the liquid crystal switching retardation between 0 and π , when the half-wave plate is set at both 0° and 45° . This allows the elimination of noise associated with differing pixel sensitivity across the CCD detector. The process is repeated to obtain U, but with the half-wave plate set at 22.5° and 67.5°	99

4.15	<i>Case 1.</i> A theoretical trial arrangement of the two liquid crystals, with LC ₂ orientated at 45° to the axes of the analysing polaroid, P.	100
4.16	<i>Case 2.</i> A theoretical trial arrangement of the two liquid crystals, where now both cells are orientated at 45° to the axes of the analysing polaroid, P, but in the opposite sense to each other.	101
4.17	<i>Case 3.</i> A theoretical trial arrangement of the two liquid crystals, where now both cells are orientated at 45° to the axes of the analysing polaroid, P.	101
4.18	The <i>ideal</i> optical arrangement of the two liquid crystals. Light passes through LC ₁ and then LC ₂ . LC ₂ is aligned with its fast axis at $\frac{\pi}{4}$ to that of LC ₁	104
4.19	Cross-section of the layout used to align all optical components to correct orientations for calibration by the Sénarmont method.	106
4.20	When the retarder in question is positioned at θ to the major axis of the input light beam, the maximum modulation, upon rotation of P _{flip} , is achieved when $\phi = \frac{\pi}{4}$	108
4.21	Layout of the Sénarmont Compensator, used for the calibration of voltages which need be applied to the liquid crystal cells, to achieve the desired retardation values given in Table 4.4.	109
4.22	Plot of the retardance of the liquid crystal cell, versus the voltage applied to it. The wavelength calibrated for is 560nm.	110
4.23	Error in alignment angle between δ_1 and δ_2 . δ_2 is not at exactly $\frac{\pi}{4}$ to axis of system of system, but δ_2 is at $\frac{\pi}{4}$ from axis.	115
4.24	Error in alignment angle between δ_1 and δ_2 . δ_1 is not exactly aligned with axis of system, but δ_2 is at $\frac{\pi}{4}$ from axis.	115
4.25	δ_1 and δ_2 aligned correctly at $\frac{\pi}{4}$ with respect to each other, but combined δ_1 and δ_2 offset slightly from system axis.	116
4.26	Plot showing the effect on θ_{out} when the error, ϵ_1 , takes the values of 0°, 10°, 20°, and 35°.	117
4.27	Plot showing the effect on θ_{out} when the error, ϵ_1 , takes the values of 0°, -10°, -20°, and -35°.	117
4.28	The effects of ϵ_1 on the calculated output value of polarisation, P _{out} , for values of ϵ_1 of 0°, 5°, 10°, 20°, and 35°.	118

4.29	The effects of ϵ_1 on the calculated output value of polarisation. P_{out} , for values of ϵ_1 of $0^\circ, -5^\circ, -10^\circ, -20^\circ$, and -35°	119
4.30	Theoretical specific values of θ_{out} for $0^\circ < \epsilon_1 < 10^\circ$, for input orientations corresponding to $+Q$ and $+U$, i.e. θ_{in} equal to 0° and 45° respectively. . . .	120
4.31	Theoretical specific values of θ_{out} for $0^\circ < \epsilon_1 < 10^\circ$, for input orientations corresponding to $-Q$ and $-U$, i.e. θ_{in} equal to 90° and 135° respectively. .	120
4.32	Plot showing the effect on θ_{out} when the error, ϵ_2 , takes the values of $0^\circ, 10^\circ, 20^\circ$, and 35°	121
4.33	Plot showing the effect on θ_{out} when the error, ϵ_2 , takes the values of $0^\circ, -10^\circ, -20^\circ$, and -35°	122
4.34	Plot showing the effect on P_{out} when the error, ϵ_2 , takes the values of $0^\circ, 5^\circ, 10^\circ, 20^\circ$, and 35°	123
4.35	Plot showing the effect on P_{out} when the error, ϵ_2 , takes the values of $0^\circ, -5^\circ, -10^\circ, -20^\circ$, and -35°	123
4.36	Plot showing the effect on θ_{out} when the error, ϵ_3 , takes the values of $0^\circ, 10^\circ, 20^\circ$, and 35°	124
4.37	Plot showing the effect on θ_{out} when the error, ϵ_3 , takes the values of $0^\circ, -10^\circ, -20^\circ$, and -35°	125
4.38	Plot showing the effect on P_{out} when the error, ϵ_3 , takes the values of $0^\circ, 5^\circ, 10^\circ, 20^\circ$, and 35°	126
4.39	Plot showing the effect on P_{out} when the error, ϵ_3 , takes the values of $0^\circ, -5^\circ, -10^\circ, -20^\circ$, and -35°	126
4.40	Plot showing θ_{out} , versus the input polarisation angle, θ_{in} , for different combinations ϵ_1, ϵ_2 and ϵ_3	127
4.41	Plot showing θ_{out} , versus the input polarisation angle, θ_{in} , for different combinations ϵ_1, ϵ_2 and ϵ_3	128
4.42	Plot showing P_{out} , versus the input polarisation angle, θ_{in} , for different combinations ϵ_1, ϵ_2 and ϵ_3	128
4.43	Plot showing P_{out} , versus the input polarisation angle, θ_{in} , for different combinations ϵ_1, ϵ_2 and ϵ_3	129

4.44	Plot showing θ_{out} , versus the input polarisation angle, θ_{in} , for different combinations ϵ_1, ϵ_2 and ϵ_3 , when the the input beam is taken to be centered on 555nm with a pass band of 10nm, for which the profile is Gaussian. . . .	130
4.45	Plot showing θ_{out} , versus the input polarisation angle, θ_{in} , for different combinations ϵ_1, ϵ_2 and ϵ_3 , when the the input beam is taken to be centered on 555nm with a pass band of 10nm, for which the profile is Gaussian. . . .	131
4.46	Plot showing P_{out} , versus the input polarisation angle, θ_{in} , for different combinations ϵ_1, ϵ_2 and ϵ_3 , when the the input beam is taken to be centered on 555nm with a pass band of 10nm and a Gaussian profile.	132
4.47	Plot showing P_{out} , versus the input polarisation angle, θ_{in} , for different combinations ϵ_1, ϵ_2 and ϵ_3 , when the the input beam is taken to be centered on 555nm with a pass band of 10nm and a Gaussian profile.	133

Chapter 1

Introduction

The underlying theme of this thesis is the investigation of very low levels of stellar polarimetric variability. Stars, which have been considered as having very low levels of temporal variability, or which have been suspected as being unpolarised, are being reassessed as new data emerges. Spectroscopy and photometry, point to astrophysical mechanisms which also predict the production of polarisation, albeit very small amounts. This thesis has been divided into chapters, which will tackle different areas of interest with regard to improving our understanding of these sources.

Chapter 2 will be concerned with the results of an observing program carried out at the SAAO observatory in Sutherland, South Africa during May 1996. The purpose of the campaign was to obtain data on a sample of solar type stars in an attempt to investigate their polarimetric variability. Many solar type stars have been grouped among unpolarised star catalogues, or amongst stars with only a small level of polarisation. Rigorous statistical techniques, including Welch tests, F-tests, and testing for skewness and kurtosis of distributions of the normalised linear Stokes parameters, have been used to detect whatever miniscule changes may be present.

Chapter 3 is predominately concerned with the development of a novel device and technique for detecting the polarisation of a source. This is the Twin Liquid Crystal Polarimeter. It was hoped that by the use of electronically controlled liquid crystals, there would be no need for any moving parts within the instrument, which could only serve to

improve accuracy. Previously used techniques, such as that of the rotating half wave plate will be discussed, and compared with this new idea. It was intended to improve upon existing instrumental sensitivities, and thus aid the pursuit of the detection of low levels of polarisation variability.

Chapter 4 investigates the use of the Kolmogorov Test as a statistical technique for detecting temporal variability in the degree of polarisation, p , and the vibration angle, θ . A sample of O stars and the previously considered standard star, ϕ Cas, of type F0, are analysed. Correct procedure is emphasised to prevent wrong conclusions being made. by consideration of the effect of any error present on the determination of the centre of gravity of a sample of observed values.

Finally, Chapter 5 concludes the thesis, summarising the main findings, and points to possible future work, and further application of polarisation as an astrophysical diagnostic.

The aim of the present chapter, is as an introduction to the concepts, techniques and past relevant research. It will begin with a brief insight into polarimetric definitions and mathematical tools, such as Mueller matrices, used for the description of a polarised light beam. A discussion will then follow on the polarimetry of solar type stars, pertinent to the observational work described later in the thesis. Various devices for detecting polarisation will then be introduced and compared, in an attempt to explain the need for a new generation of sensitive instruments to detect polarisation, and variability.

Finally, a brief introduction to statistical techniques will be discussed to investigate the interpretation of polarimetric data.

1.1 Polarimetric Definitions

Electromagnetic waves may be described in terms of the electric field vector components in two orthogonal planes perpendicular to the direction in which the wave propagates. A wave with an electric vector, E , propagating along the z -axis of an x, y, z , right-handed Cartesian coordinate system, may be described in terms of two components,

$$\begin{aligned}
 E_x &= E_{x_0} e^{i(\omega t - kz + \delta_x)} \\
 E_y &= E_{y_0} e^{i(\omega t - kz + \delta_y)}
 \end{aligned}
 \tag{1.1}$$

Where,

E_x and E_y are the values of the electric field vector in the x and y directions at position z , and at time t .

E_{x_0} and E_{y_0} are the amplitudes of the x and y oscillations.

δ_x and δ_y are the phases of the x and y oscillations at $z = 0$.

ω = angular frequency

i = square root of -1

The *Stokes parameters* are the four quantities which denote ‘radiant energy per unit time, per unit frequency interval and per unit (detector or collector) area (and for extended sources : per unit solid angle)’. This representation of polarised light was suggested by Sir George Gabriel Stokes (1852) and revived and introduced into astronomy by Chandrasekhar (1946). The absolute phase of the wave does not enter into the definitions; addition of the Stokes parameter of beams of radiation represents incoherent superposition of these beams. The Stokes parameters, which describe the polarisation of the waves in Eqn. 1.1 are related to the electric vectors by the Stokes parameters I, Q, U and V , which are defined as,

$$\begin{aligned}
 I &= \langle E_{x_0}^2 + E_{y_0}^2 \rangle \\
 Q &= \langle E_{x_0}^2 - E_{y_0}^2 \rangle \\
 U &= \langle 2E_{x_0}E_{y_0} \cos(\delta_y - \delta_x) \rangle \\
 V &= \langle 2E_{x_0}E_{y_0} \sin(\delta_y - \delta_x) \rangle
 \end{aligned}
 \tag{1.2}$$

Where,

I represents the total intensity of the waves.

Q and U are the intensities associated with linear polarisation.

V is the intensity associated with circular polarisation.

Note that $I \geq 0$, but Q, U, V can be positive or negative. The *degree of polarisation*, p' , is defined by,

$$p' = \frac{\sqrt{(Q^2 + U^2 + V^2)}}{I} \quad (1.3)$$

...and the *degree of linear polarisation*, p , which is primarily the concern of this thesis, is,

$$p = \frac{\sqrt{(Q^2 + U^2)}}{I} \quad (1.4)$$

Q and U are determined with respect to some chosen coordinate system. An obvious choice of this for astronomical polarimetry, is that used to define the equatorial system, ie. right ascension (y -axis), declination (x -axis), with the direction of propagation being the z -axis in the right-handed coordinate frame. The direction of vibration, known as the *position angle*, is expressed as an angle from 0 degrees to 180 degrees, increasing from North, through East, to South. This angle, θ defined by Q and U , relates the direction of vibration to the reference frame, and is given by :

$$\tan 2\theta = \frac{U}{Q} \quad (1.5)$$

When comparing polarisation signals, it is logical to deal with the *normalised linear Stoke parameters*,

$$q = \frac{Q}{I} \quad u = \frac{U}{I} \quad (1.6)$$

The *degree of polarisation* may now be written as,

$$p = \sqrt{(q^2 + u^2)} \quad (1.7)$$

...where $p=1$ corresponds to 100% linearly polarised light, and $p=0$ to unpolarised light. The position angle of the polarised light, in terms of θ , may be expressed by :

$$q = p \cos 2\theta \quad u = p \sin 2\theta \quad (1.8)$$

$$\theta = \frac{1}{2} \arctan \left(\frac{u}{q} \right) \quad (1.9)$$

1.2 Mueller Matrices

The four Stokes parameters may be written collectively as a column matrix, generally referred to as the *Stokes vector*. When radiation propagates through a volume of space or a medium, its state of polarisation may be altered. The radiation may be polarised by the medium, and elliptical polarisation, the ratio of circular polarisation to linear polarisation of the radiation, may be converted to some other form of elliptical polarisation. This can be represented by a transformation between the input and output Stokes vector. The transformation may be represented by a 4×4 matrix \mathbf{M} ,

$$\mathbf{M} = \begin{pmatrix} M_{11} & M_{12} & M_{13} & M_{14} \\ M_{21} & M_{22} & M_{23} & M_{24} \\ M_{31} & M_{32} & M_{33} & M_{34} \\ M_{41} & M_{42} & M_{43} & M_{44} \end{pmatrix} \quad (1.10)$$

Such that,

$$\begin{pmatrix} I_{out} \\ Q_{out} \\ U_{out} \\ V_{out} \end{pmatrix} = \begin{pmatrix} M_{11} & M_{12} & M_{13} & M_{14} \\ M_{21} & M_{22} & M_{23} & M_{24} \\ M_{31} & M_{32} & M_{33} & M_{34} \\ M_{41} & M_{42} & M_{43} & M_{44} \end{pmatrix} \times \begin{pmatrix} I_{in} \\ Q_{in} \\ U_{in} \\ V_{in} \end{pmatrix} \quad (1.11)$$

Such matrices are known as *Mueller Matrices*, after H.Mueller (see Mueller (1948)) who calculated their form for a number of optical components. Since Stokes parameters are real quantities, the elements of \mathbf{M} are all real numbers; M_{11} must be positive (I is always positive), and the other elements can be positive or negative. When the radiation travels through several media in succession, the output Stokes vector for one medium ('a') is the input Stokes vector for the next ('b'):

$$S_{b_{out}} = \mathbf{M}_b \cdot S_{b_{in}} \equiv \mathbf{M}_b \cdot S_{a_{out}} = \mathbf{M}_b \cdot \mathbf{M}_a \cdot S_{a_{in}} \equiv \mathbf{M} \cdot S_{a_{in}} \quad (1.12)$$

where,

$$\mathbf{M} = \mathbf{M}_b \cdot \mathbf{M}_a \quad (1.13)$$

\mathbf{M} represents the combined action of the two media 'a' and 'b'. Note that the order of the matrix product is important, i.e. the first medium traversed comes last in the equation. Application of Mueller matrices is used in the design of polarimetric devices, to determine the effects on the light passing through the device, and is applied in chapter 4 in consideration of the development of the Twin Liquid Crystal Polarimeter. To determine the state of polarisation of light leaving an optical device, the input beam must first be *rotated* to the reference frame of the optical component through which the radiation has traversed. The *rotator matrix* ($Rot(\alpha)$) is,

$$Rot(\alpha) = \begin{pmatrix} 1 & 0 & 0 & 0 \\ 0 & \cos 2\alpha & \sin 2\alpha & 0 \\ 0 & -\sin 2\alpha & \cos 2\alpha & 0 \\ 0 & 0 & 0 & 1 \end{pmatrix} \quad (1.14)$$

The effect of the element, characterised by the matrix ($Ret(\Delta)$), is,

$$Ret(\Delta) = \begin{pmatrix} 1 & 0 & 0 & 0 \\ 0 & 1 & 0 & 0 \\ 0 & 0 & \cos \Delta & \sin \Delta \\ 0 & 0 & -\sin \Delta & \cos \Delta \end{pmatrix} \quad (1.15)$$

... where Δ (given by $\Delta_{y'} - \Delta_{x'}$) is the retardance of the element. This is the general *retardation matrix*. The matrix for a perfect polariser is given by :

$$\frac{1}{2} \begin{pmatrix} 1 & 1 & 0 & 0 \\ 1 & 1 & 0 & 0 \\ 0 & 0 & 0 & 0 \\ 0 & 0 & 0 & 0 \end{pmatrix} \quad (1.16)$$

1.3 Astrophysical Mechanisms That Produce Polarisation

The light of most stars, due to spherical symmetry, and their appearance as point sources, was at first believed to be unpolarised. However, astronomers now realise that many types of stars display polarisation, albeit, very low levels in many cases. In fact, wherever there is some asymmetry in an astronomical situation, there is likely to be some residual polarisation. These asymmetries may be magnetic fields, or an asymmetric distribution of scattered radiation. When radiation encounters small particles such as dust within circumstellar envelopes, electron clouds in extended disassociated stellar atmospheres, or dust in the interstellar medium, there is an interaction, resulting in the radiation undergoing a form of scattering. Generally, the scattering is not isotropic, with the amplitudes of the electromagnetic waves being dependent on the angle of emergence with respect to the original direction of incidence. This scattering is also sensitive to polarisation. It is deemed pertinent to briefly describe some of these polarimetric mechanisms, and particularly those relevant to the types of stars discussed within this thesis.

1.3.1 Electron and Thomson Scattering

Unpolarised light or linearly polarised radiation incident on free electrons is, in general, partially polarised after scattering, with the electric vector perpendicular to the scattering plane. The light becomes 100% polarised when the scattering angle is $= 90^\circ$. The cross section for electron scattering, known as the *Thomson cross section* is the same for all wavelengths.

$$\sigma = \frac{8\pi^4}{3m^2c^4} \quad (1.17)$$

Polarisation arising within stellar atmospheres by electron scattering, was calculated by Chandrasekhar (1950), who formulated equations of transfer allowing for anisotropic scattering. He then predicted that the polarisation due to such scattering could be observed from the atmospheres of hot early type stars, when they were partially eclipsed by a companion star. The linear polarisation of Be stars is very likely to be caused by electron scattering, thought to take place in an ionised disk around the star.

1.3.2 Atomic and Molecular Scattering

Scattering may be caused by gaseous atoms and molecules. Two cases must be distinguished: that in which the frequency of the incident light is not at any resonant frequency, and that in which it is near or coincides with a resonant frequency. For the former case the scattering cross section is proportional to $\frac{1}{\lambda^4}$ where λ is the wavelength of the incident radiation. This is known as Rayleigh Scattering. For the case of the scattering medium consisting of isotropic particles, the light scattered at 90° to the scattering plane is 100% polarised. However, when the frequency of the incident light coincides with the energies associated with the energy levels of atoms or molecules, then resonance scattering may occur. For these cases the fourth power law is only approximately satisfied. When a resonant frequency falls within the spectrum of the incident beam, scattering is very strong at those frequencies and at other frequencies is negligible by comparison.

1.3.3 Scattering by Dust Particles

Scattering by dust particles has long been recognised as an important source of linear polarisation in optical astronomy. The simplest case is that for which the scatterers are small spheres. The scattering is dependent upon the refractive index of the medium and the size of the particles. No polarisation is expected with forward scatter of the light. If these 'grains' assume a non-spherical shape and preferred orientations, then stellar light passing through such a region of particles may become polarised. This process is known as *interstellar polarisation* (IP). Serkowski (1973) modelled the grains as being long cylinders aligned in direction, and was able to satisfactorily describe the wavelength dependence of the IP. The mechanisms of grain alignment are not completely understood, but magnetic

fields are believed to be the dominant factor. It has been pointed out by van de Hulst (1957) that such media are birefringent and will thus introduce ellipticity to a linear polarised wave. Ellipticity caused by this mechanism has been discovered in the polarised light from the Crab Nebula, where the sign and wavelength of the circular component of polarisation are a characteristic component.

1.3.4 Magnetic fields

Polarimetry is a direct method of detecting magnetic fields, which in astronomy range from $10 \mu\text{G}$ in interstellar space to approximately 10^7G in white dwarfs (Angel and Landstreet (1992)), and even up to 10^{13}G in pulsars. Solar photospheric fields in magnetically active regions are determined from the Zeeman effect (see Stenflo (1994)). There is active debate regarding the presence of global polarisation of the light from solar type stars, as a direct result of this effect occurring within hot ‘spots’ within the photosphere.

Magnetically induced polarisation, may be produced by synchrotron radiation, where highly relativistic electrons are moving in a magnetic field. This can result in circular polarisation, or linear polarisation in regions of uniform magnetic field. This mechanism is thought to explain linear polarisation of the Crab Nebula. The polarisation effect of a magnetic field on thermal continuum absorption and emission is detectable at radio wavelengths for fields $\geq 10\text{G}$, and in the optical spectrum for fields $\geq 10^6\text{G}$. Kemp (1970) has studied white dwarfs and detected strong fields, by studying the Zeeman effect, and the difference in intensity between left and right handed transitions.

1.4 Polarisation of Solar and Late Type Stars

It is a well known for stars of early and late type to show intrinsic linear polarisation. Reviews may be found in Coyne and McLean (1979). for luminous red variables, Coyne and McLean (1982) on Be stars. and Schwarz (1986) on late type stars. The measurement of this polarisation may provide insights into the geometries of the stellar atmospheres. Such information can be used to model these stars and glean a greater understanding of their dynamics.

Many stars in the middle of the spectral sequence, including solar type stars, have been grouped among unpolarised standard stars, whilst those which do show polarisation, have only a small intrinsic polarisation. However there have been cases of F, G and K type stars showing temporal variations in polarisation over the order of days. Elias and Dorren (1990), and Kemp et al. (1986) discovered variable polarisation over 65 nights in α Boo (Arcturus: K2 IIp) in the blue band with an amplitude of $\approx 0.005\%$, and indicated possible periodicities. They also measured the Ca II H and K emission which showed clear variability, indicating magnetic activity during the period of observations. Piirola (1977) measured a number of F, G and K type stars within 25 parsecs of the Sun, finding that χ Her (F9V) displayed temporal variations in polarisation over 5 nights.

Leroy and LeBorgne (1989) suggested that broad band linear polarisation caused by differential saturation is a useful aid for the study of the transverse field component of active solar regions and for the investigation of stellar magnetism. It is suggested that late-type stars with a large coverage of active regions could yield polarisations of a level reaching 10^{-4} . The first experimental indications of a magnetic polarising effect were presented by Tinbergen and Zwaan (1981), in which results indicated a slight intrinsic polarisation of the order of $1-2 \times 10^{-4}$ in the spectral V band of F to M nearby dwarfs, which could result from magnetic differential saturation. Evidence for magnetic fields in dwarfs, particularly the program stars of the SAAO observations, 59 Vir (HD115383) and 9 Cet (HD1835) (see also Chapter 4), is discussed in Saar et al. (1997). Leroy and LeBorgne (1989) state that 59 Vir has no intrinsic polarisation larger than the uncertainty of the measurements. In their conclusion, they point out that studies of solar active regions show that there is no chance of measuring the polarisation due to magnetic saturation on stars of similar activity to the Sun: even in the most favourable spectral region, the linear polarisation degree will be smaller than $\approx 10^{-6}$. However, the polarisation of Solar-like active regions observed as a whole can reach some units of 10^{-4} . This means that the polarisation due to saturation could be large enough to be detected in late-type dwarfs with very big spots (as already shown by Tinbergen and Zwaan (1981)). The average uncertainty in the data of Leroy and LeBorgne (1989) is 1.4×10^{-4} , and at this sensitivity level, they show no polarisation detection at the 3σ level, and their results reasonably fit the distribution which would result from a sample of stars without intrinsic polarisation (a Rice distribution). They point out that a gain in accuracy upon their data of only

a factor of two might be sufficient to confirm, or to negate, the existence of polarisation effects due to the magnetic fields in late-type dwarfs.

1.4.1 Activity in F to M Type Stars

Evidence is presented below for magnetic activity present in some F and M type stars. This activity is likely to result in some observable polarimetric variability which should be studied to gain greater understanding of these stars. Evidence of activity, is now discussed with physical explanations of trends observed by spectroscopy and photometry. Polarisation of the light from these stars would be a suitable indicator of magnetic activity within or around the star.

F and G type stars have shown activity in the form of proven area coverage of active regions similar to the Sun. Magnetically induced stellar activity is thought to have its roots in the interaction between stellar rotation and turbulence. This interaction is believed to lead to a dynamo generation of magnetic fields in the interior of a star. Magnetic buoyancy waves cause the magnetic field to ultimately rise to the surface, where they manifest themselves directly or indirectly in the many indicators of stellar activity, such as star spots, flares, ultraviolet and X-ray emission (see Schmitt et al. (1995)). Among suitable other diagnostics, are the observation of $D_3(\lambda 5876)$ and $\lambda 10830$ lines arising from the triplet levels in neutral Helium, which appear in absorption in active (plage) regions on the Sun, and by implication in the active regions on Sun-like (F to early K) stars. These features either do not appear, or appear only very weakly, in the solar (or stellar) photosphere, and are therefore ideal diagnostics of magnetic regions outside of cool spots. The appearance of D_3 and $\lambda 10830$ in absorption immediately suggests that these lines can be utilised to infer the fractional area coverage of active regions on stellar surfaces if their intrinsic absorption strengths are known. Andretta and Giampapa (1995) indicate that the plage like regions can be $\sim 20\%$ among active solar-type stars. By example of the Sun, and by inference to that of late-type stars, ‘activity’ is spatially associated with sites of emergent magnetic flux. Again it is pointed out that the magnetic fields themselves are regarded as the surface manifestations of an interior dynamo mechanism, which in a general way involves the interaction between rotation, convection and an extant magnetic

field. Andretta and Giampapa (1995) suggest that the difference between active and quiet stars is in the fractional area coverage, or ‘filling factor’ of magnetic regions, analogous to solar plages on the stellar surface. Zarro (1982) found that, among stars of similar spectral types, the central residual flux of $H\alpha$ absorption increases with the strength of Ca II K emission. This result suggests that the $H\alpha$ core may provide a viable diagnostic of chromospheric activity, as Ca II K emission has proved to be in past studies. Shine and Linsky (1974) studied the correlation between chromospheric activity diagnosed by Ca II K emission strength and atmospheric temperatures, for the case of solar plages. Their simulations demonstrated that a steep temperature gradient above the temperature minimum (relative to quiet solar regions) was required to explain the bright K emission of the magnetic regions. The large temperature gradient, increases the degree of hydrogen ionisation in the atmosphere, and the subsequent rise in the electron density explains a coupling of the $H\alpha$ profile with the chromospheric temperature structure in the line formation region. They conclude that evidence for the existence of magnetic regions, like solar plages, on the cool dwarfs ϵ Eri (spectral type K2V) and ξ Boo(A) (type G8V), has been given by Linsky and Bornmann (1982), whose studies provide further evidence for stellar activity on these type of stars, by demonstrating that the stellar chromospheric and higher temperature emission-line surface fluxes are similar to those of solar plages. Observations of Zarro (1982) give further evidence to suggest the stellar plage theory, as the enhanced $H\alpha$ brightness among the active dwarfs in their sample parallels the contrast of chromospheric plages seen on the solar surface. It should be noted that the $H\alpha$ core brightening in higher density regions than the quiet-Sun chromosphere, is the attribute of magnetic active regions revealed in Ca II K modeling of plages by Shine and Linsky (1974).

Therefore, to conclude, the presence of polarisation from solar type stars, can be a useful indicator of stellar activity manifested in the form of chromospheric plages, spots or ‘holes’, resulting from interactions of the stars’ magnetic fields. Such activity has previously been looked for using methods such as observing the $D_3(\lambda 5876)$ and $\lambda 10830$ lines arising from the triplet levels in neutral Helium, Ca II K emission, $H\alpha$ core brightening. Polarimetry can be a useful tool to compliment UV and X-ray observations, and should be employed to determine the intrinsic properties of these stars.

1.5 General Polarimetric Modulators

Throughout the history of polarimetry, there has been continual developments in the techniques used to produce modulation of the light beam passing through a polarimeter, needed to determine the polarisation of the radiation from a source. The aim of any technique is to measure the *degree of polarisation* (or the *normalised Stokes parameters* Q/I , U/I , V/I) to the limit of the photon noise. Modulation is a way of rapidly making a differential measurement, and is useful whenever the required information is represented by a small quantity superposed on a large, irrelevant background signal. The modulation may be continuous, in which case the ratio is taken of the amplitude of the variable part of the signal, relative to the mean level. Alternatively, the signal may be measured with the optical components of the instrument at certain set orientations. It is possible to obtain signals representing $\frac{Q}{I}$, $\frac{U}{I}$, $\frac{V}{I}$ or some combination of these, depending on the adjustment of the instrument. Rapid modulation will overcome the problems associated with atmospheric noise.

The most commonly used method, is the rotating half wave plate, whereby, an analysing polaroid is placed after a continuously rotating half wave plate, the light beam then entering a detector, or spectrometer followed by detector. An alternative to continuous rotation of the wave-plate, is to measure the signal with the plate at set angles to the axis of the system, such that the Stokes' parameters Q and U may be obtained. The disadvantage of either system is the mechanical rotation of the wave-plate, which due to non-exact alignment perpendicular to the light beam, or flexing and vibrations within the plate, can result in 'image wobble' upon the slit of the spectrometer, thus introducing a spurious signal. It would therefore be of great advantage for polarimetry to develop a device which needs no mechanical movement. This leads to the search for an instrument which may switch retardation electronically, such that the internal properties of the plate change, enabling the selection of certain phases, without any physical movement.

Accurate polarimetry is best achieved through some method of modulation of the light beam, without the need for any mechanical movement of the optical elements. If it were possible to completely modulate the signal electronically, then the level of noise present could be reduced, and if the modulation could be made rapid enough, then the

spurious noise caused by atmospheric scintillation could be removed (if the modulation frequency can be made much larger than the seeing frequencies).

Among the most promising candidates for a suitable modulation device, are the *twisted-nematic liquid crystal* (NASA Conf.Publ.2374,1985), and the Piezoelectric modulator (PEM). However, it must be noted that the PEM is far from ideal. Whilst one Stokes' parameter may be obtained, without the need for any mechanical movement of optical components, ultimately there must be some movement to enable the determination of the other Stokes' parameter.

The Piezoelectric modulator is based on resonant excitation of longitudinal oscillations in a slab of optical material (eg. quartz) with a piezotransducer, leading to a strain induced modulated birefringence. The PEM then functions as a variable retarder. Using a linear polariser behind the PEM, one obtains a simple, compact and stable intensity modulator with a large angular aperture. The PEM has many positive advantages, but ultimately it's few disadvantages are its downfall. These will now be discussed.

A PEM is one of the most simple and stable modulators. They have been routinely used with great success for high precision polarimetry with one channel detector systems (accuracy of $10^{-4} - 10^{-5}$). In these cases the demodulation is done using a standard lock-in amplifier. This method however is not practical when using multichannel array detectors such as charge-coupled devices (CCDs), which have a slow frame rate (in comparison to the PEM frequency), and which generate significant noise each time the detector is read. It is also clearly not practical to mass produce lock-in amplifiers to connect one to each photometric channel (pixel). An alternative to demodulation is to use a gating technique to read out the array at each gating interval. The maximum possible readout rate for a CCD is of the order of 5 MHz. This poses limitations on the array size for a given gating frequency. If for example the readout is done every millisecond, the number of pixels used in the array cannot much exceed ~ 1000 : i.e, one would be limited to the use of arrays of a size of $\sim 32 \times 32$ or smaller (see Stenflo and Povel (1985)). Therefore the use of large detector arrays thus requires slow gating or small modulation frequencies. Also, if the integration time is short, then the large readout noise could result in the small polarisation signal being completely drowned.

It is possible to produce a slow modulation by using the beat frequencies of two or more modulators, Stenflo and Povel (1985). However, if one wants to record all four of the Stokes parameters simultaneously, the modulation efficiency is then greatly reduced. In the optimum of schemes, this reduction is as large as a factor ~ 5 .

Use of an optical demodulator in front of the detector array, is a method of eliminating these problems. The principal element of the demodulation is a piezoelastic modulator that is locked in phase frequency and phase to the respective modulation frequency. In such a system the limitations on array size and readout frequency disappear (see Stenflo and Povel (1985)). A 50-100 kHz modulation can now be obtained with slow readout (e.g., once per second), where the readout rate is determined by the requirement that charge is built up to a significant fraction of the saturation level. Advantages of this scheme are that it also alleviates the problem of readout noise, and one does not have to consider using beat frequencies, which means that the modulation efficiency can be maintained high for all Stokes parameters.

A drawback of the above system is that it contains a relatively large number of optical surfaces, which may reduce the transmission substantially. It may be possible to use anti-reflection coatings to reduce these losses, but care must be taken about the possible stress and thereby birefringence induced by such coating.

Povel and Stenflo (1990), showed how the demodulation of a rapidly modulated light beam can be achieved within a single charge-coupled device. If demodulation is done by the CCD itself, optical components such as the demodulator mentioned in Stenflo and Povel (1985), are no longer needed, since their functions are performed electronically within the CCD itself, by creating two image planes corresponding to the two orthogonal polarisation states. The two polarisation states are represented by the two half-periods of the polarisation modulation. Whilst one of the image planes is being exposed the other plane is stored in an unexposed storage region of the CCD. During the next half of the modulation cycle the two image planes trade places, i.e. they have shifted between the exposed and unexposed areas in synchrony with the PEM modulation. This process continues until the accumulated charge nearly saturates the CCD. An advantage of this system is that the electronic shifting is done much faster than the atmospheric seeing, and

therefore seeing cannot create any spurious polarisation. Also, the problem of pixel-to-pixel sensitivity is evaded, as the two polarisation mode images use the same pixels.

Recently promoted on the market, is the Meadowlark liquid crystal variable retarder. This device has an electrically adjustable retardance, and can replace a large range of fixed retarders in precision optical systems. The retardation control makes possible the conversion of polarisation state between any states of elliptical polarisation, including the special cases of linear and circular polarisation. The actual face of the cell has a large acceptance angle with a quoted variation of retardance (see Optics (1996)) over the aperture of 3% or less. Transmission is in excess of 92 % and hence is advantageous over other more cumbersome polarimetric modulators employing the use of a number of optical components. Thus, it was decided to explore this device's potential as a means of constructing a modulator suitable for undertaking stellar polarimetry. Due to the range of retardance that the basic liquid crystal may provide, it is still necessary, for some mechanical rotation to enable both linear Stokes' parameters to be obtained. However, by the use of two cells used in conjunction it has been possible to dismiss this problem, and develop a no moving parts polarimeter. The development of this Twin Liquid Crystal Polarimeter will be discussed in detail in Chapter 4.

The next section of this thesis will be concerned with the analysis of a group of stars, consisting of a number of solar types, which were observed during 1996 at the SAAO observatory, South Africa.

Chapter 2

UCT Polarimeter Observations

2.1 Introduction

The optical radiation from young stars at both ends of the spectral classification sequence frequently exhibits intrinsic linear polarization (Menard and Bastien (1992), Jain and Bhatt (1995) – and references therein). It is now well established that at least 85% (or even as many as 100%) of such stars exhibit temporal polarimetric variability on a wide range of time scales (Menard and Bastien (1992), Yudin and Evans (1998)). These include Herbig Ae/Be stars (HAEBE spectral class from B to early F) and T Tauri type stars, ranging between later F stars to early M. There is, however, little or no information on the polarimetric properties for intermediate spectral type stars ranging between late F and early G8, the so-called solar-type stars. In catalogues of young stars (Herbig and Bell (1988) and Thé et al. (1994)) this latter category represents about 15% of the total objects and most of them have not been studied polarimetrically.

Recently it has been shown that the polarimetric properties of young stars might be considered from the point of view of their circumstellar evolution (Tamura and Sato (1989) and Yudin (1994)). As suggested by Yudin (1994), at least one subgroup of HAEBE stars, namely those with algol-like brightness minima (Grinin (1988)), represents a late stage of circumstellar evolution with fragmented circumstellar disks forming protoplanetary condensations. Such asymmetries would affect the scattering with an associated polarization

being generated in the observed light. At present this subgroup contains about 10 objects which have spectral classes mainly A.

As a result of magnetic activity, young solar-type stars exhibit chromospheric disturbances which can be monitored by K-index photometry. The renowned observational program at Mt Wilson (see Vaughan et al., 1981) is a prime source of information for solar-type stars on rotation periods, typically a few days, and on magnetic cycles with periods of years. Radiation emanating from active regions is likely to be partially polarized for a variety of reasons, one such polarigenic mechanism being the integration of Zeeman split lines with differential saturation (see Leroy and LeBorgne (1989)). The expected wavelength dependence of the degree of any polarization, $p(\lambda)$, generated by this mechanism has been explored by Leroy and LeBorgne (1989). Predictions of the magnitude of p to be observed globally from stars are generally not sanguine for the promotion of extensive polarimetric studies and there has been controversy about some of the reported observations – see discussions in Clarke and Fullerton (1996). Fox (1995) has modelled the behaviour of star spots using Rayleigh scattering as the polarigenic mechanism and suggests that their presence might be detected with polarimetric accuracies $\sim \sigma_p = 0.005\%$, a challenging but not impossible task. On the positive and observational side, Tinbergen and Zwaan (1981) have used statistical arguments to suggest that polarimetric phenomena, at low levels, are fairly common in middle spectral type stars and with reports of polarimetric variability of individual objects (see e.g. Piirola (1977) [χ Her – F9V] and Kemp et al. (1986) [α Boö – K1.5 III]), there is evidence for promoting polarimetric studies of solar-type stars, albeit with the requirement of extremely high precision.

Recently, an attempt to record rotationally induced polarimetric variability has been undertaken by Gullbring and Gahm (1996) but with null results, an outcome which may have been influenced by the short run of observations and/or measurement uncertainties which were too large. Clarke and Fullerton (1996) report on novel measurements of the global radiation from the Sun near to the solar maximum and have recorded changes in p just larger than 0.0001 at the time of the appearance of large spots traversing the disk, promoting the possibilities of making solar-stellar connections by polarimetry.

A further dimension to polarimetry of stars in the middle part of the spectral sequence is offered by the measurements of circular polarization resulting from the presence of

magnetic field structures. Kemp et al. (1987), for example, have recorded variations of the circular polarization of the RV CVn star λ And and Elias and Dorren (1990) have recorded both linear and circular polarization variations in the young solar-type star HD 129333, thought to have spots covering 6% of its surface, these being responsible for low amplitude light variations. It is important to note that, according to Bastien et al. (1989), circular polarization has been detected in most of the investigated young T Tauri stars, whereas for young HAEBE stars, circular polarization was detected for only a few objects (Yudin and Evans (1998) – and references therein).

With the above ideas in mind, a polarimetric investigation of some southern hemisphere objects has been undertaken with the aim of detecting variability in solar-type stars and the results are reported below.

2.2 The Measurements

Seven nights were allocated for May 1996 on the 0.75m SAAO telescope at Sutherland using the University of Cape Town Polarimeter. This instrument, designed by Cropper (1985), operates with a single channel and filter set to provide UBVR_I measurements. The modulator comprises oppositely rotating quarter-wave and half-wave (achromatic) phase plates at 10 revs s^{-1} , the oscillatory signal providing means of determining both the linear and circular components simultaneously, the system being ideal for polarimetry of solar-type stars. This optical module is placed between the offset guider and filter box. The module is located above any apertures or filters which could otherwise introduce spurious polarisations. Because of the single channel configuration of the photometer, a Glan-Thompson analyser is employed, in preference to a Wollaston or Foster prism. This arrangement unfortunately wastes half of the light. The five-position filter slide holds two pieces of linear polaroid at different orientations, a piece of polaroid followed by a plastic quarter-wave plate to give circular polarised light, and a depolariser. The fifth position is empty for observations. The slide provides rough calibration sources. However, time was given, on the limited observing run, attempting to determine the amount to which the instrument is responsible for converting circular to linear polarisation, or vice versa. Unfortunately no reference is made in Cropper 1985, to the extent of this effect, if

any. Pulse counting is employed with the recorded photons being binned into computer memory according to the phase of the modulator. Polarimetric accuracies limited only by photon counting statistics can be achieved under good working conditions. For the purpose of making data comparisons, the normalised linear Stokes components q and u were calculated with the degree of linear polarization, $p = (q^2 + u^2)^{1/2}$, together with the normalised circular Stokes parameter, v .

The emphasis of the study was towards high accuracy, and early experience indicated that the best results accrued by concentrating the observational effort on measurements in the B and V bands. With these passbands, the photon count rates were sufficient to achieve $\Delta p \sim \pm 0.0001$ in about 20mins. For the brighter stars, a 2.5D neutral density filter was introduced into the beam after the polarizer to keep the count rate to acceptable levels so that dead-time errors were unimportant (see Clarke and Naghizadeh-Khouei (1994)). To establish a data set, repeated records for the degrees of linear and circular polarization and brightness levels (photon counts and magnitudes) were obtained using a preset integration time typically several tens of seconds. Telescope tracking reliability was checked from the quality of the polarimetric modulated signal and at interruptions of the sequence for visual inspections. From the collection of records contributing to a mean measurement, it was later possible to undertake internal statistical analyses of the behaviour of the data sets. Following the observing run, the data were cleaned with integrations removed which were obviously distorted by cloud or inadequate telescope tracking. The measurements were also honed to remove the effects of the sky background although they proved to be inconsequential at the achieved polarimetric accuracy.

It was hoped to relate any polarimetric variations of a star to magnitude changes but, without the full procedure involving observations of photometric standard stars, this was not possible. At no time were the conditions “photometric” and on some nights the effects of buoyancy waves on the atmospheric extinction were clearly seen.

The list of observed stars is given in Table 2.1. The main program stars were selected by having spectral classification around G5V, for their comparative youth, by having known estimates of their rotation period, by having some known variable characteristic and by having sufficient brightness to allow high accuracy polarimetry in short integration times. In addition to the program stars, observations were made of two listed unpolarized

Table 2.1: The observed program stars including unpolarized and polarized standards.

Star Identification	Other Name	Mag	Spectral Type	Notes
SAO 154972	TU Pyx	8.7	G0	
SAO 251015		8.1	G0	
HD 100623		6.0	K0V	Unpol Std.
HD 115383	59 Vir	5.23	F8V	3. ^d 3 P
HD 128400		6.7	G5V	
HD 147084	<i>o</i> Sco	4.6	A5II-III	Pol Std.
HD 155555	V824 Ara	6.67-6.84	G5	Sp 1. ^d 682
HD 160529		6.7	A2Ia	Pol Std.
HD 202940		6.6	G5V	Unpol Std.
HD 1835	9 Cet	6.44	dG2	8 ^d P

standard stars (HD 100623 and HD 202940 – in Appendix 1 and 2 respectively of Serkowski, 1974) to allow investigation of the instrumental polarization and two recognised polarized stars (HD 147084 and HD 160529 – in Appendix 3 of Serkowski (1974)) to check out the modulator efficiency and the orientation of the polarimeter's reference axes relative to equatorial co-ordinates.

2.3 Statistical analyses

At the stage of reducing the data and also assessing if any star is exhibiting temporal variability or if there are polarimetric differences between sets of stars, various statistical tests were performed.

The first procedure involved checking that the various normalised Stokes parameters, q , u and v , generated by repeated integrations, could be considered as coming from the same respective parent Normal distributions. This exercise was useful to check for any spurious records and to search for any drifts in the underlying mean values during the data accumulation caused either by effects in the instrument or in the stellar radiation itself. Normality checks were performed by determining the skewness and kurtosis coefficients and comparing the resulting values with those in tables presented by Brooks et al. (1994).

In order to test if there were polarimetric differences between mean values of q , u and v , the Welch statistic (see Brown and Forsythe (1974)) was applied to the data assemblies providing the individual means. The test was performed covering groups of data sets from different stars, particularly those which might be considered as being unpolarized sources, and on groups of data sets from individual stars to see if there were any temporal changes between their accumulation. Features of the Welch test are that it can be applied to several data sets simultaneously and that the number of values constituting any of the data sets can be small. The only prerequisite is that each of the compared data sets should be indistinguishable from having a Normal distribution, such tests being performed as a matter of course as outlined above.

2.3.1 Testing for Temporal Variability of Polarisation Using the Welch Test

Temporal changes in the normalised Stokes' parameters may not be immediately apparent by observation, and so a test is needed to determine significant changes in polarisation. Brown and Forsythe (1974) concluded that in terms of the size and power (power being the probability of rejecting the hypothesis of equality of means when it is indeed false), the Welch test is the recommended statistical test.

For a set of g data points for q (or u), with unequal sample sizes $n_1 \neq n_2 \neq \dots \neq n_g$ and standard mean errors $\hat{\sigma}_1^2 \neq \hat{\sigma}_2^2 \neq \dots \neq \hat{\sigma}_g^2$, the Welch statistic, \mathbf{W} , is calculated from

$$\mathbf{W} = \frac{\sum W_i (q_i - \tilde{q})^2 / (g - 1)}{[1 + \frac{2(g-2)}{(g^2-1)} \sum (1 - W_i/u)^2 / (n_i - 1)]} \quad (2.1)$$

where

$$W_i = \frac{1}{\hat{\sigma}_i^2}$$

$$u = \sum W_i$$

$$\tilde{q} = \sum W_i q_i / u$$

with the summations over $i = 1, 2, \dots, g$.

When all the population means are equal (the standard mean errors being equal or unequal), \mathbf{W} is approximately distributed as an F statistic with $(g - 1)$ and f degrees of freedom, where f is defined by :

$$\frac{1}{f} = \left[\frac{3}{(g^2 - 1)} \right] \frac{\sum (1 - \frac{W_i}{u})^2}{(n_i - 1)} \quad (2.2)$$

2.3.2 Unpolarised Standard Stars

An accurate interpretation of polarimetric results is not complete without a full knowledge of the way in which the observational instrument might affect the data obtained. An instrumental polarisation may be introduced when the optical elements of a reflecting telescope, or any polarimetric instrument, do not have the same transmission/reflection efficiency for the orthogonal directions of vibration of the incident light. It is therefore required that unpolarised standard stars are observed to measure the instrumental polarisation of the telescope. It is also possible that this instrumental contribution is not stable over time. This, for example, could be due to an ambient temperature change. The unpolarised standards measured were :

HD 202940

HD 100623

The unpolarised standard HD202940 was observed on the nights of 21, 22, 25, 26 May 1996 (JD[245 +] 0225, 0226, 0229, 0230) using UBVRI filters. Tables A.1 and A.2 show the raw data, uncorrected for instrumental polarisation, and without any rotation to the instrumental frame. The unpolarised standard HD 100623 was observed on the night of 25 May 1996 in the V and R bands. Table A.3 displays the raw data (uncorrected for instrumental polarisation and without any rotation to the instrumental frame). All the data are displayed in Figures 2.1, 2.2 and 2.3 for HD 202940, and Figures 2.4 and 2.5 for HD 100623.

Only one single observation was taken in the U and I bands on the night of 25 May, and unfortunately this has led to a relatively large error in these bands.

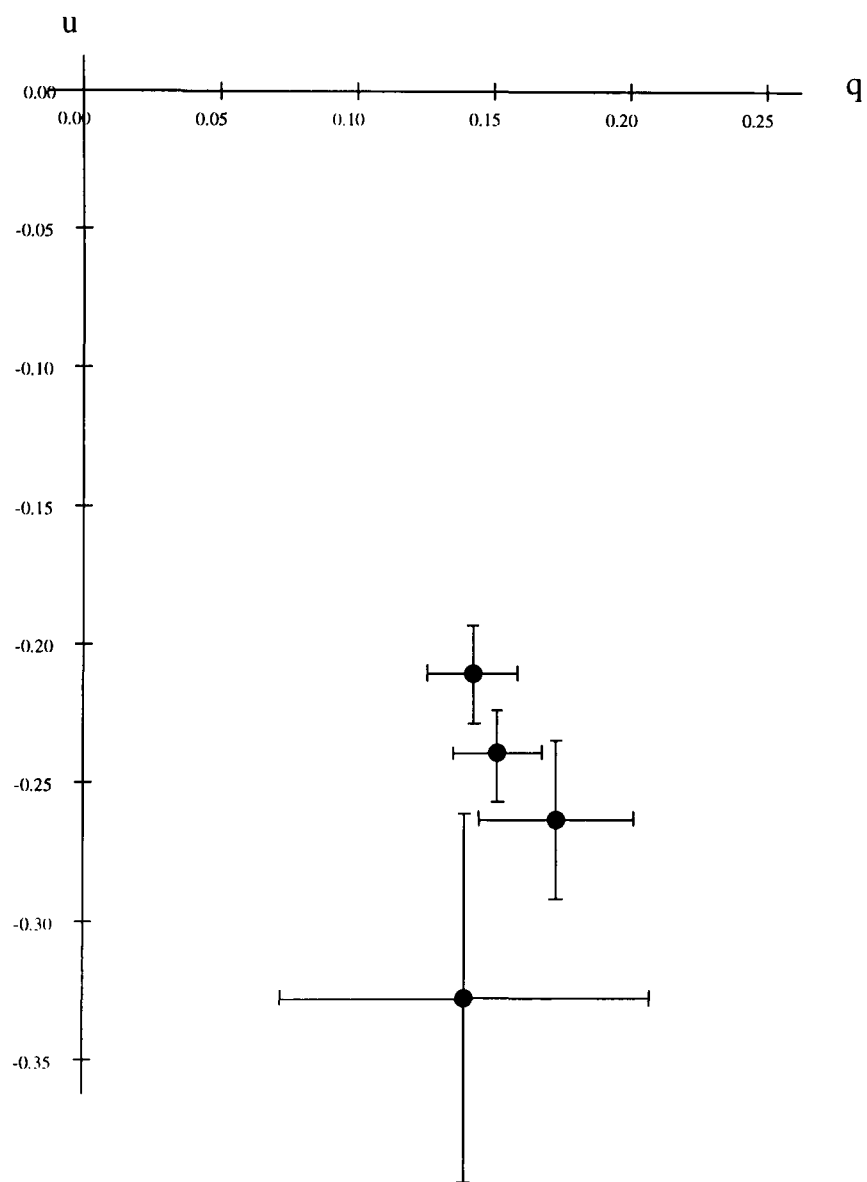


Figure 2.1: The Stokes parameter plot (q, u in %) displays the four B band polarisation measurements of HD 202940 made on the nights of JD 0225, 0226, 0229, 0230. Each point is the weighted mean of all measurements taken on those nights. The star is an unpolarised standard, but the data clearly reveal an instrumental polarisation of $\sim 0.3\%$.

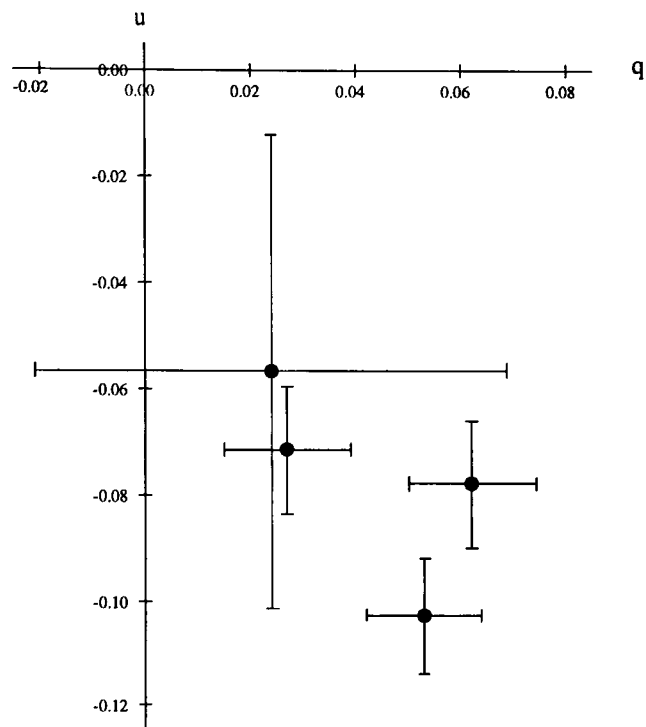


Figure 2.2: The Stokes parameter plot (q, u in %) displays the four V band polarisation measurements of HD 202940 made on the nights of JD 0225, 0226, 0229, 0230. Each point is the weighted mean of all measurements taken on those nights.

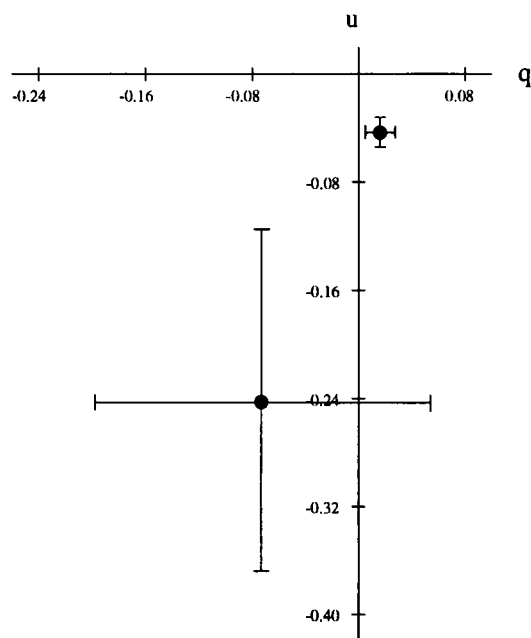


Figure 2.3: The Stokes parameter plot (q, u in %) displays the two R band polarisation measurements of HD 202940 made on the nights of JD 0225, 0230. Each point is the weighted mean of all measurements taken on those nights.

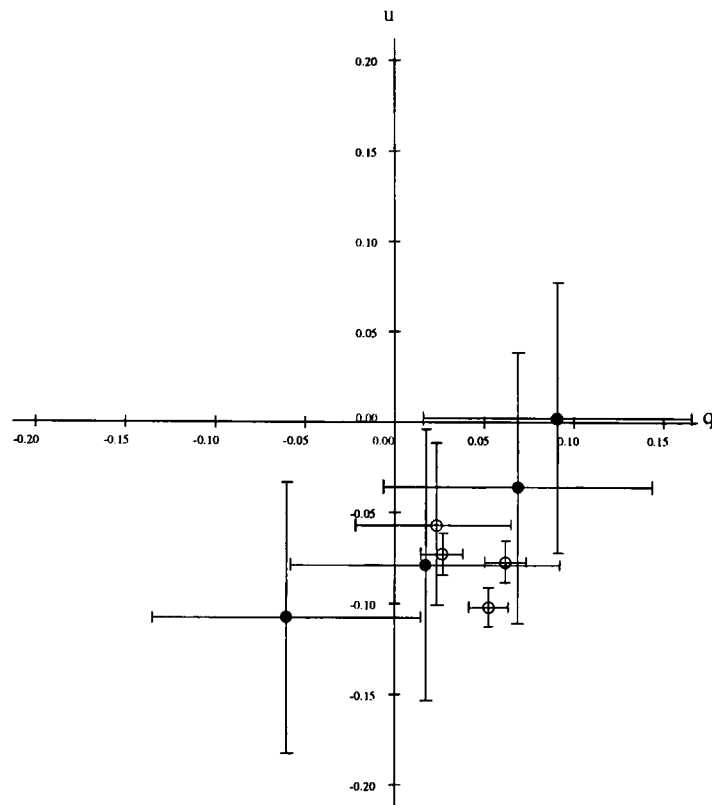


Figure 2.4: The Stokes parameter plot (q, u in %) displays the four V band (●) polarisation measurements of HD 100623 made on the night of JD 0229; 25 May 1996. Comparison is made with the higher quality data for HD 202940 (⊕)

Figure 2.4 is the Stokes parameter plot (q, u in %) for HD 100623 of the normalised linear Stokes parameters, expressed in terms of percentage polarisation, in the V band. It is compared with HD 202940, to indicate the relative poor quality of the data for HD 100623. This was due to the lower integration time, and fewer integrations for this star.

Figure 2.5 is a similar plot in the R band, displaying the data for HD 100623 with that of HD 202940.

From the kinds of stars selected for the program, it was anticipated that any measured polarizations, other than the polarized standard stars, would be fairly small. One of the basic questions to be asked of each star is whether the measurements are consistent with the radiation being unpolarized by comparison with data from the unpolarized standard stars, assuming the latter to be designated correctly.

Early in the observing run it was apparent that the system displayed a high level

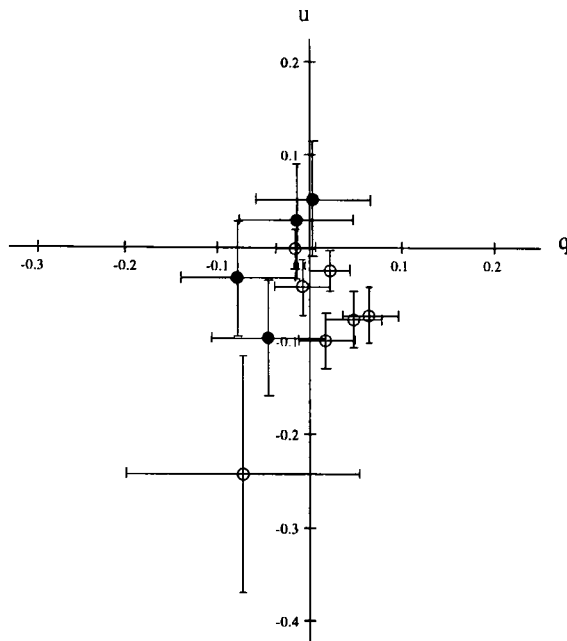


Figure 2.5: The Stokes parameter plot displays the four R band polarisation measurements (●) of HD 100623 made on the night of JD 0229;25 May 1996. Also plotted are the individual observations for HD 202940 (□)

of instrumental polarization and that its value was strongly wavelength dependent. This has no consequence on deciding whether there are differences in the low levels of polarization between compared stars but imposes restrictions on its absolute description (amount and position angle). Such a problem cannot be resolved without spending an inordinate amount of observing time calibrating this off-set with many more “unpolarized” stars being measured to provide a larger statistical base. This was not pursued.

Table 2.2 lists the basic polarimetric determinations for the two observed catalogued unpolarized stars. The mean values q_o , u_o and v_o are the normalised Stokes parameters as calculated directly by the reduction process with their 1σ uncertainty obtained from the fitting of the coefficients of the harmonics describing the polarimetric modulation and from the combination of repeated measurements used to determine the quoted means. The data for each star suggest that the underlying distribution of measurements in the q, u plane have circular symmetry and that the variances of the individual Stokes parameters are equal to each other. Each listed 1σ value has been taken from the mean of the sample variances obtained for the q and u parameters individually.

Table 2.2: The measurements of the unpolarized standard stars according to the mean Julian Date (245 +) and the filter passband. The headings q_o , u_o , and v_o correspond to the raw normalised Stokes parameters in the instrumental frame, with the standard error (1σ) attached. The number of integrations is designated by N , each with integration time of T seconds.

HD 100623							
JD	Band	q_o	u_o	σ	v_o	T	N
0229.239	R	-0.00033	-0.00014	± 0.00031	$+0.00025 \pm 0.00022$	120	4
0229.216	V	+0.00029	-0.00056	± 0.00037	-0.00058 ± 0.00026	120	4
HD 202940							
JD	Band	q_o	u_o	σ	v_o	T	N
0225.606	U	+0.00594	-0.00387	± 0.00177	-0.00200 ± 0.00125	120	1
0225.608	B	+0.00142	-0.00328	± 0.00068	-0.00024 ± 0.00048	120	1
0225.585	V	+0.00024	-0.00057	± 0.00045	-0.00071 ± 0.00032	120	1
0225.616	R	-0.00074	-0.00242	± 0.00127	-0.00175 ± 0.00090	120	1
0225.623	I	-0.00171	-0.00098	± 0.00146	-0.00001 ± 0.00103	120	1
0226.653	B	+0.00173	-0.00263	± 0.00029	-0.00047 ± 0.00020	750	1
0226.621	V	+0.00027	-0.00072	± 0.00012	-0.00010 ± 0.00009	750	2
0229.556	B	+0.00152	-0.00240	± 0.00017	$+0.00004 \pm 0.00012$	180	10
0229.565	V	+0.00053	-0.00103	± 0.00011	-0.00023 ± 0.00008	180	10
0230.542	B	+0.00143	-0.00211	± 0.00018	$+0.00015 \pm 0.00013$	180	10
0230.544	V	+0.00062	-0.00078	± 0.00012	-0.00018 ± 0.00008	180	10
0230.603	R	+0.00016	-0.00044	± 0.00011	-0.00010 ± 0.00008	180	6

A statistical comparison (Welch tests) of the measurements showed that, for a given passband, no distinction could be made between the mean values of the stars or between measurements made on different nights. To act as the unpolarised reference for all other measurements, the data sets and mean values of HD 2902940 were taken as their quality was far superior to those of HD 100623. Thus the assumed instrumental linear polarization was

$$U: q = +0.00594, u = -0.00387: \equiv p = 0.00709 \pm 0.00177$$

$$B: q = +0.00151, u = -0.00235: \equiv p = 0.00279 \pm 0.00011$$

$$V: q = +0.00047, u = -0.00085: \equiv p = 0.00097 \pm 0.00007$$

$$R: q = +0.00015, u = -0.00046: \equiv p = 0.00048 \pm 0.00011$$

$$I: q = -0.00171, u = -0.00098: \equiv p = 0.00197 \pm 0.00146 .$$

It may be noted that the values for the U and I bands are from single measurements carrying low accuracy and are only listed for reference in respect of the general spectral trend of the instrumental polarization, clearly seen over the B, V and R bands, being in the same quadrant in the Stokes parameter plane and exhibiting a progressive reduction.

The weighted mean values for the circular polarization were

$$\text{B: } v = -0.00001 \pm 0.00007$$

$$\text{V: } v = -0.00019 \pm 0.00004$$

$$\text{R: } v = -0.00007 \pm 0.00007 \quad .$$

These data suggest that for the V band, circular polarization has nominally been detected, this probably originating within the telescope, although it cannot be ruled out as being present in the stellar radiation. This is the first time HD 202940 has been measured for circular polarization. In fact it is always difficult to obtain firm offset calibrations for v as a catalogue of reliable standards is not available. For the B and R bands the measurements provide null values with uncertainties of $\pm 0.007\%$.

2.3.3 Polarised Standard Stars

All data from the SAAO 0.75m telescope are obtained in the instrumental frame. It is usual practice to discuss any results in the equatorial frame, where the q axis is parallel to the North-South axis. To achieve this, the standard stars HD 147084 and HD 160529 were observed. The data are depicted in Figure 2.6 and Figure 2.7.

Table 2.3 summarises the measurements made of the two polarized standard stars HD 147084 (*o*Sco) and HD 160529. Following the subtraction of the proposed instrumental values, the reduced values for q and u are consistent with the polarimeter's axes being set at angle of 1.45° for the B band and 0.4° for V, the difference being caused by the dispersion in the principal axis of the achromatic modulator.

The values of the degree of polarization as calculated in the instrumental and corrected frames may also serve as a check on the suggested instrumental values by comparison

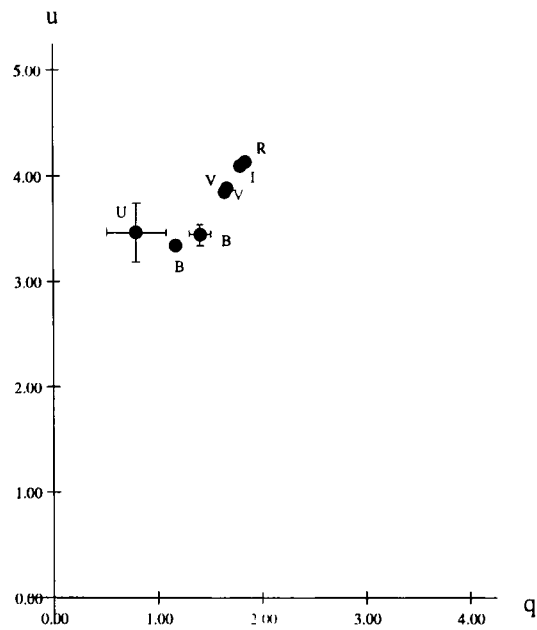


Figure 2.6: The Stokes parameter plot (q, u in %) for HD 147084 showing the weighted mean data points for the U,B,V,R,I bands, in percentage polarisation.

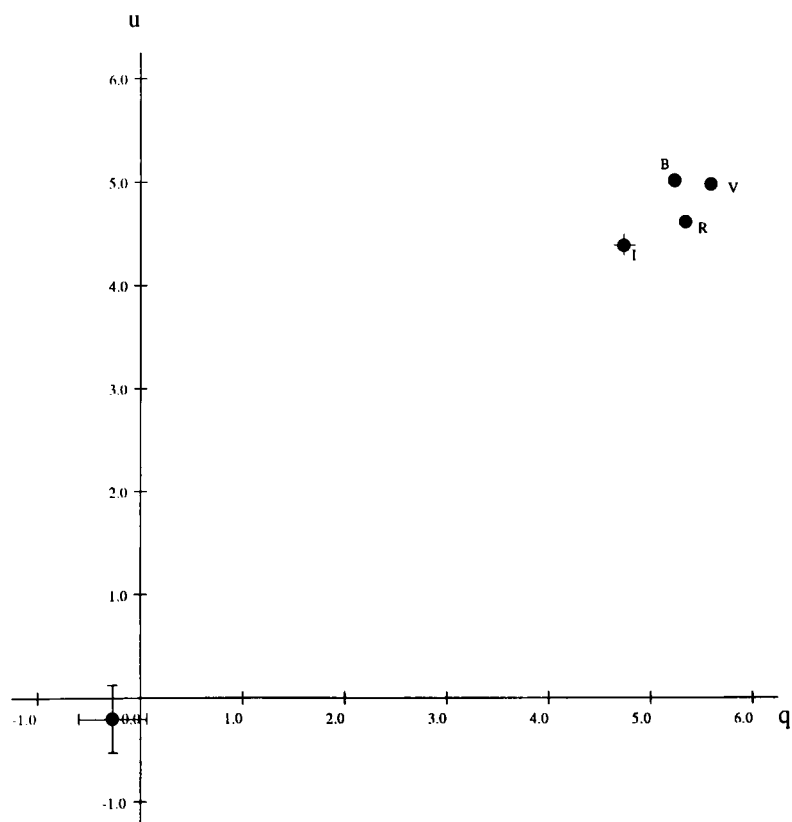


Figure 2.7: The Stokes parameter plot (q, u in %) for HD 160529 showing the weighted mean data points for bands U,B,V,R,I in percentage polarisation.

Table 2.3: The measurements of the polarized standard stars according to the mean Julian Date (245 +) and the filter passband. The headings q_o , u_o , and v_o correspond to the instrumental normalised Stokes parameters with their standard errors (1σ) attached. The number of integrations is designated by N , each with integration time of T seconds. Columns identified by q and u contain the values of the normalised Stokes parameters corrected for instrumental polarization but in the instrumental frame; the uncertainties of these values are taken as being the same as the basic measurements without the inclusion of the estimate of any systematic effect from the subtraction of the instrumental polarization.

HD 147084									
JD	Band	q_o	u_o	σ	v_o	T	N	q	u
0225.421	U	+0.01390	+0.03093	± 0.00284	-0.00129 ± 0.00202	120	1	+0.00796*	+0.03480*
0225.423	B	+0.01576	+0.03217	± 0.00099	-0.00159 ± 0.00070	120	1	+0.01425	-0.03452
0225.427	V	+0.01684	+0.03786	± 0.00056	$+0.00038 \pm 0.00039$	120	1	+0.01637	-0.03871
0225.432	R	+0.01860	+0.04095	± 0.00043	$+0.00024 \pm 0.00030$	120	1	+0.01845	-0.04141
0225.440	I	+0.02108	+0.04183	± 0.00041	-0.00001 ± 0.00029	120	1	+0.02279	-0.04281
0228.455	B	+0.01330	+0.03113	± 0.00046	$+0.00053 \pm 0.00032$	160	1	+0.01179	-0.03348
0228.462	V	+0.01724	+0.03805	± 0.00027	-0.00033 ± 0.00019	160	1	+0.01677	-0.03890
0228.474	R	+0.01773	+0.04067	± 0.00021	-0.00033 ± 0.00015	160	1	+0.01758	-0.04113
HD 160529									
JD	Band	q_o	u_o	σ	v_o	T	N	q	u
0225.673	V	+0.05825	+0.04791	± 0.00044	-0.00058 ± 0.00031	120	1	+0.05778	-0.04876
0225.678	R	+0.05382	+0.04578	± 0.00036	-0.00011 ± 0.00026	120	1	+0.05367	-0.04876
0225.680	I	+0.04522	+0.04268	± 0.00102	-0.00002 ± 0.00073	120	1	+0.04693	-0.04366
0229.525	B	+0.05386	+0.04767	± 0.00031	-0.00043 ± 0.00022	180	5	+0.05235	-0.05002
0229.547	V	+0.05633	+0.04908	± 0.00015	-0.00030 ± 0.00011	180	5	+0.05586	-0.04990

* Poorly determined instrumental polarization offset in the U band

Table 2.4: The determined raw (p_o) and corrected (p) values of the degree of linear polarization for comparison with the standard values (p_{HB}) of Hsu and Breger (1982).

<i>o</i> Sco			
	p_o	p	p_{HB}
B	3.42 ± 0.04	3.58	3.50
V	4.17 ± 0.02	4.23	4.18
HD 160529			
	p_o	p	p_{HB}
B	7.19 ± 0.03	7.24	6.97
V	7.26 ± 0.03	7.52	7.31

with measurements listed in the literature serving as “standards”.

Table 2.4 provides the degree of polarization based on the mean values of q and u for the B and V bands with respect to the instrumental (p_o) and corrected frames (p) together with measurements (p_{HB}) taken from Hsu and Breger (1982). For *o* Sco, the correction procedure has converted the raw values from being marginally less than the standard values to being marginally greater. For HD 160529 the raw value for B is already greater than the standard value and the correction increases the disparity; for the V band the outcome is similar to that for *o* Sco. Unfortunately there is no record of pass band for these filters, and as such, any comparison between the quoted values for the standards, must be treated with caution.

Thus for the V band it might be construed that the instrumental polarization has been marginally overestimated while for the B band the picture is inconclusive. Based on this very limited data, it was decided not to reconsider any reworking of the reductions for the program stars with alternative values for the instrumental polarization, but to bear it in mind their reported values may carry small systematic errors, adding complications to discussions on whether individual stars do or do not display low levels of polarization.

For *o* Sco, raw circular polarization was not detected in any of the bands, with the weighted mean values of v being insignificant in relation to their uncertainties. Measurements made by Kemp and Wolstencroft (1972) indicate that, for the B band, the value of v is ~ -0.00030 being of the same order of accuracy as the reported measurements; the values obtained by Kemp and Wolstencroft for the V and R bands progressively approach zero

and are certainly smaller than the detectivity used here. Circular polarization is nominally detected for HD 160529 in the V band with a weighted mean value of -0.00033 ± 0.00010 . It is impossible to say, however, if this originates in the stellar radiation (e.g. an interstellar component), or if it is the same offset as recorded for the unpolarized standard stars, or if there is some linear-to-circular conversion by the telescope, this star exhibiting a high value of p .

2.4 The program stars

Tables 2.5 and 2.6 summarise the reduced measurements of the program stars. The quoted q and u values have been corrected for the sky background, the instrumental polarization and have been rotated from the instrumental frame to the equatorial co-ordinate frame.

Table 2.5: The measurements of the program stars according to the mean Julian Date (245 +) and the filter passband. The headings q , u , and σ are the corrected normalised Stokes parameters (equatorial frame) and 1σ uncertainty. The raw value of v_o , with its uncertainty, is also tabulated. The number of integrations is designated by N , each with integration time of T seconds.

SAO 154972							
JD	Band	q	u	σ	v_o	T	N
0226.240	V	-0.00077	-0.00296	± 0.00068	$+0.00045 \pm 0.00045$	750	1
0227.218	V	-0.00093	-0.00248	± 0.00046	-0.00010 ± 0.00033	750	2
0227.245	R	-0.00077	-0.00284	± 0.00023	-0.00036 ± 0.00016	750	2
0229.206	V	-0.00170	-0.00591	± 0.00043	$+0.00072 \pm 0.00030$	240	4
0229.222	R	-0.00055	-0.00267	± 0.00029	-0.00026 ± 0.00015	240	4
0230.266	V	+0.00036	-0.00423	± 0.00053	$+0.00016 \pm 0.00037$	360	4
0230.299	R	+0.00108	-0.00304	± 0.00024	$+0.00009 \pm 0.00017$	360	4
0231.231	V	+0.01011	-0.01167	± 0.00082	$+0.00095 \pm 0.00058$	120	6
SAO 251015							
JD	Band	q	u	σ	v_o	T	N
0225.334	U	+0.00403	-0.00016	± 0.01734	-0.00194 ± 0.01219	120	1
0225.335	B	-0.01184	+0.02024	± 0.00666	-0.01186 ± 0.00471	120	1
0225.342	V	-0.01126	+0.00562	± 0.00131	-0.00017 ± 0.00093	120	1
0225.344	R	-0.01248	+0.00335	± 0.00063	$+0.00054 \pm 0.00045$	120	1
0225.352	I	-0.00776	+0.00403	± 0.00039	$+0.00038 \pm 0.00028$	120	1

It has been assumed that the underlying distribution of measurements in the q, u

Table 2.6: Further measurements of the program stars according to the mean Julian Date (245 +) and the filter passband. The headings q , u , and σ are the corrected normalised Stokes parameters (equatorial frame) and 1σ uncertainty. The raw value of v_o , with its uncertainty, is also tabulated. The number of integrations is designated by N , each with integration time of T seconds.

HD 115383							
JD	Band	q	u	σ	v_o	T	N
0226.249	B	-0.00021	+0.00015	± 0.00010	+0.00010 ± 0.00007	750	3
0226.330	V	-0.00022	-0.00027	± 0.00022	-0.00020 ± 0.00016	750	2
0227.351	B	-0.00039	-0.00003	± 0.00029	-0.00007 ± 0.00021	180	1
0227.353	V	-0.00027	-0.00113	± 0.00065	-0.00047 ± 0.00046	180	1
0227.374	V	-0.00018	+0.00103	± 0.00046	-0.00089 ± 0.00033	750	1
0227.388	V	-0.00016	+0.00064	± 0.00032	-0.00060 ± 0.00022	750	1
0227.406	B	+0.00018	+0.00046	± 0.00014	+0.00006 ± 0.00010	800	1
0227.427	B	-0.00042	+0.00027	± 0.00015	-0.00025 ± 0.00010	800	1
0229.000	B	+0.00048	-0.00017	± 0.00014	+0.00006 ± 0.00010	180	4
0229.368	V	+0.00148	-0.00054	± 0.00031	-0.00071 ± 0.00022	180	4
0230.382	B	+0.00066	+0.00027	± 0.00015	+0.00037 ± 0.00010	180	4
0230.387	V	+0.00013	+0.00080	± 0.00033	-0.00040 ± 0.00023	180	4
HD 128400							
JD	Band	q	u	σ	v_o	T	N
0229.411	B	+0.00038	+0.00017	± 0.00027	+0.00016 ± 0.00019	180	5
0229.414	V	+0.00032	-0.00011	± 0.00017	-0.00009 ± 0.00012	180	5
0230.426	B	-0.00070	-0.00045	± 0.00020	+0.00036 ± 0.00014	180	10
0230.428	V	+0.00056	+0.00095	± 0.00013	-0.00024 ± 0.00009	180	10
HD 155555							
JD	Band	q	u	σ	v_o	T	N
0225.465	U	-0.00388	-0.00404	± 0.00178	-0.00016 ± 0.00126	120	2
0225.467	B	+0.00050	+0.00017	± 0.00065	+0.00035 ± 0.00046	120	3
0225.473	V	+0.00007	+0.00021	± 0.00021	-0.00039 ± 0.00012	120	3
0225.475	R	+0.00047	-0.00039	± 0.00030	+0.00048 ± 0.00021	120	2
0225.481	I	+0.00259	-0.00006	± 0.00032	-0.00016 ± 0.00023	120	2
0227.521	V	+0.00035	+0.00043	± 0.00020	-0.00036 ± 0.00014	960	1
0229.478	B	+0.00053	-0.00077	± 0.00030	+0.00007 ± 0.00021	180	5
0229.480	V	+0.00057	-0.00044	± 0.00018	-0.00024 ± 0.00013	180	5
0230.485	B	-0.00010	-0.00036	± 0.00022	+0.00037 ± 0.00016	180	9
0230.487	V	+0.00036	-0.00035	± 0.00014	+0.00000 ± 0.00010	180	9
HD 1835							
JD	Band	q	u	σ	v_o	T	N
0229.639	B	+0.00013	-0.00076	± 0.00023	+0.00013 ± 0.00016	180	5
0229.663	V	-0.00029	+0.00017	± 0.00015	-0.00003 ± 0.00010	180	5
0230.635	B	+0.00048	-0.00069	± 0.00021	+0.00006 ± 0.00015	180	6
0230.637	V	-0.00011	-0.00011	± 0.00014	-0.00033 ± 0.00010	180	6

plane have circular symmetry and that their variances are equal to each other and are independent of the chosen co-ordinate frame. Any inter-star data comparison to decide on polarimetric differences is unaffected by the reduction and transformation procedures.

2.4.1 Observations of Tu Pyx - SAO 154972

Although the measurements of this star are relatively few, it displayed by far the largest temporal changes. In the V band, the nights of JD 0226 and 0227 had too few internal values to warrant full normality tests, but the nights of JD 0229 and 0230 provided normally distributed data sets. However, for the night of JD 0231 the data were distinctly non-normal with an approximately 3σ change occurring over the course of an hour. A Welch test concluded that the data sets for JD 0229, 0230 and 0231 could both be considered as being generated from the same parent distribution with the night of JD 0231 being the deviant (see Fig 2.8). The measurements indicate an intrinsic polarisation of about 0.5% which suddenly increases to $\sim 2\%$ on the night of JD 0231. Figure 2.8 depicts the movement of the polarisation vector in the q,u plane. Of the six separate measurements made on this night, the first three are grouped together with a low level of polarisation, while the latter three are similarly grouped together but with the much higher value of p (see Figure 2.10). Although a full photometric procedure was not performed during the observations, there was no commensurate change in the star's brightness as recorded in the raw photon count.

It is also noteworthy that, for the V band, the values of v are persistently positive with an overall weighted mean of $+0.037 \pm 0.016$. On the night of JD 0231 the mean value was $+0.095 \pm 0.058$, the first value of the six measurements, prior to the sudden change in linear polarisation being $+0.210 \pm 0.137$. All other stars provided negative values of v .

The weighted mean value for all the measurements in the R band is -0.019 ± 0.009 signifying the detection of a weak linear polarisation, which can be differentiated from measurements made of the unpolarised standard stars (see Figure 2.9).

According to the General Catalogue of Variable Stars (Kholopov (1987)) TU Pyx is classified as a semi-regular variable (SRB), spectral type M5, with a nominal period of 88

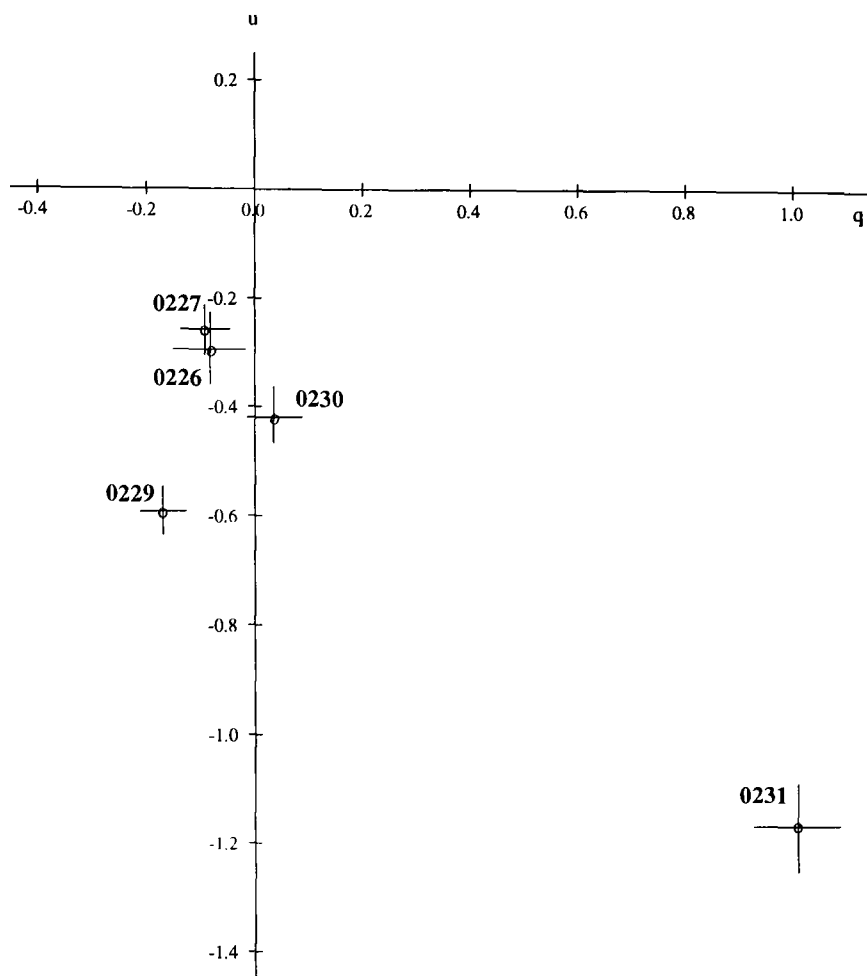


Figure 2.8: The Stokes parameter plot (q, u in %) displays the 5 data points, for TU Pyx, representing the average point for the nights of JD 0226, 0227, 0229, 0230 and 0231 respectively. The measurements indicate an intrinsic polarisation of about 0.5% which suddenly increased to $\sim 2\%$ on the night of JD 0231.

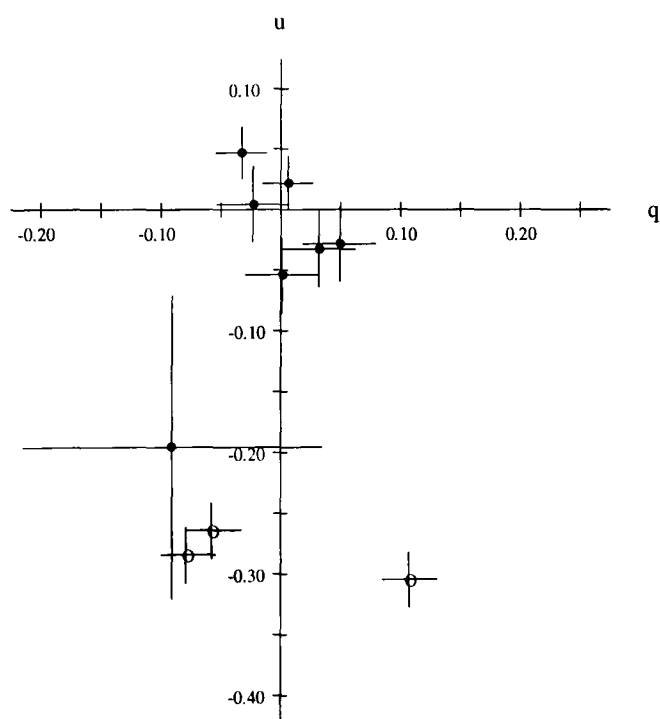


Figure 2.9: The Stokes parameter plot (q, u in %) displays the average data points, in the R band, for the nights of JD 0227, 0229 and 0230 respectively, indicating that the data sets for the unpolarised standard HD 202940 (●) and TU Pyx (○), can not be considered as being generated from the same parent distribution.

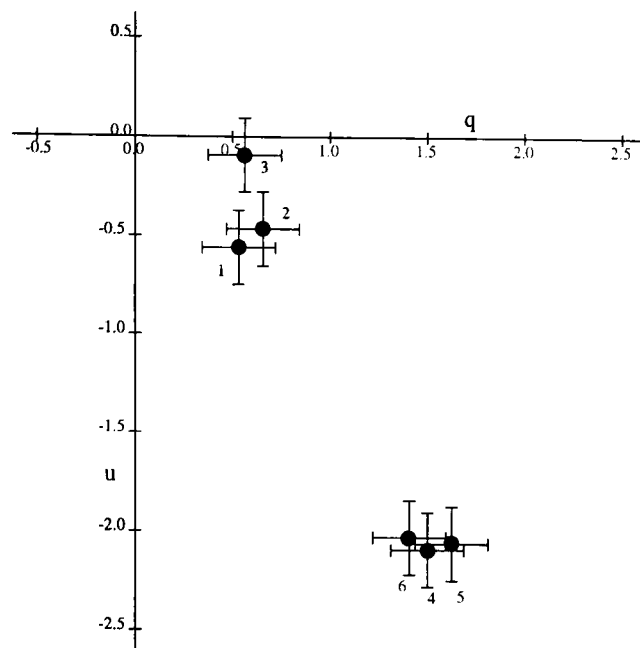


Figure 2.10: The Stokes parameter (q, u in %) plot displays the six V band polarisation measurements of TU Pyx made on the night of JD 0231. The time sequence covering about 20 minutes shows that the first three are bunched close to the origin while the final three display $p \sim 2\%$.

days and displaying a magnitude variation from 10.7 to 9.9. It was included in a ground based infrared photometric synoptic study of such stars by Kerschbaum (1995). However, according to the lists of SAO stars with infrared excess in the IRAS Point Source Catalog (see Oudmaijer et al. (1992)), this star is classified as G0 with $V = 8.7$ mag, reflecting a better match to the telescopic visual impression at the time of the observations reported here. Its entry suggests the presence of a circumstellar dust shell with a temperature of 1200 K.

Scattering of the stellar radiation by such dust with some kind of non-spherical distribution would give rise to an intrinsic polarization but it is very difficult to provide the means whereby such a large polarimetric change could occur without any noticeable change in the brightness and on a time scale of a matter of minutes. In view of the indication that circular polarization might be associated with this star and the recorded outburst of linear polarization, it is important that TU Pyx should be monitored further.

2.4.2 Observations of SAO 251015

Measurements of this star were made on one night only with moderate accuracies. Nonetheless, linear polarization appears to be present at a level just greater than 1% being significantly greatest in the B band, suggesting a polarigenic mechanism associated with the abundance of metal lines in this waveband. However it may be noted that this star has an infrared excess (Oudmaijer et al. (1992)), suggesting the presence of a circumstellar cloud. From the recorded $p(\lambda)$ data and from the location of this star, it is suggested that the polarization is intrinsic rather than having an interstellar origin. The raw measurements of v suggest null detections, except perhaps for the B band, but the absolute value of the uncertainty associated with this measurement is large. From this preliminary study, it is important that this star should be included in any future monitoring program.

2.4.3 Observations of 59 VIR : HD115383

Previous U band observations of this star over three consecutive nights have been made by Leroy and LeBorgne (1989) but with a null result. The reported measurements here on four nights for the B and V bands suggest, however, that a variable polarization is present. The nightly mean values are plotted in Fig 2.12, there being similarity of the locations in the q, u plane for the two colours. The p value in the V band for JD 0229 achieves $\sim 0.15\%$ and Welch tests in association with measurements of the unpolarized standard, HD 202940, confirm the significant difference in their q parameters on this occasion, this being the component dominating the polarization. It is interesting to note that the raw value of v for the V band on this night is also statistically significant. In fact the overall weighted value of v from the four nights is -0.00046 ± 0.00009 . No doubt some of this apparent circular polarization is instrumental as the measurements of the standard unpolarized star and of all the other stars below suggest, but this value is an extreme which is statistically significant.

Inspection of Fig 2.12 suggests that the temporal behaviour of the data for the B and V bands is coherent with the V band displaying a larger scale movement in the locus path. If the origin of the q, u plot has been correctly determined, the impression is that the underlying locus may be an elliptical figure with the origin towards an extreme end

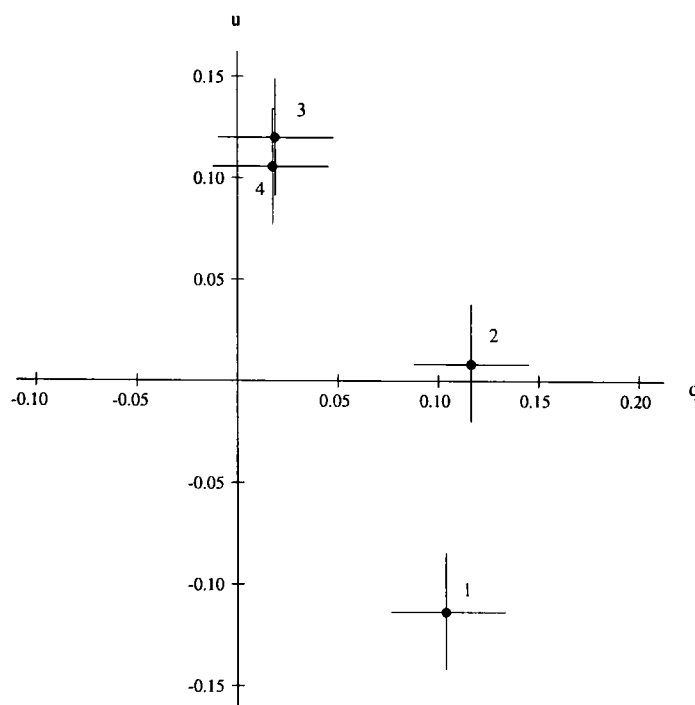


Figure 2.11: The Stokes parameter plot for 59 Vir in the B band on the night JD 0230, showing a possible fluctuation.

of the major axis (see, for example, Fig. 2(b) in Clarke and McGale (1986)). This is in keeping with a star exhibiting spot activity in its equatorial belt with the inclination, i , of the rotation axis being close to 90° . According to Donahue et al. (1996), 59 Vir displays a photometric rotational signature which has been persistent over five seasons, with a mean period of 3.33 days. This figure is not incompatible with the data shown in Fig 2.12, where, although more data is clearly needed for a realistic determination of the period of any cycle in p , a 3 day cycle (or even the polarimetric overtone of 1.5 days) is possibly present.

Although the Normality tests suggested that the polarization values were noisy or drifting during the time span of the measurements on JD 0230 (see Fig 2.11), the data set was insufficiently large to be able to confirm this. It is noteworthy, however, that if the locus of the data is following the suggested ellipse in the q, u plane, the phase associated with JD 0230 (see the points labelled 6 in Fig 2.12) corresponds to a time when it is moving at its fastest rate.

It is important that the detected polarimetric variability for 59 Vir should now be monitored more comprehensively to check on its coherence with its well established photometric period. Investigation of the circular polarization also needs a more thorough approach with the application of longer integration times.

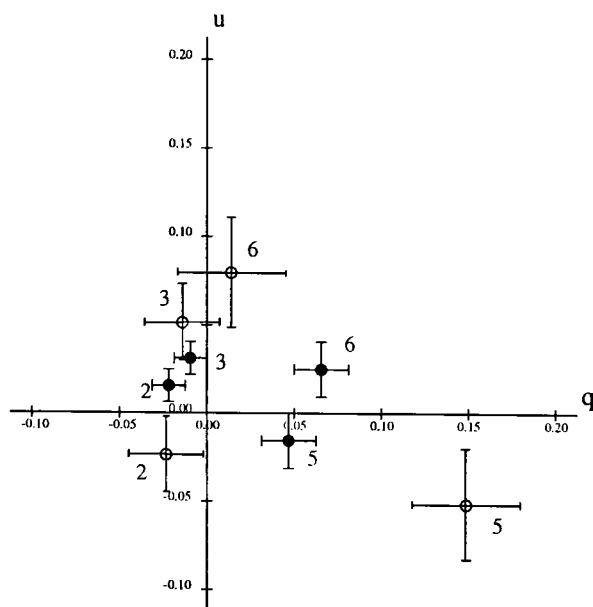


Figure 2.12: The Stokes parameter plot (q, u in %) of the **B** (•) and **V** (o) band measurements made of 59 Vir on four different nights indicate polarimetric changes that may be related to its associated photometric period. The numbers 2, 3, 5, 6 refer respectively to the nights of JD 0226, 0227, 0229 and 0230.

2.4.4 Observations of HD128400

On JD 0229 neither sets of data (B and V) were distinguishable from being representative of an unpolarised source. However, on JD 0230 Welch tests indicate a departure from the unpolarised reference in q just greater than the 90% confidence level for the B band (see Fig 2.13) and a similar significance of departure in u for the V band (Fig 2.14). However, polarisation is not detectable on any of the data at the 99% confidence level. Even if the 90% level is taken as being acceptable it would be difficult to reconcile why it should display inconsistent position angles for the two colours.

The weighted mean value for the two nights for the raw v measure in the V band indicates a detection (-0.019 ± 0.007) which is consistent with an instrumental offset. Welch tests indicate no difference in the distributions of v for each night, in both B and V, and no discernible presence of circular polarisation in Welch tests when compared to all other program stars.

2.4.5 Observations of HD 155555

Welch tests applied to the overall set of B band measures show that they can be considered as belonging to the same parent distribution and cannot be differentiated from

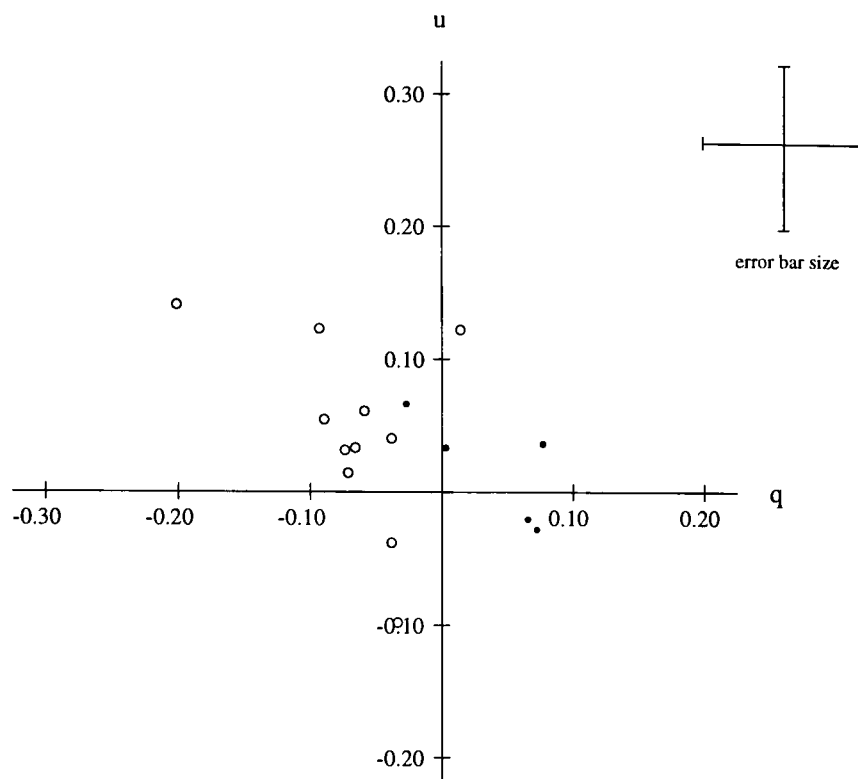


Figure 2.13: The Stokes parameter plot (q, u in %) displays the B band measurements for HD 128400 on the nights of JD0229 (\bullet) and JD 0230 (\circ). Welch tests indicate that the two distributions cannot be considered as belonging to the same parent distribution in q .

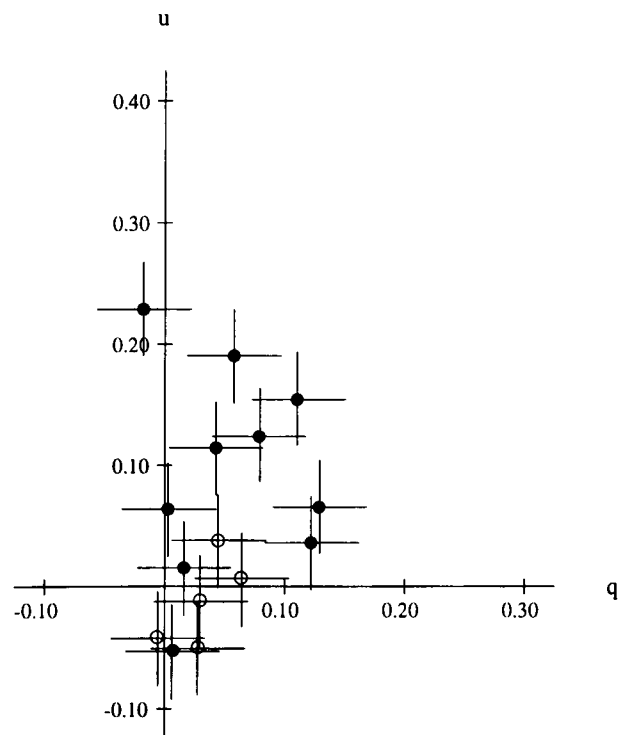


Figure 2.14: The Stokes parameter plot displays the V band measurements for HD 128400 on the nights of JD0229 (\circ) and JD 0230 (\bullet). Welch tests indicate that the two distributions cannot be considered as belonging to the same parent distribution in u .

data of the unpolarized standard. For the V band, however, Welch tests suggest that the measurements of the u parameter on JD 0229 are deviant. The q, u plot (Fig 2.15) of the data for the separate integrations from each night displays bunching with all of the five values appearing in the fourth quadrant. From its high Li/H ratio, HD 155555 has been classified as an active close binary system with both stars not having completed their contraction to the main sequence (see Pasquini et al. (1991)). Cutispoto (1990) has included HD 155555 in UBVRI photometric studies of active southern hemisphere stars. It is of interest to note that his data shows that it is also the V band which displays by far the largest rotationally modulated signal with a variation of ~ 0.1 mag associated with a period of $= 1.^d68$. Unfortunately the reported polarimetric data are insufficient to consider any correlation of its suspected variability with the photometric behaviour but the star is a prime candidate for further high accuracy studies.

HD 155555 was included in circular spectropolarimetric studies by Donati et al. (1997) and clear magnetic signatures have been detected with the high signal-to-noise records they were able to obtain. Although the weighted mean values for the raw v measurements in the V band reported here indicate a detection (-0.00021 ± 0.00006), again this can only be considered as an instrumental effect.

2.4.6 Observations of HD 1835

The hour angle of this star was such that it could only be observed at large zenith distance just before sunrise and consequently the time coverage was insufficient to investigate any possible rotational modulation. In the V band the two sets of measurements could not be distinguished from representing unpolarized radiation. In the B band there is a marginal suggestion that the star may exhibit a polarization $\sim 0.07\%$ K-index programme (see Donahue et al. (1996)) exhibiting photometric variations with periods ranging from $7.^d23$ to $8.^d30$ due to changes in the mean latitude of the active regions and effects of surface differential rotation. These preliminary measurements are sufficiently encouraging to promote a more intensive high precision polarimetric study.

Yet again, weighted mean values for the raw v measurements in the V band indicate a detection (-0.00018 ± 0.00007) but this can only be considered as an instrumental effect.

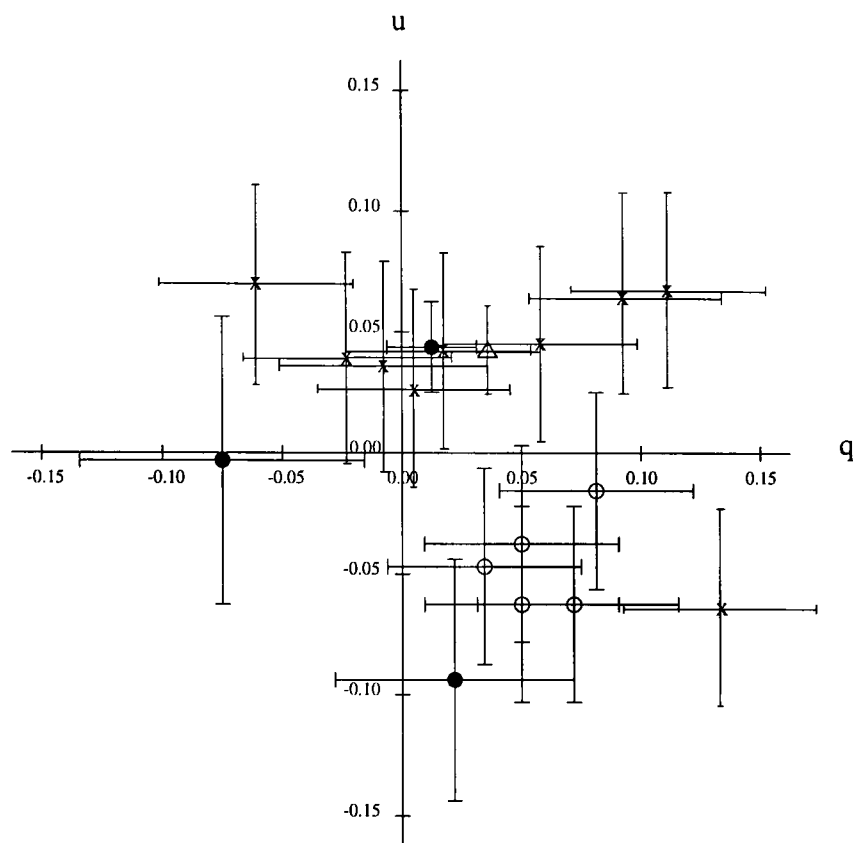


Figure 2.15: The Stokes parameter plot (q, u in %) depicts the V band polarimetric values for HD 15555 for each period, on the four nights of observation; \bullet = JD 0225, \triangle = JD 0227, \circ = JD 0229 and \times = JD 0230. It may be noted that for JD 0229, all the data lie in the fourth quadrant and Welch tests indicate variations in the parent distributions from which night-to-night data have been sampled, suggesting a low level of polarimetric variability.

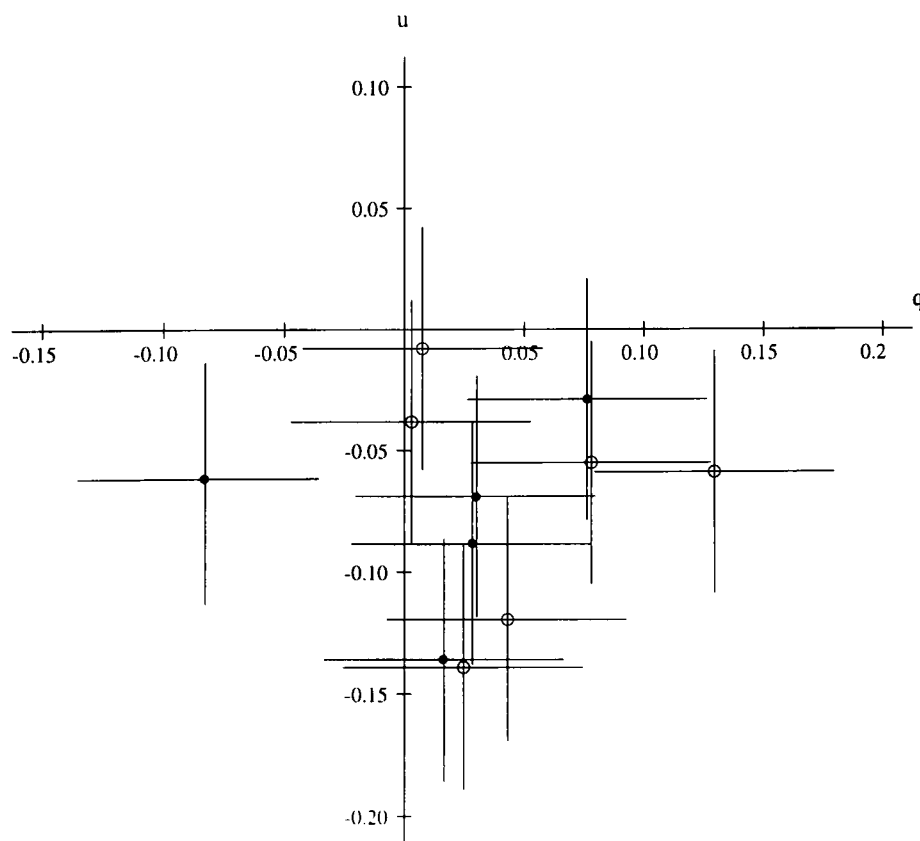


Figure 2.16: The Stokes parameter plot (q, u in %), for HD 1835, in the B band. There is a marginal suggestion that the star may exhibit a polarisation $\sim 0.07\%$.

2.5 Conclusion of G-Type Discussion

A preliminary synoptic study has been made of a sample of young solar type stars with the aim of detecting activity via polarimetry. Previous studies, both theoretical and observational, suggest that the levels of any polarization are likely to be small. As the stars are effectively solar type in terms of their luminosity and display high apparent brightness, they are relatively close and unlikely to be contaminated by interstellar polarization.

For the work reported here, both the linear and circular components have been investigated with typical measurement uncertainties in q, u and $v \sim \pm 0.0003$. This high level of accuracy causes problems with the assessment and removal of instrumental polarization due to the inadequacy of the catalogued unpolarized and polarized standard stars. In addition, even if the reference stars provided well calibrated values, an inordinate amount of time from the observational run would be required to perform the measurements to the required levels of accuracy. For the analysis of the program stars, the instrumental polarisation has been taken as constant, and not changing from night to night. Consequently the tabulated polarimetric values for the programme stars may be subject to systematic errors of the order of the uncertainties of their measurements but this in no way negates the investigations and detections of any variable intrinsic polarization.

The sample of investigated stars is small and the time window for the measurements is very limited. Of the stars suspected of displaying polarimetric variability, there are no similarities of behaviour. The most remarkable recorded event was for SAO154972 (TU Pyx) which displayed a sudden change in polarization from a level $\sim 0.5\%$ to $\sim 2.0\%$ in a time interval of about 15 minutes. There is also a strong indication of circular polarization associated with this star, suggesting the presence of magnetic activity. It is important that this star be included as a prime target in future polarimetric programmes.

Measurements of HD 115383 (59 Vir) on four nights display polarization variations ($\sim 0.1\%$) which are coherent in the B and V bands, the latter providing the larger amplitude about the origin. There is also evidence for a detection of circular polarization in the V band. The data for HD 155555 also display night-to-night variations in the V band but not in B; these may be related to previously monitored photometric variability which is also most strongly apparent in the V band.

The data for HD 1835 are very limited but there is marginal evidence for detection of a weak polarization in the B band.

All of these stars require further observations to characterise their polarimetric behaviour and to confirm that the observed effects are related to active regions traversing the projected disk as a result of stellar rotation or to other causes.

2.6 Observations of HD 139614

HD 139614 is an early-type (A7Ve) emission-line star with infrared excess (Oudmaijer et al. (1992)) and has been recognized as a member of Vega-type stars (Silvester et al. (1997) and references therein; Dunkin et al. (1997)). According to Malfait et al. (1998) it is certainly a member of the young Herbig Ae/Be group considering its spectral energy distribution (SED) in the IR and its single-peaked H_α emission. In reality its SED in the IR (using the IRAS data) is similar to the behaviour of Herbig Ae/Be stars or is like β Pic (i.e. a comparable young A star near the end of the Pre-Main Sequence evolutionary phase, displaying a disk). There is a consensus that most of the Herbig Ae/Be and β Pic-type stars are surrounded by disk-like dust envelopes (see for example Grady et al. (1996)). For the case of optically thin dust distributions, any IR excess from the heated grains does not depend on the inclination of the system, whereas the value of polarization generated from the scattered stellar radiation, is sensitive to the structure of the cloud and its viewing aspect. For lenticular envelopes, the recorded polarization is likely to be at a maximum for disks which are oriented edge-on.

2.6.1 Observations

V-band polarimetry of HD 139614 was undertaken on four nights at the SAAO in May 1996 (JD 2450226–2450229); on JD...226 a single measurement was made in R-band. The data are presented in Table 2.7. The columns give the Julian Date for the mean time of each observation, the filter used, the normalised Stokes parameters (q and u both in percent), their standard error ($\sigma_{q,u} \equiv 1\sigma$) and the calculated value of p . The listed q and u values have been corrected for sky background and instrumental polarization and are

Table 2.7: Polarimetric data for HD 139614.

JD2450000+	Filter	q	u	$\sigma_{q,u}$	p
226.3975	R	-0.038	+0.017	0.035	0.042
226.4649	V	+0.076	-0.018	0.040	0.078
226.4815	V	-0.025	+0.104	0.039	0.107
226.4958	V	-0.029	+0.036	0.039	0.046
226.5114	V	+0.005	+0.082	0.038	0.082
226.5240	V	+0.033	+0.116	0.039	0.121
227.4647	V	+0.060	+0.049	0.038	0.077
227.4794	V	+0.052	+0.016	0.038	0.054
228.4913	V	+0.007	+0.006	0.036	0.009
229.4461	V	-0.093	-0.138	0.055	0.166
229.4508	V	-0.104	-0.136	0.055	0.171
229.4557	V	-0.144	-0.159	0.055	0.215
229.4616	V	-0.085	-0.141	0.055	0.165
229.4664	V	-0.072	-0.149	0.055	0.165

plotted in Fig. 2.17.

2.6.2 Discussion

As can be seen immediately from both Table 2.7 and Fig. 2.17 that HD 139614 exhibits low levels of polarization of 0.05%–0.2% changing from night-to-night with JD... 228 showing a level close to zero. Moreover, it may be suggested that nightly mean values, as plotted in the qu -plane, form a locus along an arc, being part of a closed phase curve.

If this notion is correct, the full period of polarimetric variation is about 8–10 days and probably results from some kind of rotational modulation. Whether this is the case or not, the observations clearly reveal the presence of a variable intrinsic polarization.

It is interesting to compare the polarimetric data for HD 139614 presented here with those obtained for other Herbig Ae stars: HD 141549 (e), HD 142666 (A8Ve) and HD 169142 (B9Ve) (Yudin & Evans 1998). All of these stars are also recognized as Vega types by Silvester et al. (1996) and Harvey et al. (1996) but, taking into account the IRAS data, they are also members of the Herbig Ae/Be group. Detailed comparison of the photometric behaviour of HD 139614 and HD 142666 has been described recently by

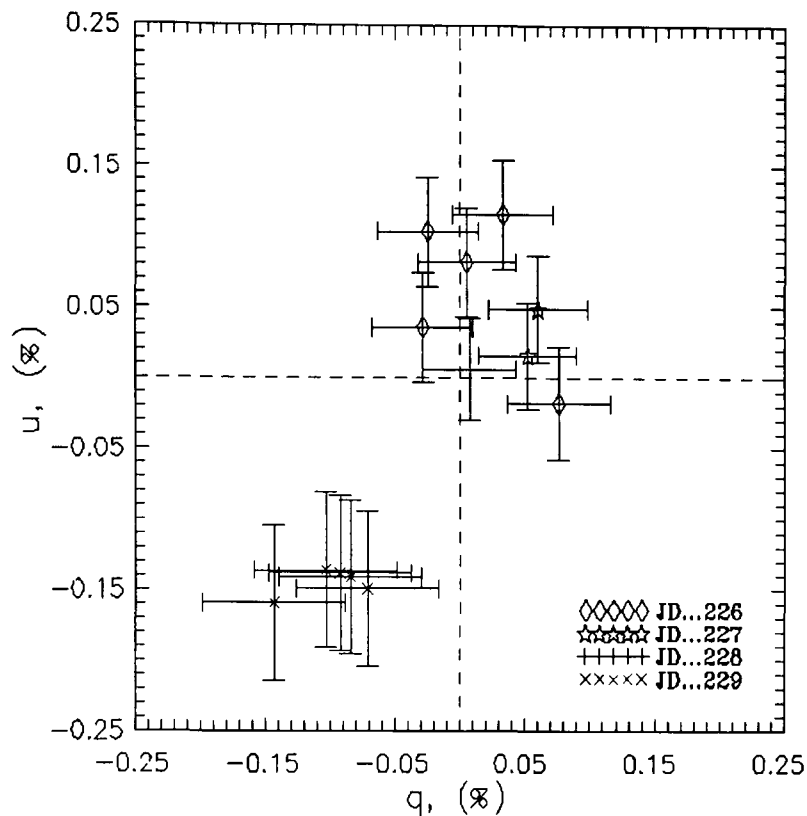


Figure 2.17: V band polarisation measurements of HD 139614 plotted in the q, u -plane.

Meeus et al. (1998) who discussed evidence for circumstellar disks around these stars. According to Silvester et al. (1996), the total extinction towards HD 142666 is significantly larger than towards HD 139614 ($E[B - V] = 0.22^m$ and 0.08^m respectively). Meeus et al. (1998) noted that both stars have almost identical spectral types, UV-optical SEDs and observed IR excesses. However, they pointed out that HD 142666 has a substantial amount of circumstellar material in the line of sight, while HD 139614 shows no evidence for material in the line of sight. In terms of a model proposed by Meeus et al. (1998) for HD 142666, the irregular brightness variations are caused by dense nodules in the dust clouds which occasionally cross the projected stellar disk, i.e. the disk is being viewed edge-on. The non-variable photometric behaviour of HD 139614 suggests a more (but probably not exactly) pole-on orientation of a disk.

Consideration of the polarization data obtained here and of Yudin and Evans (1998) for HD 142666 is consistent with the above descriptive model. The single measurements in the VR_cI_c bands for HD 142666 show a degree of polarization $\approx 0.7\%$, much larger than any of the values obtained for HD 139614. Note that the behaviour of $p(\lambda)$ for HD 142666 is unlike that of interstellar polarization with p probably increasing in the red. Thus the

polarization is again intrinsic to the stellar system. Moreover, the visual magnitude of HD 142666 at the time of the polarimetry was about 8.7^m , i.e. the star was observed at maximum light. One can predict the detection of a much larger value of polarization for this star in minima because according to Bogaert and Waelkens (1990) its amplitude of photometric variability is about 3^m in the V band and it may be a member of Herbig Ae/Be stars with Algol-like minima of brightness (Meeus et al. (1998)).

Two other Herbig Ae/Be stars (HD 141549 and HD 169142) also show evidence of intrinsic polarization on the level of about $\approx 0.6\%$ and $\approx 0.5\%$ respectively in the V band (Yudin and Evans (1998)) behaving similarly to HD 142666). HD 169142 displays night-to-night polarimetric variability from 0.1% to 0.6% (i.e. the amplitude of variability being greater than that for HD 139614 reported here). Dunkin et al. (1997) noted that HD 139614 has the lowest $v \sin i$ value from all Vega-type stars in their sample and suggested that the disk around this star may be closer to pole-on. The $v \sin i$ values for HD 141549 and HD 142666 are much larger and together with their higher levels of polarization and larger amplitude of polarimetric variability support the hypothesis that HD 141549, HD 142666 and HD 169142 exhibit circumstellar disks with edge-on aspects.

2.6.3 Future Work

It is important to undertake precise multicolour observations to investigate the $p(\lambda)$ behaviour of HD 139614 and to obtain a longer time series of measurements to confirm the periodicity of the polarimetric variations. More generally, it is also important to extend photometric/polarimetric studies of Herbig Ae/Be stars with approximately the same IR excesses and physical properties (spectral types and brightness) to allow better interpretation of the model and the role that disk orientation plays on their observed behaviour.

2.7 Observations of HD 100546

It is well known that Be stars display linear polarizations $\sim 1\%$ with a characteristic wavelength dependence dominated by the influence of hydrogen opacity in the extended

atmosphere (e.g. see the review of Coyne (1976)). Once the contamination of any interstellar component is removed, the intrinsic $p(\lambda)$ behaviour usually follows some particular direction – the intrinsic line – in the normalised Stokes parameter (q, u) plane, with the vector angle relatable to the viewing aspect of the stellar equatorial disk. Many Be stars also display temporal variability on a range of time-scales from hours to months, the mapped behaviour in the q, u plane again being related to the intrinsic line. A classic example for the behaviour of $p(\lambda)$ and its temporal changes is the Be star, γ Cas (e.g. see Clarke (1990)).

The southern hemisphere Be star HD100546, spectral type B9Vne, has been included in the list of Herbig Ae/Be stars of Thé et al. (1994). It has also been selected for investigation as a young star by Henning et al. (1994) who discussed the presence of a disk-like dust component around it. Short-term variability of the $H\alpha$ and He line profiles on time scales of days and probably hours has been reported by Vieira et al. (1998). It was therefore decided to extend the observational diagnostic study by performing polarimetry with a view to determining the star's basic geometry and aspect. A preliminary polarimetric study was made by Yudin and Evans (1998) and with uncertainties in $p \sim \pm 0.1\%$ for each reported measure, they suggest there is clear evidence of variability on time-scales of days to minutes. We report on new measurements obtained during an observational run in May 1996 at the South African Astronomical Observatory, Sutherland, using the polarimeter of the University of Cape Town.

2.7.1 Measurements

Measurements were made on three nights, each covering about 2 hours. Alternate B and V band integrations (180s) were obtained and later reduced to remove the instrumental polarization and to relate the Stokes parameters to the celestial equatorial frame. The nightly mean values of the polarization are summarised in Table 2.8 and displayed in Fig 2.18.

At face value the measurements suggest that HD100546 displays a small polarization $\sim 0.25\%$. The measurements also show that $p(V)$ is greater than $p(B)$. This is contrary to the polarimetric behaviour of other Be stars and suggests that these basic values are

Table 2.8: The measurements of the Be star, HD100546, according to the commencing Julian Date (245 +) and the filter passband. The headings q , u correspond to the normalised linear Stokes parameters with the standard error (1σ) attached; uncorrected circular polarization measurements with their associated error are listed under the heading v_o . The number of integrations is designated by N , each with integration time of 180 seconds.

JD	Band	q	u	σ	v_o	N
0227.272	B	-0.00077	+0.00180	± 0.00014	-0.00020 ± 0.00010	11
0227.274	V	-0.00086	+0.00311	± 0.00012	-0.00027 ± 0.00009	11
0229.286	B	-0.00039	+0.00156	± 0.00010	$+0.00007 \pm 0.00007$	17
0229.288	V	-0.00113	+0.00227	± 0.00009	-0.00017 ± 0.00007	17
0230.324	B	-0.00084	+0.00082	± 0.00013	$+0.00046 \pm 0.00009$	12
0230.326	V	-0.00165	+0.00232	± 0.00011	-0.00030 ± 0.00008	12

contaminated by interstellar polarization, altering the origin in the q, u plane for the description of the intrinsic polarization.

One of the procedures for estimating the interstellar component is to examine the values of field stars. Inspection of the Strasbourg polarimetric catalogue (1970) and the data of Klare and Neckel (1977) offers only sparse clues, the nearest objects being several degrees away and closer to the galactic equator. Typical values are 1 or 2% with position angles in the vicinity of 80° . If the interstellar contamination for HD100546 is of this order, the origin from which the intrinsic component is referred is in the 2nd quadrant of the q, u diagram at some 10 times distant from the depicted origin of Fig 1. than the plotted data. Based on a value of $p \sim 1.5$ with $\theta = 80^\circ$, the interstellar point would be at $q \approx -0.940\%$ and $u \approx +0.342\%$. It may be noted that by a transposition to this offset origin, the intrinsic $p(B)$ component would now be greater than $p(V)$. Thus the intrinsic polarization is effectively crossed with the interstellar component, the former almost annihilating the polarization generated by the star. Unfortunately a precise value for the interstellar component cannot be obtained neither from the field star assessment nor from colour data presented here which is limited to two passbands.

The method of data logging with repeated measurements (N) of $p(B)$ and $p(V)$ is ideal for applying statistical tests to explore short term polarimetric flickering and night to night changes.

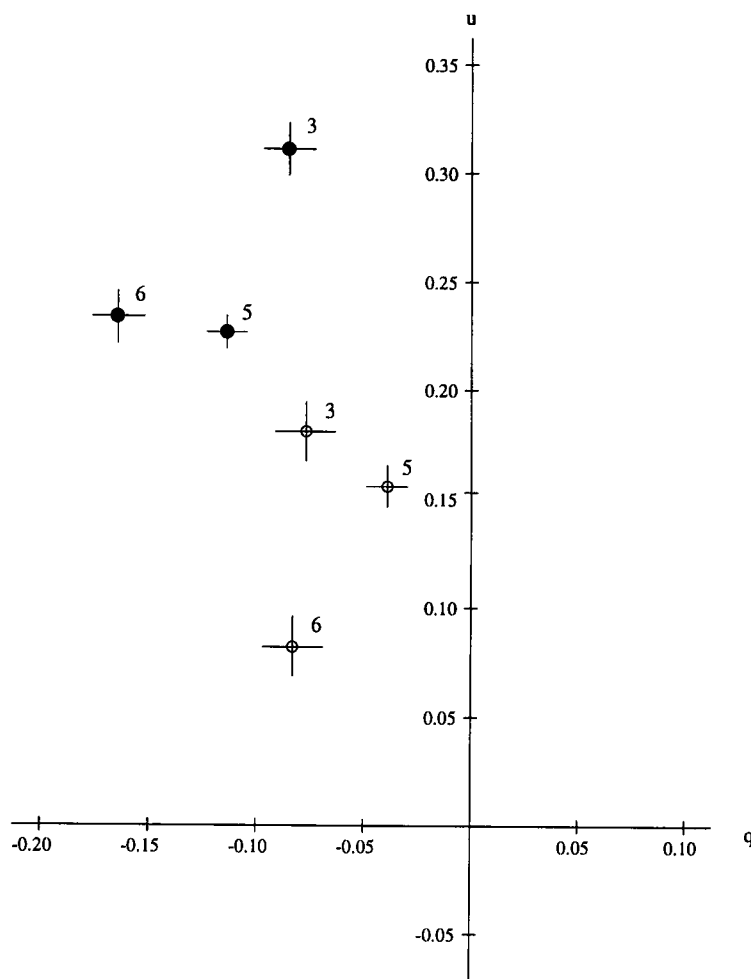


Figure 2.18: The Stokes parameter plot (q, u in %) depicts the mean polarimetric values for HD 100546 for each of the three nights of observation, for the B and V bands.

For each night tests (see Brooks et al. (1994)) showed that the assembly of q and u values for both passbands could be considered as being Normally distributed with a variance that was no larger than expected as a result of the experimental noise. Time plots of the data in the q, u plane also revealed random paths through the distribution. No distinctions could be made between measurements made at the beginning of each night relative to the data recorded towards the end of each 2hr run. Each set of nightly values appeared to be consistent as being repeated measurements of a constant underlying value. A typical set of measurements from a single night is depicted in Fig 2.19. Thus no flickering at a level of $\sim \pm 0.0002$ was observable on any of these nights with a total observation coverage of about 6 hours.

Welch tests (see Brown and Forsythe (1974)) reveal that for both the B and V passbands, the three q means for each night are indistinguishable and can be considered as coming from the same underlying parent constant value. The u parameter, however, does show movement. On JD 0230, the B band measurements are significantly displaced

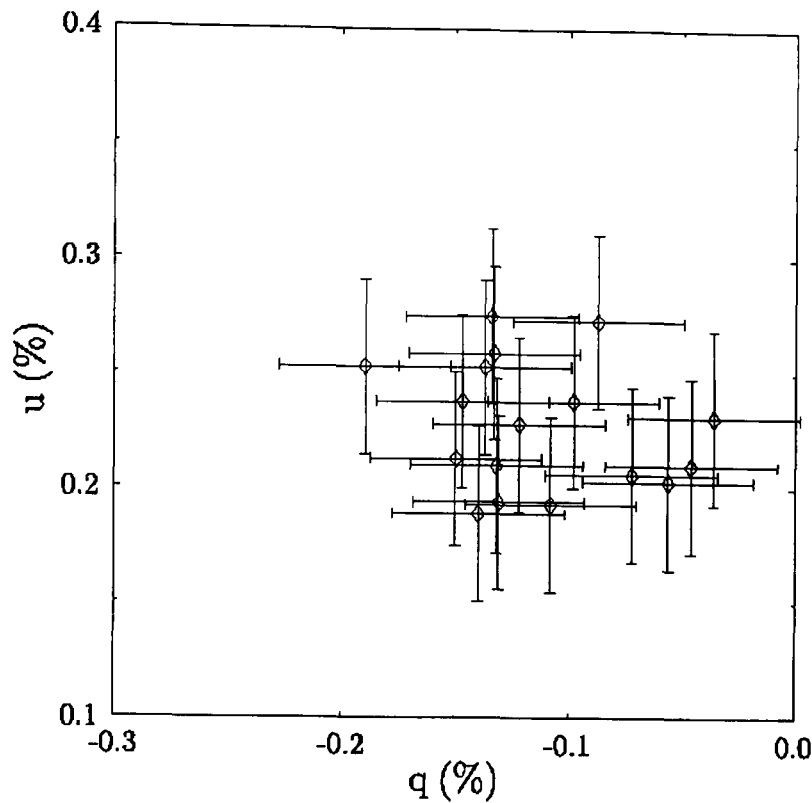


Figure 2.19: The Stokes parameter plot depicts the individual V-band polarimetric records for HD 100546 for the night of JD 245 0229.

from the values of the other two nights and, on JD 0227, the V band measurements are significantly displaced relative to the other two nights, the differences being clearly seen in Fig 2.18. Unfortunately the observing run was too short to obtain hints of any systematic changes in the q, u plane that would allow the major principal axis or intrinsic line (see Clarke and McGale (1987)) to be determined.

Although the circular polarization measurements have not been treated properly for effects of instrumental polarization, it does appear that a change in the B band is detectable over the observing run.

Welch tests show that on JD 0230 the underlying value is different from the other two nights, possibly associated with the noted change of the linear polarization on the same night. At this stage it is impossible to say whether this circular polarization is generated in the stellar atmosphere or whether it is the intrinsic linear component being partially converted to circular by the birefringent interstellar medium. The three mean records for the V band are indistinguishable and although they provide a systematic non-zero value, reference to data from the other program stars would suggest that it is an instrumental

effect and that its mean value is essentially zero.

2.7.2 Discussion and Conclusion of Results for HD 100546

Three nights of observation have revealed night-to-night polarimetric changes in HD100546, both linear and circular. Over windows of ~ 2 hours, however, no polarimetric variation either secular or of a more stochastic nature was detected with measurement uncertainties $\sim \pm 0.02\%$. No hint of the temporal behaviour as reported by Yudin and Evans (1998) was detected over a total monitoring time ~ 6 hours, even though the measurements were recorded with experimental uncertainties which were some 5 times smaller. Comparison of the data of Yudin and Evans shows that the $p(V)$ values occupy a similar region in the q, u plane but that the $p(B)$ are displaced as a result of u values being negative. Thus the ratio $p(B)/p(V)$ has changed significantly between the data sets of Yudin and Evans and those presented here. Such a variation may be brought about by a change in the average opacity in the stellar disk or by a change in the contribution of the circumstellar dust component.

It is important that this star should be monitored more extensively to explore the nature of the variation in p and to investigate the circular polarization further with a view to confirming its origin. In order to help determine the degree of clumpiness in the circumstellar structure which produces the night-to-night variations in p , it is important to record the rate at which the polarimetric changes occur. Measurements made with a broader range of wavelength coverage would also be useful to distinguish between electron scattering and Mie scattering from the dust in the stellar environment.

Chapter 3

Kolmogorov Testing for Temporal Variability

When attempting to detect the presence of temporal variability in the polarisation of a star, the employment of sensitive, and rigorous statistical tests are needed. The first and most convenient method is to determine whether the polarimetric data are normally distributed or not. A statistically significant deviation from normality, would point to the presence of some polarisation variability. A commonly used process is the testing for the skewness and kurtosis of a single distribution. The Welch test may be used to detect if there is any significant variation in the level of polarisation from data set to data set, where each individual set is in itself normal. For example, the presence of any night to night variability may be tested, when it is known that there is no variability within the timescale of one night. The F-test is used as a means of comparing the variances of the distributions in q and u . The presence of a significant difference in their magnitudes, would suggest the presence of some variability. All three of these methods have been demonstrated and used effectively in Chapter 2 to investigate the polarisation of solar type stars observed at SAAO with the 0.75m telescope. However, the purpose of this chapter is to describe the use of the Kolmogorov-Smirnoff technique. This method has been used traditionally to assess the similarity between two distributions. It is particularly useful as means of obtaining a reasonable hypothesised distribution, as an approximation to a real distribution. The aim in this chapter will be to use the technique to compare the data from a set of polarised

stars, with their calculated theoretical normal distributions.

An ideal candidate data set for this investigation, was selected from private communication with David McDavid at the Limber Observatory, Texas, during 1996, where polarisation data for several stars was presented from observations from 16th-20th October 1989 at the McDonald Observatory, Texas, USA. The program stars were λ Cep (O6I(n)fp), ξ Per (O7.5III(n)(f)) and ϕ Cas (FO Ia). All data were taken using a filter designated B5 (for the B band) in conjunction with a neutral density filter allowing 50% transmission. ϕ Cas was observed as a polarised standard, but will also be analysed, to confirm it's status. These stars have also been investigated for both photometric and spectroscopic variability. Kaper and Heinrichs (1997) conducted simultaneous ultraviolet and H α spectroscopy of λ Cep and ξ Per, and observed changes in the H α line at low velocity ($0 - 0.2v_{\infty}$) on time scales that are consistent with the development and evolution of discrete absorption components (DACs) in UV resonance lines. Heinrichs (1998) also present findings from a multi-wavelength campaign to observe ξ Per and investigate the cause of variability of the stellar wind, suggesting that magnetic activity on patches on the stellar surfaces be the the most promising candidate for generating structures in the wind. It is necessary to further investigate these stars, and an analysis of polarimetric data from the program stars would be of benefit in an interpretation of the processes intrinsic to them. The presence of any temporal variability in polarisation is likely to be small, and therefore good quality data are required, and sensitive statistical techniques are needed. The basic Kolmogorov test is used in this chapter, and extended, to search rigorously for any variability.

3.1 Kolmogorov-Smirnoff Technique

An effective method of determining how well two distributions resemble each other, has been developed by Kolmogorov and Smirnoff (see Conover (1980)). Kolmogorov type tests are an alternative to the often used χ^2 Test for goodness of fit, which was designed for nominal type data. The Kolmogorov technique is exact if the sample size is small, where as the χ^2 Test assumes that the number of observations is large enough, so that the χ^2 distribution provides a good approximation as the distribution of the test statistic. It is

generally excepted that the Kolmogorov test is probably the more powerful test in most situations (see Slakter (1965)).

If it is necessary to see if two or more random distribution samples are governed by the same unknown distribution, it is good practice to compare the empirical distributions of these samples, where the empirical distribution function, $S(x)$, is the fraction of a sample's values, x_i 's, that are less than or equal to x , for each x lying in the range $-\infty < x < +\infty$. It should be noted that some level of disparity between or among these functions, is needed. Kolmogorov and Smirnov developed statistical procedures that use the maximum vertical distance between these functions, to determine how well the functions resemble each other.

The usual procedure for testing the goodness of fit, involves taking a random sample from an unknown distribution and then testing the null hypothesis that the unknown distribution is in fact a known specified function. For example, the null hypothesis specifies some theoretical distribution function, $F^*(x)$, as a mathematical function that may be shown graphically. A random sample is taken from some population, and is then compared to, $F^*(x)$, in order to determine whether $F^*(x)$ is a reasonable approximation of the true underlying distribution function of the random sample, $F(x)$. As the empirical distribution function is a good approximation of $F(x)$, then by comparing $S(x)$, and $F^*(x)$, if there is not good agreement, the null hypothesis may be rejected, i.e. it may be concluded that the unknown distribution function, $F(x)$, is not in fact given by the function, $F^*(x)$.

The easiest way of comparing $S(x)$, and $F^*(x)$, is by way of the *Kolmogorov Statistic*, T , which is a measure of the maximum vertical distance between the two graphs of $S(x)$, and $F^*(x)$, taken in the vertical direction, (Fig 3.1). This value is then compared with tabulated values of the quantiles of the Kolmogorov test statistic (see Miller (1956)), where large values of T lead to rejection of $F^*(x)$ as a reasonable approximation to the true unknown distribution function, $F(x)$. See Table 3.2.

It is important to point out the difference between tests of the Kolmogorov type and tests of the Smirnov type. Statistics that are functions of the maximum vertical distance between $S(x)$, and $F^*(x)$, are considered to be Kolmogorov-type statistics. Statistics that are functions of the maximum vertical distance between two empirical distribution functions, are of the Smirnov type.

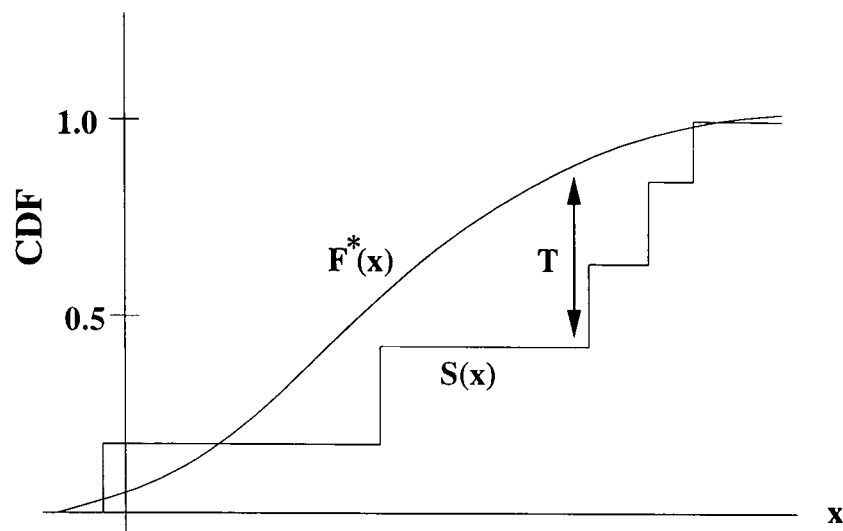


Figure 3.1: The hypothesized distribution function $F^*(x)$, the empirical distribution function (EDF), $S(x)$, and the Kolmogorov Statistic, T .

Employing the Kolmogorov Goodness-of-fit Test, there are three individual tests to consider, and these are specified below, for data of a random sample $x_1, x_2, x_3, \dots, x_n$ of size n associated with an unknown distribution function, $F(x)$. $F^*(x)$ is the hypothesised distribution function.

A. Two-Sided Test

$$H_0 : F(x) = F^*(x) \text{ for all } x \text{ from } -\infty \text{ to } +\infty$$

$$H_1 : F(x) \neq F^*(x) \text{ for at least one value of } x$$

B. One-Sided Test

$$H_0 : F(x) \geq F^*(x) \text{ for all } x \text{ from } -\infty \text{ to } +\infty$$

$$H_1 : F(x) < F^*(x) \text{ for at least one value of } x$$

C. One-Sided Test

$$H_0 : F(x) \leq F^*(x) \text{ for all } x \text{ from } -\infty \text{ to } +\infty$$

$$H_1 : F(x) > F^*(x) \text{ for at least one value of } x$$

For these three individual hypotheses, there are three individual test statistics. These are given below.

A. $T = \sup_x |F^*(x) - S(x)|$

B. $T^+ = \sup_x [F^*(x) - S(x)]$

One-Sided Test											
$p =$.90	.95	.975	.99	.995	$p =$.90	.95	.975	.99	.995
Two-Sided Test											
$p =$.80	.90	.95	.98	.99	$p =$.80	.90	.95	.98	.99
$n = 1$.900	.950	.975	.990	.995	$n = 21$.226	.259	.287	.321	.344
2	.684	.776	.842	.900	.929	22	.221	.253	.281	.314	.337
3	.565	.636	.708	.785	.829	23	.216	.247	.275	.307	.330
4	.493	.565	.624	.689	.734	24	.212	.242	.269	.301	.323
5	.447	.509	.563	.627	.669	25	.208	.238	.264	.295	.317
6	.410	.468	.519	.577	.617	26	.204	.233	.259	.290	.311
7	.381	.436	.483	.538	.576	27	.200	.229	.254	.284	.305
8	.358	.410	.454	.507	.542	28	.197	.225	.250	.279	.300
9	.339	.387	.430	.480	.513	29	.193	.221	.246	.275	.295
10	.323	.369	.409	.457	.489	30	.190	.218	.242	.270	.290
11	.308	.352	.391	.437	.468	31	.187	.214	.238	.266	.285
12	.296	.338	.375	.419	.449	32	.184	.211	.234	.262	.281
13	.285	.325	.361	.404	.432	33	.182	.208	.231	.258	.277
14	.275	.314	.349	.390	.418	34	.179	.205	.227	.254	.273
15	.266	.304	.338	.377	.404	35	.177	.202	.224	.251	.269
16	.258	.295	.327	.366	.392	36	.174	.199	.221	.247	.265
17	.250	.286	.318	.355	.381	37	.172	.196	.218	.244	.262
18	.244	.279	.309	.346	.371	38	.170	.194	.215	.241	.258
19	.237	.271	.301	.337	.361	39	.168	.191	.213	.238	.255
20	.232	.265	.294	.329	.352	40	.165	.189	.210	.235	.252
				Approximation for $n > 40$			1.07	1.22	1.36	1.52	1.63
							\sqrt{n}	\sqrt{n}	\sqrt{n}	\sqrt{n}	\sqrt{n}

SOURCE. Adapted from Table of Miller (1956).

"The entries in this table are selected quantiles w_p of the Kolmogorov test statistics T , T^+ , and T^- as defined by Equation 6.1.1 for two-sided tests and by Equations 6.1.2 and 6.1.3 for one-sided tests. Reject H_0 at the level α if T exceeds the $1 - \alpha$ quantile given in this table. These quantiles are exact for $n \leq 40$ in the two-tailed test. The other quantiles are approximations that are equal to the exact quantiles in most cases. A better approximation for $n > 40$ results if $(n + \sqrt{n/10})^{1/2}$ is used instead of \sqrt{n} in the denominator.

Figure 3.2:

C. $T^- = \sup_x [S(x) - F^*(x)]$

...where, for example, for A, the test statistic T is the greatest (denoted by "sup" for supremum) vertical distance between $S(x)$ and $F^*(x)$, over all x , of the absolute value of the difference $F^*(x) - S(x)$. H_0 is rejected at the level of significance α if the appropriate test statistic, T , T^+ , or T^- exceeds the $1 - \alpha$ quantile $w_{1-\alpha}$, given in Fig 3.2 taken from Miller (1956)

Quantiles are provided for use in the two-sided tests at $\alpha = .20, .10, .05, .02,$ and $.01$ and for the one-sided tests at $\alpha = .10, .05, .025, .01,$ and $.005$. The tables are exact for $n \leq 20$ in the two-sided test. For the one-sided test and for $n > 20$ in the two-sided test, the tables provide good approximations that are exact in most cases.

3.2 Kolmogorov Technique Analysis to Detect Real Temporal Variability by Consideration of Errors

The Kolmogorov technique has been used to compare two distributions – one real data set, and one hypothesised approximation of the set. When comparing the empirical distribution, $S(x)$, of a real set with the theoretical normal distribution, $F(x)$, generated from the observed mean and standard deviation, it is not enough just to consider the Kolmogorov Statistic for the maximum vertical distance between the two distributions. When examining sources with possibly very low levels of polarisation variability, it is increasingly important to take account of the intrinsic uncertainty on the determination of the mean of the normal distribution, $F(x)$. This error on the mean is the Standard Error, s.e. . It is an acceptable proposition to compare $S(x)$ with all possible normal distributions, between that generated from the mean plus the standard error, and that generated from the mean minus the standard error. If the measured value of T between $S(x)$ and any of the $F(x)$ distributions exceeds the $1-\alpha$ quantile given in Table 3.2, then the hypothesis, H_0 , that the real distribution may be described as a sample from a parent normal distribution, may be rejected at the level α .

Presented in the following subsections is the analysis using the above technique, for each of the program stars. A description of the errors and the observing technique was provided by private correspondence with David McDavid. The errors include contributions from photon counting statistics ($\delta q = \delta u = \delta p$) and contribution from noise in the sky background correction. A small instrumental polarisation (on the order of 0.1%) was removed from all the measurements, but its uncertainty was not propagated into the final results. The measurements were taken in sets of three interspersed with a sky background measurement (star 200 secs, star 200 secs, sky 200 secs, star 200 secs) to obtain a more realistic error estimate than the photon counting statistics errors given with each individual observation.

The analysis of the individual normalised Stokes parameters is dealt with first, followed by a discussion of the techniques involved to assess whether there is any non-normality evident in the data of the polarisation angle, θ . It must be pointed out that whilst there maybe no observed polarisation in the q and u normalised Stokes parameters,

there may be special conditions which might show a variability in θ alone.

The process of analysis is summarised in Fig 3.3. Where as it is possible to conduct a Kolmogorov test upon the data in the original frame, and this would certainly be prudent if there is an immediately obvious non-normality along either of the q or u axes, it is preferable to first rotate the data to any preferred axis within the data. This is done by conducting F-tests before and after rotation, to compare the variances of the q and u distributions. The preferred axis is that for which the largest F-statistic is obtained. Rather than examining the set along the arbitrary instrumental axis, there is a greater probability of detecting polarimetric variability in the rotated frame, which is likely to be coincident with any intrinsic polarimetric axis of the star. By doing so, any non-normality produced by temporal variability is more likely to be detected.

3.2.1 Analysis ϕ Cas

Before considering ξ Per and λ Cep, the data for ϕ Cas were tested, to determine whether this latter star could indeed be considered as showing no temporal variability in either the q or u Stokes parameters, and therefore whether it may be used as a reliable polarised standard. Initially, an F-test on the data for the normalised Stokes parameters, q and u , on the night of the 16th October 1989 revealed a value of the F statistic, $F_1=1.53$, identical to the value, F_2 , obtained from a F-test performed after the data had been rotated by $\sim 5.4^\circ$ in the q,u plane, to coincide with the determined preferred axis of the system. Kolmogorov tests were performed on both q and u to detect any non-normality in either of the individual data sets. Fig 3.4 (a) and Fig 3.5 (a) display the cumulative distribution functions for this night. $S(q)$ and $S(u)$ are the empirical distribution functions of the observed data. The three smooth curves, $F^*(q)$, $F^*(q+se)$ and $F^*(q-se)$, are the three normal distributions for q generated from the observed mean and standard deviation. $F^*(q)$ is the hypothesised distribution function generated from the observed mean, and $F^*(q+se)$ and $F^*(q-se)$ are the hypothesised distribution functions generated from the observed mean plus and minus the standard error, s.e. . It is clear from the figure that the two sided Kolmogorov test is the appropriate test to use.

It should be noted that these three curves are identical in shape, and are merely

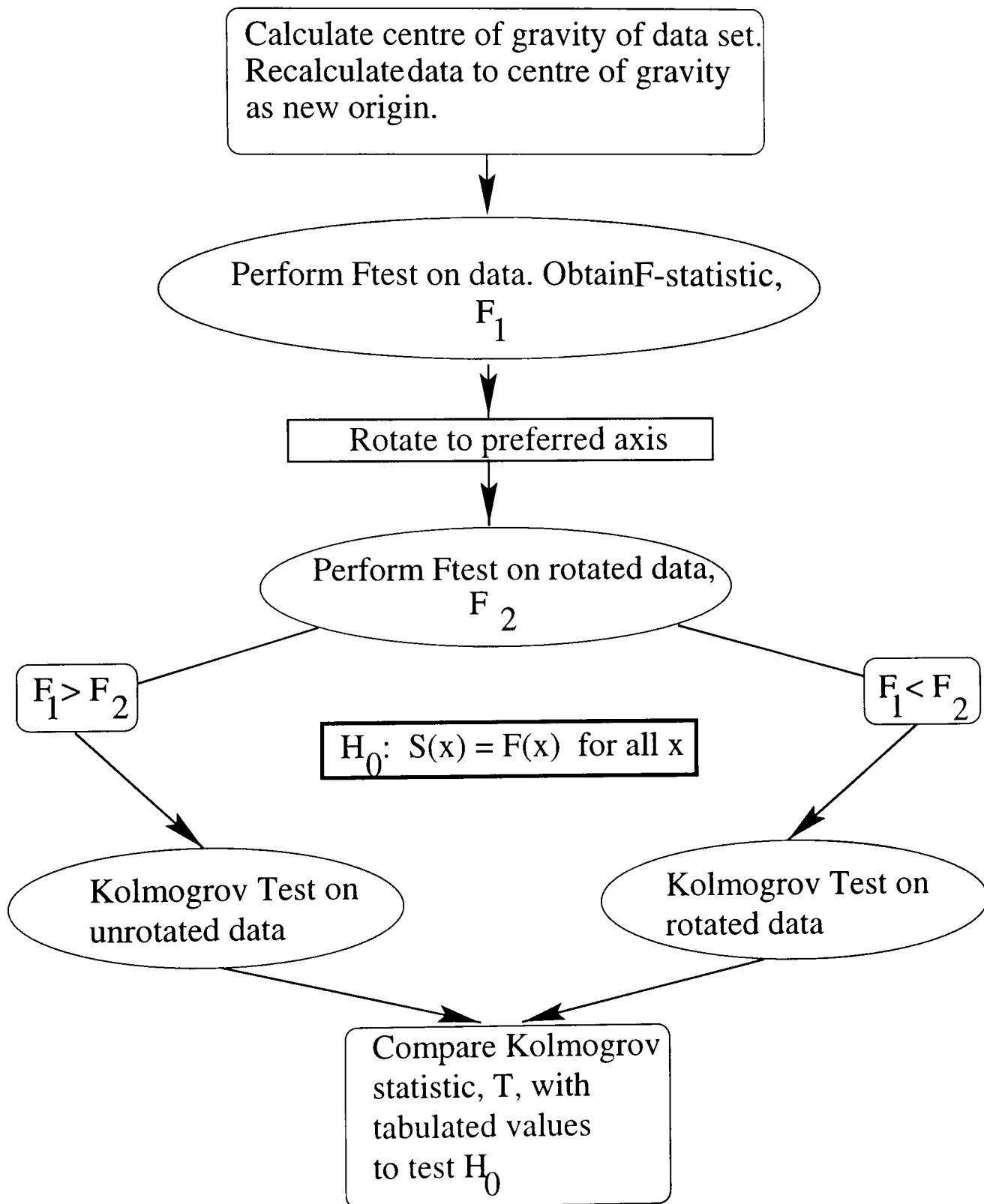


Figure 3.3: Flow chart showing the analysis process for the program stars. The data for the normalised Stokes parameter in question, may be considered as showing some temporal variability, if H_0 is rejected at the level α .

shifted in the x -direction by ± 1 s.e. It is not acceptable to just consider whether $F^*(q)$ provides a reasonable approximation to $S(q)$, as there is an intrinsic error on the position of the $F^*(q)$ curve in the x -direction due to the error on the calculated observed mean. If any of the hypothesised distribution functions for q provide a statistically significant fit with $S(q)$, then the hypothesis, H_0 is proved at that level of significance.

It is immediately apparent from the plots that for both q and u , $F^*(q)$ and $F^*(u)$ provide good fits to $S(q)$ and $S(u)$ respectively, without the need to shift either of the hypothesised distributions in either direction. The statistics confirm this, and only point to failure, and subsequent rejection of H_0 at the 95% confidence level for $F^*(q+se)$ and $F^*(u+se)$, and the 80% level for $F^*(q-se)$ and $F^*(u-se)$. It is apparent from the plots that the maximum vertical separation, T , from $S(q)$ and $S(u)$, is by $F^*(q+se)$ and $F^*(u+se)$ respectively, confirming these results. However, the acceptance of H_0 for $F^*(q)$ and $F^*(u)$ is proof that there is no sign of temporal variability in polarisation during the observations on the 16th.

Observations for the night of the 17th October showed a preferred axis upon a rotation of $\sim 141.7^\circ$, but F-tests indicated a larger value of the F statistic before rotation. Therefore, it is in this frame, that there is a greater likelihood of detecting whether or not the distributions in q and u respectively, can be considered as being part of the same parent distribution. However, comparison with tabulated values indicated that there is no evidence that they could **not** be considered as coming from the same parent population. Kolmogorov tests conducted on the data produced the plots shown in Fig 3.4 (b) and Fig 3.5 (b). Again, these tests indicate that both $F^*(q)$ and $F^*(u)$ are significantly similar to $S(q)$ and $S(u)$, for the hypothesis H_0 to be accepted, i.e. there is no evidence of temporal variability during the observations.

Analysis of the data for the night of the 19th October, provided some unexpected results for a star previously taken as a polarised standard. An F-test performed after a rotation to the preferred axes in the q,u plane, of $\sim 104.2^\circ$ produced a value of the F statistic, $F_2=12.02$, which was significantly greater than that before rotation. $F_1=6.81$. Comparison with tabulated values proved that there is a 99% certainty that the distributions of q and u can not be considered as being samples from the same underlying parent distribution. This points to the possible conclusion that there is some temporal

variability of the source. Plots of the cumulative distribution functions from the subsequent Kolmogorov tests are shown in Fig 3.4 (c) and Fig 3.5 (c). Calculated values of the Kolmogorov statistic, T , indicate that there is a 99% certainty that H_0 is not true for $F^*(q)$. Therefore it is necessary to shift $F^*(q)$ by $\pm s.e.$ to create $F^*(q+se)$ and $F^*(q-se)$, and attempt to fit these distributions to $S(q)$. Unfortunately this proves that there is a 99% certainty that H_0 is not true for $F^*(q-se)$, and a 95% certainty that H_0 is not true for $F^*(q+se)$. This is evidence therefore, that there is some temporal variability in the normalised Stokes parameter, q , on this night of observation. Examination of the cumulative distribution plots for u shows that no hypothetical distribution function between the limits dictated by the observed mean plus or minus the standard error, may be proved to not fit $S(u)$ with a certainty greater than 95% (in the case of $F^*(u+se)$). There is a 90% certainty that $F(u)$ is not successfully modeled by $S(u)$.

F-tests performed on the observations for the night of 20th October, after a rotation of 135.6° to the preferred axis in the Stokes plane, give evidence that the q and u distributions cannot be considered as being samples from the same underlying parent distribution, at the 95% confidence level. Again, the results of the Kolmogorov tests on the individual Stokes parameters, are shown in Fig 3.4 (d) and Fig 3.5 (d). Analysis of the resultant statistics show that $F^*(q)$ and $F^*(u)$, show no deviation from normality. However, Welch tests performed on the data sets for the four nights of observation, reveal no evidence of any temporal variability from night to night.

In conclusion, there appears to be some polarisation variability in both q and u on this night, indicating that this star cannot be considered standard, despite its nomination by Serkowski (1973).

3.2.2 Analysis ξ Per

The assessment of the O star ξ Per was performed in the same manner as for ϕ Cas. F-tests were performed initially on the data for the night of the 16th. These indicated that there was a preferred axis at $\sim 21^\circ$ to that of the observing frame, and that after rotation to this new frame, there was a 99% certainty that the individual q and u distributions cannot be considered as samples from the same underlying parent distribution. Results of

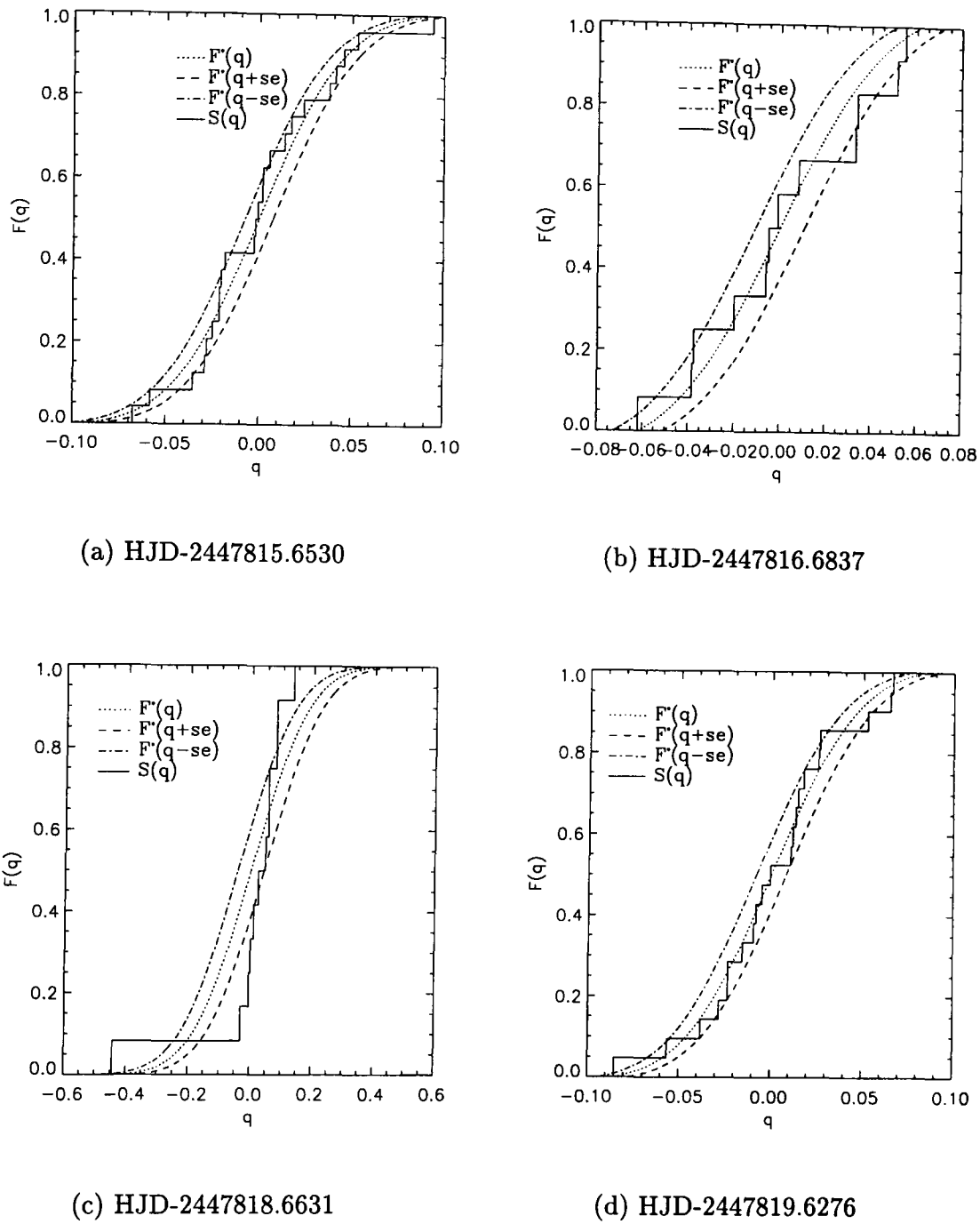
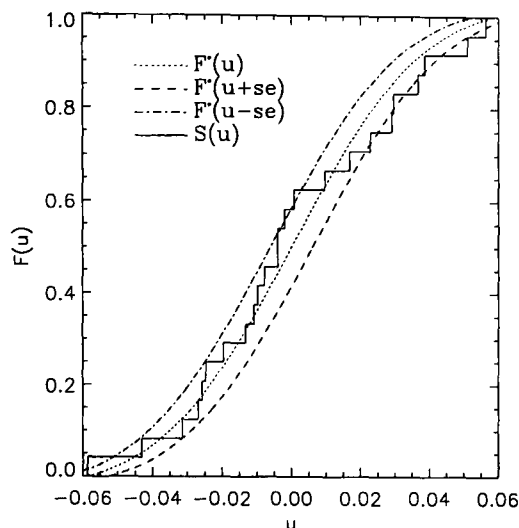
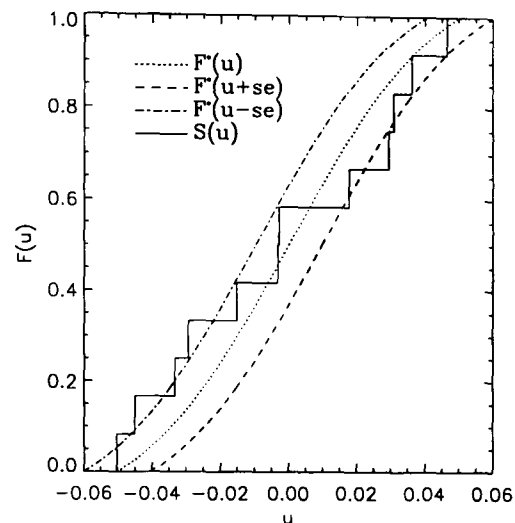


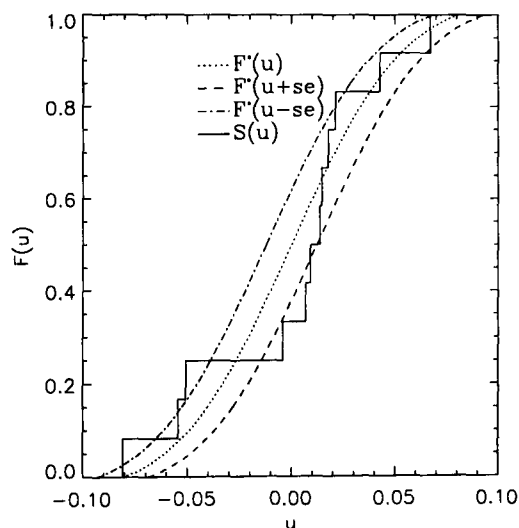
Figure 3.4: ϕ Cas. Plots of the empirical distribution function $S(q)$, and the hypothesised distribution functions $F^*(q)$, $F^*(q+se)$ and $F^*(q-se)$, where se is the standard error of the observed mean. The four plots (a), (b), (c) and (d), correspond to the four nights of observation 16th, 17th, 19th and 20th October 1989. The Julian dates given are for the first data point of that night. Kolmogorov tests for the 19th reveal temporal variability on this night at the 95% confidence level.



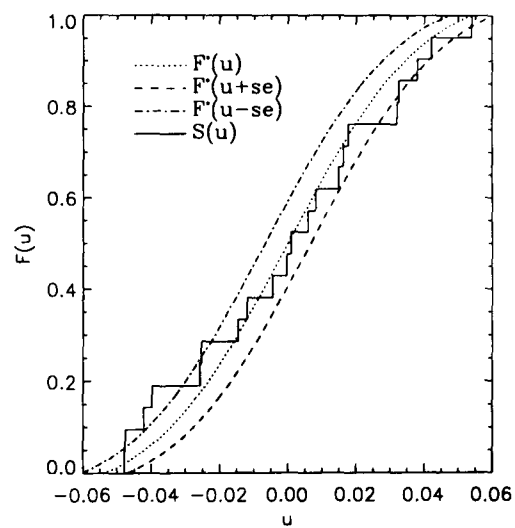
(a) HJD-2447815.6530



(b) HJD-2447816.6837



(c) HJD-2447818.6631



(d) HJD-2447819.6276

Figure 3.5: ϕ Cas. Plots of the empirical distribution function $S(u)$, and the hypothesised distribution functions $F^*(u)$, $F^*(u+se)$ and $F^*(u-se)$, where se is the standard error of the observed mean. The four plots (a), (b), (c) and (d), correspond to the four nights of observation 16th, 17th, 19th and 20th October 1989. The Julian dates given are for the first data point of that night. Kolmogorov tests for the 19th reveal temporal variability on this night at the 90% confidence level.

the Kolmogorov tests are shown in Fig 3.6 (a) and Fig 3.7 (a). The quantitative results indicate that for u , $F^*(u)$ provides a good approximation of $S(u)$, and therefore the real data may be considered as being normally distributed. However, for q , where the best fit to $S(q)$ is provided by $F^*(q)$, there is an 80% certainty that the hypothesis, H_0 is untrue.

F-tests of the data for the night of the 17th indicate that the individual q and u distributions may be considered as belonging to the same parent distribution indicating that there is no temporal variability. Kolmogorov tests add weight to this argument, proving H_0 is true for both q and u , as $F^*(q)$, and $F^*(u)$ both approximate $S(q)$ and $S(u)$ respectively, particularly well. These results are presented in Fig 3.6 (b) and Fig 3.7 (b).

Evidence is provided for some possible temporal variability in both q and u on 19th October. Firstly, after a rotation of $\sim 100.0^\circ$, an F-test yields a value indicating that there is a 99% probability that the individual q and u data sets do not belong to the same underlying parent distribution. Secondly, the results of Kolmogorov tests point to a 95% confidence that the data sets can not be modeled by their generated normal distributions. The shifting of the $F^*(q)$ and $F^*(u)$ hypothesised distributions by up to the standard error, along either direction in q and u respectively, only serves to increase the likelihood of showing a temporal variability, i.e. the statistic T is at a minimum for $F^*(q)$ and $F^*(u)$.

An F-test performed on the data for 20th indicated that there is a 99% probability that the distributions for q and u can not be considered as belonging to the same parent population. Kolmogorov tests on the individual Stokes parameters show no evidence that they are not normally distributed. It is clear then, that the two distributions for q and u , have different variances, where the random variability of the star can be considered as adding in quadrature with the normal noise associated with the observational practice. This difference, could perhaps be as a result of some effect such as blobs of material being emitted from a fixed region on the stellar surface, but on a random time scale. As a result, there will be an underlying intrinsic level of polarisation, which is normal in both q and u , but which shows different variances in the two, since the blobs are moving away from the star along the one axis.

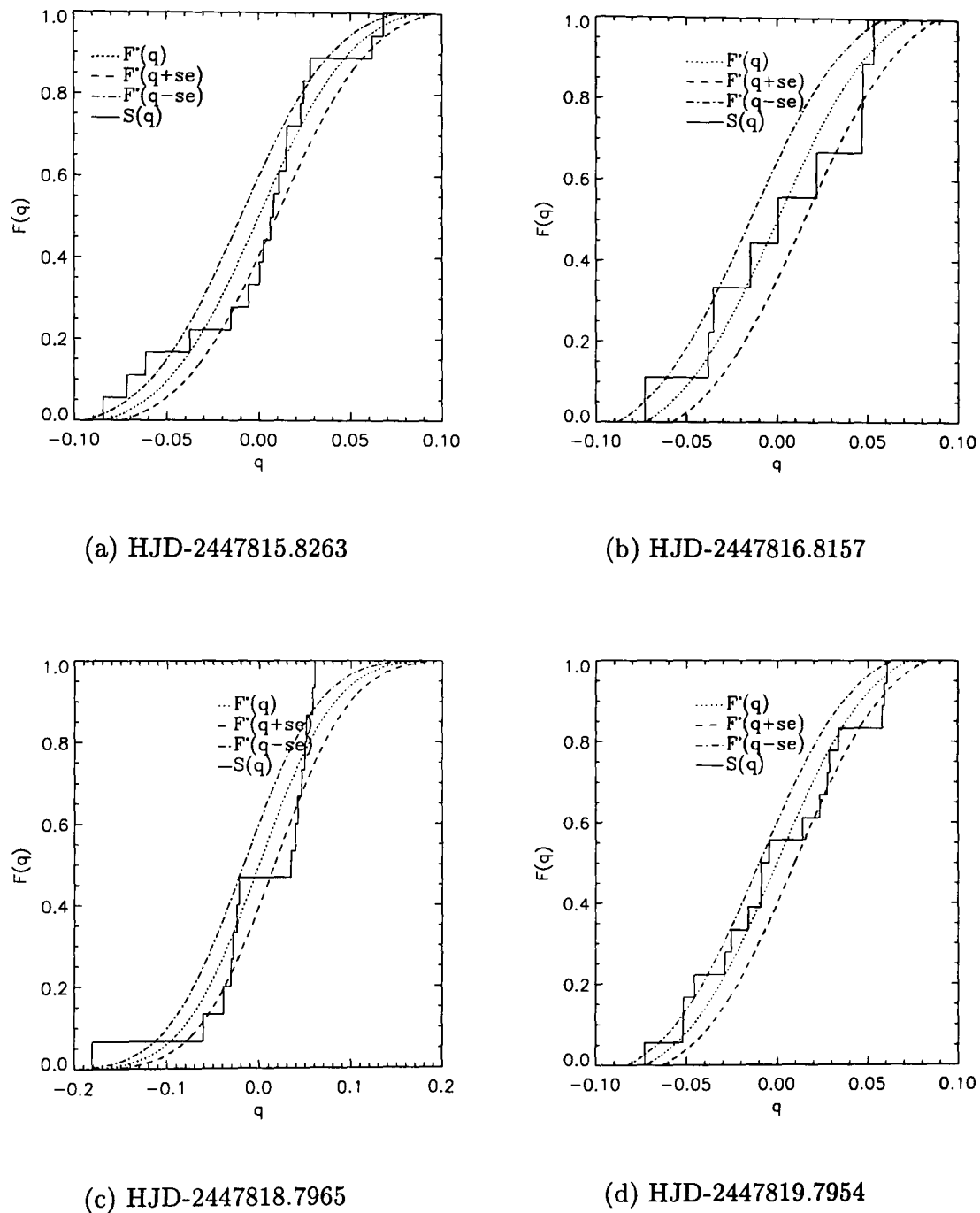
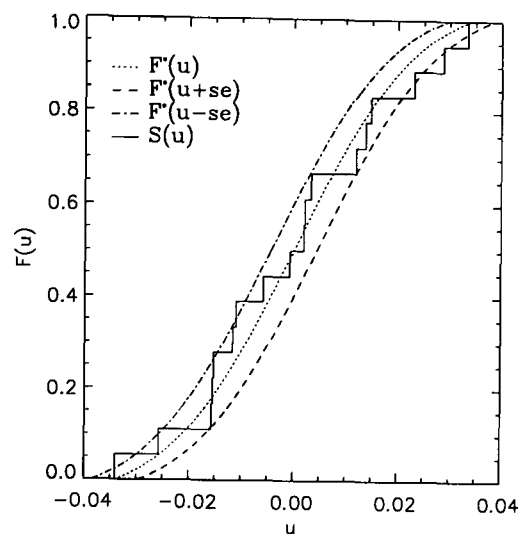
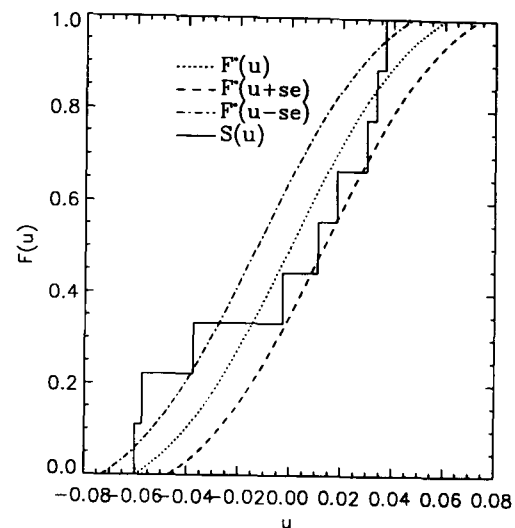


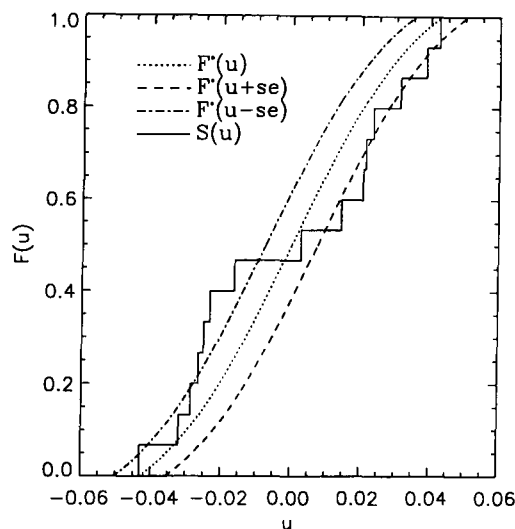
Figure 3.6: ξ Per. Plots of the empirical distribution function $S(q)$, and the hypothesised distribution functions $F^*(q)$, $F^*(q+se)$ and $F^*(q-se)$, where se is the standard error of the observed mean. The four plots (a), (b), (c) and (d), correspond to the four nights of observation 16th, 17th, 19th and 20th October 1989. The Julian dates given are for the first data point of that night. Kolmogorov tests for the 19th reveal temporal variability on this night at the 95% confidence level.



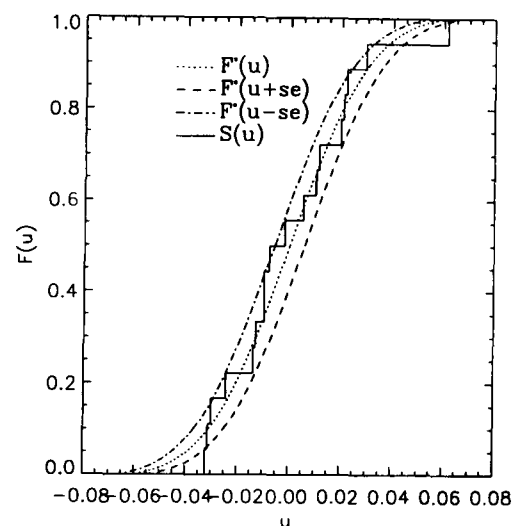
(a) HJD-2447815.8263



(b) HJD-2447816.8157



(c) HJD-2447818.7965



(d) HJD-2447819.7954

Figure 3.7: ξ Per. Plots of the empirical distribution function $S(u)$, and the hypothesised distribution functions $F^*(u)$, $F^*(u+se)$ and $F^*(u-se)$, where se is the standard error of the observed mean. The four plots (a), (b), (c) and (d), correspond to the four nights of observation 16th, 17th, 19th and 20th October 1989. The Julian dates given are for the first data point of that night. Kolmogorov tests for the 19th reveal temporal variability on this night at the 95% confidence level.

3.2.3 Analysis λ Cep

Data for the star λ Cep from David McDavid was analysed and then compared with previously obtained observations (Hayes (1977)), displayed in the next section. McDavid's data was analysed for each individual night to detect any temporal variability within the time scale of a few hours, and then collectively to detect any night to night fluctuations in polarisation.

F-tests performed on data for the night of 16th October indicate that there is no significant difference in the variances of the distributions for q and u . Kolmogorov tests point to the empirical distributions for q and u being modeled well by the theoretical distribution functions $F^*(q)$ and $F^*(u)$ respectively, thus indicating that there was no temporal variability during the time of these observations. Analysis performed for the nights of 17th, 19th and 20th yields the same result. This result is easily seen graphically in Figs 3.8 and 3.9. This is a somewhat disappointing result. It was hoped that p would provide an extended diagnostic to complement work involving the investigation of photometric variability and the development of DACs with this star.

Fig 3.10 displays the cumulative distribution plots for the cumulative data of all the nights of observation. Welch tests performed on the four data sets for the four nights reveal a 99% certainty that the sets can not be considered as belonging to the same parent distribution, i.e. there is some temporal variability from night to night. However, Kolmogorov tests performed on the collective data, indicate there is only an 80% certainty that q is not normally distributed, and there is no evidence that u is not normally distributed. The contradiction between the results of the Welch Test and the Kolmogorov tests may be explained by the different powers of the two tests. It must also be remembered that for a Welch test to be conducted, the individual data sets must all be normally distributed. For a more conclusive result to be determined, it would clearly be necessary to obtain much more data on this star. Although the Kolmogorov Test is recognised as a reliable test for a number of data points as low as 10, the likelihood of detecting any variability, and of agreement between the two different tests, can only be improved by a more comprehensive observing campaign.

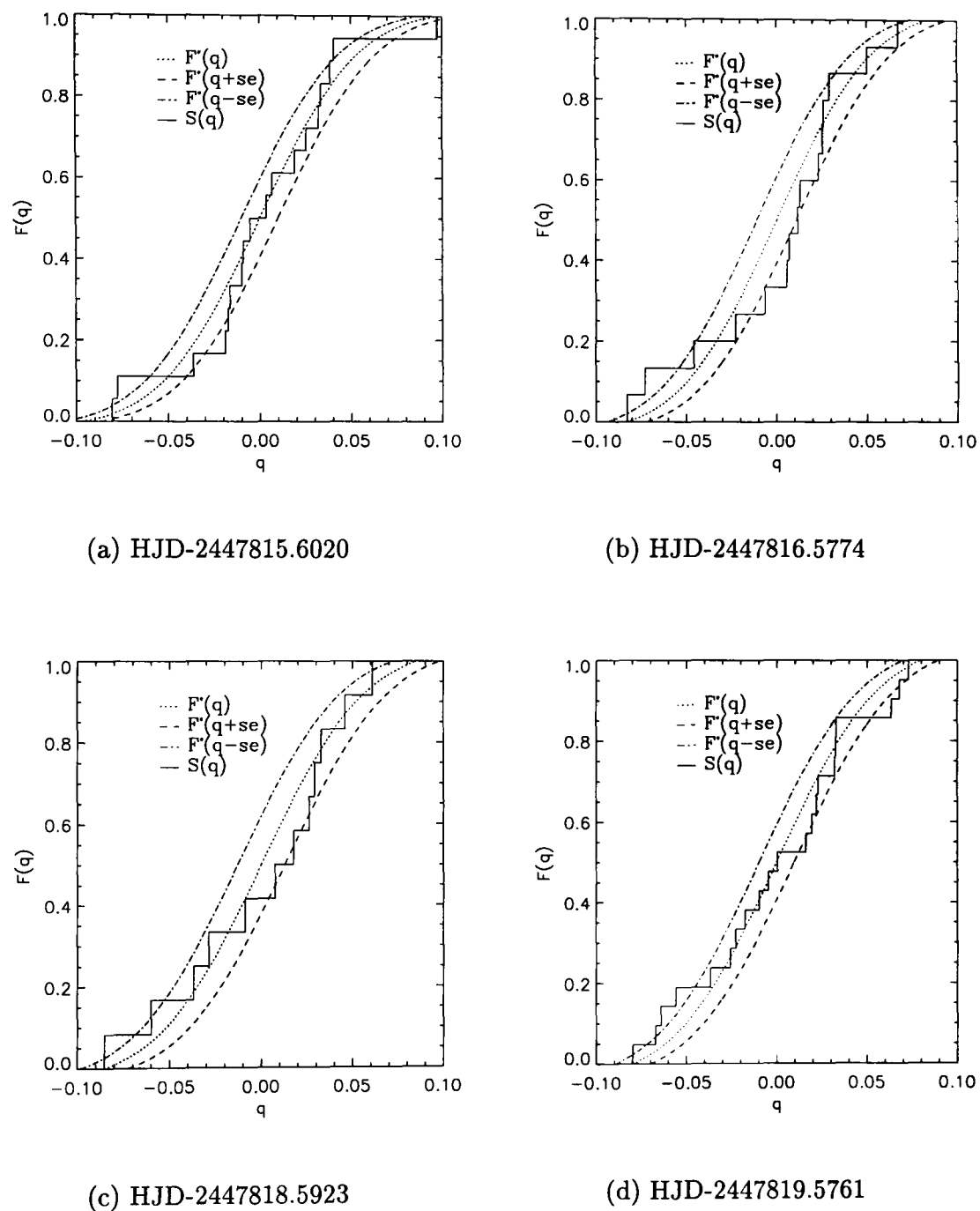
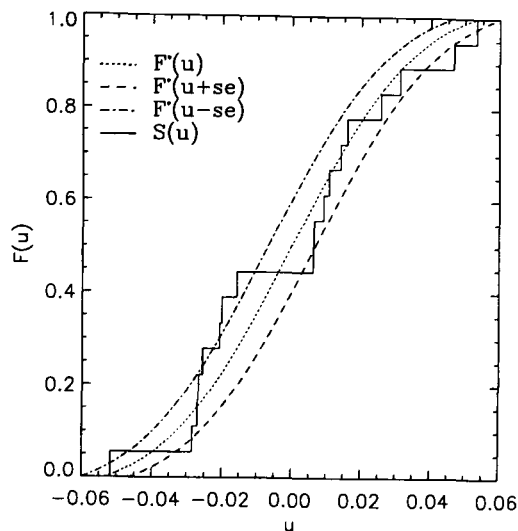
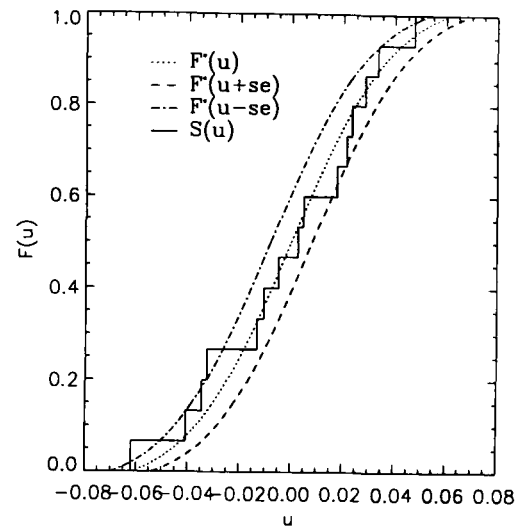


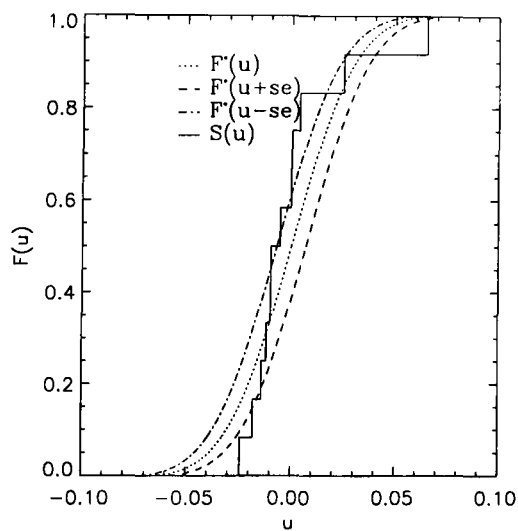
Figure 3.8: λ Cep. Plots of the empirical distribution function $S(q)$, and the hypothesised distribution functions $F^*(q)$, $F^*(q+se)$ and $F^*(q-se)$, where se is the standard error of the observed mean. The four plots (a), (b), (c) and (d), correspond to the four nights of observation 16th, 17th, 19th and 20th October 1989. The Julian dates given are for the first data point of that night. Kolmogorov tests detect no temporal variability of q during any of the observed nights.



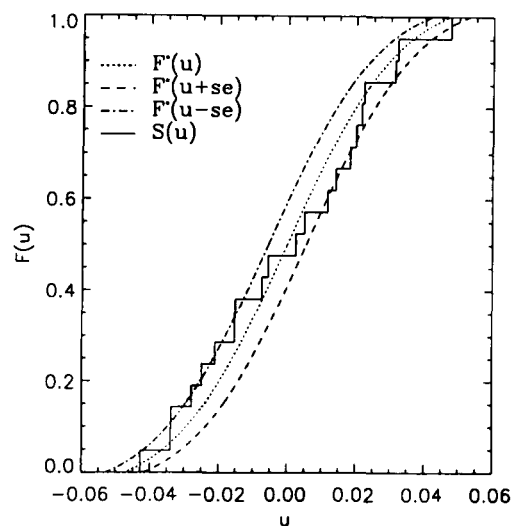
(a) HJD-2447815.6020



(b) HJD-2447816.5774

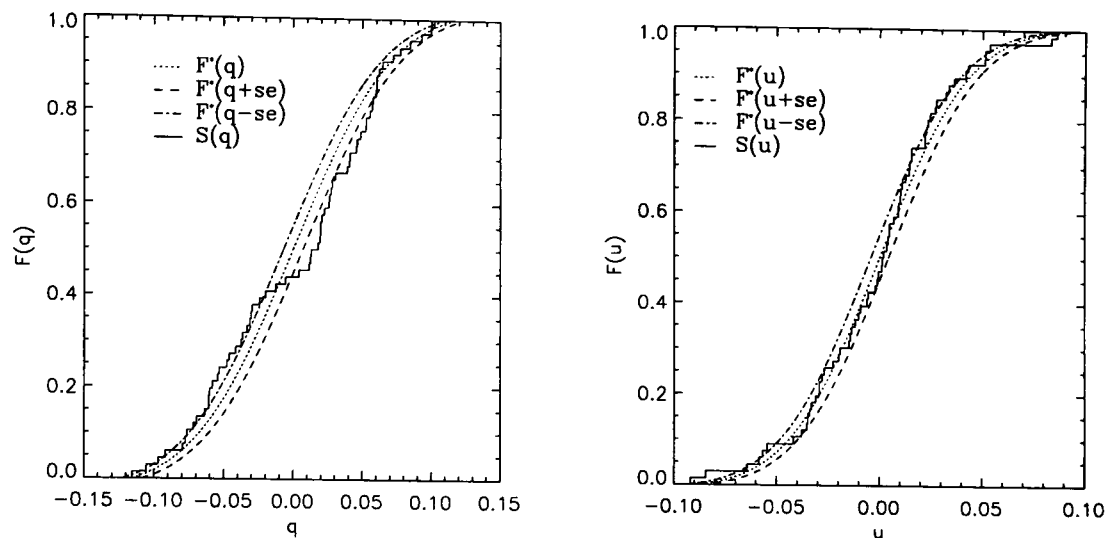


(c) HJD-2447818.5923



(d) HJD-2447819.5761

Figure 3.9: λ Cep. Plots of the empirical distribution function $S(u)$, and the hypothesised distribution functions $F^*(u)$, $F^*(u+se)$ and $F^*(u-se)$, where se is the standard error of the observed mean. The four plots (a), (b), (c) and (d), correspond to the four nights of observation 16th, 17th, 19th and 20th October 1989. The Julian dates given are for the first data point of that night.



(a) Cumulative distribution plots of q (b) Cumulative distribution plots of u

Figure 3.10: λ Cep. Plots of the empirical distribution function $S(q)$, $S(u)$ and the respective hypothesised distribution functions, where se is the standard error of the observed mean. Each plot represents the cumulative data over the four nights of observation.

3.2.4 Analysis of Alternative Data on λ Cep

Hayes (1977) collected data on λ Cep spanning 32 months, from an observing campaign at the Harriman Observatory of Columbia. Tests were conducted on all 74 observations of this star from March 1974 to October 1976, by comparing the sample variances with the theoretical variances derived from photon counts. He concluded that there is an intrinsic variability at a significance level of less than 0.05 %. It is stated that the observed and theoretical variances were found to differ at a significance level of less than 0.05% over the following intervals : 1974 March 26-27, October 8-9, October 10-11, October 11-12; 1975 May 8-9; 1976 August 31-September 1, September 29-30. The data provided by David McDavid would tend to dispute the presence of polarimetric variability. When Hayes' data were tested using the Kolmogorov test (see Fig 3.11), the statistics point to there being no evidence that the empirical distribution functions for q and u may not be modeled well by the normal distributions $F^*(q)$ and $F^*(u)$ respectively. In fact reference to the histograms shown in the figure, reveal the normal shape of these distributions. It must be noted, however, that for q there is no data on the histogram of less than $q = -0.1$ %, implying a departure from the normal distribution in this left side wing. This can also be detected

in the cumulative distribution plot for q , where $S(q)$ does not coincide well with the hypothesised distributions for $q < -0.1$. However, the Kolmogorov test indicates that this departure is not significant enough to prove that the real distribution can be considered as anything other than normal. It must be remembered that whilst a histogram provides a good picture of any behaviour and leads to a comparison with the theoretical normal distribution, the number of bins and the bin sizes are arbitrary. It is also necessary to have a large number of data points. Therefore, greater weight should be given to the results of the Kolmogorov tests.

An F-test performed on the data in the frame corresponding to the preferred axis indicates that at the 99% confidence level, the distributions in q and u may not be considered as belonging to the same parent population. It is apparent from Fig 3.11 (a) and (b), that both q and u are normally distributed, but that their variances are different. When shifted to the centre of gravity frame, u reaches a minimum at ~ -0.08 and a maximum of $\sim +0.08$, whilst q shows a minimum and maximum of ~ -0.15 and $\sim +0.15$ respectively. Hence, the F-test picks out this difference in the two variances.

The required rotation from the original frame of all the data points to the preferred axis corresponds to a rotation of $\sim 61^\circ$ which is in agreement to the polarisation angle of $\sim 56.4^\circ$ given in Hayes (1977). If emission line stars and known intrinsically polarised stars are omitted, there are 64 stars listed in Hall's (1958) blue-band polarisation catalog that are located in an area of sky 8° square centered on the galactic coordinates of λ Cep. The mean position angle of these stars is $57^\circ \pm 2^\circ$. It, therefore appears that the interstellar polarisation in this region of the galaxy is reasonably well determined. Thus, it is possible that the preferred orientation of the data may be as a result of interstellar polarisation. However, this must be treated with caution. As the angle of the preferred axis of the data, is so close to the polarisation angle of 56.4° , one must not ignore the effect of Serkowski Bias, which has not been accounted for in Hayes (1977). Apparent non-normality along the direction of p may result from effects of variable Serkowski bias, which itself may vary from night to night as the uncertainties of any measurements varies from one night to the next.

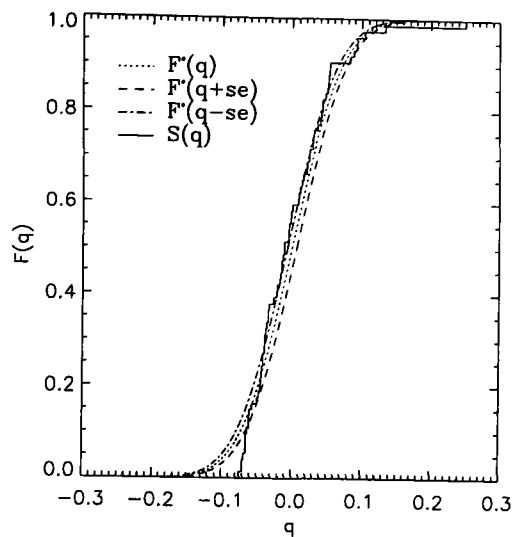
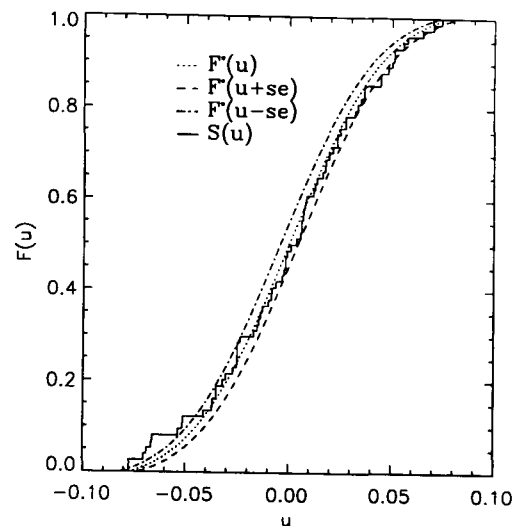
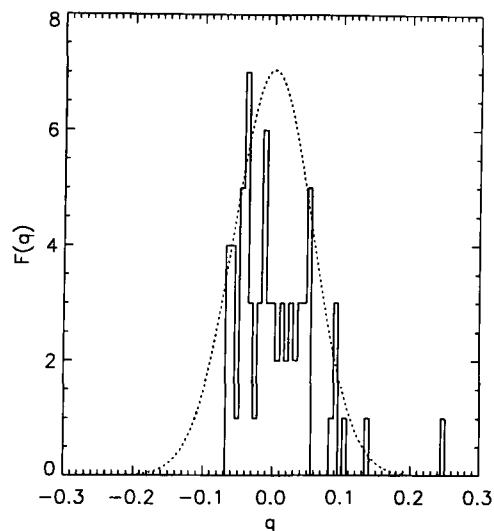
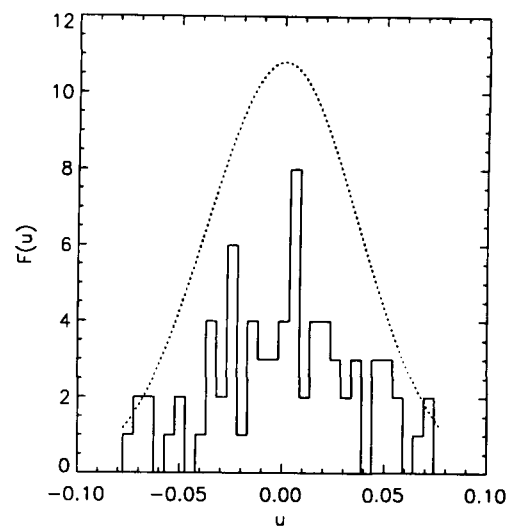

 (a) Cumulative distribution functions for q

 (b) Cumulative distribution functions for u

 (c) Histogram of q binned into 50 bins

 (d) Histogram of u binned into 30 bins

Figure 3.11: λ Cep. Daniel Hayes data (Hayes, 1977). (a) and (b) show plots of the empirical distribution function $S(x)$, and the hypothesised distribution functions $F^*(x)$, $F^*(x+se)$ and $F^*(x-se)$, where for (a) $x=q$, and for (b) $x=u$. se is the standard error of the observed mean. (c) and (d) show the individual normalised Stokes parameters binned to produce histograms as an approximation of the real distribution, plotted with the normal distribution generated from the observed mean and standard deviation. The data is from the Harriman Observatory of Columbia, and spans 32 months. In all, 74 observations were made on 31 nights.

3.3 Kolmogorov Technique for Analysis of the Polarisation Angle

If a source is unpolarised, it would be expected that all position angles, $\theta(=\frac{1}{2}\arctan(\frac{u}{q}))$ are equally probable within the data in the range 0-180° and hence any empirical cumulative distribution function of this parameter can be compared with a cumulative distribution function, CDF, which is linear, Fig 3.12. It follows that if a source is polarised, then to test whether there is any temporal variability, the data should be transferred to the centre of gravity coordinate system, and a comparison made between the empirical distribution function and the linear theoretical distribution. A significant deviation would indicate a temporal variability, or perhaps a difference in the magnitude of the variances in q and u respectively. Such a differences in the variances, would not lead to a distribution of θ around the centre of gravity which was circularly symmetrical, but which would be more elliptical, thus producing a CDF which would not be linear.

When constructing the CDF plots to analyse θ , it easier to show the three empirical distribution functions representing those calculated with three different origins representing the centre of gravity, (q_0, u_0) ; and $(q_0+s.e., u_0)$, and $(q_0, u_0+s.e.)$, where s.e. is the standard error of the observed mean. These plots may then be compared with the straight line which would result from a normally distributed parent population, where all values of θ are equally probable. If the data shows some temporal variability, or if the variance on the distributions in q and u are not equal, then the EDF's will deviate from the straight line. However, if any EDF can be shown to fit significantly well with the straight line, then the sample data may be said to be normally distributed around that respective origin.

Due to the standard uncertainty on the observed mean, there is an error on the determination of the centre of gravity position. Fig 3.13 shows the data displayed in q, u space, with the centre of gravity, q_0, u_0 as the origin. Of course, due to the error, s.e. on the determination of this position, the origin for the coordinate system may be taken anywhere inside the circle. The preceding sections present the analysis of the program stars by Kolmogorov testing θ .

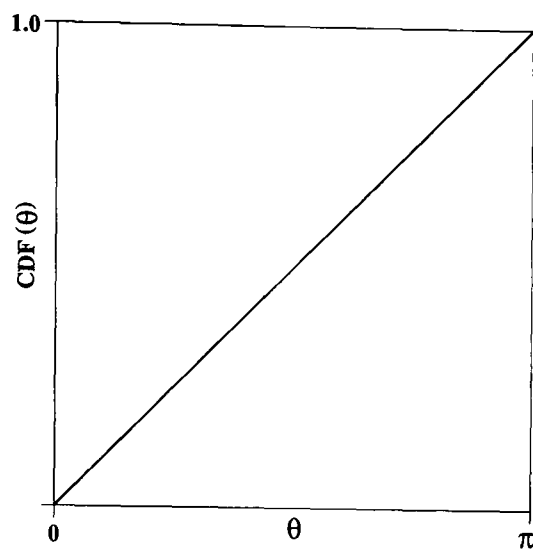


Figure 3.12: The CDF for θ for an unpolarised source, or a polarised standard viewed in the centre of gravity coordinate system.

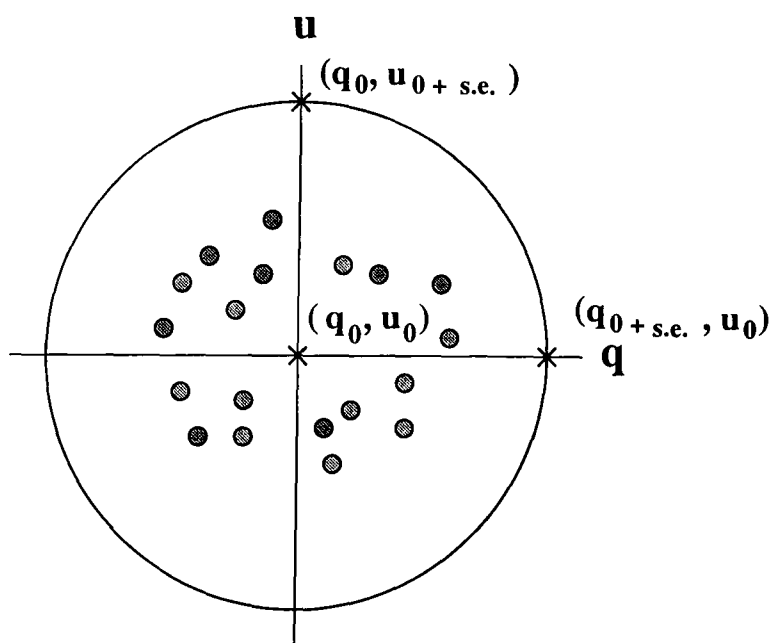
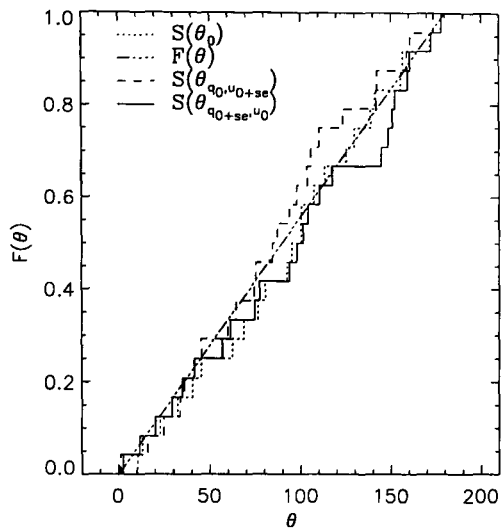


Figure 3.13: Plot in q,u space with the centre of gravity, q_0, u_0 as the origin. Due to the standard error on the observed mean, there is an error on the determination of the centre of gravity position. It is possible that it may be anywhere within the 1σ circle. The EDF plots in the Kolmogorov plots for the polarisation angle, θ , will show three sample EDF's calculated with origins at (q_0, u_0) , $(q_0 + s.e., u_0)$ and $(q_0, u_0 + s.e.)$, where s.e. is the standard error of the observed mean.

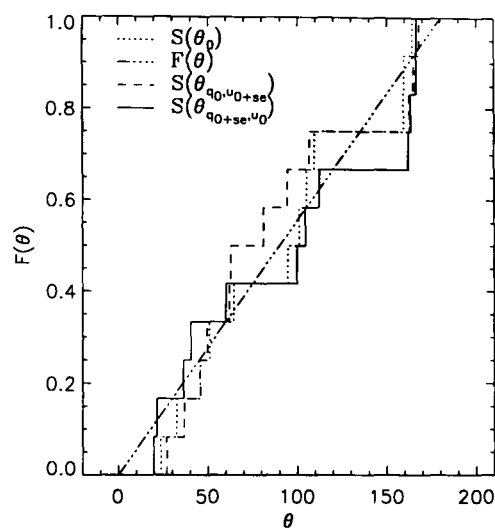
3.3.1 Analysis ϕ Cas

The CDF plots of the polarisation angle for the data of ϕ Cas on the nights of observation, are displayed in Fig 3.14. Kolmogorov tests on the observations of both the 16th and the 17th show that the data for θ fit well with the straight line $F(\theta)$, and hence that θ is normally distributed. However, observations taken on the 19th appear to indicate that at the 80% confidence level, $S\theta$ does not fit $F(\theta)$. This should be treated cautiously. Further analysis, reveals that the EDF, $S(\theta_{q_0-(0.7)s.e.}, u_0)$ is an acceptable fit to $S(\theta)$ (see Fig 3.15). So, therefore, when the error on the the calculated mean of the centre of gravity coordinates, is taken into account, it is not possible to discount the possibility that the data is normally distributed. Fig 3.15 shows how a change in the position of the calculated centre of gravity, due to the uncertainty on this position, moves and **changes the shape** of the empirical distribution functions.

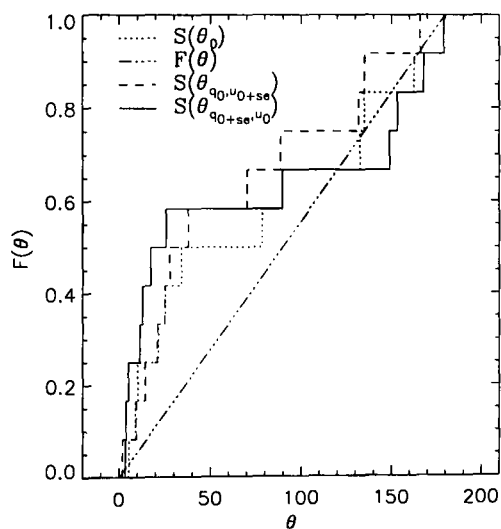
The EDF plots for the night of the 20th reveal a good fit, indicating that there is no temporal variability in θ on this night.



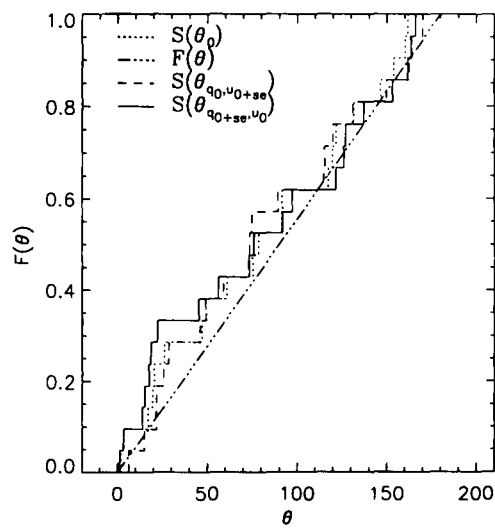
(a) HJD-2447815.6530



(b) HJD-2447816.6837

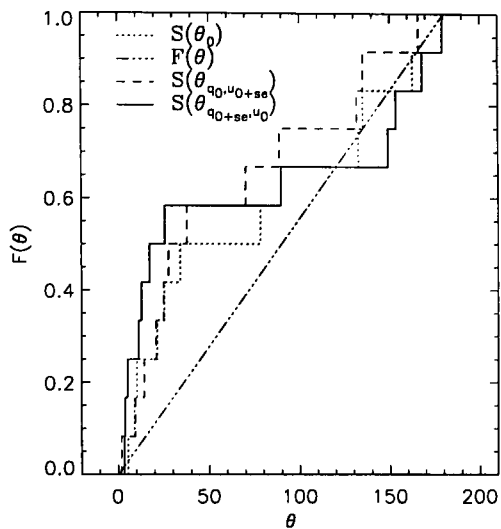


(c) HJD-2447818.6631

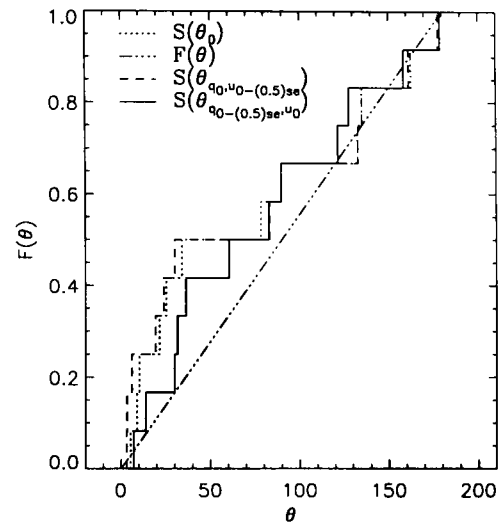


(d) HJD-2447819.6276

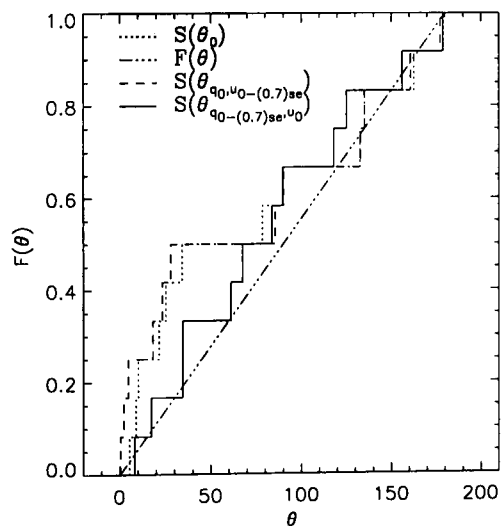
Figure 3.14: ϕ Cas. Plots of the empirical distribution functions $S(\theta_0)$, $S(\theta_{q_0+se, u_0})$ and $S(\theta_{q_0, u_0+se})$ where se is the standard error of the observed mean, and the hypothesised distribution function $F(\theta)$ for a normally distributed set of θ . The four plots (a), (b), (c) and (d), correspond to the four nights of observation 16th, 17th, 19th and 20th October 1989. The Julian dates given are for the first data point of that night.



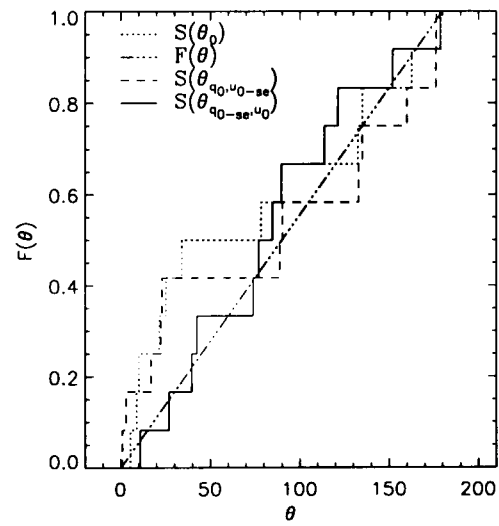
(a)



(b)



(c)



(d)

Figure 3.15: ϕ Cas. The four CDF plots for ϕ Cas on the night of 19th October 1989 showing the effect upon the empirical distribution functions of the real data, calculated from different centre of gravity positions, where u_0 and q_0 are varied by different factors of the s.e., up to -1.0 s.e. A better fit to $S(\theta_0)$ is obtained with $S(\theta_{q_0-se, u_0})$.

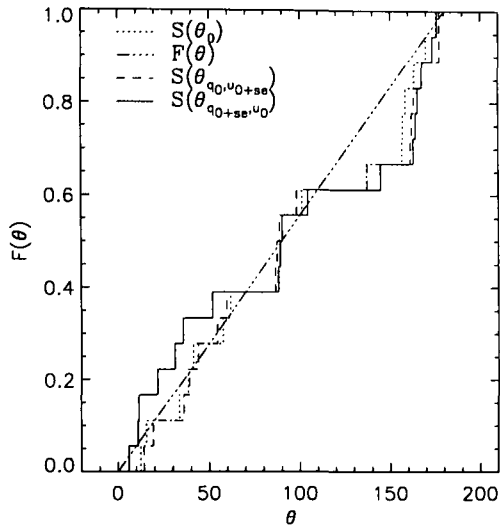
3.3.2 Analysis ξ Per

The same analysis as was performed on ϕ Cas was applied to ξ Per. Kolmogorov tests proved that there was good fit on all nights of observation. There was no evidence of temporal variability of the polarisation angle on any night. This result can be seen quite clearly in the plots of the cumulative distribution functions in Fig 3.16

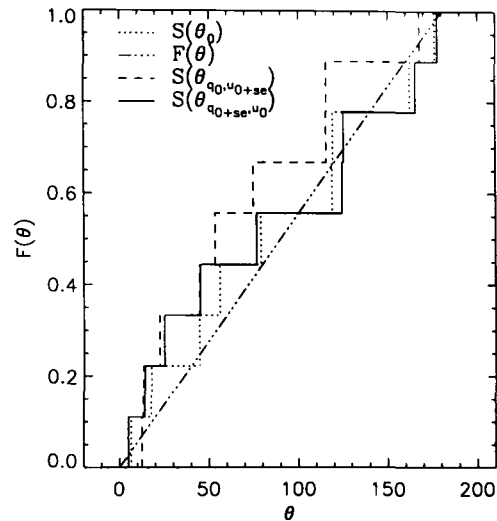
3.3.3 Analysis λ Cep

Kolmogorov tests performed on the polarisation angle data on the nights 16th, 17th and 20th indicate that the observed values may be considered as belonging to an underlying parent normal distribution. Preliminary analysis of the data for the 19th show that the EDF, $S(\theta_0)$ calculated for the centre of gravity position, is not modeled well by the straight line $F(\theta)$, and therefore the polarisation angle data for this night may not be considered as belonging to an underlying parent distribution. However, Fig 3.17(c) shows quite clearly that if the centre of gravity is just one standard error, s.e., out in the u direction, that there is then a good fit, and the Kolmogorov statistic indicates a good fit with $F(\theta)$.

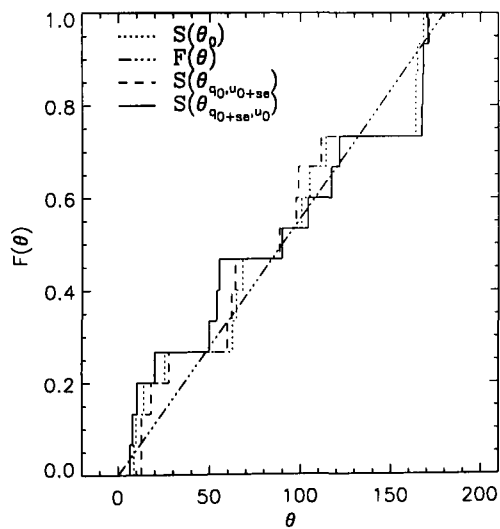
Fig 3.18 displays the CDF plots for the total data file of all four nights of observation. Kolmogorov tests show that there is no evidence for any temporal fluctuation in polarisation angle from night to night.



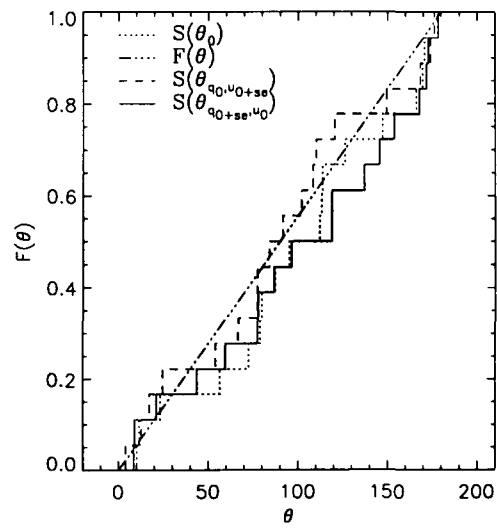
(a) HJD-2447815.8263



(b) HJD-2447816.8157

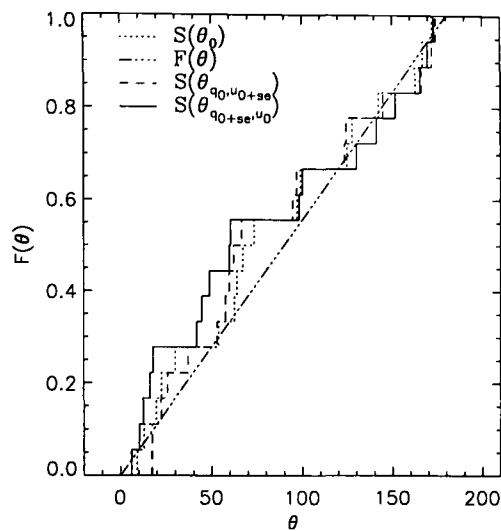


(c) HJD-2447818.7965

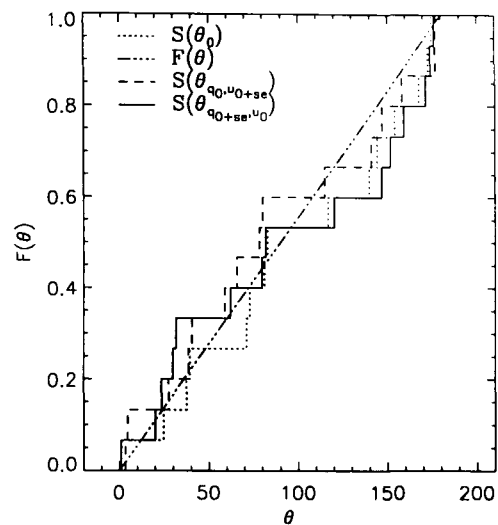


(d) HJD-2447819.7954

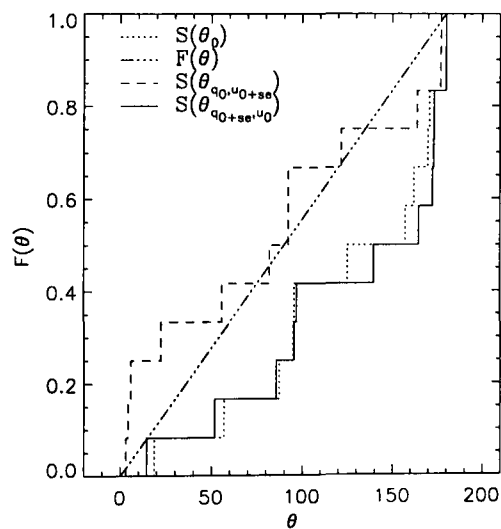
Figure 3.16: ξ Per. Plots of the empirical distribution functions $S(\theta_0)$, $S(\theta_{q_0+se, u_0})$ and $S(\theta_{q_0, u_0+se})$ where se is the standard error of the observed mean, and the hypothesised distribution function $F(\theta)$ for a normally distributed set of θ . The four plots (a), (b), (c) and (d), correspond to the four nights of observation 16th, 17th, 19th and 20th October 1989. The Julian dates given are for the first data point of that night.



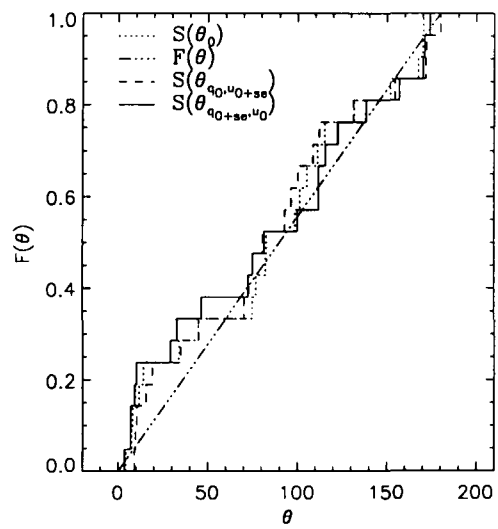
(a) HJD-2447815.6020



(b) HJD-2447816.5774



(c) HJD-2447818.5923



(d) HJD-2447819.5761

Figure 3.17: λ Cep. Plots of the empirical distribution functions $S(\theta_0)$, $S(\theta_{q_0+se, u_0})$ and $S(\theta_{q_0, u_0+se})$ where se is the standard error of the observed mean, and the hypothesised distribution function $F(\theta)$ for a normally distributed set of θ . The four plots (a), (b), (c) and (d), correspond to the four nights of observation 16th, 17th, 19th and 20th October 1989. The Julian dates given are for the first data point of that night.

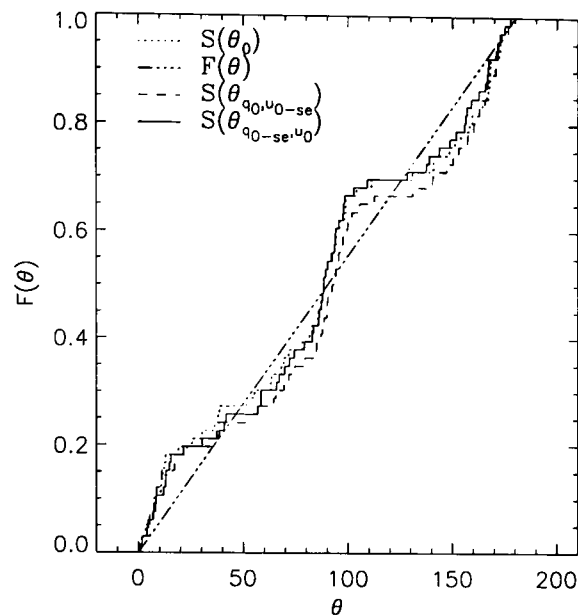


Figure 3.18: CDF plots for the total data of the four nights of observation of λ Cep. It is interesting to note the wave-like nature of the curve. The curve expected elliptical distribution in q, u space, would be expected to cross the straight line $F(\theta)$ only twice.

3.4 Conclusion

The Kolmogorov technique has been investigated as a means of detecting low levels of temporal variability in polarisation, and polarisation angle, of two O stars, and a previously believed standard star of type F0. The technique, usually used to compare two distributions, has been used here to compare observed data, with the theoretical normal distributions generated from the observed mean and standard deviation. Calculation of the Kolmogorov test statistic, T , and comparison with tabulated values has allowed the testing of the null hypothesis, H_0 ,

$$H_0 : F(x) = F^*(x) \text{ for all } x \text{ from } -\infty \text{ to } +\infty$$

Particular attention has been made towards assessing the influence of not knowing the mean values perfectly, and on the statistical interpretation. Examples are shown, where comparison between the CDF and EDF of data from a star, initially lead to the conclusion that H_0 fails, but when the error on the position of the centre of gravity of the data is taken into account, H_0 can be taken as being true. It is therefore concluded that for any realistic determination of temporal variability of the polarisation of a star, by the Kolmogorov statistical test, a more conservative approach should be taken, allowing for the uncertainty of the distribution against which the data are being compared.

3.4.1 ϕ Cas

It is concluded that the star ϕ Cas does show some polarisation variability within the time scale of one night. Kolmogorov tests on the night of 19th October 1989 indicate failure at the 99% confidence level of the hypothesis, H_0 , for q . By considering the standard error on the centre of gravity position, and all possible CDF curves generated, it was not possible to alter this conclusion, and hence there is a significant indication of temporal variability during this night. There is also temporal variability in u at the 90% confidence level. An F-test performed on the two distributions for q and u , indicate that there is a 99% confidence that the two distributions can not be considered as belonging to the same parent population, further pointing to the presence of variability.

Examination of the polarisation angle, θ , leads to the conclusion that there is no variability on the 16th, 17th and 20th. Initial comparison of the straight line CDF expected for a normally distributed data set of θ , with the EDF of the data for the 19th point to there being further evidence of temporal variability on this night, as at the 80% confidence level, H_0 is shown to be false. However, by recalculating the EDF, by varying the centre of gravity of the data, by up to \pm s.e., it is clear that an EDF may be made to fit significantly well with the normal CDF, thus proving that there is indeed no evidence of any variability of θ on this night. A Welch test does not detect the presence of any variability in q or u , from night to night.

The presence of a temporal variation of the level of polarisation, p , of this star, but with no evidence of any variability of θ is consistent with a model of blobs of material being emitted from a spot on the stellar surface, which move away from the star along the same axis. As such, the level of p would be expected to change, as the number of blobs present at any one time varies, and their distances from the surface increases. The value of θ would be expected to remain unaltered. The presence of variability in this star is in contradiction with previous acceptance as a polarised standard (see Gehrels (1974)). It should be noted that the determined preferred axis of the total data set for all observations, is $\sim 103^\circ$, which compares favourably with the quoted value of interstellar polarisation for this star, $\theta(\lambda_{max})=9.4^\circ$ given in Gehrels (1974). Therefore, it is possible that any polarimetric axis intrinsic to the star on the night of the 19th, is almost coincident

with the axis of interstellar polarisation. However, this conclusion must be treated with caution, as such an effect would be apparent due to the effect of Serkowski bias.

3.4.2 ξ Per

Kolmogorov tests conducted on the data for ξ Per indicate that the data for both q and u on 17th and 20th may be considered as being normally distributed, and therefore that there was unlikely to be any temporal variability in polarisation present on these nights. However, it must be noted that the results of an F-test on the 20th show that at the 99% confidence level, the distributions in q and u may not be considered as belonging to the same parent population. It is clear then that on this night, the two distributions have different variances, which could perhaps be the result of an effect such as blobs of material being emitted from a fixed region on the stellar surface, but on a random time scale. As a result, there will be an underlying intrinsic level of polarisation, which is normal in both q and u , but which shows different variances for these parameters, since the blobs are moving away from the star along the one axis. F-tests performed on observations for 16th and 19th provide a similar result, and a Kolmogorov test on data for 16th show that at the 80% confidence level, H_0 is false for the q distribution. Further more, the Kolmogorov statistics from the 19th indicate a temporal variability in q and u at the 95% confidence level. There is therefore strong evidence for temporal variability within the time scale of a few hours within this star. Similarly to ϕ Cas, there is however no evidence of any temporal variability of θ , either within the time scale of one night, or from night to night.

3.4.3 λ Cep

Kolmogorov tests performed on the McDavid data for all four nights of observation for this star, reveal that for each night, they fit well with the normal distributions generated from the observed mean and standard deviation for that respective night. However, F-tests reveal that there is evidence that the q and u distributions may be considered as not belonging to the same underlying parent population at the 95% confidence level on the 19th, and at the 99% confidence level on the 20th, indicating that there is a difference in the variances in q and u at this level of significance.

Welch tests performed on the four data sets, representing the four nights of observation, indicate that at the 99% confidence level, the four data sets in q and u may not be considered as belonging to the same distribution. Surprisingly, a Kolmogorov test performed on the collective data set for all four nights, yields a different result, and instead points to there only being a confidence of 80% that q is not normally distributed, i.e. that the four data sets are samples from the same underlying parent normal distribution. There is no evidence from the Kolmogorov test that there is any night to night variation in u . This apparent contradiction between the two tests is as a result of the difference in their respective powers. More data is clearly needed before a more definite conclusion may be reached.

Analysis of the the polarisation angle, θ , reveals no evidence of night to night fluctuation, or any evidence of variability within the time scale of one night. Initial findings from a Kolmogorov test on θ on the 19th indicate that there is some temporal variability present, but when the error on the determined centre of gravity of the data is allowed for, any temporal variability has no statistical foundation.

Comparison has been made between the data provided by David McDavid and that of Hayes (1977). Hayes concluded that there was an intrinsic variability at a significance level of less than 0.05% over the intervals : 1974 March 26-27, October 8-9, October 10-11, October 11-12; 1975 May 8-9; 1976 August 31-September 1, September 29-30. However, when this data was analysed using the Kolmogorov test, the conclusion reached was that there was no firm evidence of any temporal variability.

In conclusion it is clear that there is need for a long and sustained observation program on λ Cep, in order to clarify the situation, especially since the star has been selected for special study of DACs.

3.4.4 Summary

The existence of polarimetric variability within the timescale of one night, inherent to the previously considered polarisation standard, ϕ Cas, has been detected by Kolmogorov testing . A Welch test reveals no indication of variability from night to night. Evidence

of temporal variability has been demonstrated for ξ Per, in accordance with spectroscopic variability discussed in Heinrichs (1998). Evidence for variability of p in λ Cep has been put into question, and clearly further data is needed on this star.

The use of the Kolmogorov technique has been examined as a means of detecting low levels of variability in both p and θ . The Welch test and F-test have been used as a control on the technique, to compare conclusions about variability detected with each method. Differing results due to the respective power of each of the statistical tests, have been commented on. Particular attention has been given to the intrinsic error present on the determination of the centre of gravity of a distribution, and its propagation to the theoretical normal CDF plots generated from the real observed mean and standard deviation. It has been shown that where normally a Kolmogorov test would lead to the conclusion of the presence of some variability, the inclusion of the standard error on the observed mean, can result in the rejection of this conclusion. Hence, this method of testing is more conservative and appropriate to the investigation of possible polarimetric variability.

Chapter 4

A Liquid Crystal Polarimeter

Traditionally, the general detection of polarisation is achieved by rotating a half wave plate before a fixed polarising element. The polarimetric modulation is achieved by the continuous rotation of the wave plate. Light passing through the optical elements is then fed to a photo-multiplier with a Fabry lens. However, when performing spectropolarimetry, the photo-multiplier (PM) is inefficient as it is a single element detector and sequential scanning is required. In fact when comparing the use of a PM to the use of CCD detector with N pixels, it would take N times as long to achieve the same signal with the PM. When performing spectropolarimetry, to obtain one spectrum by sequential scanning usually takes an inordinate amount of time, and fluctuations in the Earth's atmosphere become a significant problem. Conventionally a spectrometer is used as the means of exploring the variation of stellar polarisation with wavelength. The optical system requires the modulator to be placed prior to it and an image of the star to be formed on the entrance slit. In such a design, beam wobble induced by the rotatable wave plate will cause an image motion on the slit and give rise to false modulations, particularly if the image spread by 'seeing' is larger than the slit width.

No matter the chosen system, rotation of the wave plate may cause movement of the light beam passing through it, thus producing spurious signals which may be larger than the polarimetric signal of interest.

By using a wave plate where retardation is controlled by electronic means, it should

be possible to record individual Stokes' parameters by 'switching' the polarisation state of the modulator rather than rotating it. Therefore, the problem of image wobble is negated.

To this end, a Liquid Crystal Variable Retarder manufactured by Meadowlark, has been investigated, as a means of performing polarimetry. Inevitably mechanical rotation will be required to allow measurement of pairs of Stokes' parameters (Q,U) needed to define the linear polarisation state of the stellar light. However, with the incorporation of two liquid crystals in succession, it should be possible to develop a system which can be controlled entirely electronically.

4.1 The Meadowlark Liquid Crystal Variable Retarder

The Meadowlark Liquid Crystal Variable Retarder, may operate in the visible to near infrared region, and can produce electrically controllable attenuation, linear polarisation or phase modulation. The liquid crystal may be implemented just as a typical traditional fixed wave plate. Pure phase modulation may be achieved by aligning the optic axis of the liquid crystal parallel to a linearly polarised input beam. The liquid crystal cell construction is shown in Fig 4.1. Fig 4.2 displays the range of supply voltages needed to achieve various output polarisation forms, from linear, through to elliptical, to circular polarisation. The retarders are constructed using optically flat fused silica windows coated with a transparent conductive indium tin oxide (ITO). This ITO coating is designed for a maximum transmission from 450-1800nm. A thin dielectric layer is applied which has been gently rubbed to create parallel micro-grooves for liquid crystal (LC) molecular alignment. The two windows are designed only a few microns apart, and the cavity is filled with a birefringent nematic LC material. The cell is environmentally sealed, and electrical contacts are attached, to allow external electronic, tunable control of retardation, by changing the effective birefringence of the material with applied voltage. Thus the transmitted light is converted to some elliptical polarisation form, if it was originally polarised to begin with.

Within the cell, the anisotropic nematic liquid crystal molecules form uniaxial birefringent layers. A feature of nematic material is that, on average, molecules are aligned

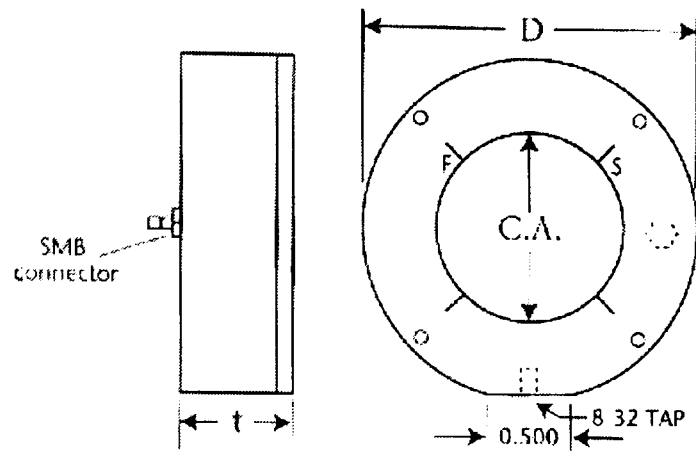


Figure 4.1: Cross-sections of the liquid crystal variable retarder cell. Dimensions are shown in inches and fast, f, and slow, s, axes are indicated. D is 1.99 inches, the Clear Aperture, C.A., is 0.80 inches, and the thickness, t, is 0.79 inches. The SMB connector is attached to the power supply.

Voltage (volts)	Retardance	Output
$V \sim 2$	$\delta = \lambda/2$	
$2 < V < 4$	$\lambda/4 < \delta < \lambda/2$	
$V \sim 4$	$\delta = \lambda/4$	
$4 < V < 7$	$0 < \delta < \lambda/4$	
$V \sim 7$	$\delta = 0$	

Figure 4.2: The output polarisation forms for the different retardance values, when the liquid crystal is positioned with fast axis at 45° to the horizontally polarised input.

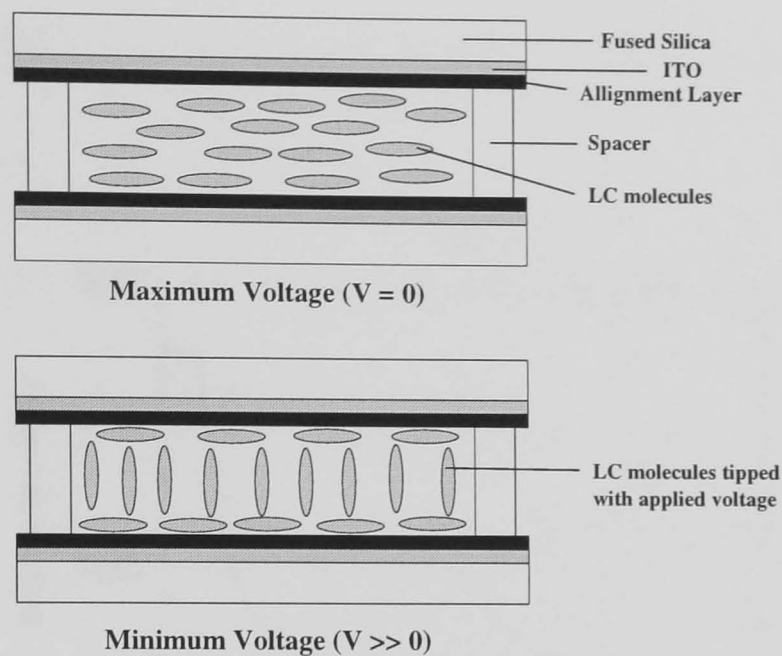


Figure 4.3: The construction of the liquid crystal variable retarder, showing molecular alignment with no voltage applied, and at high voltage.

with their long axes parallel and pointing in the same direction, but with their centers randomly distributed, as shown in Fig 4.3. The long axis of the LC molecules defines the extraordinary (or slow) index n_e . When no voltage is applied, the LC molecules lie parallel to the glass substrates, and therefore maximum retardation is achieved. When a voltage is applied, the molecules begin to align in a direction perpendicular to the silica windows, and become parallel to the direction of the propagation of light through the cell. As voltage increases, the molecules ‘tip’ further, and hence, the effective value of n_e and therefore, birefringence, decreases, causing a reduction in retardance. However, the molecules at the surface, undergo a ‘surface pinning effect’, as they are unable to rotate freely, since they are ‘pinned’ at the alignment layer. Unfortunately, this results in a residual retardance of $\sim 30\text{nm}$, even at high voltage (20 volts). This is demonstrated in Fig 4.4. Therefore, to achieve zero retardance, it is necessary to attach a ‘compensator’ plate to the LC cell, which would behave as a subtractive fixed retarder. This is achieved by attaching the compensator such that its fast axis is set perpendicular to the fast axis of the LC. Fig 4.5 shows how the whole retardance v. voltage curve, is shifted down when a subtractive compensator plate is fixed to the liquid crystal. The shape of the curve remains the same, but it is now possible to obtain lower values of retardance.

A characteristic of the LC material, is that the retardance decreases at longer wavelengths (see Fig 4.6). The cells offer good performance over large incidence angles. The

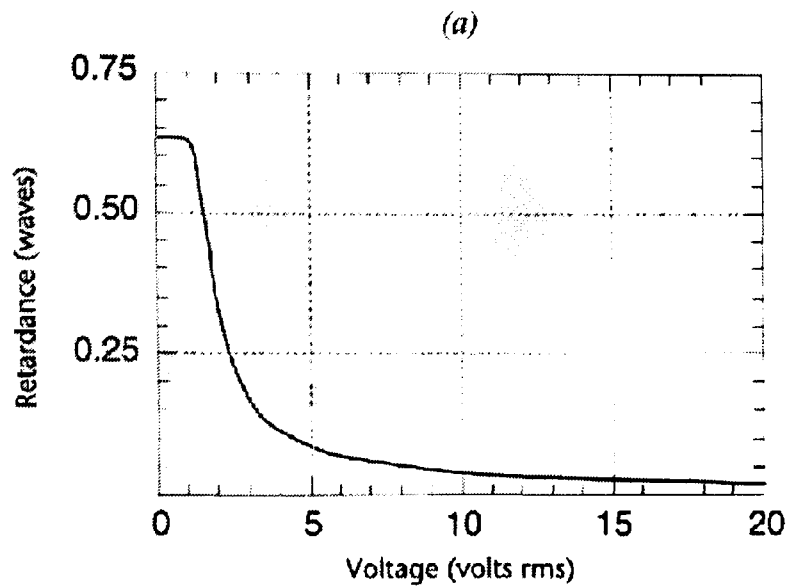


Figure 4.4: Performance curve for the retarder at 632.8nm, and 21°C.

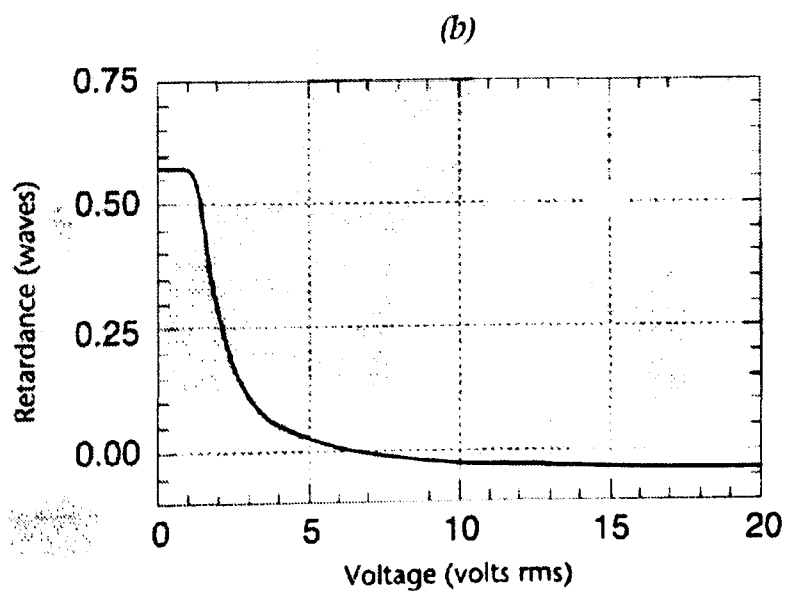


Figure 4.5: Performance curve for the retarder at 632.8nm, and 21°C, with a compensator attached, such that axes are aligned, (Meadowlark 1992).

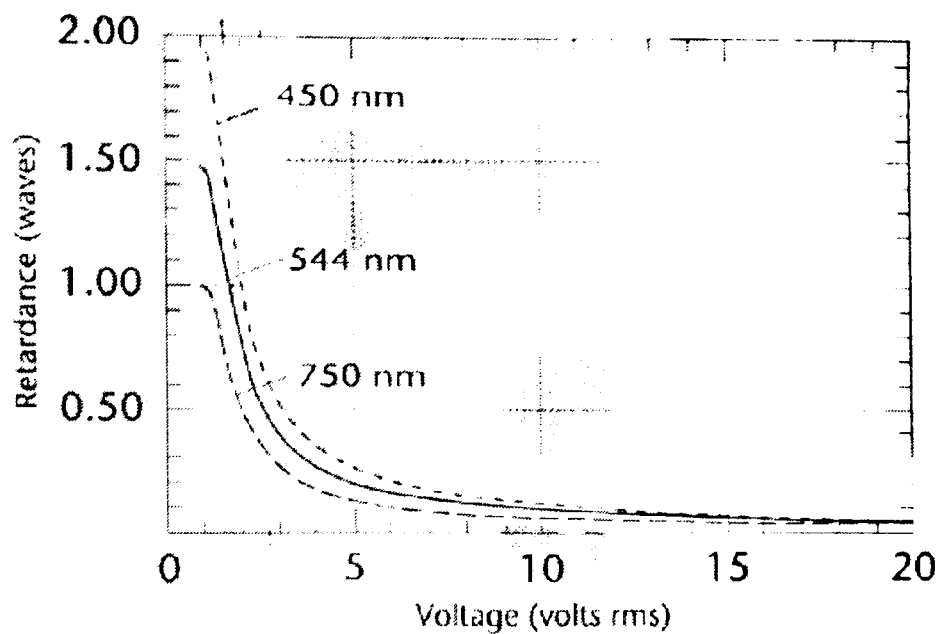


Figure 4.6: Plot demonstrating how the birefringence of the liquid crystal variable retarder decreases at longer wavelengths.

retardance of the LC is dependent upon thickness and birefringence, where this birefringence is dependent upon operating wavelength, drive voltage, and temperature. Meadowlark quote the overall retardance of the LC as decreasing with increasing temperature such that there is a 0.4% change per °C, within a range of 10° to 50°. The temperature sensitivity of the basic cell is demonstrated in Fig 4.7. It is apparent that at a wavelength of 560nm, a 16° increase in temperature, from 24°C to 40°C, can result in a change in retardance of only 0.04 waves~22nm. The calibration of the cell for wavelength will be shown in a later section. Calibration for temperature sensitivity was considered unnecessary for the development of the Twin Liquid Crystal Polarimeter, as the filter pass band of the light used was ~100nm. However, the importance of maintaining a constant temperature of the liquid crystal, during the calibrative procedure, was not neglected.

When the LC cell is positioned between crossed polaroids, with the fast axis at 45°. then as the AC voltage amplitude is increased from half to zero-waves retardance, the relationship between *transmittance*, T , and *retardance* r (in degrees), is given by :

$$T(r) = \frac{1}{2} [1 - \cos(r)] T_{max} \quad (4.1)$$

where T_{max} is the maximum transmittance when retardance is exactly one half wave.

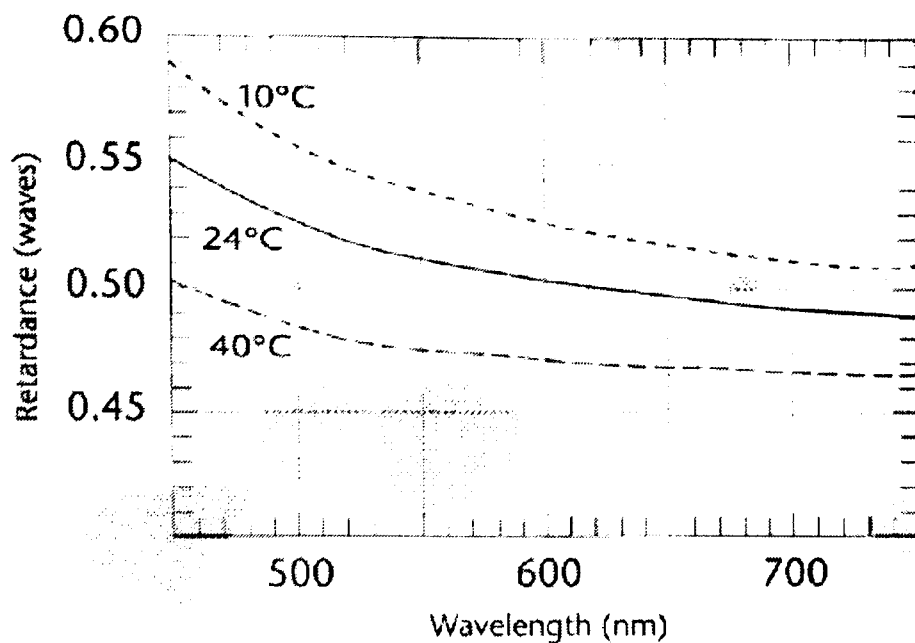


Figure 4.7: Plot demonstrating the temperature sensitivity of the liquid crystal variable retarder.

Fig 4.8 shows transmittance as a function of voltage. Maximum transmittance is dependent upon properties of the LC cell, as well as the polarisers used. With HN38S crossed polarisers, the behaviour of transmittance with wavelength is shown in Fig 4.9, for an unpolarised illumination. Note, that this is fairly uniform from $\sim 500\text{nm}$ - 750nm , and is $\approx 32\%$ at 550nm , the wavelength chosen for future calibration. In this same configuration, the *contrast ratio* may be defined as :

$$R = \frac{T_{max}}{T_{min}} \quad (4.2)$$

where T_{min} is when the LC cell is operating at zero-wave retardance (Fig 4.10).

The response time of a LC depends upon several parameters including layer thickness, temperature and variations in drive voltage. Response time is proportional to the square of the layer thickness, and therefore, the square of the total retardance. It is important to note that response time is also dependent on the *direction* of the retardance change. For example, if the retardance changes from $\frac{\lambda}{4}$ to $\frac{\lambda}{2}$, response time is determined only by mechanical relaxation of the molecules. However, if retardance decreases in value, response time is much faster due to the increased electrical field across the LC layer. Typical response time for a standard liquid crystal variable retarder is shown in Fig 4.11. It takes about 5 ms to switch from $\frac{\lambda}{2}$ to 0 waves (low to high voltage), and about 20

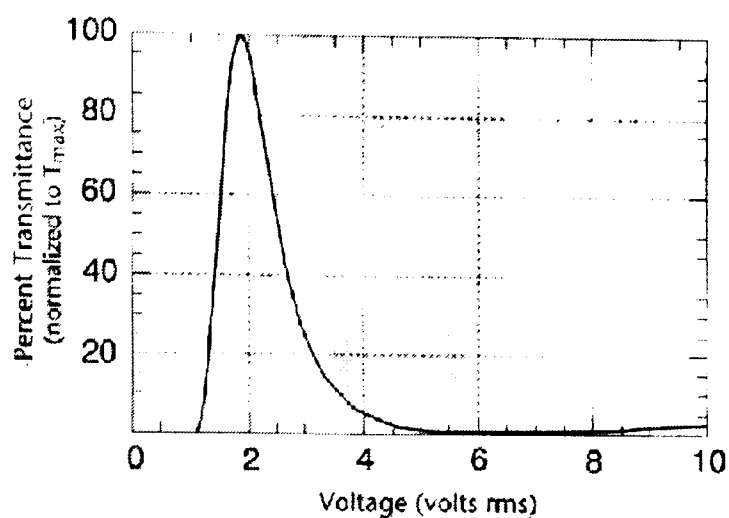


Figure 4.8: Normalised transmittance of a liquid crystal variable retarder between crossed polaroids, at a single wavelength, (Meadowlark 1992).

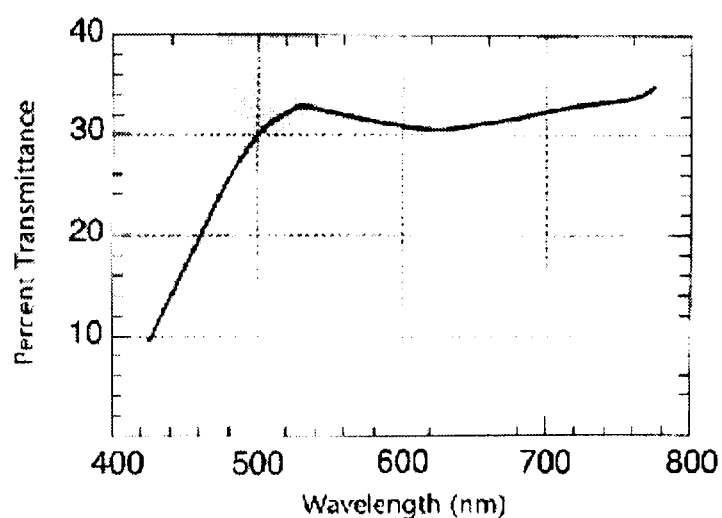


Figure 4.9: The transmittance as a function of wavelength for a liquid crystal variable retarder between crossed polaroids, optimised at 550nm.

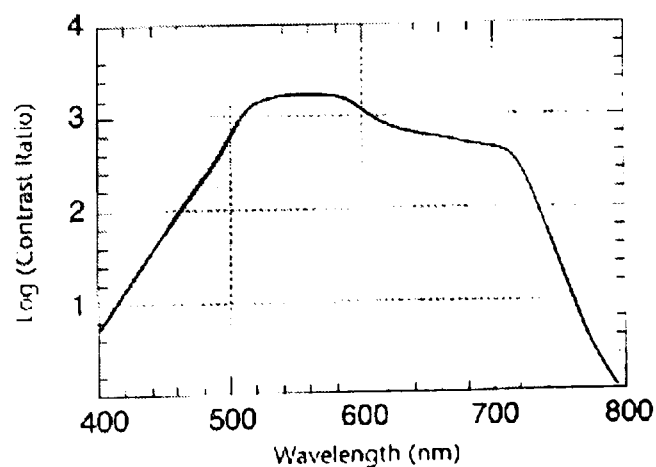


Figure 4.10: Typical contrast ratio of a liquid crystal variable retarder between crossed polaroids, optimised at 550nm.

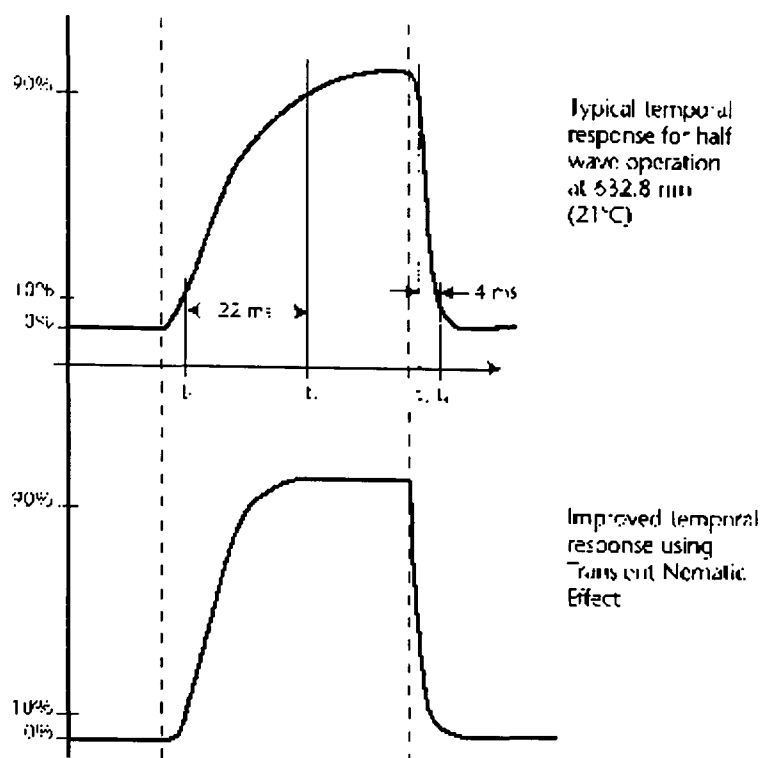


Figure 4.11: Typical response time for a liquid crystal variable retarder. The upper diagram shows normal response, whereas the lower diagram shows the more rapid response employing the Transient Nematic Effect (see Meadowlark 1992).

ms to switch from 0 to $\frac{\lambda}{2}$ (high to low voltage). Fortunately, with the use of the D1040 Interface described below, the *Transient Nematic Effect*, TNE may be employed. With this drive method, a high voltage spike is applied to accelerate the molecular alignment parallel to the applied field. Voltage is then reduced to achieve the desired retardance. When switching from low to high retardance, all voltage is momentarily removed allowing the LC molecules to undergo natural relaxation. Improved response time achieved with TNE is also shown in Fig 4.11.

4.1.1 D1040 Liquid Crystal Digital Interface

Control of the voltage to the LC is achieved by the use of the a D1040 Digital Interface (see Fig 4.12), allowing complex variations with time. This device allows convenient computer control of the cell. Once the required retardation value needed is known, the appropriate voltage is selected at the PC keyboard. Computer software sends digitally encoded voltage information to the model D1040. Four independent voltage states may be stored for sequential operation. These digitised voltage values are sent from the PC to the interface through a 16-bit data path with an upper and lower output byte select. All



Figure 4.12: The Meadowlark liquid crystal digital interface, used to allow precision control of the liquid crystal by PC.

sixteen bits can be sent simultaneously, or upper and lower bytes can be set separately, using an 8-bit connection, making the device very versatile. The output voltage from the D1040 is a 2kHz AC square wave, digitally adjustable from 0 to 20 V rms, with a resolution of 0.61mV.

Thus the D1040 allows electronic control of the LC via computer operation. A PC interface is used enabling complex retardance variations with time, including those suitable for polarimetric modulation.

4.2 Selection of Liquid Crystal Configuration

4.2.1 The Single Liquid Crystal Polarimeter

Initial research concentrated on the development of a polarimetric device employing just one liquid crystal cell. To obtain just one linear Stokes parameter, the device must provide electronically generated retardance values, such that light passing through the system, may switch between orthogonal polarisations. To obtain the other Stokes parameter, it will be necessary to :

- (1) mechanically rotate the LC cell, or

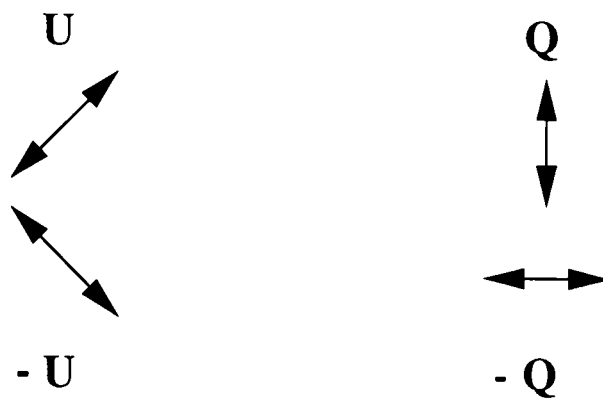


Figure 4.13: The output linear polarisation forms needed for the determination of the Stokes parameters, Q and U .

(2) rotate a half wave plate in front of the LC cell.

The required output polarisation forms, needed for determination of the Stokes' parameters, are as shown in Fig 4.13.

The method whereby a half-wave plate is used, is demonstrated pictorially in Fig 4.14. With the half-wave plate set at 0° to the axis of the system, the liquid crystal switches its retardance between 0 and π to allow the Stokes parameter Q to be obtained. The half wave-plate is then rotated such that its axis is at 45° to the axis of the system. Switching the LC between 0 and π , again allows the determination of Q such that the noise associated with differing pixel sensitivity across a CCD detector, may be eliminated.

The half-wave plate is necessary, so that the light entering the LC, can be rotated, thus allowing the other Stokes parameter to be obtained. To obtain a single parameter at a given wavelength, the retardance of the LC cell will switch between zero and π retardance, so that it is actually acting firstly as a zero order plate, and then as a half wave plate. To aid the subtraction of atmospheric noise, a CCD is used with a frame rate equal to the switching/modulating rate of the LC. The two images at 0 and π retardance, are stored in a PC memory, and steadily built up over time. If the half wave plate in front of the LC is then rotated by 45° , such that the light entering the cell has rotated by 90° , then the same Stokes parameter will be obtained again, and this will enable the elimination of the problem of varying pixel sensitivity across the CCD surface, thus bypassing the need for flat fielding. The other Stokes parameter is obtained by the same method, but by fixing the half wave plate at 22.5° and 67.5° to the reference axis, respectively.

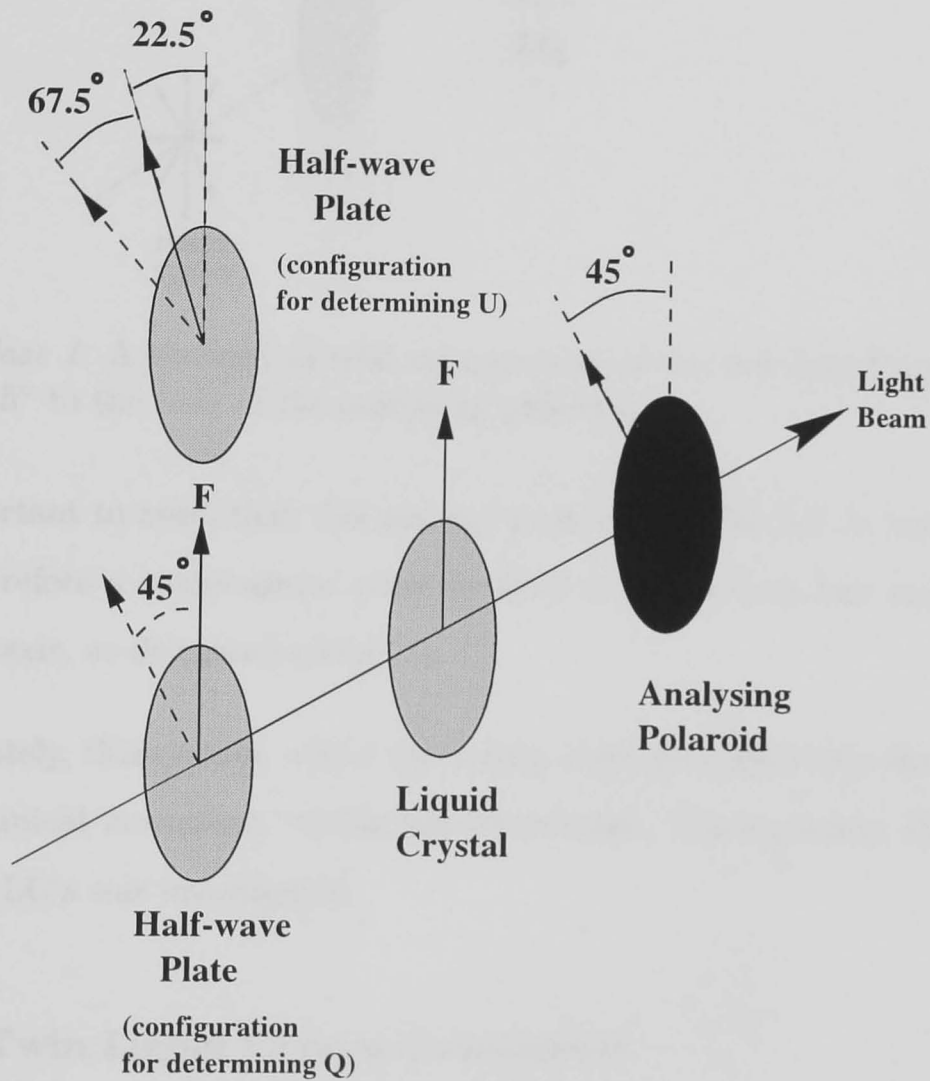


Figure 4.14: Instrumental setup, for the Single Liquid Crystal Polarimeter. The Stokes parameter Q , is determined with the liquid crystal switching retardation between 0 and π , when the half-wave plate is set at both 0° and 45° . This allows the elimination of noise associated with differing pixel sensitivity across the CCD detector. The process is repeated to obtain U , but with the half-wave plate set at 22.5° and 67.5° .

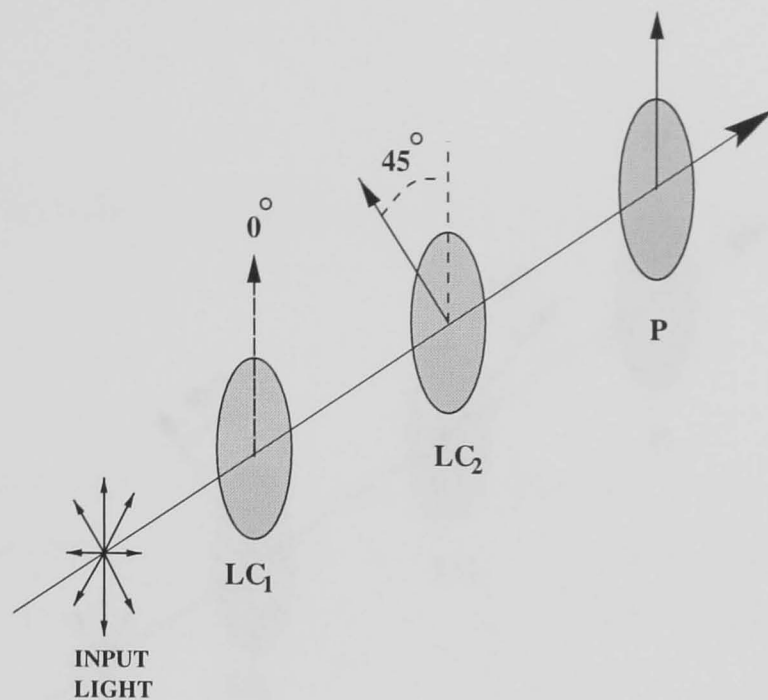


Figure 4.15: *Case 1.* A theoretical trial arrangement of the two liquid crystals, with LC_2 orientated at 45° to the axes of the analysing polaroid, P.

It is important to note, that this method does require the LC to provide zero retardance, and therefore a compensator must be fixed to it, with its fast axis perpendicular to the LC fast axis, as discussed earlier.

Unfortunately, this system, whilst attractive, does not completely eliminate the need for some mechanical movement, within the instrument. Consequently, the possibility of combining two LC's was investigated.

4.2.2 The Twin Liquid Crystal Polarimeter

It should be possible to combine two liquid crystal variable retarders so that they are aligned in such a way that, with the first one acting as a zero order wave plate, the other may switch its state of retardance to allow the determination of one Stokes parameter; then, by switching the second LC to zero retardance, the first LC may change its retardation between two states, to obtain the other Stokes parameter. Three, perhaps immediately intuitive methods of doing this are presented in Figs 4.15, 4.16 and 4.17.

The Mueller matrix equations of these optical arrangements, needed to determine the resultant emergent intensities from the systems, are calculated thus :

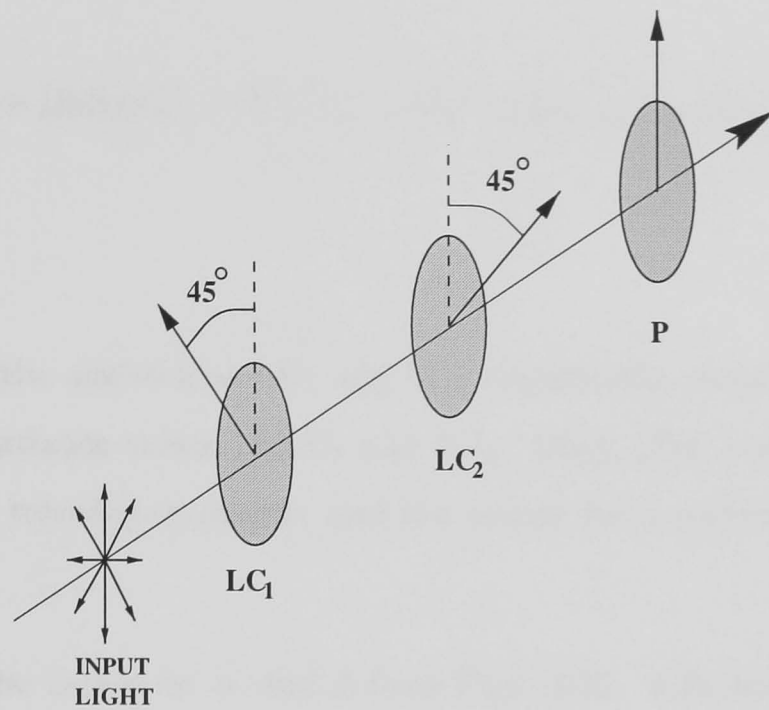


Figure 4.16: *Case 2.* A theoretical trial arrangement of the two liquid crystals, where now both cells are orientated at 45° to the axes of the analysing polaroid, P, but in the opposite sense to each other.

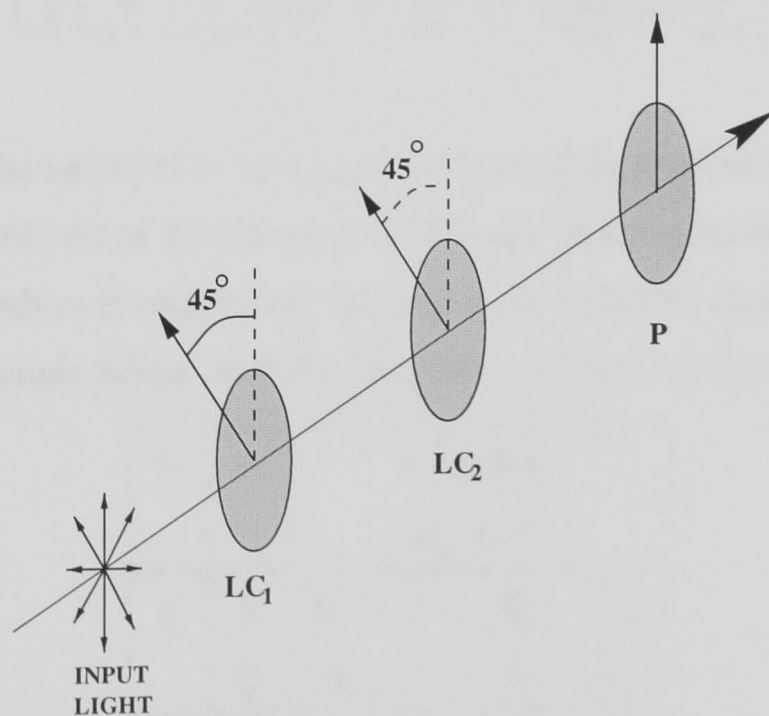


Figure 4.17: *Case 3.* A theoretical trial arrangement of the two liquid crystals, where now both cells are orientated at 45° to the axes of the analysing polaroid, P.

$$[Pol] \times [Rot(\beta)] \times [Ret(\delta_2)] \times [Rot((\beta - \alpha))] \times [Ret(\delta_1)] \times [Rot(\alpha)] \times \begin{bmatrix} I \\ Q \\ U \\ V \end{bmatrix} \quad (4.3)$$

where α and β are the angles that LC_1 and LC_2 respectively, make with the vertical. δ_1 and δ_2 are the retardance values of LC_1 and LC_2 . $[Rot]$, $[Ret]$ and $[Pol]$, represent the *rotator matrix*, the *retardation matrix*, and the matrix for a perfect polariser defined in Chapter 1.

Substituting the values for α , and β from Figs 4.15, 4.16 and 4.17, the resultant intensities are shown below.

α	β	Emergent Intensity
0	$\frac{\pi}{4}$	$\frac{I}{2} + Q\frac{1}{2}\cos\delta_2 + U\frac{1}{2}\sin\delta_2\sin\delta_1$
$\frac{\pi}{4}$	$-\frac{\pi}{4}$	$\frac{I}{2} + Q\frac{1}{2}\cos\delta_1\cos\delta_2 + Q\frac{1}{2}\sin\delta_2\sin\delta_1$
$\frac{\pi}{4}$	$\frac{\pi}{4}$	$\frac{I}{2} + Q\frac{1}{2}\cos\delta_1\cos\delta_2 - Q\frac{1}{2}\sin\delta_2\sin\delta_1$

By changing the values of δ_1 and δ_2 , it is immediately evident that, only in the first case, is there a possibility of determining both linear Stokes parameters. Selecting *Case 1*, there should be values of retardation for both liquid crystals, which enable Q and U to be determined. Example values, and the resultant emergent intensities are shown below.

δ_1	δ_2	Emergent Intensity
$\frac{\pi}{2}$	$\frac{\pi}{4}$	$E_1 = \frac{I}{2} + \frac{Q}{2\sqrt{2}} + \frac{U}{2\sqrt{2}}$
	$\frac{3\pi}{4}$	$E_2 = \frac{I}{2} + \frac{Q}{2\sqrt{2}} - \frac{U}{2\sqrt{2}}$
$\frac{\pi}{4}$	$\frac{\pi}{2}$	$E_3 = \frac{I}{2} + \frac{U}{2\sqrt{2}}$
	$\frac{3\pi}{4}$	$E_4 = \frac{I}{2} - \frac{U}{2\sqrt{2}}$

It can be seen that both linear Stokes parameters, and the total intensity, I , may be obtained, as shown :

$$U = \sqrt{2}(E_3 + E_4) \quad (4.4)$$

$$I = E_3 + E_4 \quad (4.5)$$

$$Q = \sqrt{2}[(E_1 + E_2) - (E_3 + E_4)] \quad (4.6)$$

Equation 4.4 gives U , but also introduces a scaling factor, meaning maximum possible modulation of the signal will not be obtained. Therefore the signal-to-noise is not as high as it might be. Equation 4.6 is not as compact as would be preferred, and the effective addition of **four** signals will increase noise. Further calculations reveal that, the ideal values for obtaining the greatest modulation of the signal in *Case 1*, and therefore the best signal-to-noise, are as shown in the table below.

δ_1	δ_2	Emergent Intensity
π	0	$I + Q$
π	π	$I - Q$
$\frac{5\pi}{2}$	$\frac{\pi}{2}$	$I + U$
$\frac{3\pi}{2}$	$\frac{\pi}{2}$	$I - U$

Table 4.3: The preferred retardation values of δ_1 and δ_2

Therefore, by taking the appropriate ratios for the signals :

$$R_q = \frac{I - Q}{I + Q} \quad R_u = \frac{I - U}{I + U} \quad (4.7)$$

Thus q and u may be determined from,

$$q = \frac{1 - R_q}{1 + R_q} \quad (4.8)$$

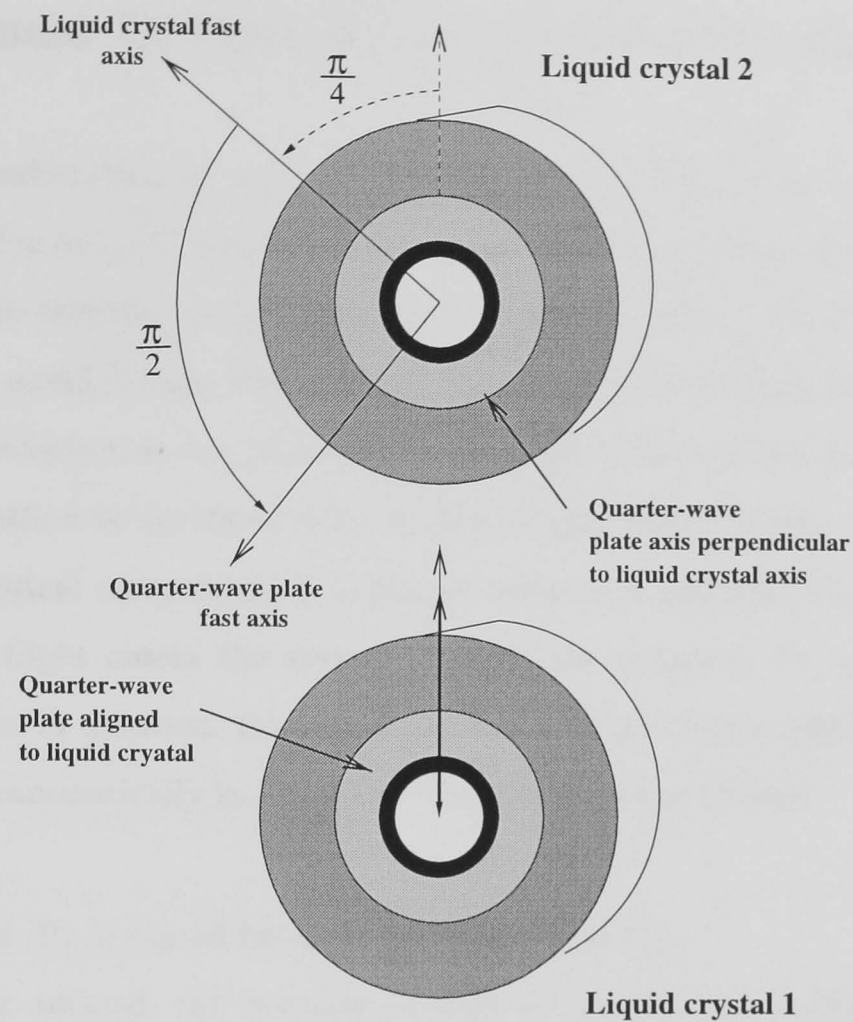


Figure 4.18: The *ideal* optical arrangement of the two liquid crystals. Light passes through LC₁ and then LC₂. LC₂ is aligned with its fast axis at $\frac{\pi}{4}$ to that of LC₁.

and,

$$u = \frac{1 - R_u}{1 + R_u} \quad (4.9)$$

This *ideal* optical arrangement, which requires no moving parts is shown pictorially in Fig 4.18.

For δ_1 to have $\frac{3\pi}{2}$ retardance, LC₁ has a quarter-wave compensator plate attached to it, with its fast axis aligned to that of the liquid crystal. With δ_1 set at $\frac{5\pi}{2}$, LC₁ provides 2π retardance, which is possible for wavelengths from $\sim 150 - 750$ nm. For δ_2 to be able to have 0 retardance, it has a quarter-wave compensator attached to it, with fast axis perpendicular to the fast axis of LC₂. Note, that to obtain the emergent intensity of $I + U$, δ_1 is set at $\frac{5\pi}{2}$ retardance, rather than the immediately intuitive $\frac{\pi}{2}$, since for δ_1 to be $\frac{\pi}{2}$, then LC₁ must provide zero retardance, which of course it cannot achieve without the further addition of another compensator plate.

4.3 Alignment Of Optical Components For Calibration

For an effective calibration of the Twin Liquid Crystal Polarimeter (via the Sénarmont method discussed in the next section), it is essential that the axes of all optical components are at exactly the specified angles with respect to each other. This is achieved by the employment of a novel device, involving the use of a polaroid which is able to turn 180° , through an axis which is in the plane of the polaroid. This axis has been selected as the vertical. The method is described fully in Rowell and Levitt (1969). To determine the fast axis of an optical component, it is placed between a polaroid, P_1 , and the spinning polaroid, P_{flip} . Light enters the system through the polaroid, P_1 , passes through the optical component in question, through P_{flip} , and into a detector/photo-multiplier. This is displayed diagrammatically in Fig 4.19. The method is as follows:

- (1) Polaroid, P_1 is placed between the source and P_{flip} .
- (2) As P_1 is rotated, the intensity of light at the detector is observed. This is done with P_{flip} in **position₁** (normal orientation), and **position₂** (rotated through 180°).
- (3) At the position of P_1 , such that there is no change of intensity at the detector upon rotation of P_{flip} , greater than the noise of the signal, the fast axis of P_1 is then known to be vertical (i.e. aligned to the spin axis of P_{flip}). P_1 is fixed in position.
- (4) LC_1 is inserted between P_1 and P_{flip} . Process is repeated, until zero modulation of the output is again obtained, i.e. when the fast axis of LC_1 is aligned with P_1 . Accuracy is aided by the precision rotary mount.
- (5) LC_1 is fixed in position, and a compensating quarter-wave plate is added, and the process is again repeated, until it's axis is also exactly vertical.
- (6) LC_1 and compensator locked permanently together.
- (7) The quarter-wave plate, Q , necessary for calibration by the Sénarmont method, is inserted between LC_1 and the 'flip' polaroid. Process is repeated until axis vertical. Then the plate is fixed within its mount.
- (8) Sénarmont quarter-wave plate, Q , and LC_1 /compensator combination are removed.

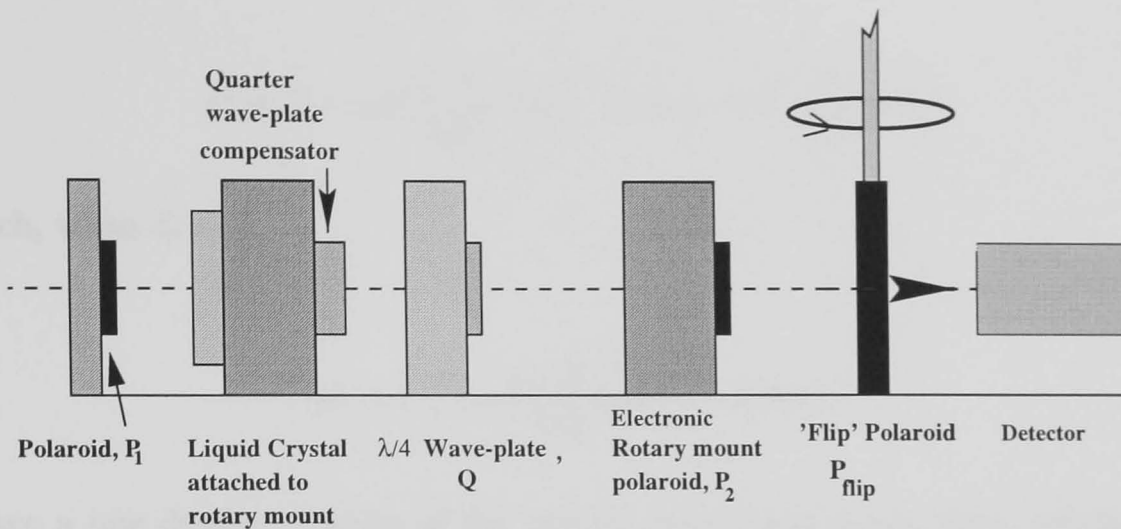


Figure 4.19: Cross-section of the layout used to align all optical components to correct orientations for calibration by the Sénarmont method.

- (9) Alignment procedure repeated for LC_2 and its respective compensator.
- (10) LC_2 /compensator combination, and P_1 are removed.
- (11) P_2 is placed in system. Steps (1) and (2) are repeated for P_2 until its axis aligned to vertical.

The light source used was a HeNe laser (632.8nm), for ease of alignment of the components in the x, y, z directions.

Upon completion of this, all components are known to be accurately aligned to the vertical reference axis. The components are now rotated within their respective precision rotary mounts (allowing a resolution of 10 arcsecs), to the required angles necessary for calibration by the Sénarmont method.

A discussion of the expected precision in the positioning of the optical components is necessary. It will now be calculated and compared to the precision attainable by just rotating a retarder between two parallel polaroids.

When an optical retarder, R , of retardance Δ , is placed between parallel polaroids, and a light beam is passed through all components, the expected percentage change in the intensity of light emergent from the assembly can be calculated. The difference in intensity, D , of light passing through the retarder in question, at the position of R for maximum transmission (fast axis of polaroid and R aligned), and at one degree from this position is ...

$$D = 1 - \cos^2 \left(\frac{2}{57} \text{rads} \right) - \cos \Delta \sin^2 \left(\frac{2}{57} \text{rads} \right) \quad (4.10)$$

which, when $\Delta = \frac{\pi}{2}$,

$$D = 1 - \cos^2 \left(\frac{2}{57} \text{rads} \right) \sim 0.0012 \quad (4.11)$$

Hence a one degree rotation of the optical component in question, produces a percentage change in transmitted intensity of,

$$D \sim 0.12\% \quad (4.12)$$

It is worth noting that the human eye is capable of detecting approximately a 2% change in intensity between two stars within a field, and is capable of slightly improved detection when only looking for extinction of light passing through a rotating optical retarder placed between two crossed polaroids.

Now, when using a photo-multiplier for the detection, it is important to achieve a count rate of $\leq 10^5 \text{s}^{-1}$ to avoid saturation. The expected photon noise on such a signal, N would be ...

$$\frac{1}{\sqrt{N}} = \frac{1}{\sqrt{10^5}} \sim 0.3\% \quad (4.13)$$

Therefore to be able to detect a 0.12% change in intensity associated with the rotating of R by 1° , i.e. above the level of photon noise, would require an integration time, T of ~ 10 seconds.

Using the 'flip polaroid' method shown in Fig 4.19 it is possible to reduce the integration time necessary to detect a 0.12% intensity change, and in fact allow the detection, with ease, of a rotation of the retarder of merely $\theta = \frac{1}{2}^\circ$. Referring to Fig 4.20, the difference in intensity, D, of light exiting the system upon a one degree rotation of the retarder, when turning P_{flip} through 180° , is.

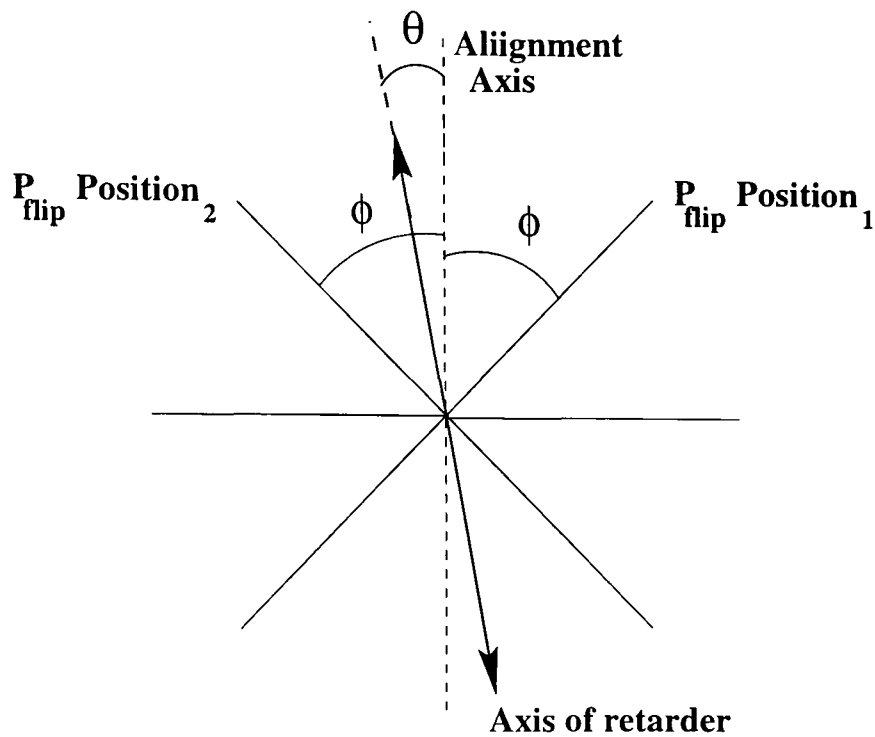


Figure 4.20: When the retarder in question is positioned at θ to the major axis of the input light beam, the maximum modulation, upon rotation of P_{flip} , is achieved when $\phi = \frac{\pi}{4}$.

$$D = 2 \sin 2\phi \sin 2\theta \cos 2\theta \quad (4.14)$$

Maximum modulation upon rotation of P_{flip} , is observed when $\phi = \frac{\pi}{4}$, i.e. when,

$$D = \sin 4\theta \quad (4.15)$$

Therefore, taking $\theta = 0$ to be the retarder aligned such that it allows maximum transmission, then a one degree shift in position of the retarder produces a percentage change in intensity of ...

$$D \sim 2 \sin \left(\frac{2}{57} \text{ rads} \right) \sim 7\% \quad (4.16)$$

Since photon noise is only $\sim 0.3\%$, it should therefore be theoretically possible to align the axis of the retarder to approximately 3 arc minutes, with only a one second integration time.

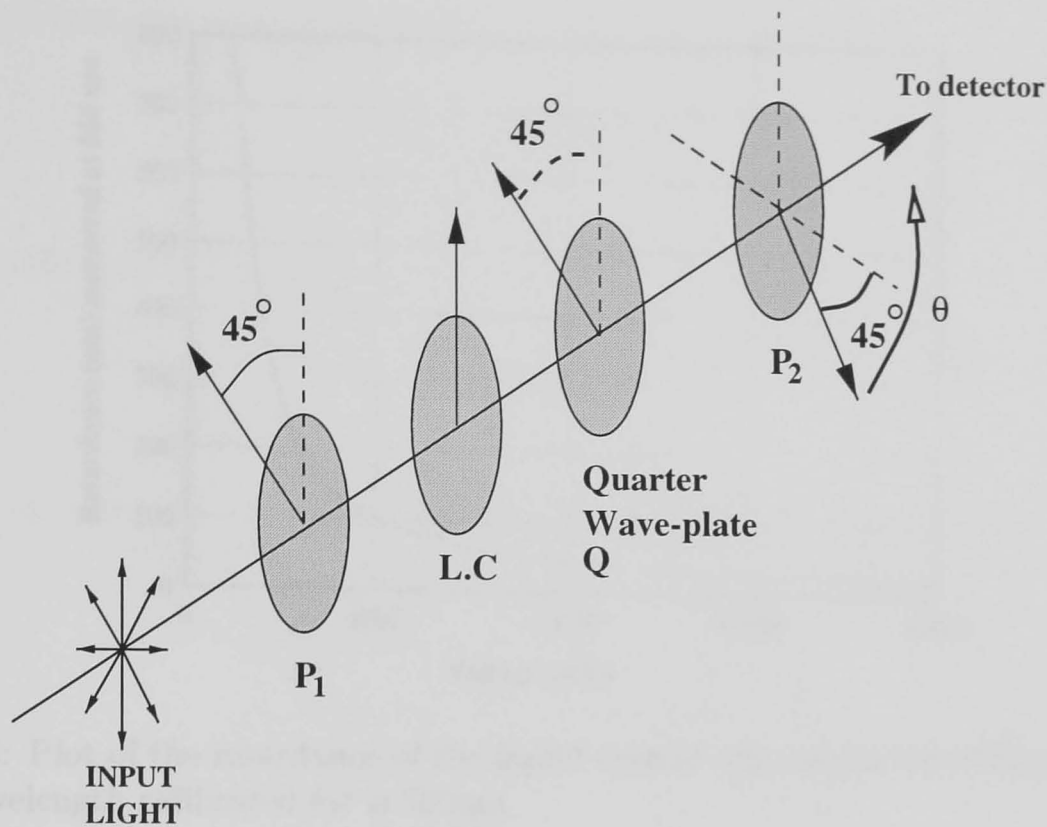


Figure 4.21: Layout of the Sénarmont Compensator, used for the calibration of voltages which need be applied to the liquid crystal cells, to achieve the desired retardation values given in Table 4.4.

4.4 Sénarmont Compensator

The Sénarmont Compensator is a device which may be used to determine the phase retardation, ϕ , of two orthogonally polarised components of a beam emerging from a birefringent wave plate. Therefore, it may be employed to calibrate the two liquid crystals. This method allows the determination of the necessary voltages which need be applied to the LC cells to achieve the required retardation values given in Table 4.4. It consists of two polaroids, P_1 and P_2 , the birefringent plate in question, and a fixed quarter wave plate, Q , for the range 460 to 680 nm (see Fig 4.21). Polarised light leaving P_1 , passes through the wave plate, whereupon the two linearly polarised components entering the quarter wave-plate, are converted into opposite circular polarisations, with a phase difference of ϕ . The superposition of these two circular components produces a linearly polarised beam, which is then incident on P_2 . The Mueller matrix equation for the system is

$$[Pol] \times [Rot(\theta)] \times \left[Retar\left(\frac{\pi}{2}\right) \right] \times \left[Rot\left(\frac{-\pi}{4}\right) \right] \times [Retar(\phi)] \times \left[Rot\left(\frac{\pi}{4}\right) \right] \times [P] \quad (4.17)$$

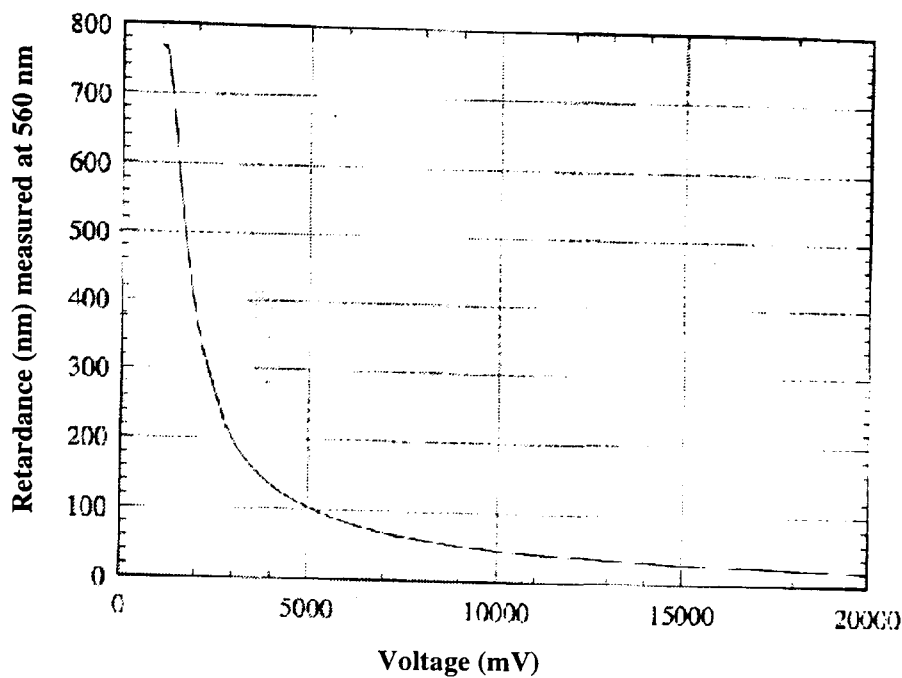


Figure 4.22: Plot of the retardance of the liquid crystal cell, versus the voltage applied to it. The wavelength calibrated for is 560nm.

which, when P_2 is rotated to extinction means that,

$$\theta = \frac{\phi}{2} \quad (4.18)$$

Hence, for a particular voltage, the retardation of the wave plate may be determined by measuring θ . However, it must be noted that this method is only valid for the wavelength at which Q , is a quarter of a wave. At other wavelengths, the two beams leaving Q will be elliptically polarised.

A discussion of the expected precision of the calibration is necessary, to point out the accuracy which can be achieved with the liquid crystal variable retarders, particularly as compared to more conventional wave plates.

The wavelength of light used for this calibration was $\lambda = 560 \pm 10$ nm, and thus referring to the gradient of Fig 4.22, $\frac{dR}{dV}$, the incremental change of voltage with wavelength at $\delta_1 = \pi$, is calculated as follows :

When,

$$\delta_1 = \pi \quad (4.19)$$

then LC_1 provides a retardation of,

$$\frac{\pi}{2} = \frac{\lambda}{4} \sim 138\text{nm} \quad (4.20)$$

Hence referring to Fig 4.22,

$$\frac{dR}{dV} \sim 23\text{mV/nm} \quad (4.21)$$

Table 4.4 summarises the approximate values of $\frac{dR}{dV}$ for the necessary values of δ_1 and δ_2 .

δ_1	$\frac{dR}{dV}$	δ_2	$\frac{dR}{dV}$
π	23mV/nm	0	23mV/nm
$\frac{5\pi}{2}$	3mV/nm	π	3mV/nm
$\frac{3\pi}{2}$	6mV/nm	$\frac{\pi}{2}$	6mV/nm

Table 4.4: The preferred retardation values of δ_1 and δ_2 , tabulated with the $\frac{dR}{dV}$ values obtained from the voltage v. retardance curve given in Fig 4.22.

To determine the voltage which need be applied to the liquid crystal cells to achieve the necessary retardation, P_2 was set to the pre-determined angle, $\theta = \frac{\delta_n}{2}$, and then the voltage to the individual cell being calibrated, LC_n , was increased in steps, until extinction was achieved. From the table above, the minimum and maximum value of $\frac{dR}{dV}$ are 3mV/nm and 23mV/nm respectively. These figures indicate that using 10mV voltage increments for light of $\lambda \sim 560\text{nm}$, the current retardation value may be determined to within ~ 3 nm and ~ 0.5 nm for a 10mV step in voltage. This corresponds to within 0.5% and 0.1% of the desired retardation, respectively. A typical fixed achromatic half-wave plate can be used and quoted to an accuracy of 1° , i.e. to approximately 1%. Hence it was concluded that 10mV increments would be sufficiently precise for calibration.

Upon performing calibration of the LC cells using the Sénarmont method, the necessary voltages required to obtain the retardation values of δ_1 and δ_2 , were calculated. Table 4.5 displays the voltages, V_0 , which must be applied LC_1 and LC_2 to achieve the

retardation values.

δ_1	V_0	δ_2	V_0
π	3490mV	0	4069mV
$\frac{5\pi}{2}$	1552mV	π	1891mV
$\frac{3\pi}{2}$	2353mV	$\frac{\pi}{2}$	2419mV

Table 4.5: The calibrated voltages for corresponding values of δ_1 and δ_2 .

4.5 Experimental Testing of the Polarimeter

To determine the modulation of the system, light of the calibrated wavelength (560nm with a passband of 10nm) of 100% polarisation was passed through the system. The temperature of the apparatus was kept as close to 23°C as possible, to prevent the retardance of the LC fluctuating. The CCD camera temperature was set to -20°C, to ensure consistency of results. The initial chosen input orientation was arbitrary, as only repeatability of measurements, was of concern. The determined ‘output’ polarisation values, P_{out} , and the calculated direction of polarisation, θ_{out} , were calculated with the aid of the Starlink packages, Kappa and Gaia, for the analysis of CCD array images. These results are shown in Table 4.6.

Temperature of CCD head	P_{out} %	θ_{out}
-20° Centigrade	97.9	27.87°
	97.9	27.86°
Exposure Time 2.5 secs	97.8	27.84°
	97.6	27.75°

Table 4.6: Determined values of polarisation, and direction of polarisation, P_{out} and θ_{out} , for an input polarisation of 100%, with an arbitrary polarisation angle, θ_{in} .

The standard deviation of P_{out} and θ_{out} respectively are,

$$\sigma_{P_{out}} = 0.14 \qquad \sigma_{\theta_{out}} = 0.06 \qquad (4.22)$$

It was deemed pertinent to observe the values of P_{out} and θ_{out} for the specific input orientations of the light beam corresponding to $+Q$, $-Q$, $+U$ and $-U$. The observed results are shown in Table 4.7.

Orientation of Input Beam, θ_{in}	Orientation in Stokes space	$P_{out}(\%)$	Orientation of Output Beam, θ_{out}	$\theta_{in}-\theta_{out}$
180°	$+Q$	78.42	178.60°	+1.40°
90°	$-Q$	78.60	83.87°	+6.03°
45°	$+U$	65.9	52.26°	-7.26°
135°	$-U$	75.4	140.98°	-5.98°

Table 4.7: Table showing values of input polarisation and orientation, with the determined corresponding output values.

It can be seen that at these specific orientations of the input beam, the calculated output values of polarisation show some considerable deviation from 100% or even the values of $\sim 97\%$ given in Table 4.6. Also, the discrepancy in calculated position angle, θ_{out} and input position angle, θ_{in} has a magnitude from $\sim 1^\circ$ to 7° . Interestingly, the offset $\theta_{in} - \theta_{out}$ cannot be simply explained in terms of an instrumental offset, which would be simple to correct for. In fact, there is a positive deviation in Q and a negative deviation in U , with $\theta_{out} < \theta_{in}$, and $\theta_{out} > \theta_{in}$ respectively. To fully understand these differences it is necessary to conduct an analysis of the errors involved in the system, and their effect on the determined values of P_{out} and θ_{out} .

4.6 Theoretical Analysis of Errors and the Effect on Determined Polarisation and Polarisation Angle

To fully understand the observed/calculated results from the Twin Liquid Crystal Polarimeter, it is important to analyse the effects of errors on the alignment of all optical components within the device. The instrument has been tested using an input light beam which is 100% polarised, at various input angles with reference to the optical axis of the system. To summarise, there are three important errors, which must be investigated. These are shown in Table 4.8.

Label	Description of error
ϵ_1	Error in alignment angle between LC ₁ and LC ₂ . LC ₂ is not at exactly $\frac{\pi}{4}$ to axis of system
ϵ_2	Error in alignment angle between LC ₁ and LC ₂ . LC ₁ is not exactly aligned with axis of system, but LC ₂ is at $\frac{\pi}{4}$ from axis
ϵ_3	LC ₁ and LC ₂ aligned correctly at $\frac{\pi}{4}$ with respect to each other, but combined LC ₁ and LC ₂ offset slightly from system axis

Table 4.8: Possible errors present in the optical alignment of the system. LC₁ and LC₂ represent the combination of the respective liquid crystals and their compensator plates.

The individual effect of each of these errors will be dealt with in turn, in an attempt to explain the discrepancies described in the previous section. ϵ_1 , ϵ_2 and ϵ_3 are displayed diagrammatically in Figs 4.23, 4.24 and 4.25.

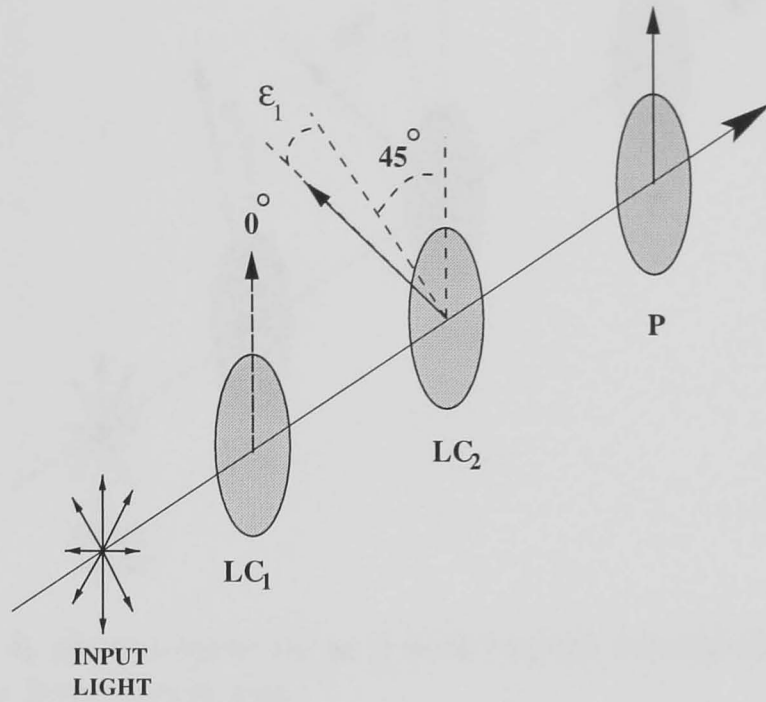


Figure 4.23: δ_1 and δ_2 error angle.

Figure 4.23: Error in alignment angle between δ_1 and δ_2 . δ_2 is not at exactly $\frac{\pi}{4}$ to axis of system of system, but δ_2 is at $\frac{\pi}{4}$ from axis.

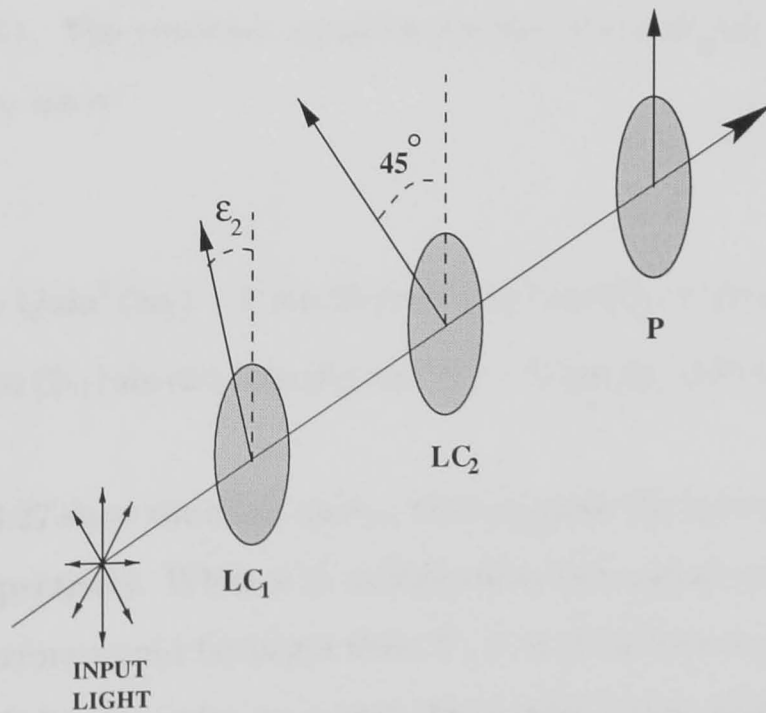


Figure 4.24: δ_1 and δ_2 error angle.

Figure 4.24: Error in alignment angle between δ_1 and δ_2 . δ_1 is not exactly aligned with axis of system, but δ_2 is at $\frac{\pi}{4}$ from axis.

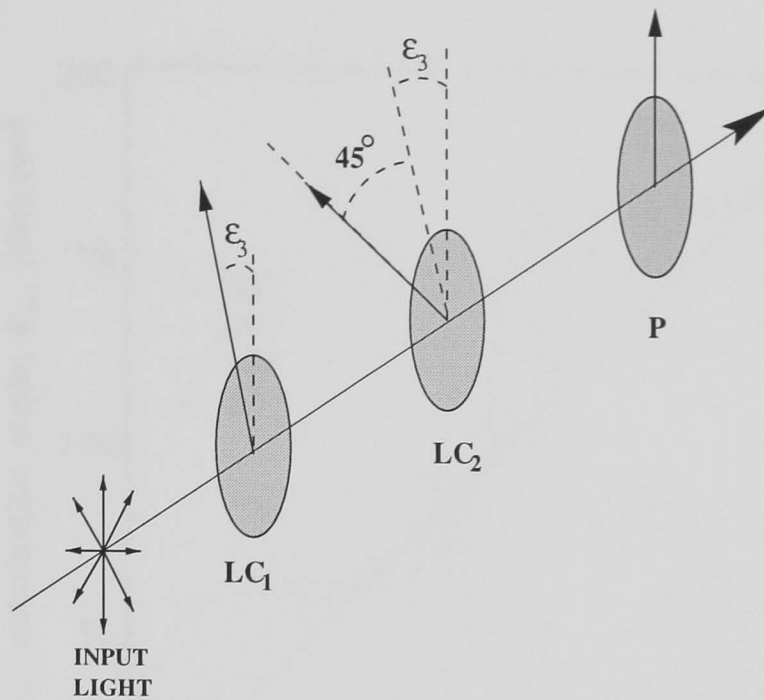


Figure 4.25: δ_1 and δ_2 aligned correctly at $\frac{\pi}{4}$ with respect to each other, but combined δ_1 and δ_2 offset slightly from system axis.

4.6.1 The Individual Effect of the Three Important Errors

The effect of the error, ϵ_1 , of different magnitudes, has been analysed by incorporating it into the Mueller matrix equations for the Twin Liquid Crystal Polarimeter, and determining the resultant effects on P_{out} and θ_{out} for all orientations of the input beam (which is polarised at 100%). The resultant equation for the emergent intensity, E_1 , neglecting terms in V , is shown below.

$$E_1 = \frac{1}{2} (1 + Q \sin^2 (2\epsilon_1) - U \sin (2\epsilon_1) \cos (2\epsilon_1) \cos (\delta_1) + Q \cos^2 (2\epsilon_1) \cos (\delta_2) + U \cos (2\epsilon_1) \sin (2\epsilon_1) \cos (\delta_1) \cos (\delta_2) + U \cos (2\epsilon_1) \sin (\delta_1) \sin (\delta_2)) \quad (4.23)$$

Figs 4.26 and 4.27 show the effect on θ_{out} when ϵ_1 takes the values of 0° , 10° , 20° , 35° , -10° , -20° , and -35° respectively. While it is unlikely that the optical alignment procedure is so inaccurate that errors would be larger than 5° , it is of interest to perform the analysis with larger values of the error also, to detect the general trends and behaviour of the instrument. The values were selected to emphasise the problems associated with non-exact alignment of the components.

From these plots it can be seen that for $\epsilon_1 = 0$, that $\theta_{in} = \theta_{out}$ as expected. However

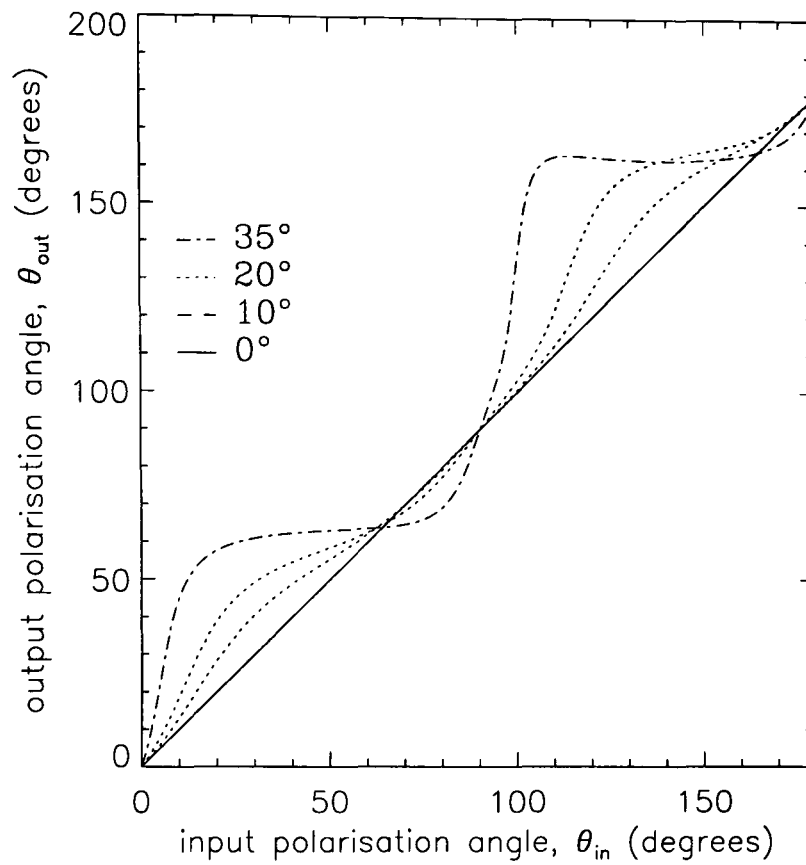


Figure 4.26: Plot showing the effect on θ_{out} when the error, ϵ_1 , takes the values of 0° , 10° , 20° , and 35° .

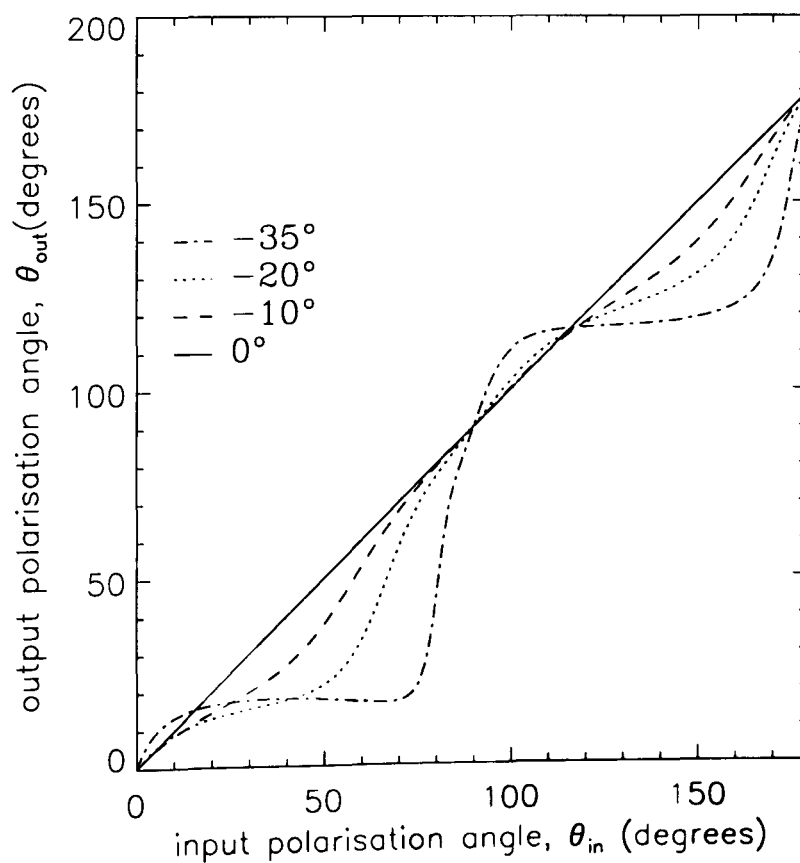


Figure 4.27: Plot showing the effect on θ_{out} when the error, ϵ_1 , takes the values of 0° , -10° , -20° , and -35° .

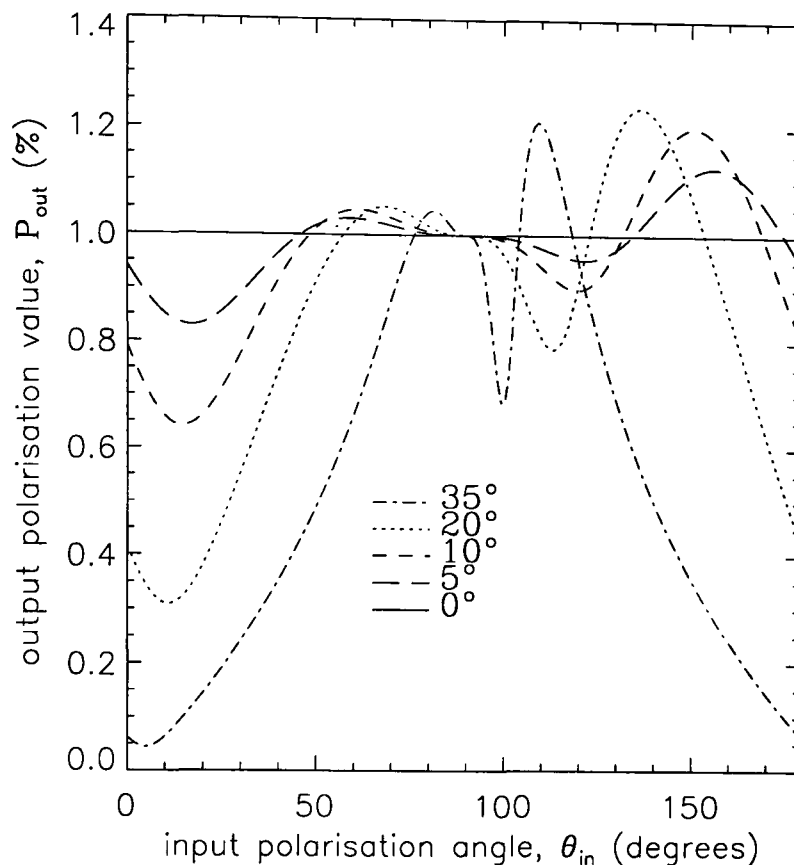


Figure 4.28: The effects of ϵ_1 on the calculated output value of polarisation, P_{out} , for values of ϵ_1 of 0° , 5° , 10° , 20° , and 35° .

as ϵ_1 increases, the maximum deviation of $\theta_{in} - \theta_{out}$ also increases. Obviously, for large errors above $20^\circ/-20^\circ$, the instrument is very inaccurate, giving a determined θ_{out} of as much as 50° different than θ_{in} . It should also be noted that at the input angles corresponding to $+Q$ and $-Q$, that $\theta_{out} = \theta_{in}$, and hence one would expect to see this mirrored in the results of Table 4.7. Although Table 4.7 indicates only a small deviation of $\sim 1^\circ - 6^\circ$ for these input orientations, the fact remains that there should be virtually no deviation, if ϵ_1 is to be considered the only error within the system. However, the deviation of the experimental values of θ_{out} for the input angles corresponding to $+U$ and $-U$, may be explained by a positive value of ϵ_1 of $\sim 7^\circ$.

The effects of ϵ_1 on the calculated output value of polarisation, P_{out} is shown in Figs 4.28 and 4.29

It can be seen that P_{out} is strongly affected by ϵ_1 , even for small values of error $\leq 5^\circ$. With $\epsilon_1 = 5^\circ$, P_{out} may read as high as 112% ($P_{in} = 100\%$) for $\theta_{in} \sim 25^\circ$, and as low as 84% for $\theta_{in} \sim 165^\circ$. At $\theta_{in} = 90^\circ$ corresponding to an input of $-Q$, $P_{out} = 100\%$, for all

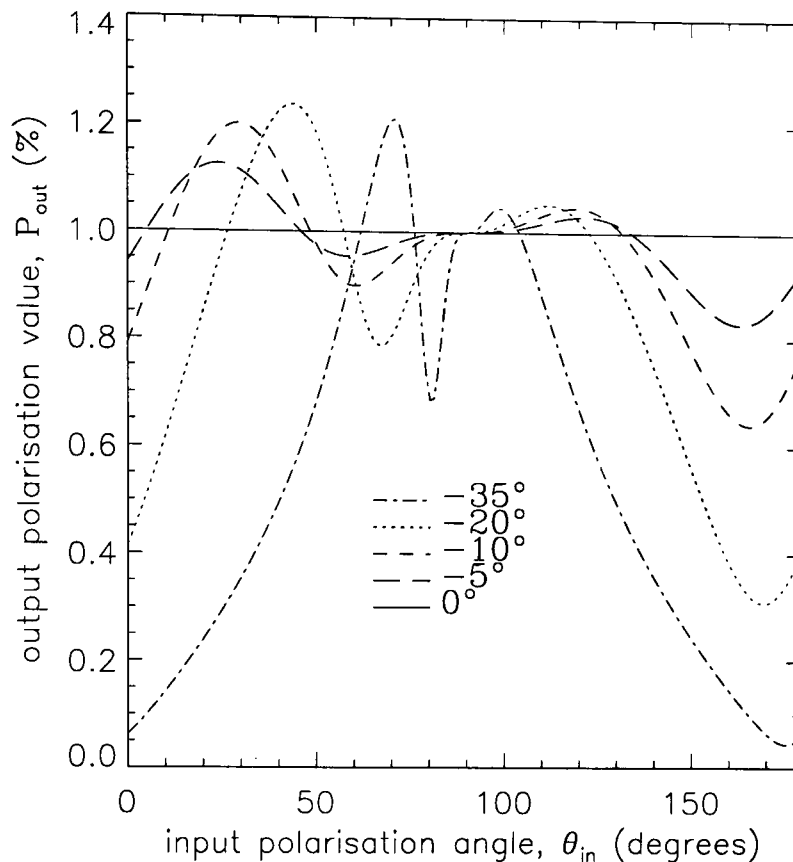


Figure 4.29: The effects of ϵ_1 on the calculated output value of polarisation, P_{out} , for values of ϵ_1 of 0° , -5° , -10° , -20° , and -35° .

ϵ_1 . However, the experimental value of P_{out} for $-Q$ input is only 83.87%. Also, due to the asymmetrical shape of the curve around the $P_{out} = 100\%$ line, then P_{out} must be greater than 100% for $+U$ input, and less than 100% for $-U$ input, when ϵ_1 is negative, or vice versa when ϵ_1 is positive. However, the experimental results show that $P_{out} < 100\%$ for both $+U$ and $-U$ input orientations.

In conclusion, ϵ_1 alone cannot explain the discrepancy between the experimentally observed output values, and the theoretically determined values. Only the deviation of θ_{out} from θ_{in} at the specific input angles corresponding to $+U$ and $-U$, may be explained by an $\epsilon_1 \sim 7^\circ$. Figs 4.30 and 4.31 display the theoretical specific values of θ_{out} for $0^\circ < \epsilon_1 < 10^\circ$. Note that $+Q$ and $-Q$ input orientations are unaffected.

Below is the calculated equation of the system, for Mueller matrices which include ϵ_2 , the error in alignment angle between δ_1 and δ_2 , when δ_1 is not exactly aligned with the axis of the system, but δ_2 is at $\frac{\pi}{4}$ from axis.

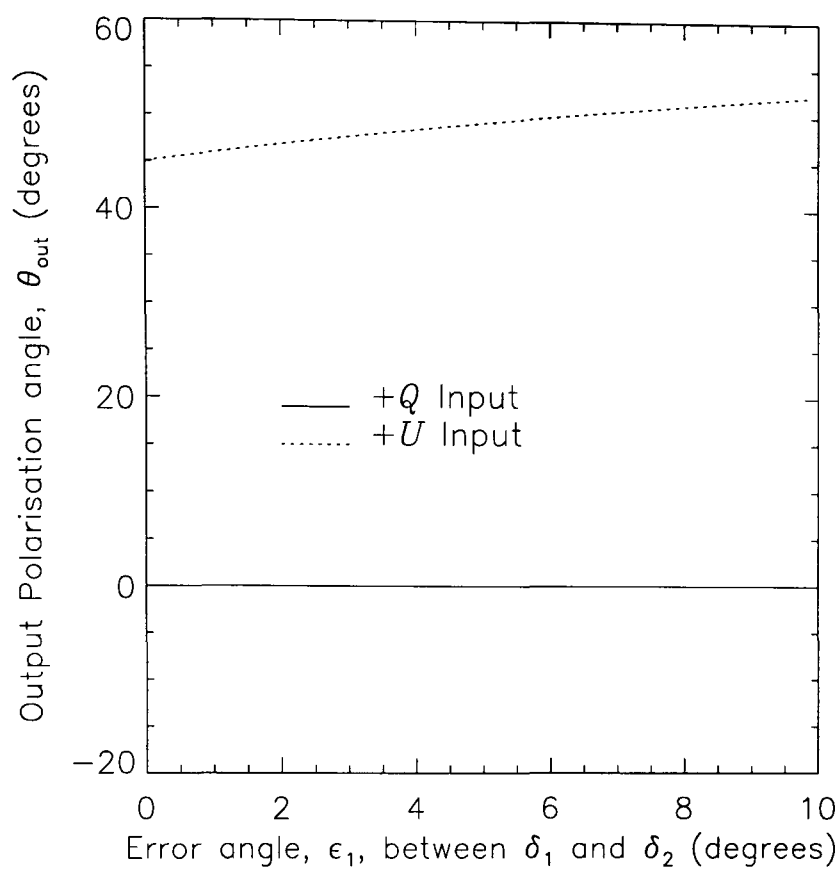


Figure 4.30: Theoretical specific values of θ_{out} for $0^\circ < \epsilon_1 < 10^\circ$, for input orientations corresponding to $+Q$ and $+U$, i.e. θ_{in} equal to 0° and 45° respectively.

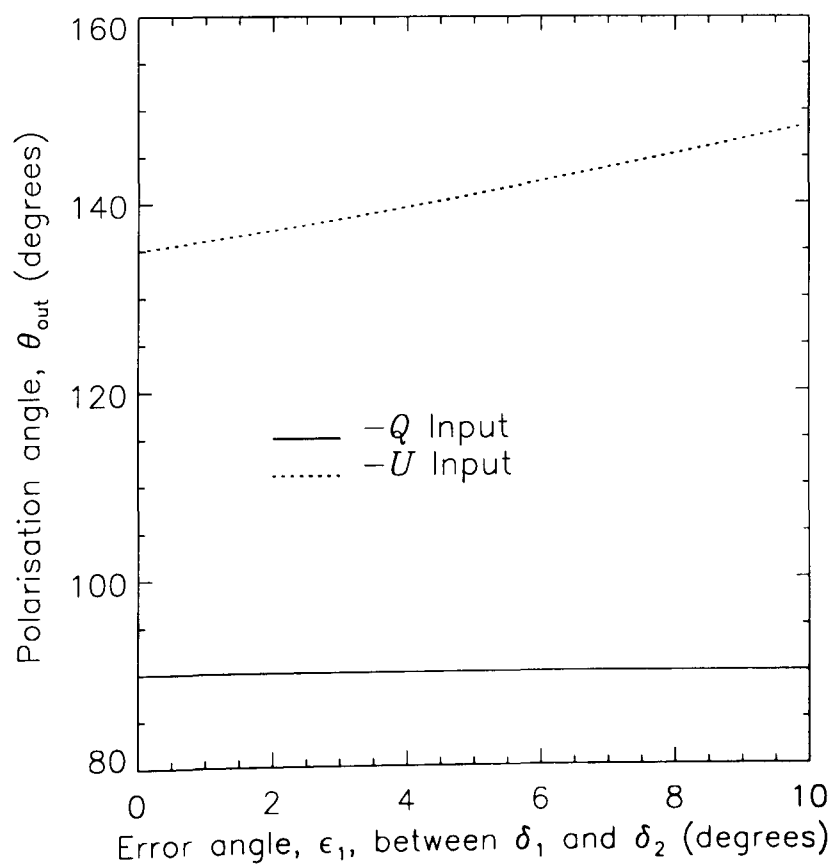
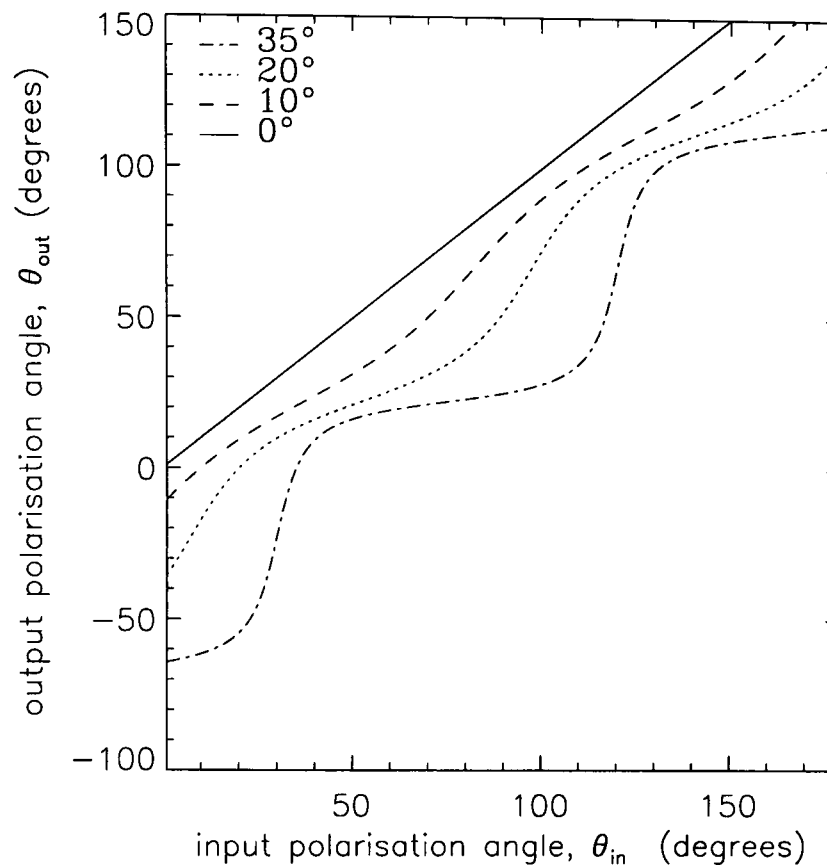


Figure 4.31: Theoretical specific values of θ_{out} for $0^\circ < \epsilon_1 < 10^\circ$, for input orientations corresponding to $-Q$ and $-U$, i.e. θ_{in} equal to 90° and 135° respectively.



aligned

Figure 4.32: Plot showing the effect on θ_{out} when the error, ϵ_2 , takes the values of 0° , 10° , 20° , and 35° .

$$\begin{aligned}
 E_2 = & \frac{1}{2} (1 + Q \cos^2 (2\epsilon_2) \cos \delta_2 + U \sin 2\epsilon_2 \cos 2\epsilon_2 \cos \delta_2 + Q \sin^2 (2\epsilon_2) \cos \delta_2 \cos \delta_1 \\
 & - U \cos 2\epsilon_2 \sin 2\epsilon_2 \cos \delta_1 \cos \delta_2 - Q \sin 2\epsilon_2 \sin \delta_1 \sin \delta_2 \\
 & + U \cos 2\epsilon_2 \sin \delta_2 \sin \delta_1)
 \end{aligned} \tag{4.24}$$

The expected effect upon θ_{out} , when only ϵ_2 is considered, is seen in Fig 4.32 and Fig 4.33. Immediate observations of these figures, indicate that the effect of changing all positive values of ϵ_2 to negative values, is just to flip the curves over the $\epsilon_2 = 0$ line. Taking the case of $\epsilon_2 \leq 10^\circ$, it can be seen that for all values of θ_{in} , the corresponding values of θ_{out} are all less than θ_{in} . Therefore, ϵ_2 cannot explain the experimentally observed trend of $\theta_{out} < \theta_{in}$ for an input of $+Q$ and $-Q$, and $\theta_{out} > \theta_{in}$ for an input of $+U$ and $-U$.

Inspection of Figs 4.34 and 4.35 reveals that the effect of introducing negative values of ϵ_2 , compared to positive values, is to reflect the curves in the y-plane. It is evident that even for ϵ_2 as small as 5° , that the value of P_{out} fluctuates from a maximum of nearly 110% to a minimum of nearly 90%. It is therefore crucial that δ_1 and δ_2 are aligned

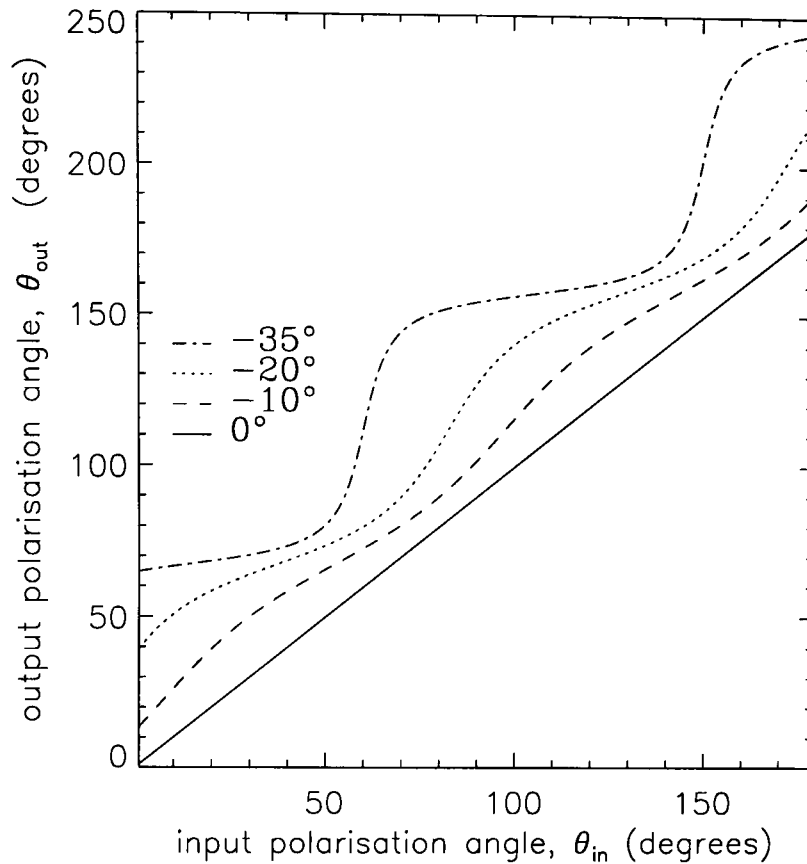


Figure 4.33: Plot showing the effect on θ_{out} when the error, ϵ_2 , takes the values of 0° , -10° , -20° , and -35° .

correctly with respect to each other. Indications are that for the specific input orientations corresponding to $+Q$, $-Q$, $+U$ and $-U$, that each corresponding value of P_{out} is removed from $P_{in} = 100\%$. Unfortunately, as for ϵ_1 , the theoretical plots do not correspond to the experimental values. Although, values as low as $P_{out} \sim 70\%$ for $-U$ and $+U$ input orientations, may be achieved theoretically, this would require a value of $\epsilon_2 \sim 35^\circ$. It is highly unlikely that the calibration, and optical alignment procedure, was this inaccurate. Also, no values of $P_{out} > 100\%$ were observed for these four input orientations.

It is of course possible that ϵ_1 and ϵ_2 are negligible, but that the combined unit consisting of δ_1 and δ_2 is offset from the system axis by the error, ϵ_3 . This error alone generates the equation below for the resultant intensity emergent from the polarimeter, E_3 . The effect of such an error is displayed in Figs 4.36 and 4.37.

$$E_3 = \frac{1}{2}(1 + Q \sin^2(2\epsilon_3) \cos \delta_1 - U \sin 2\epsilon_3 \cos 2\epsilon_3 \cos \delta_1 + Q \cos^2(2\epsilon_3) \cos \delta_2 + U \cos 2\epsilon_3 \sin 2\epsilon_3 \cos \delta_2 - Q \cos 2\epsilon_3 \sin 2\epsilon_3 \sin \delta_1 \sin \delta_2)$$

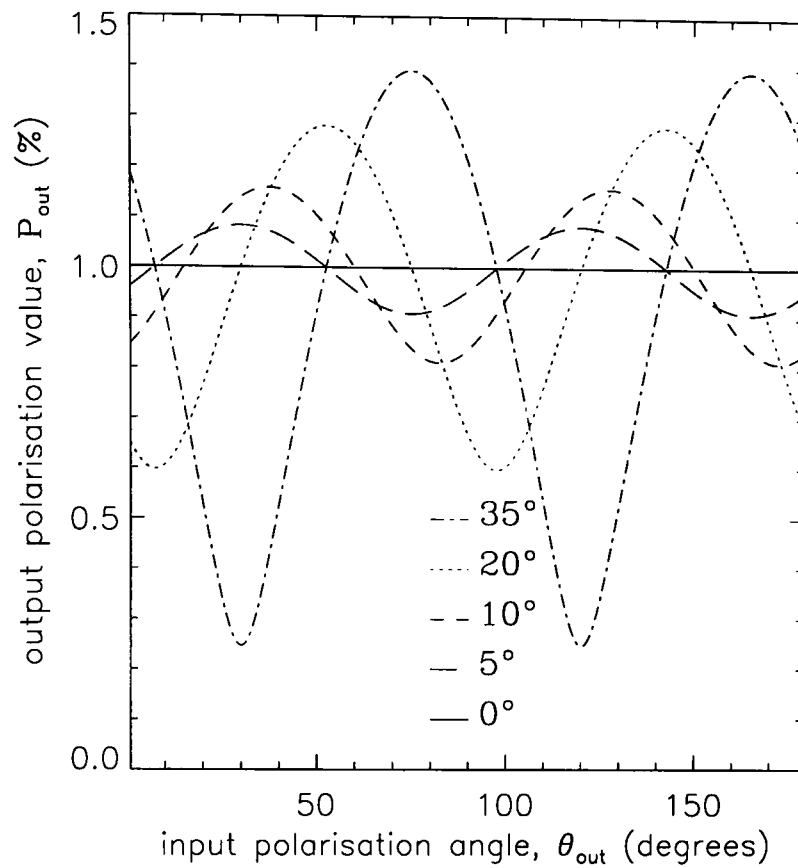


Figure 4.34: Plot showing the effect on P_{out} when the error, ϵ_2 , takes the values of $0^\circ, 5^\circ, 10^\circ, 20^\circ$, and 35° .

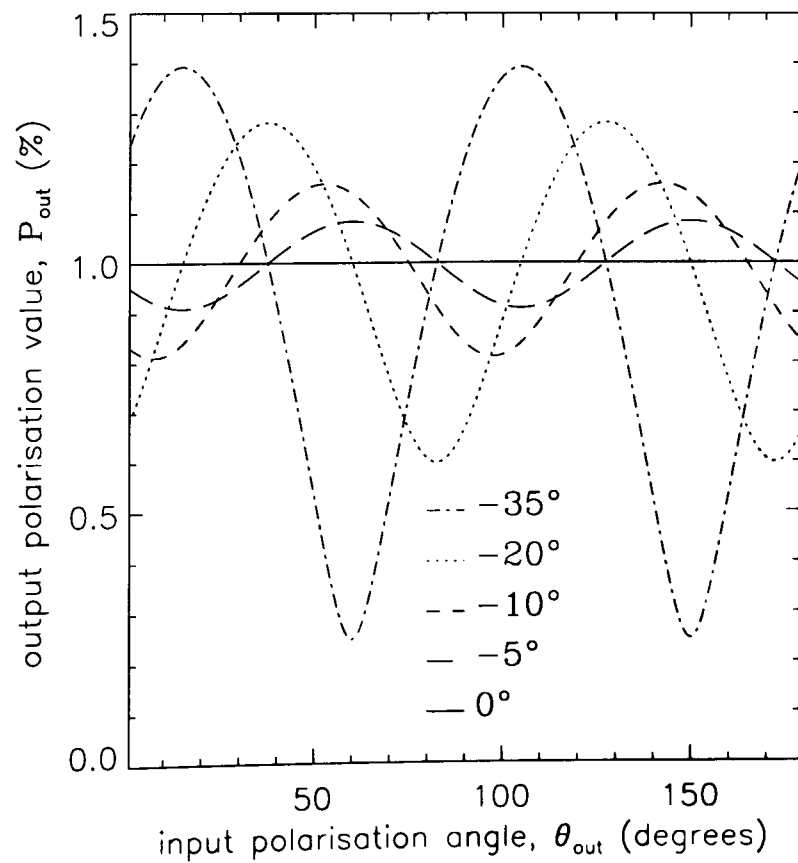


Figure 4.35: Plot showing the effect on P_{out} when the error, ϵ_2 , takes the values of $0^\circ, -5^\circ, -10^\circ, -20^\circ$, and -35° .

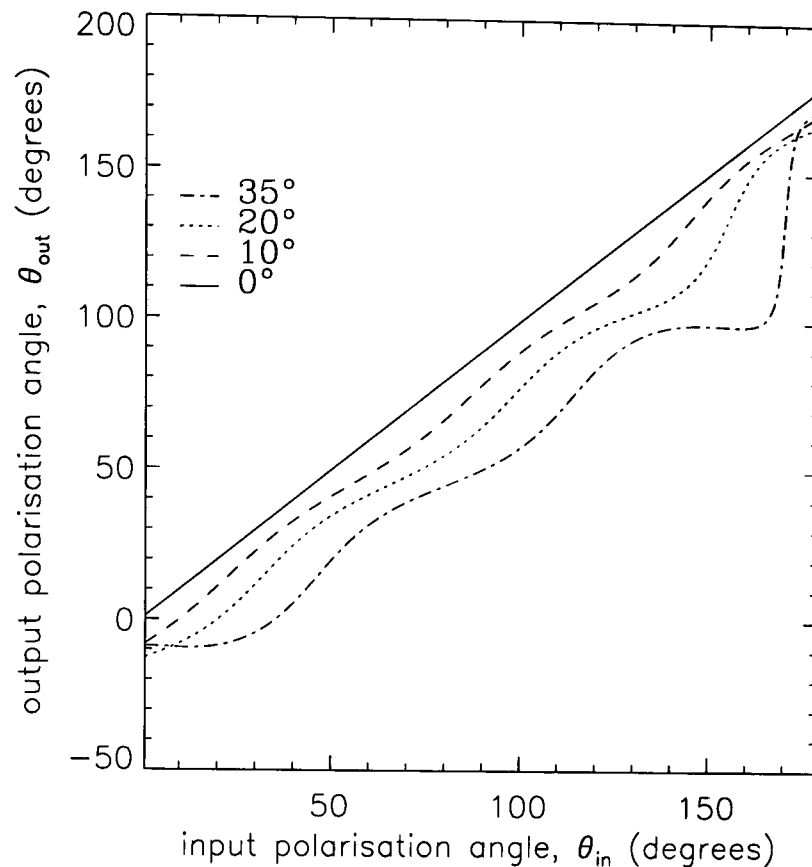


Figure 4.36: Plot showing the effect on θ_{out} when the error, ϵ_3 , takes the values of 0° , 10° , 20° , and 35° .

$$+U \cos^2(2\epsilon_3) \sin \delta_2 \sin \delta_1 \quad (4.25)$$

For large values of ϵ_3 , the curves become increasingly further removed from the $\theta_{in} = \theta_{out}$ line, but also become more distorted, such that the relationship for all θ_{in} , is no longer a mere offset of a fixed value. For a fixed ϵ_3 , the magnitude of $\theta_{in} - \theta_{out}$, actually varies depending on θ_{in} . For values of ϵ_3 less than 10° the curves become straighter, and, therefore for such small values of error, the system may be considered as having an instrumental fixed offset in position angle. Obviously, for negative values of ϵ_3 , the offset would also change sign.

Evidently, ϵ_3 alone cannot explain the observed experimental effect given in Table 4.7, since for all values of θ_{in} , all corresponding values of θ_{out} are altered in the same direction, i.e. either increased or decreased in value.

Inspection of Figs 4.38 and 4.39 reveals that there is a possibility of achieving $P_{out} < 100\%$ for $\theta_{in} = 0^\circ, 45^\circ, 90^\circ$ and 135° corresponding to input orientations of $+Q, +U, -Q$ and $-U$. However, to achieve values similar to the experimental results would require

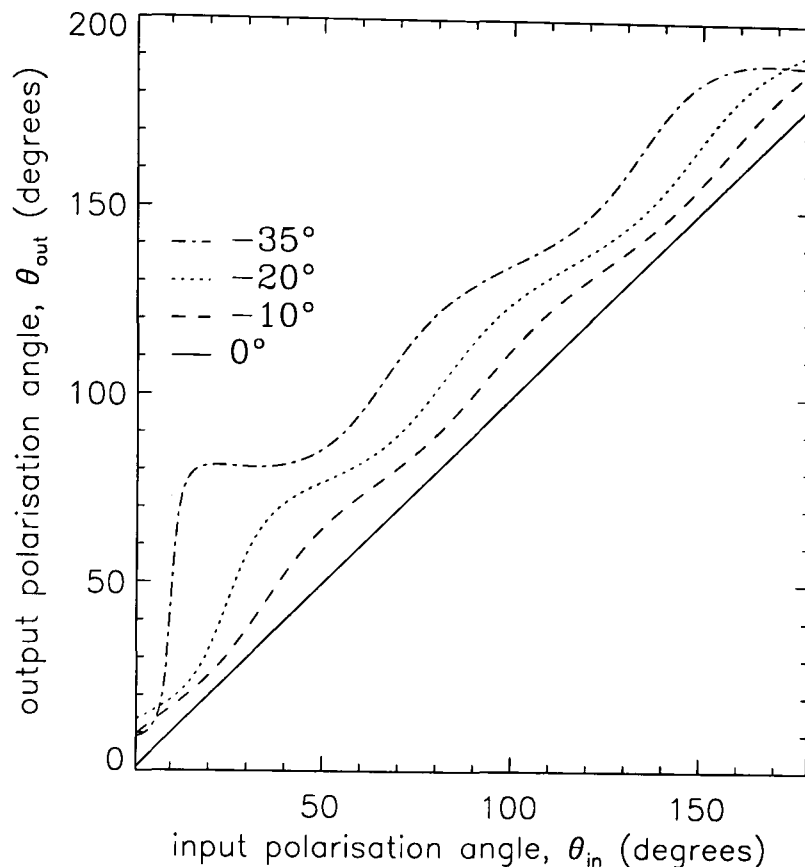


Figure 4.37: Plot showing the effect on θ_{out} when the error, ϵ_3 , takes the values of 0° , -10° , -20° , and -35° .

$\epsilon_3 \sim 20^\circ$. Again, it is unlikely that this error could be so large.

To conclude, it appears that none of the three errors declared in Table 4.8 are individually capable of explaining the observed trends of θ_{out} and P_{out} with θ_{in} . It was therefore necessary to investigate the combined effect of ϵ_1 , ϵ_2 and ϵ_3 .

4.6.2 The Combined Effect of the Three Important Errors

Only the special case of each of the three important errors being equal to 5° was considered, but the effect of changing ϵ_1 , ϵ_2 and ϵ_3 , from $+5^\circ$ to -5° was investigated by experiment. Figs 4.40 and 4.41 show the theoretical results, for all combinations of the three errors. At first glance it is notable that for $\theta_{in} = 90^\circ, 180^\circ$ corresponding to $-Q$ and $+Q$, the special case of $\epsilon_1 = \epsilon_2 = \epsilon_3 = +5^\circ$ may explain the experimentally observed deviation of $\theta_{in} - \theta_{out} \sim +1^\circ$ to $+6^\circ$. In fact the plot shows that this discrepancy would be as large as 10° for a $+5^\circ$ error in ϵ_1 , ϵ_2 and ϵ_3 . However, for this combination of errors, theory predicts that for $\theta_{in} = 45^\circ, 135^\circ$ (input of $+U$ and $-U$), that the discrepancy

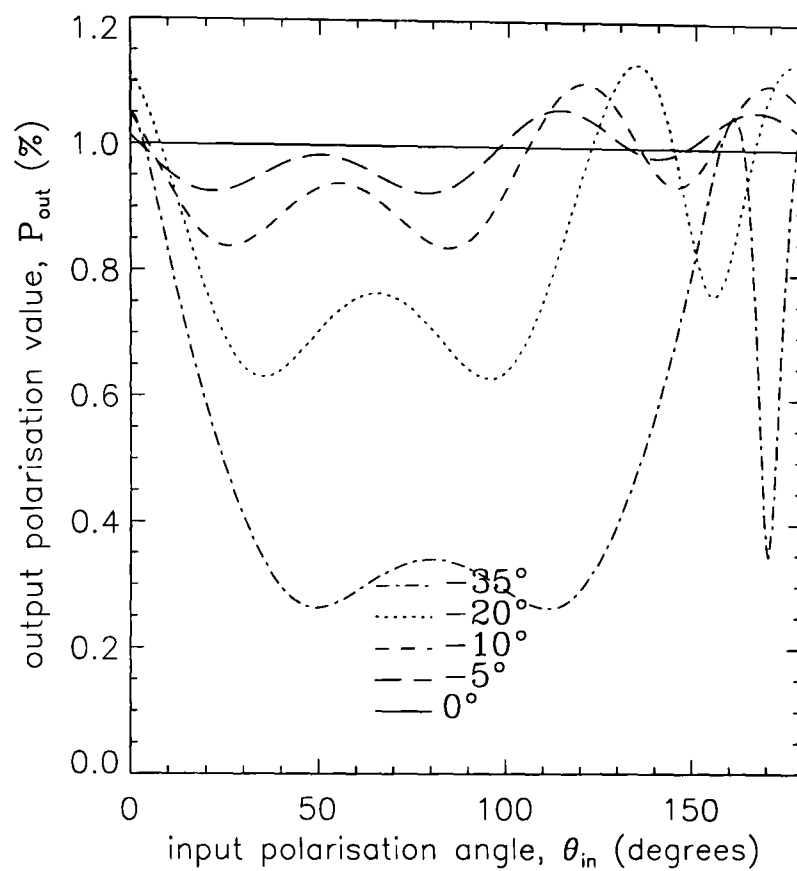


Figure 4.38: Plot showing the effect on P_{out} when the error, ϵ_3 , takes the values of $0^\circ, 5^\circ, 10^\circ, 20^\circ$, and 35° .

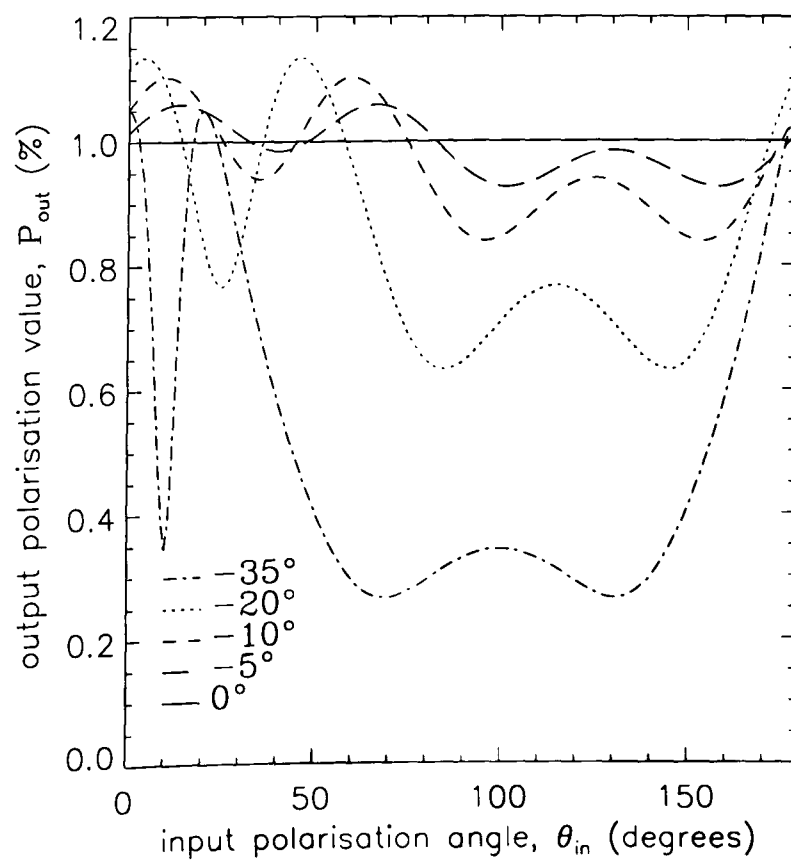


Figure 4.39: Plot showing the effect on P_{out} when the error, ϵ_3 , takes the values of $0^\circ, -5^\circ, -10^\circ, -20^\circ$, and -35° .

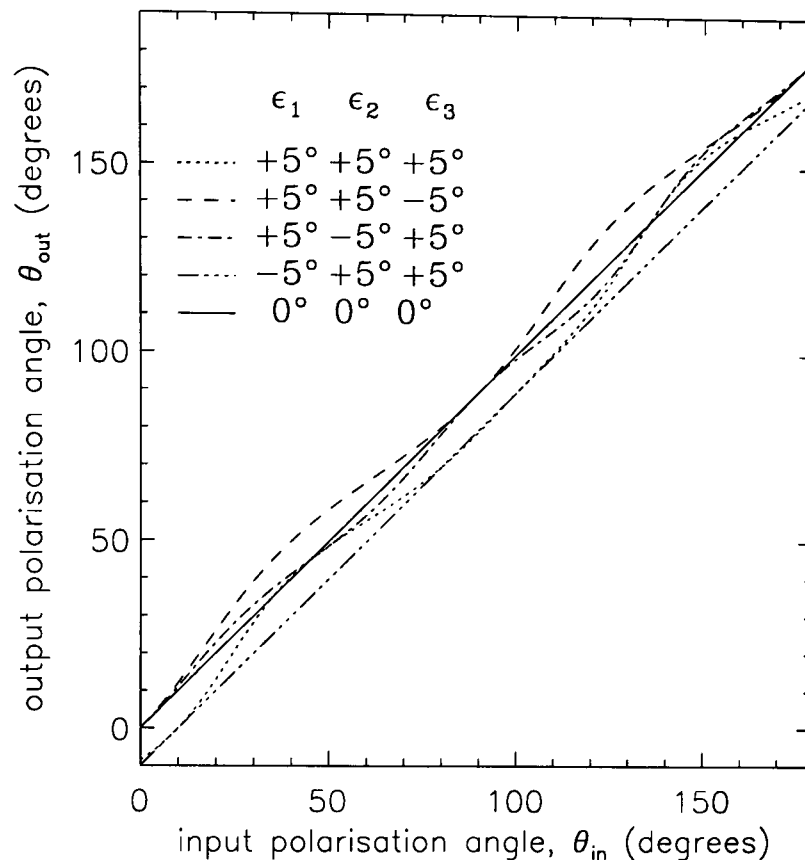


Figure 4.40: Plot showing θ_{out} , versus the input polarisation angle, θ_{in} , for different combinations ϵ_1, ϵ_2 and ϵ_3 .

$\theta_{in} - \theta_{out} = 0$. Alternatively, $\epsilon_1 = \epsilon_2 = +5^\circ$ and $\epsilon_3 = -5^\circ$, offers an explanation for the deviation of $\theta_{in} - \theta_{out} \sim -6^\circ$ to -7° for $\theta_{in} = 45^\circ, 135^\circ$, but does not explain the positive deviation for $\theta_{in} = 90^\circ, 180^\circ$. At the specific input orientations of $+Q, -Q, +U$ and $-U$, it is seen that for the cases $\epsilon_1 = +5^\circ, \epsilon_2 = -5^\circ, \epsilon_3 = +5^\circ$, and $\epsilon_1 = -5^\circ, \epsilon_2 = +5^\circ, \epsilon_3 = -5^\circ$, that there should be **NO** discrepancy and $\theta_{in} = \theta_{out}$.

Observation of Figs 4.42 and 4.43 reveals that there is only one of the given combinations of ϵ_1, ϵ_2 and ϵ_3 , which can explain why at all four input angles corresponding to $+Q, -Q, +U$ and $-U, P_{out} < 100\%$. This combination is $\epsilon_1 = -5^\circ, \epsilon_2 = +5^\circ, \epsilon_3 = -5^\circ$. Unfortunately, whilst this gives $P_{out} \sim 80\%$ for $\theta_{in} = 90^\circ, 180^\circ$, it does not offer an explanation as to why the experimental values of P_{out} for $\theta_{in} = 45^\circ, 135^\circ$, are significantly greater than the theoretical values.

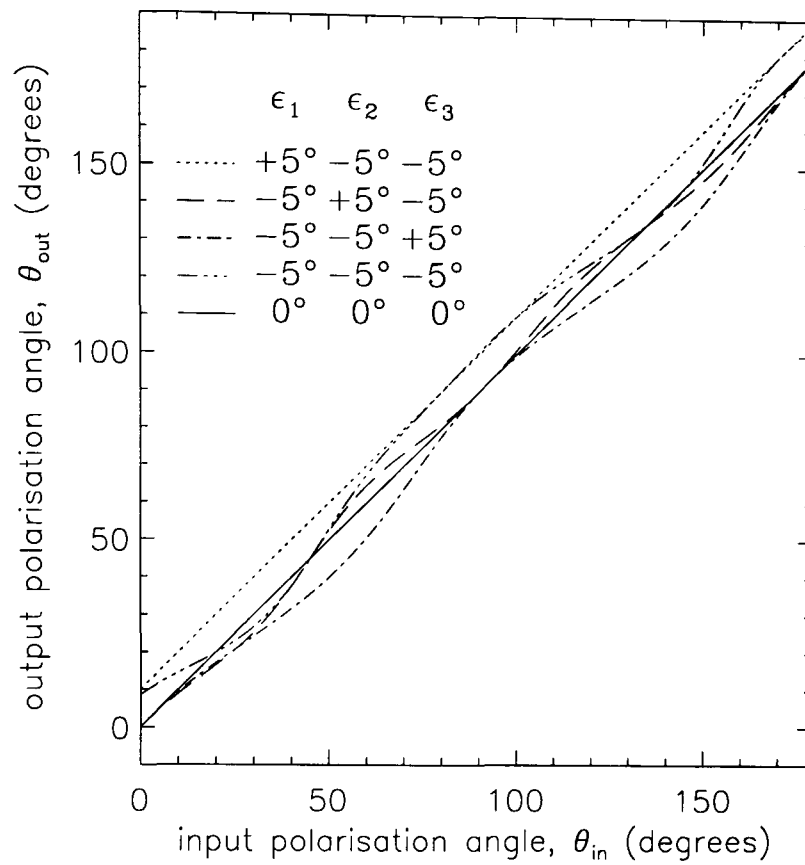


Figure 4.41: Plot showing θ_{out} , versus the input polarisation angle, θ_{in} , for different combinations ϵ_1, ϵ_2 and ϵ_3 .

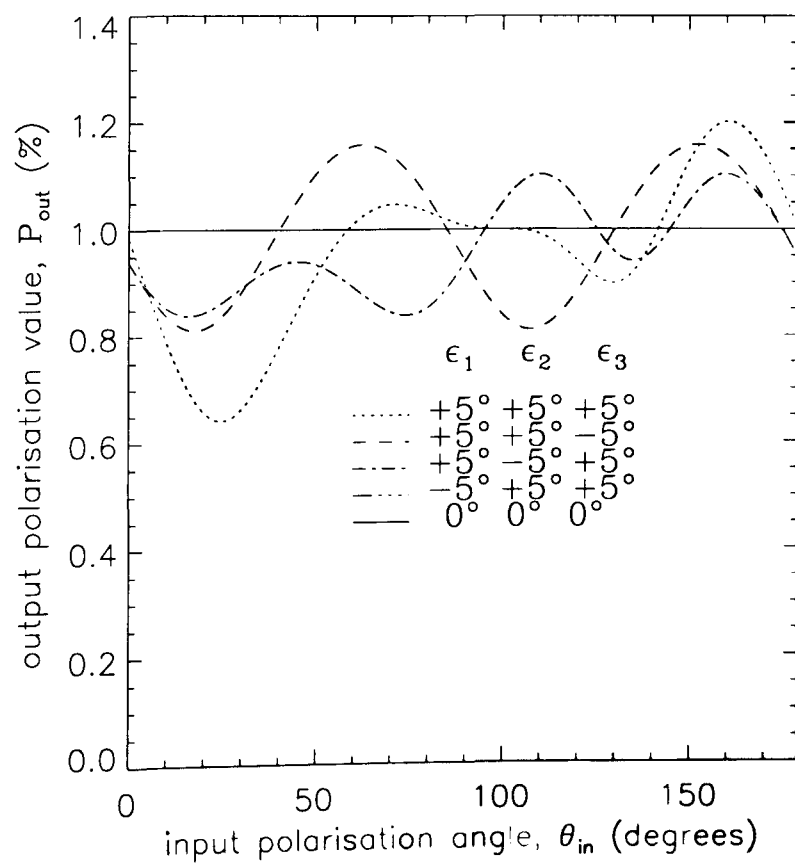


Figure 4.42: Plot showing P_{out} , versus the input polarisation angle, θ_{in} , for different combinations ϵ_1, ϵ_2 and ϵ_3 .

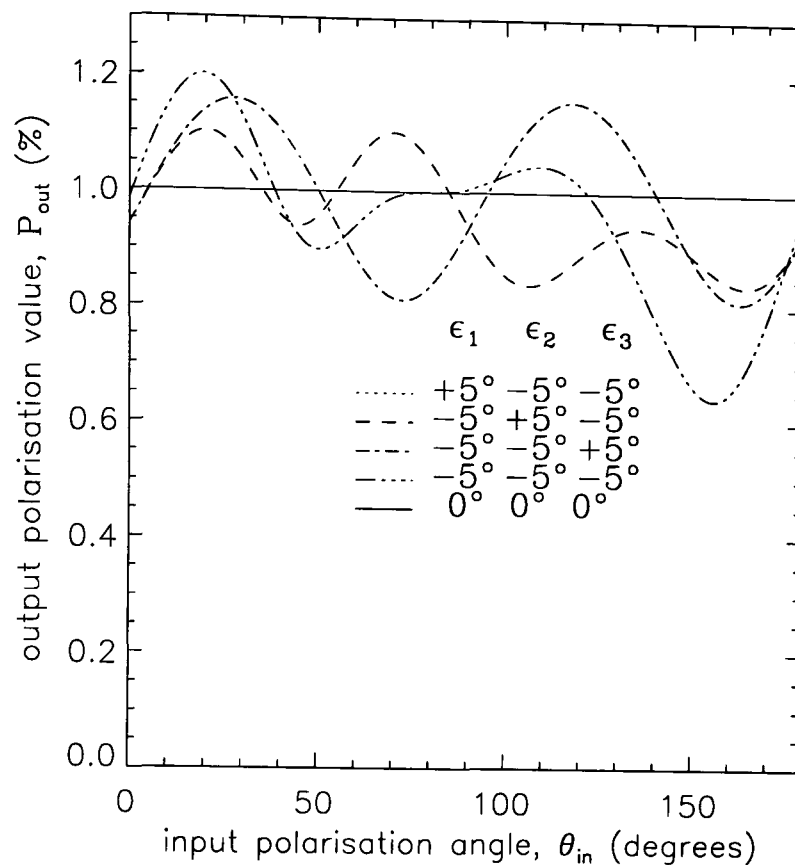


Figure 4.43: Plot showing P_{out} , versus the input polarisation angle, θ_{in} , for different combinations ϵ_1 , ϵ_2 and ϵ_3 .

4.6.3 Effects of the Passband

It must be remembered that the light beam passing through the polarimeter, is actually not at the one specific wavelength of 560nm, as has been assumed in the preceding error analysis, but is in fact centered on 560nm, with a pass band of 10nm. It was therefore worthwhile to determine what effect this actual beam would have on P_{out} and θ_{out} . In Figs 4.44, 4.45, 4.46 and 4.47, it has been assumed that the shape of the filter pass band is Gaussian, with maximum transmittance centered on 555nm. Analysis shows that introduction of such a passband merely raises all the curves of θ_{out} v. θ_{in} by $\sim 3^\circ$, even for the case of $\epsilon_1 = \epsilon_2 = \epsilon_3 = 0^\circ$. This effect, allows for an explanation as to why $\theta_{in} - \theta_{out}$ is positive for an input of $+Q$ and $-Q$, and negative for $+U$ and $-U$. Reference to Figs 4.44 and 4.45 proves that when $\epsilon_1 = \epsilon_2 = \epsilon_3 = 5^\circ$ the observed behaviour can be explained. At $\theta_{in} = 180^\circ, 0^\circ$ ($+Q$ input), $\theta_{in} - \theta_{out} \sim 7^\circ$, and this is repeated for $\theta_{in} = 90^\circ$ ($-Q$ input). At $\theta_{in} = 45^\circ$, and 135° corresponding to $+U$ and $-U$ input, $\theta_{in} - \theta_{out} \sim -3^\circ$.

The most significant deviation, is seen for the effect upon P_{out} . Figs 4.46 and 4.47

show that even for $\epsilon_1 = \epsilon_2 = \epsilon_3 = 0^\circ$, the plot has been distorted from a simple straight line of $P_{out} = 100\%$ to an oscillatory curve. Inspection also reveals that the minima and maxima of each curve have decreased and increased, respectively, when compared to Figs 4.42 and 4.43.

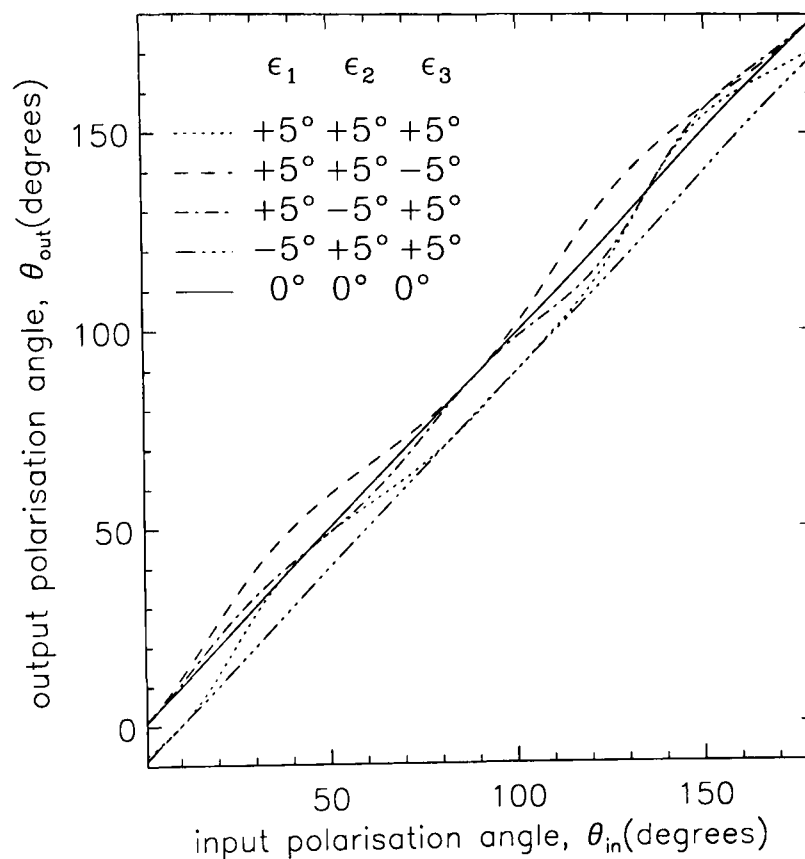


Figure 4.44: Plot showing θ_{out} , versus the input polarisation angle, θ_{in} , for different combinations ϵ_1, ϵ_2 and ϵ_3 , when the the input beam is taken to be centered on 555nm with a pass band of 10nm, for which the profile is Gaussian.

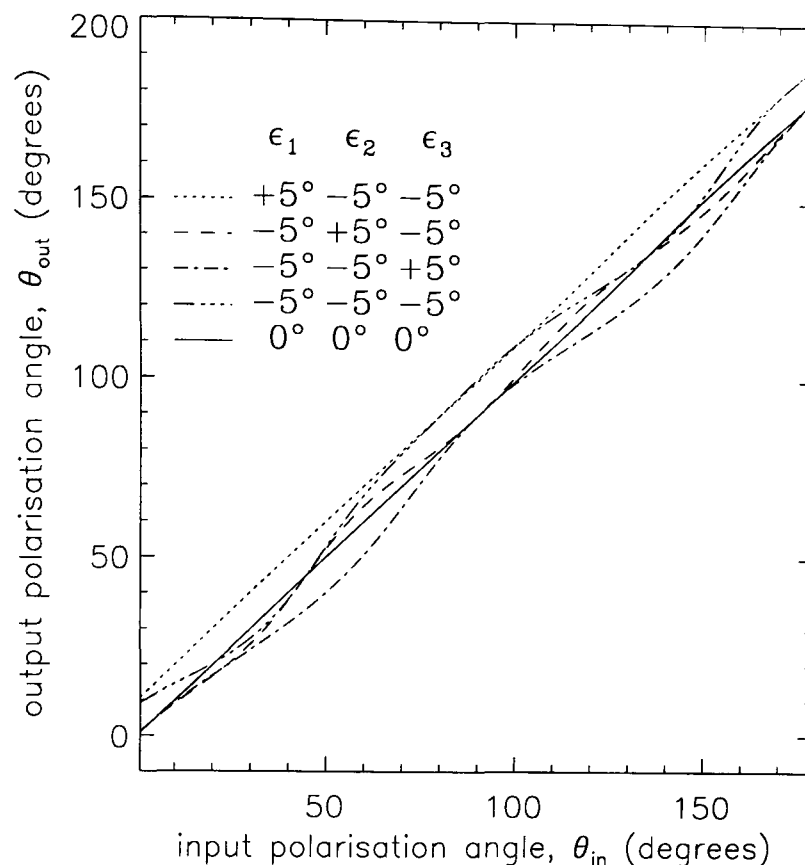


Figure 4.45: Plot showing θ_{out} , versus the input polarisation angle, θ_{in} , for different combinations ϵ_1, ϵ_2 and ϵ_3 , when the the input beam is taken to be centered on 555nm with a pass band of 10nm, for which the profile is Gaussian.

4.7 Summary

In conclusion, it is immediately evident from Figs 4.46 and 4.47, that the alignment of the two composite liquid crystal/compensator plate, units (δ_1 and δ_2), is of paramount importance. For only $\epsilon_1 = \epsilon_2 = \epsilon_3 = 5^\circ$, it is evident that P_{out} may be reduced from near 100% to as low as 62%, or increased to as high a value as 117% ! However, for certain combinations of the three important errors, their addition may result in the behaviour of P_{out} with θ_{in} , being very nearly coincident with the case when all errors are equal to zero (eg. $\epsilon_1 = -5^\circ, \epsilon_2 = \epsilon_3 = +5^\circ$). It is therefore crucial that great care is taken in the optical alignment procedure detailed in section 4.3, as even a slight deviation at each step may combine to produce a large resultant error in P_{out} .

Even if the alignment procedure is 100% accurate, and $\epsilon_1 = \epsilon_2 = \epsilon_3 = 0^\circ$, it is of particular interest that for a 10nm bandpass with a Gaussian transmittance profile, that P_{out} is dependent on θ_{in} , fluctuating between near 100% and 93%. If indeed, all errors

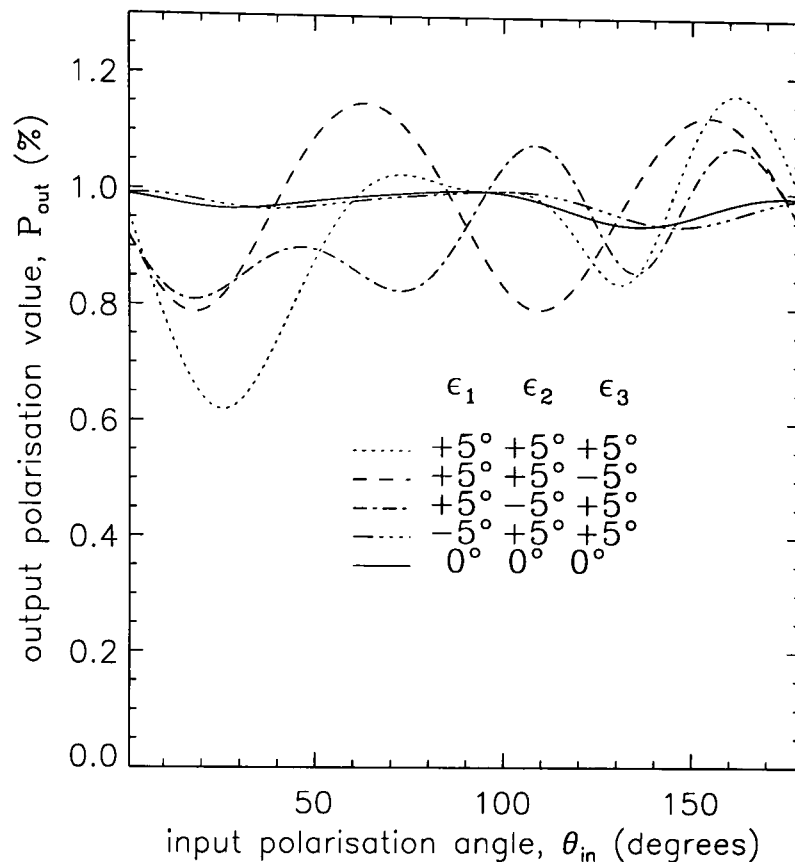


Figure 4.46: Plot showing P_{out} , versus the input polarisation angle, θ_{in} , for different combinations ϵ_1, ϵ_2 and ϵ_3 , when the input beam is taken to be centered on 555nm with a pass band of 10nm and a Gaussian profile.

were equal to zero, then it would be simple to correct for this offset in experimental data as θ_{in} is known, and hence the deviation that would be expected on P_{out} .

Unfortunately, it appears that there are large errors inherent within the polarimeter, since the experimentally determined values of P_{out} and θ_{out} , are significantly deviant from the theoretical predictions. However, explanation is provided for the trend of the experimentally determined values of $\theta_{in} - \theta_{out}$, and this is in the case of $\epsilon_1 = \epsilon_2 = \epsilon_3 \sim +5^\circ$, for when the beam passing through the system is assumed to have a Gaussian shaped pass band centered on 555nm.

Observation of Figs 4.42 and 4.43 reveals that there is only one of the given combinations of ϵ_1, ϵ_2 and ϵ_3 , which can explain why at all four input angles corresponding to $+Q, -Q, +U$ and $-U$, $P_{out} < 100\%$. This combination is $\epsilon_1 = -5^\circ, \epsilon_2 = +5^\circ, \epsilon_3 = -5^\circ$. Unfortunately, whilst this gives $P_{out} \sim 80\%$ for $\theta_{in} = 90^\circ, 180^\circ$, it does not offer an explanation as to why the experimental values of P_{out} for $\theta_{in} = 45^\circ, 135^\circ$, are significantly greater than the theoretical values.

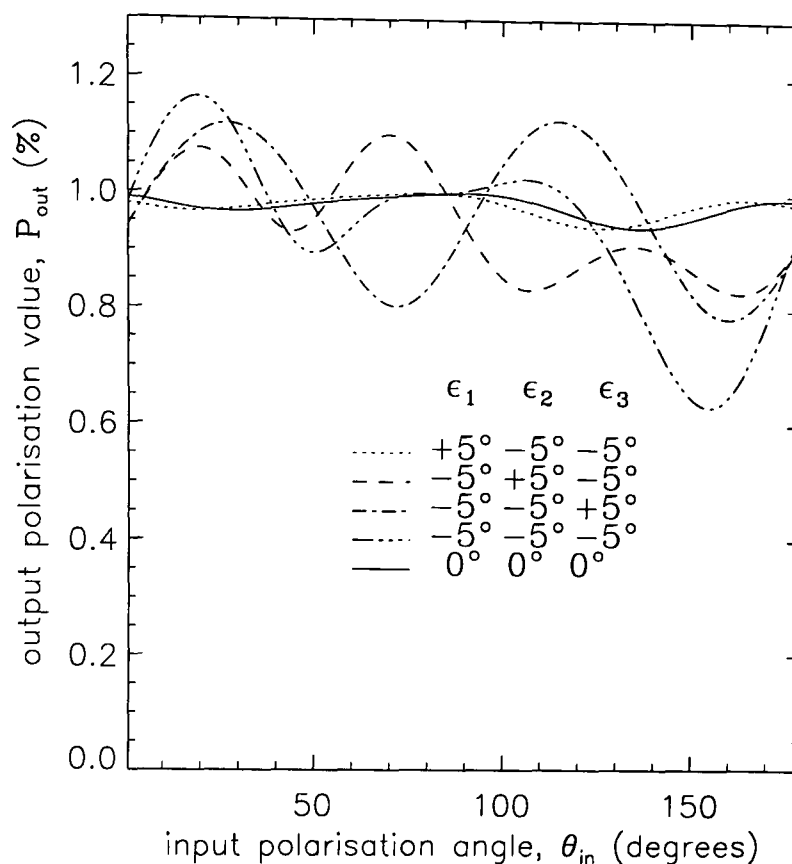


Figure 4.47: Plot showing P_{out} , versus the input polarisation angle, θ_{in} , for different combinations ϵ_1, ϵ_2 and ϵ_3 , when the the input beam is taken to be centered on 555nm with a pass band of 10nm and a Gaussian profile.

It is of great advantage to develop a polarimetric modulator with no mechanically moving elements. To this end the development of a device incorporating two Meadowlark liquid crystals has been investigated. This method is highly suitable for spectropolarimetry, with a slit spectrometer, where movement of the image on the slit will be minimised. However, upon analysis of the effects of passing light of a wide band pass through the instrument, it is evident that its use for spectropolarimetry is restricted. Clearly, the different spectral elements will be modulated with different levels of efficiency. It is this effect of the band pass, and not the method used to align the optical components, which is the dominant factor causing the disparity between observed values from the Twin Liquid Crystal Polarimeter, and the theoretical results.

Chapter 5

Conclusion

This chapter concludes the work of this thesis, summarising the findings and main achievements. Each individual theme will be discussed in turn, bringing together the main points to note from each chapter. Suggestions will be made for possible future work and research in the appropriate fields, to enhance and build upon the work done here.

Chapter 2 is concerned with measurements taken over seven nights in May 1996 on the 0.75m telescope at Sutherland, South Africa, using the Cape Town Polarimeter. The purpose of the program was to observe solar type stars, and the stars were selected by having a spectral classification around G5V. Whilst it is known that the optical radiation of about 85 % of young stars at both ends of the spectral classification sequence, exhibit intrinsic linear polarisation, there is little information on the polarimetric properties for intermediate spectral types. These types range between F and early G8, and they represent about 15% of the total objects, and most have not been studied polarimetrically. Recently it has been considered that such polarimetric properties of these stars might be considered from the point of view of their circumstellar evolution (Tamura and Sato (1989) and Yudin (1994)). Such ideas are discussed in Chapter 2 and the results of the observing campaign are analysed for temporal variability, using known statistical tests, with the aim of detecting any change in polarisation.

In summary, a preliminary synoptic study has been made of a sample of young solar type stars with the aim of detecting activity via polarimetry. Previous studies, both

theoretical and observational, suggest that the levels of any polarization are likely to be small. As the stars are effectively solar type in terms of their luminosity and display high apparent brightness, they are relatively close and unlikely to be contaminated by interstellar polarization.

For the work reported here, both the linear and circular components have been investigated with typical measurement uncertainties in q, u and $v \sim \pm 0.0003$. This high level of accuracy causes problems with the assessment and removal of instrumental polarization due to the inadequacy of the catalogued unpolarized and polarized standard stars. In addition, even if the reference stars provided well calibrated sources, an in-ordinate amount of time from the observational run would be required to perform their measurement to the required levels of accuracy. Consequently the tabulated polarimetric values for the programme stars may be subject to systematic errors of the order of the uncertainties of their measurements but this in no way negates the investigations and detections of any variable intrinsic polarization.

The sample of investigated stars is small and the time window for the measurements is very limited. Of the stars suspected of displaying polarimetric variability, there are no similarities of behaviour. The most remarkable recorded event was for SAO154972 (TU Pyx) which displayed a sudden change in polarization from a level $\sim 0.5\%$ to $\sim 2.0\%$ in a time interval of about 15 minutes. There is also a strong indication of circular polarization associated with this star, suggesting the presence of magnetic activity. It is important that this object be included as a prime target in future polarimetric programmes.

Measurements of HD 115383 (59 Vir) on four nights display polarization variations ($\sim 0.1\%$) which are coherent in the B and V bands, the latter providing the larger amplitude about the origin. The behaviour hints at cyclic changes with a period related to that expected of rotation. There is also evidence for a detection of circular polarization in the V band. The data for HD 155555 also display night-to-night variations in the V band but not in B; these may be related to previously monitored photometric variability which is also most strongly apparent in the V band.

The data for HD 1835 are very limited but there is marginal evidence for detection of a weak polarization in the B band.

All of these stars require further observations to characterise their polarimetric behaviour and to confirm that the observed effects are related to active regions traversing the projected disk as a result of stellar rotation or to other causes. A more comprehensive study would help to further present understanding of the placing solar type stars have in stellar evolution, and aid in the continuing development of a comprehensive theory explaining the connection between early type stars and G types. It is fundamental to stellar physics and the interpretation of data from stars, to be able to understand how they evolve, and the relevant processes occurring within, and around them, during each stage.

Within Chapter 2, polarimetric data have also been presented for the Ae star HD 139614, and its behaviour relative to similar stars has been discussed. In spite of a low level of polarisation ($\sim 0.05\text{-}0.2\%$), polarimetric variability on a time-scale of days was detected during a four night synoptic study. It is suggested that the difference in the level of polarisation for HD 139614 relative to other Herbig Ae/Be stars such as HD 141549, HD 142666 and HD 169142 might be due to the inclinations and viewing aspects of their circumstellar disks. The $v \sin i$ values for the latter three stars, together with their high levels of polarisation and large amplitude of polarimetric variability, support the hypothesis that these stars exhibit circumstellar disks with edge-on aspects. In terms of a model proposed by Meeus et al. (1998) for HD 142666, the irregular brightness variations are caused by dense nodules in the dust clouds which occasionally cross the projected stellar disk, i.e. the disk is being viewed edge-on. The non-variable photometric behaviour of HD 139614 suggests a more (but probably not exactly) pole-on orientation of a disk.

It is important to undertake precise multicolour observations to investigate the $p(\lambda)$ behaviour of HD 139614 and to obtain a longer time series of measurements to confirm the periodicity of the polarimetric variations. More generally, it is also important to extend photometric/polarimetric studies of Herbig Ae/Be stars with approximately the same IR excesses and physical properties (spectral types and brightness) to allow better interpretation of the model and the role that disk orientation plays on their observed behaviour.

One other star measured and analysed within Chapter 2 was the Be star HD 100546.

Three nights of observation have revealed night-to-night polarimetric changes in this star, both linear and circular. Over windows of ~ 2 hours, however, no polarimetric variation either secular or of a more stochastic nature was detected with measurement uncertainties $\sim \pm 0.02\%$. No hint of the temporal behaviour as reported by Yudin and Evans (1998) was detected over a total monitoring time ~ 6 hours, even though the measurements were recorded with experimental uncertainties which were some 5 times smaller. Comparison of the data of Yudin and Evans shows that the $p(V)$ values occupy a similar region in the q, u plane but that the $p(B)$ are displaced as a result of u values being negative. Thus the ratio $p(B)/p(V)$ has changed significantly between the data sets of Yudin and Evans and those presented here. Such a variation may be brought about by a change in the average opacity in the stellar disk or by a change in the contribution of the circumstellar dust component.

It is important that this star should be monitored more extensively to explore the nature of the variation in p and to investigate the circular polarization further with a view to confirming its origin. In order to help determine the degree of clumpiness in the circumstellar structure which produces the night-to-night variations in p , it is important to record the rate at which the polarimetric changes occur. Measurements made with a broader range of wavelength coverage would also be useful to distinguish between electron scattering and Mie scattering from the dust in the stellar environment.

The concern of Chapter 3 was to investigate the Kolmogorov statistical technique as a means of detecting low levels of polarimetric variability. Traditionally used as a means of assessing the similarity between two distributions, it is particularly useful for obtaining a reasonable hypothesised distribution, as an approximation to a real distribution. The aim of Chapter 3, was to compare the data from a set of polarised stars, with their calculated theoretical normal distributions, generated from the observed mean and standard deviation. Particular attention has been made towards assessing the effect of the standard error on the observed means, and the subsequent effect on any conclusions made from the statistical test. This consideration leads to a more conservative test than previously appreciated, which is especially important when looking for very low levels of temporal variability.

The candidate stellar data set chosen for the investigation, were measurements of λ

Cep, ξ Per and ϕ Cas. These stars have all been investigated for other types of variability, e.g. photometric. Kaper and Heinrichs (1997) conducted simultaneous ultraviolet and H α spectroscopy of λ Cep and ξ Per, and observed changes in the H α line at low velocity ($0 - 0.2v_\infty$) on time scales that are consistent with the development and evolution of discrete absorption components (DACs) in UV resonance lines. Heinrichs (1998) also present findings from a multi-wavelength campaign to observe ξ Per and investigate the cause of variability of the stellar wind, suggesting that magnetic activity on patches on the stellar surfaces be the most promising candidate for generating structures in the wind. It was thus considered a worthwhile experiment to investigate these stars for signs of temporal variability in polarisation, using the statistical test described above, as the presence of variability of polarisation is likely to be small, and therefore a sensitive statistical technique is needed.

The chapter ends with a summary of the main findings. The existence of polarimetric variability inherent to the previously considered polarisation standard, ϕ Cas has been detected by Kolmogorov testing within the time-scale of one particular night. A Welch test reveals no indication of any other variability from night to night. Evidence of temporal variability has been demonstrated for ξ Per, in accordance with spectroscopic variability discussed in Heinrichs (1998). Evidence for variability of p in λ Cep has been put into question, and clearly further data are needed on this star. The use of the Kolmogorov technique has been examined as a means of detecting low levels of variability in both p and θ . Particular attention has been given to the intrinsic error present on the determination of the centre of gravity of a distribution, and its propagation to the theoretical normal CDF plots generated from the real observed mean and standard deviation. It has been shown that where a straight forward Kolmogorov test would lead to the conclusion of the presence of some variability, the inclusion of consideration of the standard error on the observed mean, can result in the rejection of this initial conclusion. Hence, this method of testing is more conservative and rigorous than the usual method of Kolmogorov testing.

The theme of Chapter 4 was the development of the Twin Liquid Crystal Polarimeter. The intention was to design a polarimeter which was capable of determining both linear Stokes parameters, without the need for any mechanical rotation or movement of the optical components within the instrument. No matter the chosen system, rotation of a wave

plate within a polarimeter, may cause movement of the light beam passing through it, thus producing spurious signals which may be larger than the polarimetric signal of interest. By investigating the Meadowlark Liquid Crystal Cell it has been possible to initially develop a polarimeter using just one cell. However, the use of this device, still required a mechanical rotation to determine both linear Stokes' parameters. By the employment of two cells in series, configured in a set configuration, it has been possible to develop a twin liquid crystal polarimeter, which is capable of determining both parameters, without any need for mechanical movement of the individual components. This can only serve to improve the accuracy with which the polarisation of a source, may be determined.

It is evident that upon the experimental testing of the final instrument, there is some discrepancy between the values of polarisation input to the polarimeter, and those measured and determined by the instrument. In an attempt to explain this discrepancy, the main errors which may be present in the alignment of the optical components are considered, and the calculated output values determined when the magnitude of these errors are adjusted. It is apparent from this analysis, that alignment of the components is absolutely crucial, and examples have been given which explain the observed discrepancies between input and determined output values of polarisation, when the errors are assumed to take specific values. However it is clear that the most important factor, is the effect of the wavelength pass band of the light used for testing. When the experimentally determined values of polarisation and polarisation angle are compared with the actual values of the light beam input to the polarimeter, the discrepancy is best modeled when the effect of a 100 nm Gaussian shaped pass band for the filter is assumed, allowing for small errors in the alignment of the optical components.

In Summary, the development of a device incorporating two Meadowlark liquid crystals has been investigated. This method is highly suitable for spectropolarimetry, with a slit spectrometer, where movement of the image on the slit will be minimised. However, upon analysis of the effects of passing light of a wide band pass through the instrument, it is evident that its use for spectropolarimetry is restricted. Clearly, the different spectral elements will be modulated with different levels of efficiency. It is this effect of the band pass, and not the method used to align the optical components, which is the dominant factor causing the disparity between observed values from the Twin Liquid Crystal

Polarimeter, and the theoretical results.

Appendix A

UCT Data Prior To Reduction

The following tables show the *raw* data, collected from the UCT Polarimeter, uncorrected for sky background or instrumental polarisation. The symbols displayed in the column headings represent the measured normalised Stokes parameters q , u and v , with the associated errors on the signal being σ .

JD	BAND	q	σ_q	u	σ_u	v	σ_v
0225.606	B	0.594	0.177	-0.387	0.177	-0.200	0.125
0225.608	B	0.142	0.068	-0.328	0.068	-0.024	0.048
0226.653	B	0.173	0.029	-0.263	0.029	-0.047	0.020
0229.568	B	0.141	0.055	-0.172	0.055	0.001	0.039
0229.573	B	0.209	0.055	-0.192	0.055	0.004	0.039
0229.579	B	0.184	0.055	-0.224	0.055	-0.026	0.039
0229.584	B	0.203	0.054	-0.196	0.054	0.003	0.038
0229.590	B	0.135	0.054	-0.265	0.054	0.066	0.038
0229.560	B	0.162	0.054	-0.313	0.054	-0.028	0.038
0229.601	B	0.112	0.054	-0.268	0.054	-0.055	0.038
0229.607	B	0.134	0.054	-0.265	0.054	0.055	0.038
0229.611	B	0.157	0.054	-0.274	0.054	-0.026	0.038
0229.616	B	0.081	0.054	-0.223	0.054	0.049	0.038
0230.542	B	0.073	0.057	-0.345	0.057	0.089	0.040

0230.548	B	0.190	0.059	-0.081	0.059	0.012	0.042
0230.553	B	0.103	0.057	-0.165	0.057	-0.046	0.041
0230.558	B	0.136	0.057	-0.212	0.057	-0.012	0.040
0230.563	B	0.015	0.057	-0.233	0.057	-0.045	0.040
0230.568	B	0.093	0.057	-0.198	0.057	-0.035	0.040
0230.573	B	0.140	0.059	-0.180	0.059	-0.053	0.042
0230.579	B	0.154	0.059	-0.171	0.059	0.080	0.042
0230.584	B	0.249	0.056	-0.305	0.056	0.059	0.040
0230.590	B	0.275	0.056	-0.205	0.056	0.098	0.040
0225.584	V	0.024	0.045	-0.057	0.045	-0.071	0.032
0226.621	V	0.048	0.017	-0.097	0.017	0.001	0.012
0226.637	V	0.006	0.017	-0.047	0.017	-0.021	0.012
0229.570	V	0.050	0.035	-0.133	0.035	-0.063	0.025
0229.575	V	-0.014	0.035	-0.113	0.035	-0.031	0.025
0229.581	V	0.032	0.035	-0.101	0.035	0.002	0.025
0229.586	V	0.040	0.035	-0.058	0.035	-0.006	0.025
0229.592	V	0.114	0.035	-0.088	0.035	-0.050	0.025
0229.597	V	0.055	0.035	-0.012	0.035	-0.033	0.025
0229.603	V	0.103	0.035	-0.106	0.035	-0.054	0.025
0229.609	V	-0.013	0.035	-0.180	0.035	-0.018	0.025
0229.614	V	0.036	0.035	-0.107	0.035	0.031	0.025
0229.618	V	0.129	0.035	-0.132	0.035	-0.012	0.025
0230.544	V	0.035	0.036	-0.048	0.036	-0.055	0.025
0230.550	V	0.010	0.037	-0.087	0.037	-0.054	0.026
0230.555	V	0.073	0.036	-0.045	0.036	-0.066	0.026
0230.561	V	0.060	0.042	-0.072	0.042	-0.033	0.030
0230.565	V	0.084	0.036	-0.080	0.036	-0.007	0.026
0230.570	V	0.102	0.036	-0.109	0.036	-0.028	0.026
0230.575	V	0.059	0.037	-0.060	0.037	0.059	0.026
0230.581	V	0.019	0.037	-0.093	0.037	-0.017	0.026

0230.587	V	0.126	0.036	-0.148	0.036	0.005	0.025
0230.592	V	0.044	0.036	-0.035	0.036	0.011	0.025

Table A.1: Weighted means, and the normalised linear Stokes parameters expressed in percentage form, for HD202940 in the B, and V bands on the nights of 21,22,25,26 May 1996

JD	BAND	q	σ_q	u	σ_u	v	σ_v
0225.616	R	-0.074	0.127	-0.242	0.127	-0.175	0.090
0230.603	R	0.021	0.022	-0.025	0.022	-0.002	0.015
0230.609	R	-0.018	0.022	-0.001	0.022	-0.007	0.015
0230.613	R	0.065	0.031	-0.074	0.031	0.006	0.022
0230.615	R	0.017	0.030	-0.100	0.030	0.021	0.022
0230.619	R	0.048	0.031	-0.077	0.031	0.017	0.022
0230.621	R	-0.008	0.031	-0.041	0.030	0.056	0.022

Table A.2: Weighted means, and the normalised linear Stokes parameters expressed in percentage form, for HD202940 in the R band on the nights of 21,26 May 1996

JD	BAND	q	σ_q	u	σ_u	v	σ_v
0229.266	V	0.069	0.075	-0.036	0.075	-0.077	0.053
0229.269	V	0.091	0.075	0.002	0.075	-0.014	0.053
0229.272	V	-0.060	0.074	-0.108	0.074	-0.058	0.052
0229.275	V	0.017	0.074	-0.079	0.074	-0.082	0.052
0229.248	R	0.003	0.061	0.052	0.062	0.032	0.043
0229.251	R	-0.044	0.062	-0.098	0.062	0.019	0.044
0229.254	R	-0.013	0.062	0.030	0.062	-0.010	0.044
0229.257	R	-0.081	0.062	-0.038	0.062	0.060	0.044

Table A.3: Weighted means, and the normalised linear Stokes parameters expressed in percentage form, for HD100623 in the V and R bands on the night of 25 May 1996

JD	BAND	q	σ_q	u	σ_u
0225.421	U	0.796	0.287	3.480	0.287
0225.423	B	1.425	0.099	3.452	0.099
0228.455	B	1.179	0.046	3.348	0.046
0225.430	V	1.637	0.056	3.871	0.056
0228.462	V	1.677	0.027	3.890	0.027
0225.432	R	1.845	0.043	4.141	0.043
0228.473	R	1.758	0.021	4.113	0.021
0225.440	I	2.279	0.041	4.281	0.041

Table A.4: Data for HD147084, corrected for instrumental polarisation, but not rotated to equatorial frame

JD	BAND	q	σ_q	u	σ_u
0225.640	U	-0.260	0.335	-0.190	0.335
0225.657	B	2.564	0.063	2.356	0.063
0229.525	B	5.187	0.069	5.119	0.069
0229.530	B	5.107	0.069	4.954	0.069
0229.534	B	5.257	0.069	4.913	0.069
0229.540	B	5.325	0.069	5.000	0.069
0229.545	B	5.301	0.070	5.023	0.070
0225.673	V	5.778	0.045	4.876	0.045
0229.527	V	5.579	0.035	5.022	0.035
0229.532	V	5.653	0.035	5.018	0.035
0229.537	V	5.581	0.035	4.952	0.035
0229.542	V	5.552	0.035	4.920	0.035

0229.547	V	5.565	0.035	5.052	0.035
0225.678	R	5.367	0.037	4.624	0.037
0225.680	I	4.693	0.104	4.366	0.104

Table A.5: Data for HD160529 corrected for instrumental polarisation but not rotated to the equatorial frame.

JD	BAND	q	σ_q	u	σ_u	v	σ_v
0226.240	V	-0.077	0.068	-0.296	0.068	0.045	0.048
0227.218	V	-0.146	0.065	-0.193	0.065	0.053	0.046
0227.231	V	-0.038	0.066	-0.304	0.066	-0.076	0.047
0229.206	V	-0.119	0.122	-0.428	0.122	0.107	0.086
0229.209	V	-0.264	0.122	-0.776	0.122	0.057	0.086
0229.212	V	-0.122	0.122	-0.568	0.122	0.162	0.086
0229.215	V	-0.175	0.123	-0.594	0.123	-0.041	0.087
0230.266	V	0.042	0.106	-0.401	0.106	0.014	0.075
0230.272	V	0.137	0.105	-0.216	0.105	-0.085	0.074
0230.277	V	0.033	0.106	-0.495	0.106	0.184	0.075
0230.287	V	-0.068	0.106	-0.585	0.106	-0.046	0.075
0231.231	V	0.531	0.195	-0.553	0.195	0.210	0.137
0231.233	V	0.636	0.196	-0.457	0.196	0.079	0.138
0231.234	V	0.561	0.195	-0.086	0.195	0.079	0.137
0231.238	V	1.495	0.199	-2.095	0.199	0.090	0.139
0231.240	V	1.616	0.215	-2.076	0.215	0.063	0.151
0231.242	V	1.413	0.212	-2.062	0.212	0.034	0.149
0227.245	R	-0.038	0.032	-0.306	0.032	-0.032	0.022
0227.257	R	-0.115	0.032	-0.261	0.032	-0.040	0.023
0229.222	R	-0.086	0.058	-0.343	0.058	-0.072	0.041
0229.225	R	-0.117	0.058	-0.237	0.058	-0.022	0.041
0229.229	R	0.031	0.058	-0.302	0.058	-0.012	0.041
0229.232	R	-0.046	0.058	-0.186	0.058	0.001	0.041

0230.299	R	0.078	0.047	-0.248	0.047	0.054	0.033
0230.304	R	0.156	0.047	-0.245	0.047	-0.061	0.033
0230.309	R	0.066	0.047	-0.493	0.047	0.003	0.033
0230.314	R	0.135	0.048	-0.227	0.048	0.043	0.034

Table A.6: Weighted means, and the normalised linear Stokes parameters expressed in percentage form, for SAO154972 in the B, and V bands.

JD	BAND	q	σ_q	u	σ_u	v	σ_v
0225.465	U	-0.570	0.257	-0.389	0.257	0.186	0.181
0225.488	U	-0.218	0.248	-0.418	0.248	-0.177	0.175
0225.467	B	0.119	0.098	-0.032	0.098	0.015	0.069
0225.490	B	-0.003	0.086	0.055	0.086	0.050	0.061
0229.478	B	0.012	0.067	0.023	0.067	-0.027	0.047
0229.484	B	0.094	0.067	-0.041	0.067	0.000	0.047
0229.489	B	0.061	0.066	-0.097	0.066	0.099	0.047
0229.494	B	0.062	0.067	-0.163	0.067	-0.072	0.047
0229.500	B	0.036	0.067	-0.106	0.067	0.036	0.047
0230.485	B	0.036	0.067	0.008	0.067	-0.060	0.047
0230.490	B	-0.051	0.067	0.040	0.067	0.076	0.047
0230.495	B	-0.059	0.070	-0.075	0.070	-0.035	0.050
0230.500	B	-0.018	0.069	0.107	0.069	0.095	0.049
0230.504	B	0.130	0.069	-0.171	0.069	0.143	0.049
0230.510	B	-0.007	0.066	-0.036	0.066	0.120	0.047
0230.514	B	-0.050	0.066	-0.024	0.066	-0.076	0.047
0230.520	B	0.004	0.066	-0.205	0.066	0.036	0.046
0230.525	B	-0.070	0.066	0.036	0.066	0.038	0.047
0225.473	V	-0.076	0.058	-0.001	0.058	0.009	0.041
0225.500	V	0.029	0.049	-0.095	0.049	0.025	0.034
0225.531	V	0.013	0.020	0.043	0.020	-0.055	0.014

0227.521	V	0.035	0.020	0.043	0.020	-0.036	0.014
0229.480	V	0.049	0.041	-0.061	0.041	0.019	0.029
0229.486	V	0.072	0.041	-0.062	0.041	-0.006	0.029
0229.490	V	0.034	0.041	-0.046	0.041	-0.034	0.029
0229.496	V	0.082	0.041	-0.015	0.041	-0.060	0.029
0229.501	V	0.050	0.041	-0.038	0.041	-0.041	0.029
0230.487	V	0.091	0.041	0.061	0.041	-0.054	0.029
0230.492	V	0.058	0.041	0.045	0.041	0.044	0.029
0230.497	V	-0.024	0.043	0.037	0.043	-0.006	0.031
0230.502	V	-0.010	0.043	0.034	0.043	0.008	0.030
0230.507	V	0.110	0.042	0.067	0.042	0.007	0.030
0230.512	V	0.131	0.041	-0.067	0.041	0.014	0.029
0230.517	V	-0.063	0.041	0.071	0.041	0.023	0.029
0230.522	V	0.018	0.041	0.043	0.041	0.000	0.029
0230.527	V	0.003	0.041	0.029	0.041	-0.034	0.029
0225.475	R	-0.037	0.045	0.025	0.045	0.053	0.032
0225.497	R	0.116	0.041	-0.092	0.041	0.043	0.029
0225.481	I	0.239	0.050	0.025	0.050	-0.055	0.035
0225.503	I	0.273	0.042	-0.028	0.042	0.012	0.030

Table A.7: Weighted means, and the normalised linear Stokes parameters expressed in percentage form, for HD155555 in the U,B,V,R and I bands on.

JD	BAND	q	σ_q	u	σ_u	v	σ_v
0227.272	B	-0.184	0.043	0.217	0.043	-0.009	0.031
0227.278	B	-0.128	0.043	0.159	0.043	0.028	0.031
0227.282	B	-0.025	0.043	0.201	0.043	-0.015	0.030
0227.289	B	-0.048	0.046	0.200	0.046	-0.022	0.032
0227.293	B	-0.127	0.046	0.105	0.046	-0.054	0.033
0227.299	B	-0.037	0.046	0.143	0.046	0.052	0.032

0227.303	B	-0.079	0.045	0.298	0.045	-0.086	0.032
0227.309	B	-0.050	0.048	0.190	0.048	-0.069	0.034
0227.313	B	-0.060	0.049	0.150	0.049	0.026	0.034
0227.325	B	0.006	0.052	0.127	0.052	-0.011	0.037
0227.329	B	-0.076	0.053	0.163	0.053	-0.075	0.038
0229.286	B	0.005	0.042	0.186	0.042	0.044	0.030
0229.291	B	-0.050	0.042	0.182	0.042	0.027	0.030
0229.296	B	-0.091	0.043	0.123	0.043	0.002	0.030
0229.301	B	-0.040	0.043	0.202	0.043	0.005	0.030
0229.306	B	0.007	0.043	0.211	0.043	-0.005	0.030
0229.310	B	-0.050	0.043	0.117	0.043	0.006	0.030
0229.315	B	0.078	0.043	0.148	0.043	-0.033	0.030
0229.320	B	-0.083	0.043	0.101	0.043	-0.018	0.030
0229.325	B	-0.059	0.043	0.109	0.043	-0.050	0.030
0229.330	B	0.004	0.043	0.075	0.043	0.010	0.030
0229.335	B	-0.093	0.043	0.077	0.043	-0.003	0.030
0229.340	B	-0.032	0.043	0.126	0.043	0.068	0.030
0229.345	B	-0.046	0.043	0.235	0.043	0.032	0.031
0229.350	B	-0.007	0.044	0.252	0.044	-0.005	0.031
0229.355	B	-0.082	0.043	0.242	0.043	0.036	0.031
0229.360	B	-0.099	0.043	0.068	0.043	-0.016	0.031
0229.365	B	-0.031	0.043	0.194	0.043	0.019	0.031
0230.324	B	-0.030	0.043	0.111	0.043	0.124	0.031
0230.329	B	-0.016	0.043	-0.065	0.043	0.035	0.031
0230.334	B	-0.097	0.043	0.107	0.043	-0.001	0.031
0230.339	B	-0.046	0.043	0.257	0.043	0.046	0.031
0230.344	B	-0.144	0.044	0.120	0.044	0.057	0.031
0230.349	B	0.025	0.043	0.210	0.043	0.042	0.031
0230.354	B	-0.251	0.044	0.010	0.044	0.061	0.031
0230.359	B	-0.179	0.044	-0.054	0.044	0.094	0.031

0230.364	B	0.015	0.044	0.050	0.044	0.104	0.031
0230.369	B	-0.094	0.044	0.180	0.044	0.009	0.031
0230.374	B	-0.110	0.044	0.047	0.044	-0.045	0.031
0230.379	B	-0.088	0.044	0.001	0.044	0.029	0.031

Table A.8: Weighted means, and the normalised linear Stokes parameters expressed in percentage form, for HD100546 in the B band

JD	BAND	q	σ_q	u	σ_u	v	σ_v
0227.274	V	-0.048	0.039	0.347	0.039	-0.032	0.027
0227.280	V	-0.113	0.038	0.343	0.038	-0.011	0.027
0227.284	V	-0.050	0.038	0.273	0.038	-0.046	0.027
0227.291	V	-0.029	0.040	0.371	0.040	-0.072	0.029
0227.295	V	-0.044	0.041	0.252	0.041	-0.011	0.029
0227.301	V	-0.146	0.040	0.303	0.040	0.041	0.028
0227.305	V	-0.227	0.040	0.277	0.040	-0.064	0.029
0227.311	V	-0.083	0.043	0.343	0.043	-0.019	0.030
0227.315	V	-0.125	0.043	0.224	0.043	-0.062	0.031
0227.327	V	-0.072	0.046	0.318	0.046	-0.046	0.033
0227.331	V	0.011	0.047	0.377	0.047	0.028	0.033
0229.288	V	-0.122	0.038	0.228	0.038	-0.015	0.027
0229.293	V	-0.036	0.038	0.231	0.038	0.012	0.027
0229.298	V	-0.140	0.038	0.189	0.038	-0.011	0.027
0229.303	V	-0.056	0.038	0.203	0.038	-0.027	0.027
0229.308	V	-0.134	0.038	0.275	0.038	-0.011	0.027
0229.313	V	-0.132	0.038	0.210	0.038	0.006	0.027
0229.317	V	-0.190	0.038	0.253	0.038	-0.015	0.027
0229.322	V	-0.137	0.038	0.253	0.038	0.002	0.027
0229.327	V	-0.108	0.038	0.193	0.038	0.008	0.027
0229.332	V	-0.046	0.038	0.210	0.038	-0.028	0.027

0229.337	V	-0.131	0.038	0.194	0.038	-0.032	0.027
0229.342	V	-0.072	0.038	0.206	0.038	-0.008	0.027
0229.347	V	-0.147	0.038	0.238	0.038	0.001	0.027
0229.352	V	-0.133	0.038	0.259	0.038	-0.034	0.027
0229.357	V	-0.087	0.038	0.273	0.038	-0.071	0.027
0229.362	V	-0.098	0.038	0.238	0.038	-0.056	0.027
0229.367	V	-0.150	0.038	0.213	0.038	-0.005	0.027
0230.326	V	-0.245	0.038	0.075	0.038	-0.126	0.027
0230.331	V	-0.066	0.038	0.189	0.038	-0.035	0.027
0230.336	V	-0.006	0.038	0.220	0.038	-0.042	0.027
0230.341	V	-0.107	0.038	0.243	0.038	-0.045	0.027
0230.346	V	-0.118	0.038	0.248	0.038	-0.021	0.027
0230.351	V	-0.005	0.038	0.282	0.038	-0.085	0.027
0230.356	V	0.015	0.038	0.134	0.038	0.099	0.027
0230.361	V	-0.308	0.038	0.211	0.038	-0.007	0.027
0230.366	V	-0.287	0.038	0.276	0.038	-0.056	0.027
0230.371	V	-0.262	0.038	0.377	0.038	-0.064	0.027
0230.376	V	-0.399	0.038	0.341	0.038	-0.030	0.027
0230.381	V	-0.197	0.039	0.189	0.039	0.056	0.027

Table A.9: Weighted means, and the normalised linear Stokes parameters expressed in percentage form, for HD100546 in the V band

JD	BAND	q	σ_q	u	σ_u	v	σ_v
0226.252	B	0.101	0.516	-0.319	0.516	1.395	0.367
0226.370	B	-0.017	0.014	0.008	0.014	0.016	0.10
0226.385	B	-0.025	0.014	0.022	0.014	0.003	0.010
0227.351	B	-0.039	0.029	-0.003	0.029	0.007	0.021
0227.406	B	0.018	0.014	0.046	0.014	0.006	0.010
0227.428	B	-0.042	0.015	0.027	0.015	0.025	0.010

0229.380	B	0.028	0.028	-0.015	0.028	0.047	0.020
0229.385	B	0.030	0.028	0.004	0.028	0.000	0.020
0229.390	B	0.070	0.028	-0.025	0.028	0.041	0.020
0229.395	B	0.063	0.028	-0.031	0.028	-0.063	0.020
0230.397	B	0.103	0.029	-0.115	0.029	0.105	0.020
0230.402	B	0.118	0.029	0.010	0.029	-0.001	0.021
0230.407	B	0.018	0.030	0.119	0.030	-0.008	0.021
0230.413	B	0.017	0.030	0.105	0.030	0.043	0.021
0226.335	V	0.001	0.031	-0.020	0.031	-0.043	0.022
0226.354	V	-0.044	0.031	-0.034	0.031	0.003	0.022
0227.353	V	-0.027	0.065	-0.113	0.065	-0.047	0.046
0227.374	V	-0.018	0.046	0.103	0.046	-0.089	0.033
0227.388	V	-0.016	0.032	0.064	0.032	-0.060	0.022
0229.382	V	0.222	0.062	-0.063	0.062	-0.051	0.044
0229.387	V	0.099	0.062	-0.148	0.062	-0.028	0.044
0229.392	V	0.140	0.062	0.060	0.062	-0.111	0.044
0229.397	V	0.131	0.062	-0.066	0.062	-0.092	0.044
0230.400	V	-0.044	0.064	0.013	0.064	0.039	0.045
0230.405	V	0.035	0.065	-0.010	0.065	-0.133	0.046
0230.409	V	-0.025	0.069	0.287	0.069	-0.045	0.049
0230.415	V	0.085	0.065	0.056	0.065	-0.025	0.046

Table A.10: Weighted means, and the normalised linear Stokes parameters expressed in percentage form, for HD115383 in the B and V bands

JD	BAND	q	σ_q	u	σ_u	v	σ_v
0225.334	U	0.403	1.734	-0.016	1.734	-0.194	1.219
0225.335	B	-1.184	0.666	2.024	0.666	-1.186	0.471
0225.342	V	-1.126	0.131	0.562	0.131	-0.017	0.093
0225.344	R	-1.248	0.063	0.335	0.063	-0.054	0.045

0225.352	I	-0.776	0.039	0.403	0.039	0.038	0.028
----------	---	--------	-------	-------	-------	-------	-------

Table A.11: Weighted means, and the normalised linear Stokes parameters expressed in percentage form, for SAO251015 in the U,B,V,R and I bands

JD	BAND	q	σ_q	u	σ_u	v	σ_v
0229.411	B	0.065	0.061	-0.021	0.061	-0.023	0.043
0229.416	B	0.003	0.060	0.033	0.060	0.011	0.043
0229.421	B	-0.027	0.061	0.066	0.061	0.047	0.043
0229.426	B	0.077	0.061	0.036	0.061	0.065	0.043
0229.431	B	0.071	0.060	-0.027	0.060	-0.019	0.043
0230.426	B	0.014	0.062	0.122	0.062	-0.084	0.044
0230.431	B	-0.065	0.063	0.032	0.063	0.040	0.044
0230.436	B	-0.090	0.065	0.052	0.065	0.046	0.046
0230.441	B	-0.093	0.064	0.122	0.064	-0.006	0.045
0230.446	B	-0.073	0.063	0.031	0.063	0.038	0.045
0230.451	B	-0.038	0.063	-0.039	0.063	0.093	0.045
0230.456	B	-0.058	0.062	0.062	0.062	0.065	0.044
0230.461	B	-0.201	0.065	0.141	0.065	-0.033	0.046
0230.466	B	-0.070	0.067	0.014	0.067	0.114	0.047
0230.471	B	-0.035	0.066	-0.099	0.066	0.099	0.046
0229.414	V	0.064	0.039	0.006	0.039	0.001	0.027
0229.419	V	-0.006	0.039	-0.040	0.039	-0.015	0.027
0229.424	V	0.044	0.039	0.038	0.039	-0.017	0.027
0229.428	V	0.029	0.039	-0.050	0.039	0.005	0.028
0229.433	V	0.030	0.039	-0.011	0.039	-0.020	0.027
0230.428	V	0.124	0.040	0.036	0.040	-0.008	0.028
0230.433	V	0.004	0.040	0.063	0.040	0.055	0.028
0230.438	V	0.016	0.041	0.014	0.041	0.077	0.029
0230.443	V	-0.016	0.040	0.229	0.040	-0.050	0.029

0230.448	V	0.129	0.040	0.066	0.040	-0.024	0.028
0230.453	V	0.059	0.040	0.190	0.040	-0.101	0.029
0230.458	V	0.112	0.040	0.155	0.040	-0.024	0.028
0230.463	V	0.007	0.041	-0.052	0.041	-0.092	0.029
0230.468	V	0.078	0.042	0.124	0.042	-0.031	0.030
0230.473	V	0.043	0.042	0.114	0.042	-0.053	0.030

Table A.12: Weighted means, and the normalised linear Stokes parameters expressed in percentage form, for HD128400 in the B and V bands

JD	BAND	q	σ_q	u	σ_u	v	σ_v
0229.639	B	0.028	0.051	-0.088	0.051	-0.032	0.036
0229.645	B	0.016	0.051	-0.136	0.051	0.084	0.036
0229.651	B	0.030	0.050	-0.069	0.050	0.027	0.036
0229.656	B	0.076	0.050	-0.029	0.050	-0.029	0.036
0229.661	B	-0.084	0.050	-0.061	0.050	0.016	0.035
0230.635	B	0.025	0.053	-0.139	0.053	-0.054	0.037
0230.642	B	0.129	0.052	-0.059	0.052	0.010	0.037
0230.647	B	0.007	0.052	-0.008	0.052	-0.001	0.037
0230.653	B	0.003	0.052	-0.038	0.052	0.000	0.036
0230.658	B	0.043	0.051	-0.119	0.051	0.059	0.036
0230.664	B	0.078	0.051	-0.055	0.051	0.017	0.036
0229.641	V	-0.044	0.033	-0.056	0.033	-0.004	0.023
0229.647	V	-0.009	0.033	0.060	0.033	0.016	0.023
0229.653	V	-0.015	0.033	0.023	0.033	-0.005	0.023
0229.658	V	-0.016	0.033	-0.030	0.033	-0.009	0.023
0229.663	V	-0.059	0.033	0.087	0.033	-0.013	0.023
0230.637	V	0.039	0.034	-0.011	0.034	-0.097	0.024
0230.644	V	-0.022	0.034	-0.049	0.034	0.017	0.024
0230.649	V	-0.013	0.034	0.068	0.034	-0.017	0.024

0230.655	V	0.058	0.033	0.058	0.033	-0.028	0.024
0230.660	V	-0.010	0.033	-0.054	0.033	-0.011	0.024
0230.666	V	-0.113	0.033	-0.078	0.033	-0.059	0.024

Table A.13: Weighted means, and the normalised linear Stokes parameters expressed in percentage form, for HD1835 in the B and V bands

JD	BAND	q	σ_q	u	σ_u	v	σ_v
0226.465	V	0.076	0.040	-0.018	0.040	-0.037	0.028
0226.482	V	-0.025	0.039	0.104	0.039	0.010	0.027
0226.496	V	-0.029	0.039	0.036	0.039	0.055	0.027
0226.511	V	0.005	0.038	0.082	0.038	-0.013	0.026
0226.524	V	0.033	0.039	0.116	0.039	0.024	0.028
0227.465	V	0.060	0.038	0.049	0.038	-0.008	0.027
0227.479	V	0.052	0.038	0.016	0.038	-0.033	0.027
0228.491	V	0.007	0.036	0.006	0.036	-0.009	0.026
0229.446	V	-0.093	0.055	-0.138	0.055	-0.033	0.039
0229.451	V	-0.104	0.055	-0.136	0.055	-0.020	0.039
0229.456	V	-0.144	0.055	-0.159	0.055	-0.024	0.039
0229.462	V	-0.085	0.055	-0.141	0.055	-0.049	0.039
0229.466	V	-0.072	0.055	-0.149	0.055	0.057	0.039
0226.397	R	-0.038	0.035	0.017	0.035	-0.023	0.024

Table A.14: Weighted means, and the normalised linear Stokes parameters expressed in percentage form, for HD139614 in the V and R bands

Bibliography

- Andretta, V. and Giampapa, M. S.: 1995, *Astrophysical Journal* **439**, 405
- Angel and Landstreet: 1992, *Bull. Am. Astron. Soc.* **4**, 409
- Bogaert, E. and Waelkens, C.: 1990, in C. Jaschek and Y. Andrillat (eds.), *The infrared spectral region of stars*, p. 345, Cambridge Univ. Press
- Brooks, A., Clarke, D., and McGale, P. A.: 1994, *Vista in Astronomy* **38**, 377
- Brown, M. B. and Forsythe, A. B.: 1974, *Technometrics* **16**, 129
- Chandrasekhar, S.: 1950, in *Radiative Transfer*, pp 35–37, Oxford
- Clarke, D.: 1990, *Astronomy and Astrophysics* **227**, 151
- Clarke, D. and Fullerton, S. R.: 1996, *Astronomy and Astrophysics* **310**, 331
- Clarke, D. and McGale, P.: 1987, *Astronomy and Astrophysics* **178**, 294
- Clarke, D. and McGale, P. A.: 1986, *Astronomy and Astrophysics* **169**, 251
- Clarke, D. and Naghizadeh-Khouei, J.: 1994, *Astrophysical Journal* **108**, 687
- Conover, W. J.: 1980, in *Practical Non-Parametric Statistics - 2nd Edition*, pp 344–356, John Wiley and Sons, Chapter 6
- Coyne, G. V.: 1976, p. 233, A. Sletteback, D. Reidel Publishing Co., Dordrecht, Holland, IAU Symp. No. 70, ed.
- Cropper, M. S.: 1985, *MNRAS* **212(709)**, 131
- Cutispoto, C.: 1990, *Astronomy and Astrophysics Supplement* **84**, 397
- Donahue, R. A., Saar, S. H., and Baliunas, S. L.: 1996, *Astrophysical Journal* **466**, 384
- Donati, J., Semel, M., Carter, B. D., et al.: 1997, *MNRAS* **291**, 658
- Dunkin, S. K., Barlow, M. J., and Ryan, S. G.: 1997, *MNRAS* **286**, 604
- Elias, N. M. and Dorren, J. D.: 1990, *The Astrophysical Journal* pp 818–824
- Fox, G. K.: 1995, *Astrophysical Journal* **441**, 408
- Gehrels, T.: 1974, *Planets, Stars and Nebula*, Arizona

- Grady, C. A., Perez, M. R., et al.: 1996, *Astronomy and Astrophysics* **120**, 157
- Grinin, V. P.: 1988, *SvAL* **14**, 65
- Gullbring, E. and Gahm, G. F.: 1996, *Astronomy and Astrophysics* **308**, 821
- Harvey, P. M., Smith, B. J., et al.: 1996, *Astrophysical Journal* **471**, 973
- Hayes, D.: 1977, *Astronomical Journal* **219**, 952
- Heinrichs, H. F.: 1998, *In Press*
- Henning, T., Launhardt, R., Steinacker, J., and Thamm, E.: 1994, *Astronomy and Astrophysics* **291**, 546
- Herbig, G. H. and Bell, K. R.: 1988, *Lick Obs. Bull.* (1111)
- Hsu, J. C. and Breger, M.: 1982, *Astrophysical Journal* **262**, 732
- Jain, S. K. and Bhatt, H. C.: 1995, *Astronomy and Astrophysics Supplement* **111**, 399
- Kaper, L. and Heinrichs, H. E.: 1997, *Astronomy and Astrophysics* **327**, 281
- Kemp, J.: 1970, *Astrophysical Journal* **162**, 169
- Kemp, J. C., Henson, G. D., et al.: 1987, *Astrophysical Journal* 317(L29)
- Kemp, J. C., Henson, G. D., and Kraus, D. J.: 1986, *The Astrophysical Journal* 301,L35
- Kemp, J. C. and Wolstencroft, R. D.: 1972, *Astrophysical Journal* 176(L115)
- Kerschbaum, F.: 1995, *Astronomy and Astrophysics Supplement* **113**, 441
- Kholopov, P. N.: 1987, *General Catalogue of Variable Stars, 4th Edition, Vol III, Moscow, Nauka.*
- Klare, G. and Neckel, T.: 1977, *Astronomy and Astrophysics Supplement* **27**, 215
- Leroy, J. L. and LeBorgne, J. F.: 1989, *Astronomy and Astrophysics* **223**, 336
- Linsky, J. L. and Bornmann, P. L.: 1982, *Astrophysical Journal* **260**, 670
- Malfait, K., Bogaert, E., and Waelkens, C.: 1998, *Astrophysical Journal* **471**, 973
- Meeus, G., Waelkens, C., and Malfait, K.: 1998, *Astronomy and Astrophysics* **329**, 131
- Menard, F. and Bastien, P.: 1992, *AJ* **103**, 564
- Miller: 1956, *Journal of the American Statistical Association* **51**, 111
- Mueller, H.: 1948, *Journal of Optical Society of America* **38**, 661
- Optics, M.: 1996, p. 12
- Oudmaijer, R. D., van der Veen, W. E. C., et al.: 1992, *Astronomy and Astrophysics Supplement* **96**, 625
- Pasquini, L., Cutispoto, G., et al.: 1991, *Astronomy and Astrophysics* **248**, 72
- Piirola, V.: 1977, *Astronomy and Astrophysics Supplement* **30**, 213

- Povel, H. and Stenflo, J. O.: 1990, *Applied Optics* **29(8)**, 1186
- Rowell, R. L. and Levitt, A. B.: 1969, *Applied Optics* **8(8)**, 1734
- Saar, S. H., Huovelin, J., Osten, R. A., and Schcherbakov, A. G.: 1997, *Astronomy and Astrophysics* **326**, 741
- Schmitt, A. H. . J. H. M. M., Schultz, M., and Rudigery, G.: 1995, *Astronomy and Astrophysics* **294**, 515
- Schwarz, H. E.: 1986, *Vistas In Astronomy* **29**, 253
- Serkowski: 1973, in *Interstellar Polarisation (review)*, D.Reidel Publ.Co
- Serkowski, K.: 1974, in: *Planets, Stars and Nebulae studied with photopolarimetry*, ed. T. Gehrels, Univ Arizona Press, Tuscon, p. 135
- Shine, R. A. and Linsky, J. L.: 1974, *Solar Physics* **39**, 49
- Silvester, R. J., Skinner, C. J., and Barlow, M. J.: 1997, *MNRAS* **289**, 831
- Silvester, R. J., Skinner, C. J., et al.: 1996, *MNRAS* **279**, 915
- Slakter: 1965
- Stenflo, J. O.: 1994, in *Solar Magnetic Fields*, Kluwer Academic Publishers, Dordrecht
- Stenflo, J. O. and Povel, H.: 1985, *Applied Optics* **24(2)**, 3893
- Tamura, M. and Sato, S.: 1989, *AJ* **89**, 1368
- Thé, P. S., de Winter, D., and Perez, M. R.: 1994, *Astronomy and Astrophysics* **104**, 315
- Tinbergen, J. and Zwaan, C.: 1981, *Astronomy and Astrophysics* **101**, 223
- van de Hulst, H. C.: 1957, in *Light Scattering by Small Particles*, New York: Wiley
- Vieira, S., Pogodin, M. A., and Franco, G.: 1998, *In preparation*
- Yudin, R. V.: 1994, in: *The Nature and Evolutionary Status of Herbig Ae/Be Stars*, ASP Conf. Ser. 62, eds. P.S. Thé, M.R. Pérez and E.P.J. van den Heuvel, p82
- Yudin, R. V. and Evans, A.: 1998, *Astronomy and Astrophysics Supplement (Accepted)*
- Zarro, D. M.: 1982, *Astrophysical Journal* **267**, L61